

Nicolaus Copernicus University in Toruń  
Faculty of Physics, Astronomy and Informatics  
Department of Atomic, Molecular and Optical Physics

**COLLISIONAL EFFECTS  
IN ACCURATE ROVIBRATIONAL SPECTROSCOPY  
OF SIMPLE DIATOMIC MOLECULES**



MICHAŁ SŁOWIŃSKI

Dissertation submitted in partial fulfillment  
of the requirements for the degree of  
DOCTOR OF PHYSICS

Thesis supervised by dr hab. Piotr Wcisło, prof. NCU  
Department of Atomic, Molecular and Optical Physics  
Institute of Physics, Nicolaus Copernicus University in Toruń



Toruń 2022



# ACKNOWLEDGMENTS

I would like to express my sincere gratitude to my supervisor, dr hab. Piotr Wcisło, prof. NCU for the scientific supervision and help he supplied during my PhD studies. I deeply appreciate our merit discussions, which gave me an inspiration for my work. I would also like to thank prof. dr hab. Roman Ciuryło for mentoring, discussions and joint work on line-shape theory and other physical problems. I am grateful for introducing me into the field of the molecular spectroscopy and the theory of collisions.

I would like to thank all collaborators directly involved in the studies submitted in this dissertation, in particular I thank prof. Franck Thibault, prof. dr hab. Daniel Lisak, prof. Alain Campargue, prof. Konrad Patkowski, dr hab. Piotr Masłowski, prof. NCU, dr inż. Grzegorz Kowzan, mgr inż. Mikołaj Zaborowski, mgr Hubert Józwiak, mgr inż. Magdalena Konefał and mgr Nikodem Stolarczyk.

I would like to thank all people from our group I had opportunity to work with, particularly I would like to thank prof. dr hab. Ryszard S. Trawiński, prof. dr hab. Józef Szudy, dr hab. Michał Zawada, prof. NCU, dr hab. Jolanta Domysławska, prof. NCU, dr Szymon Wójtewicz, dr Katarzyna Bielska, dr Marcin Bober, mgr inż. Dominik Charczun, mgr Aleksandr Balashov, inż. Kamil Sołtys and Marcin Makowski.

Finally, I would like to express my gratitude to my wife. Without her tremendous understanding and encouragement in the past few years, it would be impossible for me to complete my study.

The research presented within this dissertation was supported and partially financed by the *A next-generation worldwide quantum sensor network with optical atomic clocks* project carried out within the TEAM IV Programme of the Foundation for Polish Science cofinanced by the European Union under the European Regional Development Fund, National Science Centre, Poland, project Nos. 2014/15/D/ST2/05281, 2017/26/D/ST2/00371, PHC POLONIUM program, UMK scholarship 2812-F grant (WFAiS UMK resource for development of young scientists). The research is a part of the program of the National Laboratory FAMO in Toruń, Poland.







# CONTENTS

	PAGE
<b>ACKNOWLEDGMENTS</b>	<b>3</b>
<b>CONTENTS</b>	<b>5</b>
<b>FORMAL PREFACE</b>	<b>6</b>
<b>ABSTRACT</b>	<b>8</b>
<b>PUBLICATIONS CONSTITUTING THE DISSERTATION</b>	<b>10</b>
<b>INTRODUCTION</b>	<b>12</b>
<b>AUTHOR CONTRIBUTION STATEMENT</b>	<b>16</b>
<b>BIBLIOGRAPHY</b>	<b>18</b>
<b>PUBLICATIONS</b>	<b>22</b>
ARTICLE A . . . . .	22
ARTICLE B . . . . .	29
ARTICLE C . . . . .	40
ARTICLE D . . . . .	53
ARTICLE E . . . . .	58
ARTICLE F . . . . .	62
<b>CO-AUTHOR CONTRIBUTION STATEMENTS</b>	<b>72</b>
<b>ALL PUBLISHED ARTICLES</b>	<b>86</b>



Niniejsza rozprawa doktorska stanowi spójny tematycznie zbiór sześciu artykułów, przygotowanych pod opieką mojego promotora, dr. hab. P. Wcisło, prof. UMK, opublikowanych w czasopismach z części A wykazu czasopism naukowym Ministra Edukacji i Nauki. Podstawą prawną przedstawienia niniejszej rozprawy doktorskiej w formie spójnego tematycznie zbioru artykułów opublikowanych w czasopismach naukowych jest *Art. 179 Ust. 1 Ustawy z dnia 3 lipca 2018 r. Przepisy wprowadzające ustawę - Prawo o szkolnictwie wyższym (Dz.U. 2018 poz. 1669, z późn. zm.)* i *Art. 13 Ust. 1 i 2 Ustawy z dnia 14 marca 2003 r. o stopniach naukowych i tytule naukowym oraz stopniach i tytule w zakresie sztuki (Dz.U. 2003, poz. 595, z późn. zm.)*. Ponadto, zgodnie z *Art. 13 Ust. 5* powyższej ustawy, na podstawie *Uchwały Rady Instytutu Fizyki Nr 108/2018 z dnia 12 grudnia 2018 w sprawie wyrażenia zgody na przedstawienie przez mgr. inż. Michała Słowińskiego rozprawy doktorskiej w języku angielskim*, rozprawa ta została przedstawiona w języku angielskim. W myśl *§ 5 Ust. 2 i 3 Rozporządzenia Ministra Nauki i Szkolnictwa Wyższego z dnia 19 stycznia 2018 r. w sprawie szczegółowego trybu i warunków przeprowadzania czynności w przewodzie doktorskim, w postępowaniu habilitacyjnym oraz w postępowaniu o nadanie tytułu profesora (Dz.U. 2018 poz. 261)* i w zgodzie z *Art. 179 Ust. 1 Ustawy z dnia 3 lipca 2018 r. Przepisy wprowadzające ustawę - Prawo o szkolnictwie wyższym (Dz.U. 2018 poz. 1669, z późn. zm.)* do niniejszej rozprawy dołączone są oświadczenia autora rozprawy określające indywidualny wkład autora w każdej z przedstawionych w rozprawie artykułów a także oświadczenia conajmniej czterech współautorów z tychże artykułów określające indywidualny wkład każdego z nich w ich powstanie.



This doctoral dissertation consists of six thematically matched scientific articles written under supervision of my doctoral dissertation supervisor, dr. Piotr Wcisło, prof. at NCU, and all published in scientific journals from the part A of the journals list of the Polish Minister of Education and Science. The legal basis for preparing this doctoral dissertation in the form of a thematically coherent set of articles published in scientific journals is *Art. 179 (1) of the Act of 3 July 2018 Provisions introducing the Act of the Law on higher education (Journal of Laws 2018, item 1669, as amended)* and *Art. 13 (1-2) Act of 14 March 2003 on academic degrees and academic titles as well as degrees and titles in arts (Journal of Laws 2003, item 595, as amended)*. Furthermore, according to the *Art. 13 (5) of aforementioned act, according to the Resolution of the Council of the Institute of Physics No. 108/2018 of 12 December 2018 on giving consent for presentation by mgr. inż. Michał Słowiński his doctoral dissertation in English*, this dissertation is prepared in English. According to the *Paragraph 5 (2-3) of the Regulation of the Minister of Science and Higher Education of 19 January 2018 on the detailed procedure and conditions for performing activities in the doctoral thesis, in the habilitation procedure and in the procedure for awarding the title of professor (Journal of Laws of 2018, item 261)* and according to the *Art. 179 (1) of the Act of 3 July 2018 Provisions introducing the Act of the Law on higher education (Journal of Laws 2018, item 1669, as amended)* attached to this dissertation are declarations of the author of the dissertation specifying the author's individual contribution to each of the articles presented in the dissertation, as well as statements of at least four co-authors from these articles specifying the individual contribution of each of them to their preparation.



## STRESZCZENIE

Niniejsza rozprawa jest poświęcona badaniom nad kształtem linii widmowych. Główna część wyników poświęcona jest możliwości wykorzystania ultradokładnej spektroskopii do testowania modeli zderzeniowych, które uzyskiwane są z wykorzystaniem kwantowych obliczeń rozproszonych. Wykorzystano model kształtu linii widmowej, który w dokładny sposób opisuje subtelne efekty zderzeniowe (używa modelu zderzeń kul bilardowych i zależności od prędkości parametrów zderzeniowych kształtu linii obliczonej z zasad pierwszych), co jest szczególnie istotne dla lekkich molekuł. Na przykładzie molekularnego wodoru pokazano, że możliwe jest odtworzenie widm eksperymentalnych na poziomie subprocentowym wychodząc z potencjału oddziaływania wyliczonego z zasad pierwszych. Na tymże przykładzie zanalizowano też wkład konkretnych przyczynków zderzeniowych do kształtu linii widmowej. Pokazano także, że wykorzystanie użytych w niniejszej rozprawie metod modelowania kształtu linii wraz z wysokiej jakości danymi eksperymentalnymi pozwala na weryfikowanie jakości potencjałów oddziaływania. Na przykładzie cząsteczki czadu zbadano różnice powodowane wykorzystaniem uproszczonych fenomenologicznych modeli kształtu linii widmowej. Pokazano, że badane tu metody opisu kształtu linii można także wykorzystać do dokładnego ustalania pozycji izolowanych linii na przykładzie linii deuteru, osiągając rekordową na dzień publikacji dokładność. Zademonstrowano również uproszczoną metodę modelowania kształtu linii widmowej, która pozwala na uzyskanie niemalże tych samych wyników przy wielokrotnie mniejszym zapotrzebowaniu na zasoby numeryczne i potwierdzono jej działanie na tej samej linii deuteru. Pokazano także, że możliwe jest wykorzystanie zademonstrowanej analizy do generowania danych wykorzystywanych w największych spektroskopowych bazach danych na świecie.



## ABSTRACT

This dissertation is devoted to the research on the shape of the spectral lines. The major part of the results is exploring the possibility of using extremely accurate spectroscopic methods for tests of collisional models obtained through quantum-scattering calculations. This thesis utilizes a line-shape profile using the billiard-ball model of collisions with *ab initio* calculation of the speed dependence of collisional line-shape parameters. This profile is capable of describing subtle collisional effects, which is particularly important for the light molecules. It was demonstrated on the molecular-hydrogen example, that starting from the *ab initio* calculated interaction potential it is possible to recreate the experimental spectra at the sub-percentage level. The impact of specific collision contributions to the shape of the spectral line was also analyzed on the same molecular-hydrogen example. It was also shown that the use of the line shape modeling methods developed in this dissertation, together with high-quality experimental data, allows for verification of the quality of the calculated potential energy surfaces. Usage of simplified phenomenological models has in the past been shown to cause differences between experimental and theoretical results. These differences were investigated on the carbon monoxide sample. Another part shows how the developed methods can be employed for accurate determination of the positions of isolated lines, as a record-breaking accuracy has been achieved for deuterium line. A simplified method of modeling the shape of the spectral line that allows to obtain almost same results with a much smaller numerical complexity was also demonstrated and tested on the aforementioned deuterium example. Finally, it was also shown that it is possible to use the analysis demonstrated in thesis to generate data to populate largest spectroscopic databases.



## PUBLICATIONS

### CONSTITUTING THE DISSERTATION

**A** H<sub>2</sub>-He collisions: *Ab initio* theory meets cavity-enhanced spectra

**Michał Słowiński**, Franck Thibault, Yan Tan, Jin Wang, An-Wen Liu, Shui-Ming Hu, Samir Kassi, Alain Campargue, Magdalena Konefał, Hubert Józwiak, Konrad Patkowski, Piotr Żuchowski, Roman Ciuryło, Daniel Lisak, Piotr Wcisło

*Physical Review A* 101, 052705 (2020)

DOI: 10.1103/PhysRevA.101.052705

**B** Collisional line-shape effects in accurate He-perturbed H<sub>2</sub> spectra

**Michał Słowiński**, Hubert Józwiak, Maciej Gancewski, Kamil Stankiewicz, Nikodem Stolarczyk, Yan Tan, Jin Wang, An-Wen Liu, Shui-Ming Hu, Samir Kassi, Alain Campargue, Konrad Patkowski, Piotr S. Żuchowski, Roman Ciuryło, Franck Thibault, Piotr Wcisło

*Journal of Quantitative Spectroscopy and Radiative Transfer* 277, 107951 (2022)

DOI: 10.1016/j.jqsrt.2021.107951

**C** Fully quantum calculations of the line-shape parameters for the Hartmann-Tran profile: A CO-Ar case study

Grzegorz Kowzan, Piotr Wcisło, **Michał Słowiński**, Piotr Masłowski, Alexandra Viel, Franck Thibault

*Journal of Quantitative Spectroscopy and Radiative Transfer* 243, 106803 (2020)

DOI: 10.1016/j.jqsrt.2019.106803



- D** Analytical-function correction to the Hartmann–Tran profile for more reliable representation of the Dicke-narrowed molecular spectra

Magdalena Konefał, **Michał Słowiński**, Mikołaj Zaborowski, Roman Ciuryło, Daniel Lisak, Piotr Wcisło

*Journal of Quantitative Spectroscopy and Radiative Transfer* 242, 106784 (2020)

DOI: 10.1016/j.jqsrt.2019.106784

- E** Ultrahigh finesse cavity-enhanced spectroscopy for accurate tests of quantum electrodynamics for molecules

Mikołaj Zaborowski, **Michał Słowiński**, Kamil Stankiewicz, Franck Thibault, Agata Cygan, Hubert Józwiak, Grzegorz Kowzan, Piotr Masłowski, Akiko Nishiyama, Nikodem Stolarczyk, Szymon Wójtewicz, Roman Ciuryło, Daniel Lisak, Piotr Wcisło

*Optics Letters* 45, 1603 (2020)

DOI: 10.1364/OL.389268

- F** The first comprehensive dataset of beyond-Voigt line-shape parameters from *ab initio* quantum scattering calculations for the HITRAN database: He-perturbed H<sub>2</sub> case study

Piotr Wcisło, Franck Thibault, Nikodem Stolarczyk, Hubert Józwiak, **Michał Słowiński**, Maciej Gancewski, Kamil Stankiewicz, Magdalena Konefał, Samir Kassi, Alain Campargue, Yan Tan, Jin Wang, Konrad Patkowski, Roman Ciuryło, Daniel Lisak, Roman Kochanov, Laurence S. Rothman, Iouli E. Gordon

*Journal of Quantitative Spectroscopy and Radiative Transfer* 260, 107477 (2021)

DOI: 10.1016/j.jqsrt.2020.107477



## INTRODUCTION

The main goal of the dissertation is to use highly accurate molecular spectra to test models of molecular collisions that are based on *ab initio* quantum scattering calculations. We developed new tools to efficiently handle the beyond-Voigt effects that are particularly important for light molecules such as molecular hydrogen. Finally, we applied the developed methodology to: validate applicability of simple phenomenological collisional models, improve the accuracy of the metrology of the deuterium rovibrational structure, and to develop the first *ab initio* dataset of beyond-Voigt parameters for the HITRAN database.

The collisional effects are manifested in molecular spectra as a perturbation of the shapes of molecular lines. It was thoroughly demonstrated that the collisionally broadened and shifted line shape in the impact approximation can be described by a Lorentzian profile [1, 2]. In the cases where the change of the velocity of the emitter can be neglected, Doppler broadening of a line can be treated separately from the collisional effects [3] thus giving rise to a Voigt profile (VP). However if one assumes that collisions induce velocity changes, then the Doppler contribution to the line width is reduced, which is called the Dicke narrowing [4]. Historically, there are two distinct velocity-changing collisions model that may include Dicke narrowing in the spectra description, i.e. the so-called soft and hard collisions [5, 6]. Recently, a more physically justified approach to velocity-changing collisions has been introduced, called the billiard-ball (BB) model [7, 8]. In most cases collision and Doppler broadening occur together. For the molecular systems featured in our articles, simple VP turns out to be fairly insufficient [9–11]. The beyond-Voigt line-shape effects are particularly pronounced for the case of the molecular hydrogen rovibrational transitions (see Fig.2 e-f in Article **A**). If the correlations between the collision kinetic energy and collision broadening and shift are strong, the dependence of these two line-shape parameters on the emitter speed has to be taken into account. Recent studies already confirmed, that in some cases it is necessary to take into account simultaneously both the speed dependence of the line-shape parameters as well as the Dicke narrowing. In general, line-



shape can also be perturbed by other effects such as line mixing. Those effects are not covered in this dissertation as those effects are not visible under the considered here conditions.

In the Articles **A** and **B**, we use highly-accurate spectra obtained with cavity ring-down spectroscopy (CRDS) to study collisions at molecular scale and validate quantum chemical calculations of the potential energy surfaces (PESs). We focus here specifically on helium-perturbed hydrogen molecule, which is the simplest neutral chemically bound system colliding with a smallest atom. The He-perturbed spectra were collected in the Hefei National Laboratory for Physical Sciences at Microscale (Hefei, China) and Interdisciplinary Physics Laboratory (Grenoble, France). In both works, we demonstrated agreement between measured and *ab initio* calculated shapes of the molecular lines at the subpercent level.

In Article **A** we use our *ab initio* originated line-shape calculations based on the generalized Hess method [12–14] (in which we replace velocity-changing model to one based on the Boltzmann operator with the rigid-sphere potential approximation [15] to create accurate line shapes for the considered transitions. Indeed, basing on the state-of-the-art PES, i.e. the extended Bakr-Smith-Patkowski PES [16, 17], we were able to reproduce the experimental spectra to the level of 0.99% and 0.33% rRMSE, for the 3-0 S(1) and 2-0 Q(1) lines, respectively. In addition to demonstrating that our methodology leads to reproducing the experimental profiles at unprecedented level, we showed, that it can also serve as a link between quantum chemical calculations and high-precision spectroscopy, as it enabling PES testing in the regions of the parameter space inaccessible with other techniques.

In Article **B**, we focus primarily on proving, that the signatures of different collisional line-shape parameters can be clearly distinguished in the experimental spectra. We have shown, that not only both speed dependence of the line-shape parameters and Dicke narrowing effect has to be taken into account to properly describe the collision-perturbed line shape, but also that the imaginary part of the complex Dicke parameters cannot be neglected for the examined lines. In this article, we also improved the results presented Article **A** by introducing the centrifugal distortion which is usually neglected in the quantum-scattering calculations for rovibrational transition line-shape calculations. This allowed us to make previous results more consistent, with the experiment-to-theory agreement at the level of 0.87% and 0.33% rRMSE,



for the 3-0 S(1) and 2-0 Q(1) lines, respectively. We also discussed how the uncertainty of the line-shape parameters propagates on the shape of the line.

In article **C** we use the same methodology as in the articles A. and B. to test and validate simple phenomenological line-shape models that are often used in molecular spectra analysis [18–21]. For this purpose, we consider diatomic molecule that is more relevant to atmospheric spectra, i.e., Ar-perturbed CO; we studied two lines, P(2) and P(8). As a reference we chose the Hartmann-Tran profile (HTP), which is the profile recommended to use by IUPAC [22] and treats the collisions in the hard-collision model. By design, it also includes the speed dependence of the collisional width and shift in quadratic approximation, but for the sake of comparison we used also modified profile in which the speed dependence was swapped to *ab initio* calculated. We demonstrated, that BB-based profiles (with both quadratic and *ab initio* versions of the speed dependence) for both P(2) and P(8) lines differ approximately 0.5% from the HTP with approximately 0.5% additional difference comes from the speed dependence model, but the latter is either same or opposed direction to the first correction. The comparison is presented in Fig. 4 in the Article **C** We can see that HTP overestimates the velocity-changing collisions in higher pressures for the lines considered in the article.

The line-shape methodology (based on the BB model) studied in all the previous articles gives a reliable description of the collision-perturbed spectra and allows one to handle sophisticated beyond-Voigt line shape effects [23–26], but it is computationally very expensive and at low pressures requires special treatment based on iterative approach to solving the transport-relaxation equation [27]. Therefore, it is difficult to widely implement this approach to molecular spectra analysis in practical applications. To address this issue, in Article **D**, we developed a correction function (called  $\beta$  correction) that can be introduced in the profiles that includes the velocity-changing collisions as in the hard-collision model. We extend the previous approach [15] (which is limited to the self-perturbed cases) to any value of perturber-to-absorber mass ratio up to five, which covers almost all atmospheric applications. The correction itself is a function of aforementioned mass ratio and Doppler width to the frequency of the velocity-changing collisions ratio and, as such, it does not include any additional parameter that has to be fitted during any fitting procedure. It can be used freely in any hard-collision based models without increasing the computational complexity.



In Article **E**, we applied the methodology tested in Articles **A**, **B** and **C** and the  $\beta$ -correction approach developed in Article **D**, to improve the accuracy of the metrology of the deuterium rovibrational structure. Using the frequency-stabilized CRDS (FS-CRDS) operating in frequency-agile, rapid scanning (FARS) spectroscopy mode, we measured the S(2) 2-0 deuterium transition in low pressure range (from 1 up to 40 Torr). Analysis of the experimental data was done with the  $\beta$ -corrected quadratic speed-dependent hard-collision model (qSDHCP). The ultimate result was repeated using the billiard-ball based one. A careful analysis of the collisional line-shape effects allowed us to find an optimal balance between the statistical and systematic contributions to the uncertainty budget, see Fig. 3 in Article **E**. The obtained accuracy allowed us to test quantum electrodynamics for molecules at fifth significant digit.

Finally, in Article **F**, we used the approach introduced in Article **D** to develop a methodology of populating spectroscopic databases with beyond-Voigt line-shape parameters. We considered the case of the He-perturbed H<sub>2</sub> rovibrational lines. We tested, that the  $\beta$ -corrected qSDHCP (the approach adopted in the HITRAN database) reproduces the accurate experimental spectra at sub-percent accuracy level, see Fig. 5 in Article **F**. We created a comprehensive (3480 entries) database consisting of *ab initio* calculated line-shape parameters from which the 370 entries contain purely *ab initio* calculated parameters, which we also included in the supplementary materials. We showed that the double power law [28,29] is capable to reproduce the *ab initio* temperature dependence of the line-shape parameters with sufficient accuracy (see Fig. 4).



## AUTHOR CONTRIBUTION STATEMENT

In articles **A** and **B** I was the main contributor to the research presented in the publications. In these two articles, I prepared the greatest part of the original manuscript. All but one figures (i.e. Fig. 5 in Article **B**) were prepared by me. I was in duty of submitting these articles to respective journals and I was the corresponding author for them. I was responsible for editing the manuscripts in response to other authors' or reviewers' comments.

### **Article A**

In Article **A**, I was responsible for the analysis of the experimental data acquired from two external laboratories, namely from Hefei and Grenoble. I used the generalized spectroscopic cross-sections prepared by other co-authors to accurately simulate the line shape behavior and compare it with the aforementioned experimental data. I have simulated line-shape behavior when it is based on used potential energy surfaces which lead to a proof that the analysis can be used to validating the potentials. A large part of that work was a development of a software, that made getting the results possible. I was fully responsible for creating the code for the analysis and debugging it during the data curation. I was the main contributor for running the analysis with the code and optimizing it for experimental-data format.

### **Article B**

In Article **B**, I was also responsible for the analysis of the experimental data acquired from two external laboratories, namely from Hefei and Grenoble. I used the generalized spectroscopic cross-sections prepared by other co-authors to accurately simulate the line shape behavior and compare it with the aforementioned experimental data. In this work I was also responsible for simulating and analyzing the impact of each collisional parameter that was included in the analysis. This lead to a proof that the imaginary part of the complex Dicke parameter may has to be included in the analysis to properly describe the shape of the line. This work also consisted of creating the software for such need.



### **Article C**

In article **C**, I was responsible for analysis regarding comparison of Hartmann-Tran model vs billiard-ball line shape model which was the main part of the article's discussion. I have simulated the shapes of the line with billiard-ball model both with *ab initio* speed-dependence and with its quadratic approximation.

### **Article D**

In article **D**, I was responsible for developing the idea of the extending the correction introduced originally in [15] for self-perturbed samples to the wide mass-ratio range. I found and corrected the error introduced in [15] regarding the correction behavior in low- $\chi$  regime. I am a sole contributor for the software preparation used for the data simulation. I was responsible for debugging the software, preparing the original manuscript and preparing all but one figures to the article.

### **Article E**

In Article **E**, I was responsible for collecting the experimental data in few-week-long 24-hours-per-day experimental campaign in the CRDS laboratory in KL FAMO, Toruń. I was also responsible for the line-shape analysis with billiard-ball and  $\beta$ -corrected profiles, also by preparing and debugging part of the software that was used (with the main work done by M. Zaborowski). I contributed to writing and editing the manuscript.

### **Article F**

In article **F**, I was responsible for conducting a full line-shape analysis for two exemplar hydrogen transitions, concluded in Fig. 5. I calculated the *ab initio* speed dependencies for line-shape parameters, concluded in Fig. 4, from generalized cross-sections, presented in Fig. 2. All three figures were prepared by me. I was also responsible for debugging and correcting the database. The analysis for the exemplar analysis was done for two line-shape profiles, i.e. the  $\beta$ -corrected qSDHCP as a main result and an ordinary one as a reference and proof of  $\beta$  correction proper operation on experimental data as well as an encouragement to use it more widely. Database was prepared with respect to the  $\beta$ -corrected line-shape parameters.



## BIBLIOGRAPHY

- [1] N Allard and J Kielkopf. The effect of neutral nonresonant collisions on atomic spectral lines. *Rev Mod Phys*, 54(4):1103–1182, 1982. doi:10.1103/RevModPhys.54.1103.
- [2] J Szudy and WE Baylis. Profiles of line wings and rainbow satellites associated with optical and radiative collisions. *Phys Rep*, 266(3):127–227, 1996. doi:10.1016/0370-1573(95)00054-2.
- [3] R Ciuryło. Shapes of pressure- and doppler-broadened spectral lines in the core and near wings. *Phys Rev A*, 58(2):1029–1039, 1998. doi:10.1103/PhysRevA.58.1029.
- [4] RH Dicke. The effect of collisions upon the doppler width of spectral lines. *Phys Rev*, 89(2):472–473, 1953. doi:10.1103/PhysRev.89.472.
- [5] L Galatry. Simultaneous effect of Doppler and foreign gas broadening on spectral lines. *Phys Rev*, 122(4):1218–1223, 1961. doi:10.1103/physrev.122.1218.
- [6] M Nelkin and A Ghatak. Simple binary collision model for Van Hove's  $G_s(r, t)$ . *Phys Rev*, 135(1A):A4–A9, 1964. doi:10.1103/PhysRev.135.A4.
- [7] DA Shapiro, R Ciuryło, JR Drummond, and AD May. Solving the line-shape problem with speed-dependent broadening and shifting and with Dicke narrowing. I. Formalism. *Phys Rev A*, 65(1):012501, 2002. doi:10.1103/physreva.65.012501.
- [8] R Ciuryło, DA Shapiro, JR Drummond, and AD May. Solving the line-shape problem with speed-dependent broadening and shifting and with Dicke narrowing. II. Application. *Phys Rev A*, 65(1):012502, 2002. doi:10.1103/physreva.65.012502.
- [9] AS Pine. Asymmetries and correlations in speed-dependent Dicke-narrowed line shapes of argon-broadened HF. *J Quant Spectrosc Radiat Transf*, 62(4):397–423, 1999. doi:10.1016/s0022-4073(98)00112-5.



- [10] P Duggan, PM Sinclair, R Berman, AD May, and JR Drummond. Testing lineshape models: Measurements for  $v = 1-0$  CO broadened by He and Ar. *J Mol Spectrosc*, 186(1):90–98, 1997. doi:10.1006/jmsp.1997.7420.
- [11] NH Ngo, D Lisak, H Tran, and JM Hartmann. An isolated line-shape model to go beyond the Voigt profile in spectroscopic databases and radiative transfer codes. *J Quant Spectrosc Radiat Transf*, 129:89–100, 2013. doi:10.1016/j.jqsrt.2013.05.034.
- [12] S Hess. Kinetic theory of spectral line shapes. The transition between doppler broadening and collisional broadening. *Physica*, 61(1):80–94, 1972. doi:10.1016/0031-8914(72)90035-3.
- [13] GC Corey and FR McCourt. Dicke narrowing and collisional broadening of spectral lines in dilute molecular gases. *J Chem Phys*, 81(5):2318–2329, 1984. doi:10.1063/1.447930.
- [14] L Monchick and LW Hunter. Diatomic–diatomic molecular collision integrals for pressure broadening and Dicke narrowing: A generalization of Hess’s theory. *J Chem Phys*, 85(2):713–718, 1986. doi:10.1063/1.451277.
- [15] P Wcisło, IE Gordon, H Tran, Y Tan, SM Hu, A Campargue, S Kassi, D Romanini, C Hill, RV Kochanov, and LS Rothman. The implementation of non-voigt line profiles in the HITRAN database:  $H_2$  case study. *J Quant Spectrosc Radiat Transf*, 177:75–91, 2016. doi:10.1016/j.jqsrt.2016.01.024.
- [16] F Thibault, K Patkowski, PS Żuchowski, H Józwiak, R Ciuryło, and P Wcisło. Rovibrational line-shape parameters for  $H_2$  in He and new  $H_2$ -He potential energy surface. *J Quant Spectrosc Radiat Transf*, 202:308–320, 2017. doi:10.1016/j.jqsrt.2017.08.014.
- [17] BW Bakr, DGA Smith, and K Patkowski. Highly accurate potential energy surface for the He- $H_2$  dimer. *J Chem Phys*, 139(14):144305, 2013. doi:10.1063/1.4824299.
- [18] IE Gordon, LS Rothman, C Hill, RV Kochanov, Y Tan, PF Bernath, M Birk, V Boudon, A Campargue, KV Chance, BJ Drouin, JM Flaud, RR Gamache, JT Hodges, D Jacquemart, VI Perevalov, A Perrin, KP Shine, MAH



- Smith, J Tennyson, GC Toon, H Tran, VG Tyuterev, A Barbe, AG Császár, VM Devi, T Furtenbacher, JJ Harrison, JM Hartmann, A Jolly, TJ Johnson, T Karman, I Kleiner, AA Kyuberis, J Loos, OM Lyulin, ST Massie, SN Mikhailenko, N Moazzen-Ahmadi, HSP Müller, OV Naumenko, AV Nikitin, OL Polyansky, M Rey, M Rotger, SW Sharpe, K Sung, E Starikova, SA Tashkun, J Vander Auwera, G Wagner, J Wilzewski, P Wcisło, S Yu, and EJ Zak. The HITRAN2016 molecular spectroscopic database. *J Quant Spectrosc Radiat Transf*, 203:3–69, 2017. doi:<https://doi.org/10.1016/j.jqsrt.2017.06.038>.
- [19] K Bielska, J Domysławska, S Wójtewicz, A Balashov, M Słowiński, M Piwiński, A Cygan, R Ciuryło, and D Lisak. Simultaneous observation of speed dependence and Dicke narrowing for self-perturbed P-branch lines of O<sub>2</sub> B band. *J Quant Spectrosc Radiat Transf*, 276:107927, 2021. doi:[10.1016/j.jqsrt.2021.107927](https://doi.org/10.1016/j.jqsrt.2021.107927).
- [20] A Castrillo, E Fasci, and L Gianfrani. Doppler-limited precision spectroscopy of HD at 1.4 μm: An improved determination of the R(1) center frequency. *Phys Rev A*, 103(2):022828, 2021. doi:[10.1103/PhysRevA.103.022828](https://doi.org/10.1103/PhysRevA.103.022828).
- [21] H Fleurbaey, ZD Reed, EM Adkins, DA Long, and JT Hodges. High accuracy spectroscopic parameters of the 1.27 μm band of O<sub>2</sub> measured with comb-referenced, cavity ring-down spectroscopy. *J Quant Spectrosc Radiat Transf*, 270:107684, 2021. doi:[10.1016/j.jqsrt.2021.107684](https://doi.org/10.1016/j.jqsrt.2021.107684).
- [22] J Tennyson, PF Bernath, A Campargue, AG Császár, L Daumont, RR Gamache, JT Hodges, D Lisak, OV Naumenko, LS Rothman, H Tran, NF Zobov, J Buldyreva, CD Boone, MD De Vizia, L Gianfrani, JM Hartmann, R McPheat, D Weidmann, J Murray, NH Ngo, and OL Polyansky. Recommended isolated-line profile for representing high-resolution spectroscopic transitions (iupac technical report). *Pure Appl Chem*, 86(12):1931–1943, 2014. doi:[doi:10.1515/pac-2014-0208](https://doi.org/10.1515/pac-2014-0208).
- [23] R Wehr, R Ciuryło, A Vitcu, F Thibault, JR Drummond, and AD May. Dicke-narrowed spectral line shapes of CO in Ar: Experimental results and a revised interpretation. *J Mol Spectrosc*, 235(1):54–68, 2006. doi:[10.1016/j.jms.2005.10.009](https://doi.org/10.1016/j.jms.2005.10.009).



- [24] P Wcisło, F Thibault, H Cybulski, and R Ciuryło. Strong competition between velocity-changing and phase- or state-changing collisions in  $\text{h}_2$  spectra perturbed by Ar. *Phys Rev A*, 91:052505, 2015. doi:10.1103/PhysRevA.91.052505.
- [25] P Wcisło, F Thibault, M Zaborowski, S Wójtewicz, A Cygan, G Kowzan, P Masłowski, J Komasa, M Puchalski, K Pachucki, R Ciuryło, and D Lisak. Accurate deuterium spectroscopy for fundamental studies. *J Quant Spectrosc Radiat Transf*, 213:41–51, 2018. doi:10.1016/j.jqsrt.2018.04.011.
- [26] G Kowzan, H Cybulski, P Wcisło, M Słowiński, A Viel, P Masłowski, and F Thibault. Subpercent agreement between ab initio and experimental collision-induced line shapes of carbon monoxide perturbed by argon. *Phys Rev A*, 102(1):012821, 2020. doi:10.1103/PhysRevA.102.012821.
- [27] P Wcisło, A Cygan, D Lisak, and R Ciuryło. Iterative approach to line-shape calculations based on the transport-relaxation equation. *Phys Rev A*, 88(1):012517, 2013. doi:10.1103/physreva.88.012517.
- [28] RR Gamache and B Vispoel. On the temperature dependence of half-widths and line shifts for molecular transitions in the microwave and infrared regions. *J Quant Spectrosc Radiat Transf*, 217:440–452, 2018. doi:10.1016/j.jqsrt.2018.05.019.
- [29] N Stolarczyk, F Thibault, H Cybulski, H Józwiak, G Kowzan, B Vispoel, IE Gordon, LS Rothman, RR Gamache, and P Wcisło. Evaluation of different parameterizations of temperature dependences of the line-shape parameters based on ab initio calculations: Case study for the HITRAN database. *J Quant Spectrosc Radiat Transf*, 240:106676, 2020. doi:10.1016/j.jqsrt.2019.106676.

**H<sub>2</sub>-He collisions: *Ab initio* theory meets cavity-enhanced spectra**

Michał Słowiński <sup>1,\*</sup> Franck Thibault <sup>2</sup> Yan Tan,<sup>3</sup> Jin Wang,<sup>3</sup> An-Wen Liu,<sup>3</sup> Shui-Ming Hu <sup>3</sup>,  
Samir Kassi <sup>4</sup> Alain Campargue <sup>4</sup> Magdalena Konefał,<sup>1,4</sup> Hubert Jóźwiak <sup>1</sup> Konrad Patkowski <sup>5</sup>,  
Piotr Żuchowski <sup>1</sup> Roman Ciuryło <sup>1</sup> Daniel Lisak <sup>1</sup> and Piotr Wcisło <sup>1,†</sup>

<sup>1</sup>*Institute of Physics, Faculty of Physics, Astronomy and Informatics, Nicolaus Copernicus University in Toruń, Grudziadzka 5, 87-100 Toruń, Poland*

<sup>2</sup>*Univ Rennes, CNRS, Institut de Physique de Rennes, UMR 6251, F-35000 Rennes, France*

<sup>3</sup>*Hefei National Laboratory for Physical Sciences at Microscale, iChEM, University of Science and Technology of China, Hefei 230026 China*

<sup>4</sup>*University of Grenoble Alpes, CNRS, LIPhy, F-38000 Grenoble, France*

<sup>5</sup>*Department of Chemistry and Biochemistry, Auburn University, Auburn, Alabama 36849 USA*



(Received 4 January 2020; accepted 27 April 2020; published 22 May 2020)

Fully quantum *ab initio* calculations of the collision-induced shapes of two rovibrational H<sub>2</sub> lines perturbed by He provide an unprecedented subpercent agreement with ultra-accurate cavity-enhanced measurements. This level of consistency between theory and experiment hinges on a highly accurate potential energy surface and a realistic treatment of the velocity changing and dephasing collisions. In addition to the fundamental importance, these results show that *ab initio* calculations can provide reference data for spectroscopic studies of planet atmospheres at the required accuracy level and can be used to populate spectroscopic line-by-line databases.

DOI: [10.1103/PhysRevA.101.052705](https://doi.org/10.1103/PhysRevA.101.052705)

**I. INTRODUCTION**

Molecular hydrogen differs in many respects from most other diatomic molecules, revealing its nonclassical nature due to a large rotational constant ( $B = 60.853 \text{ cm}^{-1}$ ) [1]. The most straightforward example can be traced back to the early twentieth century, when the heat capacity of H<sub>2</sub> at low temperatures was discovered to dramatically diverge from the expected classical behavior [2]. The lack of inelastic channels in H<sub>2</sub> scattering, up to relatively high temperatures of a few hundred kelvin [3], results in many other atypical features observed in H<sub>2</sub> collision studies. In the particular case of the optically excited H<sub>2</sub> molecule, the lack of inelasticity causes the rate of optical excitation damping to be much smaller than the rate of velocity-changing collisions. This property results in strong collisional Dicke narrowing of the H<sub>2</sub> rovibrational lines [4,5]. Furthermore, the opening of the first inelastic channel leads to a strong dependence of the generalized spectroscopic cross section on the collision energy [3], which enhances the speed dependence of the line-shape parameters. Pronounced collisional effects make the molecular hydrogen well suited to study not only the potential energy surfaces (PESs) and quantum-scattering calculation methodology, but also the models describing the collision-perturbed velocity distribution of the optical coherence [3,6–9], which constitute a long-term development at the frontier of quantum optics, collision theory, and statistical physics [10,11].

Experimental studies on the interactions between two hydrogen molecules and between a hydrogen molecule and a noble gas atom have a several-decades-long history

[6,7,12–15]. Recently, the rotationally inelastic scattering of the HD molecule colliding with D<sub>2</sub> [16,17] and with He [18] at 1 K was observed in coexpanded supersonic beams and theoretically handled by Croft *et al.* [19]. The influence of the molecular hydrogen collisions, with perturbers such as H<sub>2</sub> isotopologues or noble gas atoms, on the shapes of the rotational and rovibrational lines in H<sub>2</sub> were already established in a wide range of temperatures, from 20 to 1200 K [20–26]. In particular, the effects of the H<sub>2</sub>-He collisions on the widths and shifts of H<sub>2</sub> rovibrational lines were subjected to intense experimental and theoretical studies [3,25,27–32]. However, the collision-perturbed line profiles calculated from first principles never reached agreement with experimental data at the subpercent level.

In this work, we report a full *ab initio* description of the collision-perturbed shapes of rovibrational lines for the simplest benchmark system, i.e., He-perturbed H<sub>2</sub>. We demonstrate agreement between measured and *ab initio* computed collision-perturbed shapes of molecular lines at the subpercent level: the root-mean-square difference (calculated within  $\pm$ FWHM) between experimental and theoretical profiles is smaller than one-hundredth of the profile amplitude. We merged all of the theoretical tools that are necessary to reach this agreement; i.e., we used the state-of-the-art statistical model of the collision-perturbed shape of molecular lines [33–36], we derived all parameters of this model from quantum scattering calculations [30,37–39], and we used the highly accurate *ab initio* PES [30,40], referred to as BSP3. We demonstrate that the fully *ab initio* calculations can provide reference spectra for atmospheric studies of solar system planets and exoplanets at the required metrological (subpercent) level of accuracy. Therefore, this approach is well suited for populating line-by-line spectroscopic databases such as HITRAN [41], GEISA [42], and ExoMol [43], including the

\*mslowinski@umk.pl

†piotr.wcislo@fizyka.umk.pl

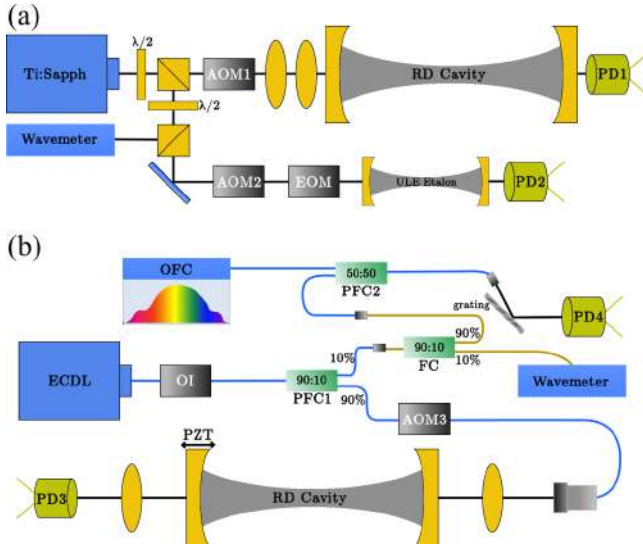


FIG. 1. Cavity ring-down spectrometers in (a) Hefei and (b) Grenoble laboratories. AOM, acousto-optic modulator; ECDL, external cavity diode laser; EOM, electro-optic modulator; FC, fiber coupler, OFC, optical frequency comb; OI, optical isolator, PD, photodiode, PFC, polarization fiber coupler; PZT, piezoelectric transducer; Ti:Sapph, Ti:sapphire laser.

recent advanced database structures [44] involving beyond-Voigt line-shape parameters and their wide ranges of temperature representations. We show that this approach can be used to experimentally test the quality of quantum-chemical calculations of the PESs [30,38,40,45,46].

## II. EXPERIMENTS

To validate our *ab initio* quantum scattering calculations, we performed measurements of the He-perturbed 3-0 S(1) H<sub>2</sub> line centered at 12 265.59 cm<sup>-1</sup> (815.33 nm) and the 2-0 Q(1) H<sub>2</sub> line centered at 8075.31 cm<sup>-1</sup> (1238.39 nm) using the experimental setups of Hefei [47] and Grenoble [48–51], respectively. Both setups, as shown in Fig. 1, are based on continuous-wave laser sources and high-finesse ring-down (RD) cavities. The two RD cavities are 1.0 and 1.4 m long, with finesse of 63 000 and 131 000, which results in effective path lengths of 20 and 59 km for the Hefei and Grenoble setups.

Acousto-optic modulators are used as optical switches to generate the RD events. The frequency of the Hefei laser source (Ti:sapphire) is set by a temperature-stabilized ( $\Delta T \approx 10$  mK at 302 K) ultralow-expansion etalon reaching 10-MHz accuracy (see Refs. [52] and [53]), whereas for the Grenoble setup the external cavity diode laser is referenced to the optical frequency comb reaching 300-kHz absolute accuracy (see Refs. [54–56]). The length of the Grenoble cavity is tunable with a piezoelectric actuator, which allows the spectra to be recorded on a much denser frequency grid. The temperatures of the cavities were controlled to within 1 and 0.15 K for the Hefei and Grenoble setups, respectively. For the 3-0 S(1) line, the H<sub>2</sub>/He mixing ratio spans between 33% and 10%, with 1% accuracy, while it has a constant value of 4.9(1)% for the 2-0 Q(1) line. The spectra were recorded at four pressures

ranging from 0.36 to 1.35 atm with an accuracy of 0.5% and signal-to-noise ratio up to 370 for the 3-0 S(1) line, as well as at nine pressures ranging from 0.07 to 1.05 atm with an accuracy of 0.15% and signal-to-noise ratio up to 2800 for the 2-0 Q(1) line.

## III. *AB INITIO* CALCULATION OF THE COLLISIONAL EFFECTS

Our line-shape calculations [34,35,57,58], originating from first principles, are based on the generalized Hess method (GHM) [37,59,60]. To better reproduce the physics of the velocity-changing collisions, we replace the commonly used hard-collision model [61,62], which is used in the GHM, with the model based on the Boltzmann operator for rigid-sphere approximation of the potential [9]. The latter model based on the isotropic part of the PES properly reproduces the dependence of the colliding partners on the mass ratio and describes the relation between velocities before and after collision [9], which is not the case for the simple hard-collision model. Moreover, we introduce the full speed dependence [63] of the collisional broadening and shift [60,64,65] into the GHM.

For the H<sub>2</sub>-He system, the PES is three-dimensional; i.e., it depends on the distance between the center of mass of the hydrogen molecule and the helium atom,  $R$ , the intramolecular distance,  $r$ , and the angle between the inter- and the intramolecular axes,  $\theta$ . To carry out the close-coupling quantum scattering calculations [66], the PES is projected on Legendre polynomials and averaged over the rovibrational wave functions of the hydrogen molecule [3,32]. The generalized spectroscopic cross sections,  $\sigma_\lambda^q$ , for the electric quadrupole lines considered here ( $q = 2$ ), as functions of the initial kinetic energy,  $E_{\text{KIN}}$ , are determined from  $S$ -matrix elements [32,60,64]. For the zero rank of the velocity tensor,  $\lambda = 0$ ,  $\sigma_\lambda^q$  reduces to the pressure broadening and shift cross sections (PBXS and PSXS, respectively) [3,65,67,68], while for  $\lambda = 1$  it provides the complex Dicke cross section [31,32,59,60,64] (RDXS and IDXS for its real and imaginary parts, respectively). The resulting cross sections are shown in Figs. 2(a)–2(d).

We use the generalized spectroscopic cross sections to calculate the corresponding line-shape parameters at a given temperature  $T$ , i.e., the speed-dependent pressure broadening,  $\Gamma(v)$ , and shift,  $\Delta(v)$  [63,69,70], as well as the complex Dicke parameter,  $\nu_{\text{opt}}$  [30,39,44,71,72],

$$\Gamma(v) + i\Delta(v) = \left(\frac{n}{2\pi c}\right) \frac{2\bar{v}_p^2}{v\sqrt{\pi}} \exp(-v^2/\bar{v}_p^2) \times \int_0^\infty x^2 e^{-x^2} \sinh(2vx/\bar{v}_p) \sigma_0^q(x\bar{v}_p) dx, \quad (1a)$$

$$\nu_{\text{opt}} = \left(\frac{n}{2\pi c}\right) \frac{m_p}{m + m_p} \int_0^\infty v_r f_m(v_r) \times \left[ \frac{2}{3} \frac{v_r^2}{\bar{v}_r^2} \sigma_1^q(v_r) - \sigma_0^q(v_r) \right] dv_r, \quad (1b)$$

where  $v$ ,  $v_p$ , and  $v_r$  are the speed of the active molecule, the speed of the perturber with the most probable value  $\bar{v}_p = \sqrt{2k_B T/m_p}$ , and their relative speed with mean value  $\bar{v}_r$ , respectively, and  $x = v_r/\bar{v}_p$ .  $m$ ,  $m_p$ , and  $\mu$  are the masses of the active molecule and perturber and their reduced mass, respec-

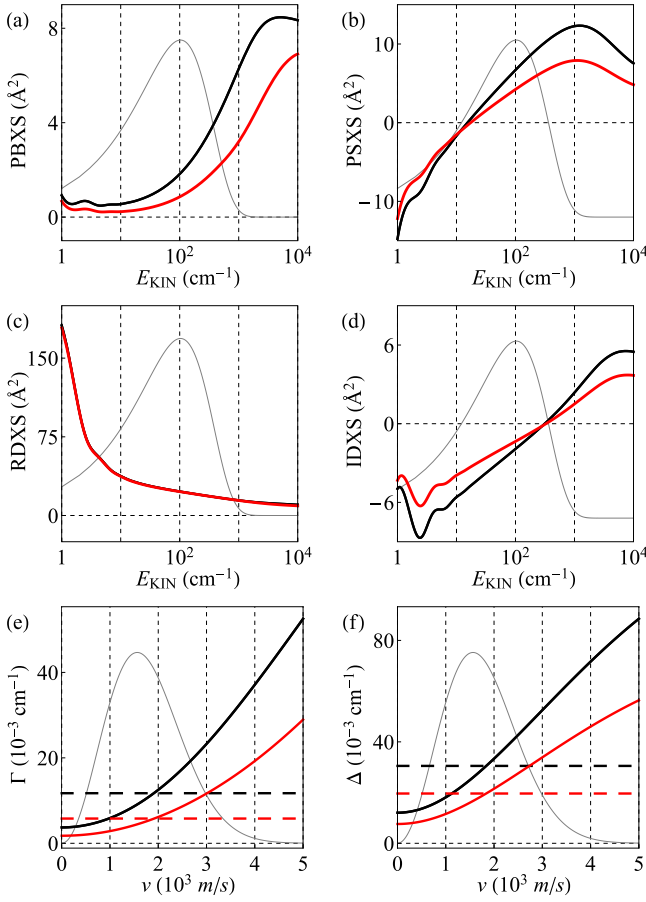


FIG. 2. (a–d) Generalized spectroscopic cross sections for the 3-0 S(1) and 2-0 Q(1) lines in helium-perturbed H<sub>2</sub>: see the respective black and red lines, respectively. PBXS, PSXS, RDXS, and IDXS are pressure broadening, pressure shift, and real and imaginary parts of complex Dicke cross sections, respectively. The two curves in (c) are overlapping. (e, f) *Ab initio* speed dependence of the line broadening,  $\Gamma$ , and shift,  $\Delta$  (same color notation), plotted for 1 amagat of He at the experimental temperatures. Black and red dashed lines are the speed-averaged collisional broadening,  $\Gamma_0$ , and shift,  $\Delta_0$ , respectively. The gray line is the Maxwell Boltzmann distribution at 296 K in arbitrary units (vertically shifted in (b) and (d)); the distribution of relative kinetic energy in (a)–(d) and the distribution of active molecule speed in (e) and (f).

tively.  $f_m(v)$  is the Maxwell-Boltzmann speed distribution,  $n$  is the number density of the perturber,  $k_B$  is the Boltzmann constant, and  $c$  is the speed of light. The *ab initio* speed-dependent broadenings and shifts are shown in Figs. 2(e) and 2(f). The calculated line-shape parameters are listed in Table I. We denote speed-averaged broadening and shift as  $\Gamma_0$  and  $\Delta_0$ , respectively: refer to the dashed horizontal lines in Figs. 2(e) and 2(f). Following Ref. [35], we introduce two parameters,  $\Gamma_{SD} = \frac{v_m}{2} \frac{d}{dv} \Gamma(v)|_{v=v_m}$  and  $\Delta_{SD} = \frac{v_m}{2} \frac{d}{dv} \Delta(v)|_{v=v_m}$ , that quantify the strength of the speed dependence of the broadening and shift, respectively, where  $v_m$  is the most probable active molecule speed. The  $\Gamma_{SD}/\Gamma_0$  and  $\Delta_{SD}/\Delta_0$  ratios, larger than 0.4, reveal extraordinarily pronounced speed dependence in the H<sub>2</sub> case; for typical atmospheric systems, these ratios are at the level of 0.1 [73–75].

TABLE I. Calculated values of the line-shape parameters for the 3-0 S(1) and 2-0 Q(1) H<sub>2</sub> lines. Calculations are performed at  $T = 296.6$  K for the 3-0 S(1) line and at  $T = 294.2$  K for the 2-0 Q(1) line. All parameters are given in units of 10<sup>-3</sup> cm<sup>-1</sup> for  $n = 1$  amagat.

Line	$\Gamma_0$	$\Delta_0$	$\Gamma_{SD}$	$\Delta_{SD}$	$v_{opt}^r$	$v_{opt}^i$
3-0 S(1)	11.72	30.51	5.40	12.42	37.96	-17.45
2-0 Q(1)	5.74	19.51	2.68	8.06	41.64	-11.31

We calculate the He-perturbed shapes of the H<sub>2</sub> lines by averaging the velocity distribution of the optical coherence [33,78,79]

$$I(\omega) = \frac{1}{\pi} \text{Re} \int d^3\vec{v} f_m(\vec{v}) h(\omega, \vec{v}). \quad (2)$$

$f_m(\vec{v})$  is the Maxwell-Boltzmann distribution of the active molecule velocity,  $\vec{v}$ , and  $f_m(\vec{v})h(\omega, \vec{v})$  is a scalar function proportional to the velocity distribution of the optical coherence. The  $h(\omega, \vec{v})$  function fulfills the transport-relaxation equation [33,79]

$$1 = -i(\omega - \omega_0 - \vec{k} \cdot \vec{v})h(\omega, \vec{v}) - \hat{S}^f h(\omega, \vec{v}), \quad (3)$$

where  $\omega$  and  $\omega_0$  are the angular frequencies of the electromagnetic radiation and the unperturbed frequency of the molecular transition, respectively,  $\vec{k}$  is the wave vector, and  $\hat{S}^f$  is the total collision operator describing relaxation and dephasing of the optical coherence as well as its flow between different velocity classes. This operator can be written as [34,35,57,58]

$$\hat{S}^f = -\Gamma(v) - i\Delta(v) + v_{opt} \hat{M}_{BB}^f, \quad (4)$$

where  $v_{opt} \hat{M}_{BB}^f$  is the velocity-changing operator for the rigid-sphere model of collisions [80,81]. By using the complex Dicke parameter derived from the GHM,  $v_{opt}$ , we introduce the correlations between internal and translational degrees of freedom to the velocity-changing operator. The ultimate collision operator used to compare *ab initio* calculations with experiment is the sum of two contributions [9]: the H<sub>2</sub>-He operator discussed here, Eq. (4), and the H<sub>2</sub>-H<sub>2</sub> operator taken from Ref. [82].

#### IV. EXPERIMENTAL VALIDATION OF THE QUANTUM SCATTERING CALCULATIONS AND TEST OF THE *AB INITIO* POTENTIALS

The direct comparison between theory and experiment is shown in Figs. 3(a) and 3(c). Despite the fact that none of the line-shape parameters were fitted, we achieved subpercent agreement between the simulated and the raw experimental profiles; i.e., the root-mean-square error of the *ab initio* model relative to the profile amplitude (rRMSE) calculated within  $\pm$ FWHM is smaller than 1%. The pressure-average values of the rRMSE are 0.99% and 0.33% for the 3-0 S(1) and 2-0 Q(1) lines, respectively. We do not know the reason why the discrepancy is larger for the 3-0 S(1) line (one possibility is a slight nonlinearity in the Hefei frequency axis; see Ref. [47]). The main conclusion of Fig. 3 is that the fully *ab initio* line-shape calculations, including not only the collisional

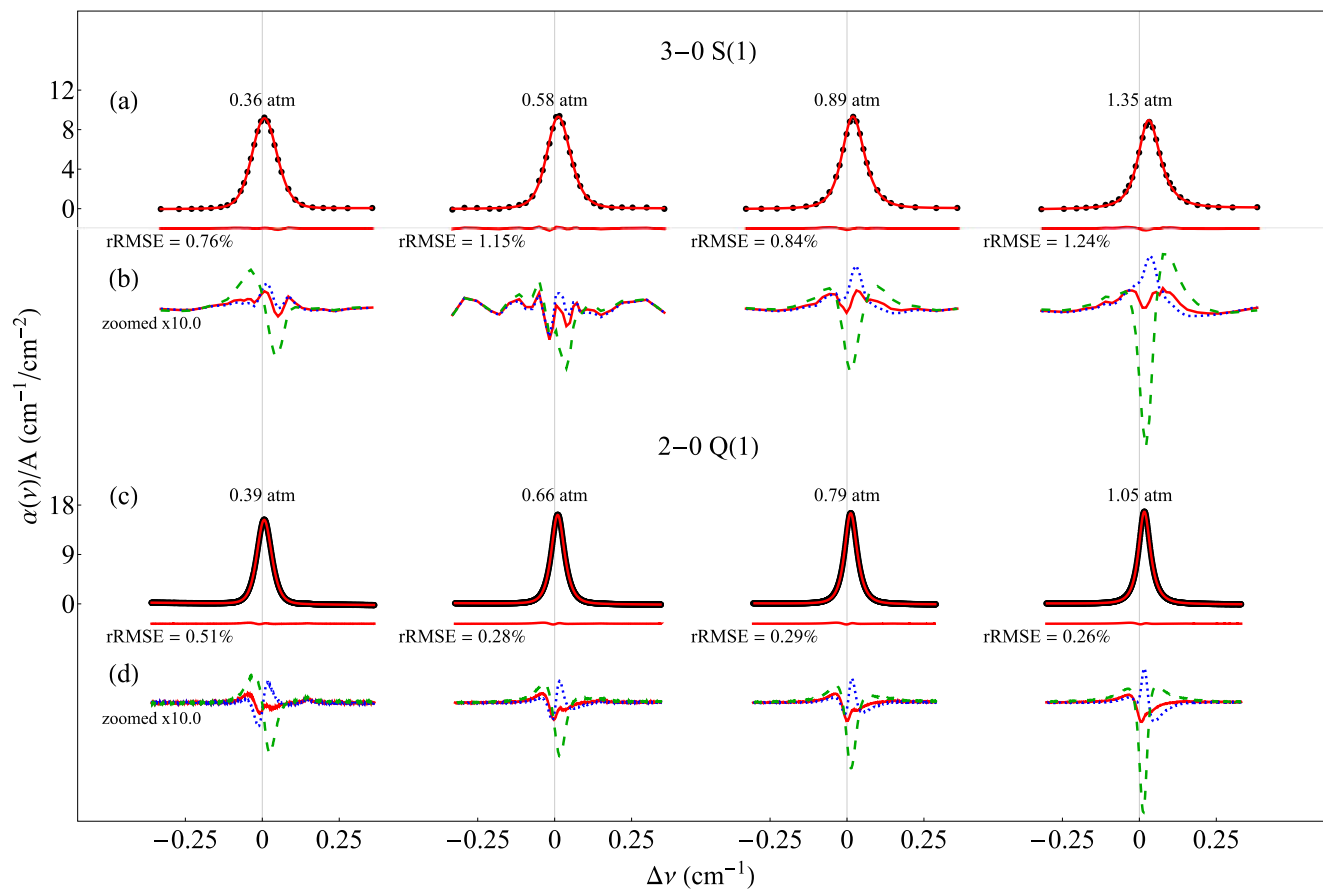


FIG. 3. (a, c) Comparison of the raw experimental spectra (black points) and the simulated line profiles (red lines). The absorption axis has been normalized to the area of the spectral line,  $A$ . Red lines under the line profiles represent the differences between experiment and theory. rRMSE values in the plots describe the root-mean-square errors relative to the profile amplitude. (b, d) Solid red, dotted blue, and dashed green lines are the zoomed residuals for the BSP3 [30,40], SK [38], and mMR [45,46] potentials, respectively. Vertical gray lines indicate the theoretical unperturbed line position [76,77]. The pressure shift is atypically large for  $H_2$  and, despite the small pressure range, is clearly visible; see the deviation of the line maximum from the vertical gray line.

perturbations of both internal and translational motions of molecules but also the correlations between them, are validated for highly accurate experimental spectra. In addition to the line-shape parameters, whose values are directly taken from our *ab initio* calculations, several other parameters (not related to the collisional effects) were fitted: the unperturbed line position frequency,  $\nu_0 = \omega_0/2\pi$ , the line intensity,  $S$ , and the background slope and baseline. The fitted values of  $\nu_0$  and  $S$  are consistent with the theoretical values [51,76,77] within the declared  $1\sigma$  uncertainties.

The  $H_2$  lines are considerably asymmetric due to collisional effects (the asymmetry is much stronger than in typical cases of atmosphere-relevant molecules with a much smaller rotational constant). We tested that if we neglect in our line-shape model the main source of the asymmetry, i.e., the speed dependence of the collisional shift, the residuals are approximately 10 times larger and have almost a purely asymmetric shape. Our *ab initio* line-shape model almost completely eliminates the strong asymmetry without fitting any line-shape parameter. The small remaining asymmetry that is seen in the residuals for the Q(1) 2-0 line is not caused by an incorrect value of the line position, which was fitted in

our analysis. It is difficult to uniquely identify the source of the remaining asymmetry. Although this paper reports the most accurate theoretical line shapes, we suspect that the source may still lie on the theory side.

The advantage of the method employed in this work is that it allows the absolute value of the collisional cross sections to be accurately tested experimentally, which is not the case for most other experimental techniques [16–18]. As an example, we consider the pressure-broadening cross section [PBXS in Fig. 2(a)], which gives the  $\Gamma_0$  parameter after thermal averaging: refer to the dashed horizontal lines in Fig. 2(e). At high pressures (at which the collisional broadening dominates), the relative error of  $\Gamma_0$  is approximately equal to the residual rRMSE. For instance, in the case of the 2-0 Q(1) line, rRMSE = 0.26% at the highest pressure corresponds to subpercent agreement between our *ab initio* and experimental values of  $\Gamma_0$ .

In addition to demonstrating that the full theoretical methodology can reproduce the collision-perturbed experimental profiles at an unprecedented level of accuracy, we show that this approach can serve as a link between high-precision spectroscopy and quantum chemical calculations,

thus enabling experimental tests of PESs in regions that are inaccessible with other techniques. In Figs. 3(b) and 3(d), we show the differences between the experimental and the theoretical profiles for three PESs: the Schaefer and Köhler (SK) PES [38], the modified Muchnik and Russek (mMR) PES [45,46], and the PES used in our main analysis, namely, the extended Bakr, Smith, and Patkowski (BSP3) [30,40]. Contrary to the main analysis, here we do not fit the line intensity but fix it to the theoretical value [51]. We do so because for the older, less accurate PESs [38,45,46] the fitted line intensities, to some extent, artificially compensate the inaccurate values of some of the line-shape parameters. This comparison clearly demonstrates that the best agreement with the experiment is achieved for the BSP3 PES. This result is consistent with our expectations, since the most recent BSP3 surface was calculated using the coupled-cluster method with single, double, and perturbative triple excitations [CCSD(T)], augmented by full configuration interaction corrections, with the relative uncertainty in the minimum estimated as 0.4% ( $\pm 0.045$  cm<sup>-1</sup>). Two other potentials studied here, SK and mMR, were obtained using much smaller Gaussian basis sets and lower levels of electronic structure theory. Moreover, the BSP3 PES involves the consistent treatment of a large range of intramolecular H-H distances and ensures a proper asymptotic behavior for large H<sub>2</sub>-He separations [30].

## V. CONCLUSION

We have demonstrated that the calculations from first principles are able to reproduce the experimental collision-perturbed molecular spectra at a subpercent-level accuracy. We used quantum scattering calculations to construct a collision operator that describes not only the dephasing and damping of the optical coherence, but also the flows of an optical coherence between different velocity classes. We solved a Boltzmann-like transport-relaxation equation to determine the velocity distribution of optical coherence and, hence, the collision-perturbed shapes of molecular lines. The calculations were validated on the highly accurate experimental spectra of the H<sub>2</sub> S(1) 3-0 and Q(1) 2-0 electric quadrupole transitions perturbed by helium. In addition to validating the theoretical methodology of accurate determi-

nation of the collision-induced shapes of molecular lines, we demonstrated that this approach can be used to test quantum-chemical calculations of the potential energy surfaces. This work demonstrates that theoretical calculations are capable of delivering line-shape parameters with the accuracy necessary to interpret experimental spectra for atmospheric, planetary, and astrophysical applications. With this approach, we show the possibility of calculating and validating beyond-Voigt line-shape parameters in order to populate line-by-line spectroscopic databases such as HITRAN [41], GEISA [42], and ExoMol [43] with requested accuracies in a wide temperature range for recent advanced database structures [44]. This approach is important for the lines relevant for atmospheric and astrophysical applications, especially for those which have not been accessed with laboratory experiments yet.

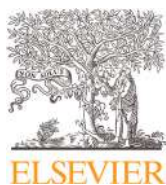
## ACKNOWLEDGMENTS

M.S.'s contribution was supported by Polish National Science Centre Project No. 2017/26/D/ST2/00371 and by the "A next-generation worldwide quantum sensor network with optical atomic clocks" project carried out within the TEAM IV Programme of the Foundation for Polish Science cofinanced by the European Union under the European Regional Development Fund. P.W. and H.J.'s contributions were supported by Polish National Science Centre Projects No. 2015/19/D/ST2/02195 and No. 2018/31/B/ST2/00720. S.-M.H. acknowledges support from the National Natural Science Foundation of China (21688102). S.K. and A.C. acknowledge funding support from the Agence Nationale de la Recherche (Equipex REFIMEVE+ANR-11-EQPX-0039). M.K. and D.L.'s contributions were supported by Polish National Science Centre Project No. 2015/18/E/ST2/00585. K.P. was supported by U.S. National Science Foundation CAREER award CHE-1351978. P.Ž.'s contribution was supported by Polish National Science Centre Project No. 2015/19/B/ST4/02707. The project was cofinanced by the Polish National Agency for Academic Exchange under the PHC Polonium program (dec. PPN/X/PS/318/2018). The research was part of the program of the National Laboratory FAMO in Toruń, Poland. It was also supported by the COST Grant No. CM1405 Action CM1405 MOLIM.

- 
- [1] G. Herzberg and L. L. Howe, *Can. J. Phys.* **37**, 636 (1959).
  - [2] A. Einstein and O. Stern, *Ann. Phys.* **40**, 551 (1913).
  - [3] F. Thibault, P. Wcisło, and R. Ciuryło, *Eur. Phys. J. D* **70**, 236 (2016).
  - [4] V. G. Cooper, A. D. May, E. H. Hara, and H. F. P. Knapp, *Can. J. Phys.* **46**, 2019 (1968).
  - [5] P. Wcisło, F. Thibault, H. Cybulski, and R. Ciuryło, *Phys. Rev. A* **91**, 052505 (2015).
  - [6] R. L. Farrow, L. A. Rahn, G. O. Sitz, and G. J. Rosasco, *Phys. Rev. Lett.* **63**, 746 (1989).
  - [7] F. Chaussard, X. Michaut, R. Saint-Loup, H. Berger, P. Joubert, B. Lance, J. Bonamy, and D. Robert, *J. Chem. Phys.* **112**, 158 (2000).
  - [8] H. Tran, F. Thibault, and J.-M. Hartmann, *J. Quant. Spectrosc. Radiat. Transf.* **112**, 1035 (2011).
  - [9] P. Wcisło, H. Tran, S. Kassi, A. Campargue, F. Thibault, and R. Ciuryło, *J. Chem. Phys.* **141**, 074301 (2014).
  - [10] S. G. Rautian and A. M. Shalagin, *Kinetic Problems of Non-linear Spectroscopy* (North-Holland, Amsterdam, 1991).
  - [11] F. R. W. McCourt, J. J. M. Beenakker, W. E. Köhler, and I. Kuscer, *Nonequilibrium Phenomena in Polyatomic Gases* (Clarendon, Oxford, UK, 1991).
  - [12] A. R. W. McKellar, *J. Chem. Phys.* **92**, 3261 (1990).
  - [13] A. R. W. McKellar and J. Schaefer, *J. Chem. Phys.* **95**, 3081 (1991).
  - [14] A. R. W. McKellar, *J. Chem. Phys.* **105**, 2628 (1996).

- [15] G. D. Sheldon, S. H. Fakh-Eslam, P. M. Sinclair, J. R. Drummond, and A. D. May, *Can. J. Phys.* **79**, 173 (2001).
- [16] W. E. Perreault, N. Mukherjee, and R. N. Zare, *Science* **358**, 356 (2017).
- [17] W. E. Perreault, N. Mukherjee, and R. N. Zare, *Nat. Chem.* **10**, 561 (2018).
- [18] W. E. Perreault, N. Mukherjee, and R. N. Zare, *J. Chem. Phys.* **150**, 174301 (2019).
- [19] J. F. E. Croft, N. Balakrishnan, M. Huang, and H. Guo, *Phys. Rev. Lett.* **121**, 113401 (2018).
- [20] K. V. D. Hout, P. Hermans, E. Mazur, and H. Knaap, *Physica A* **104**, 509 (1980).
- [21] S. L. Bragg, W. H. Smith, and J. W. Brault, *Astrophys. J.* **263**, 999 (1982).
- [22] W. K. Bischel and M. J. Dyer, *Phys. Rev. A* **33**, 3113 (1986).
- [23] L. A. Rahn and G. J. Rosasco, *Phys. Rev. A* **41**, 3698 (1990).
- [24] L. A. Rahn, R. L. Farrow, and G. J. Rosasco, *Phys. Rev. A* **43**, 6075 (1991).
- [25] J. W. Forsman, J. Bonamy, D. Robert, J. P. Berger, R. Saint-Loup, and H. Berger, *Phys. Rev. A* **52**, 2652 (1995).
- [26] P. M. Sinclair, J. P. Berger, X. Michaut, R. Saint-Loup, R. Chaux, H. Berger, J. Bonamy, and D. Robert, *Phys. Rev. A* **54**, 402 (1996).
- [27] P. Hermans, A. V. Die, H. Knaap, and J. Beenakker, *Physica A* **132**, 233 (1985).
- [28] R. Blackmore, S. Green, and L. Monchick, *J. Chem. Phys.* **91**, 3846 (1989).
- [29] X. Michaut, R. Saint-Loup, H. Berger, M. L. Dubernet, P. Joubert, and J. Bonamy, *J. Chem. Phys.* **109**, 951 (1998).
- [30] F. Thibault, K. Patkowski, P. S. Żuchowski, H. Józwiak, R. Ciuryło, and P. Wcisło, *J. Quant. Spectrosc. Radiat. Transf.* **202**, 308 (2017).
- [31] R. Z. Martínez, D. Bermejo, F. Thibault, and P. Wcisło, *J. Raman Spectrosc.* **49**, 1339 (2018).
- [32] H. Józwiak, F. Thibault, N. Stolarczyk, and P. Wcisło, *J. Quant. Spectrosc. Radiat. Transf.* **219**, 313 (2018).
- [33] R. Blackmore, *J. Chem. Phys.* **87**, 791 (1987).
- [34] R. Ciuryło, D. A. Shapiro, J. R. Drummond, and A. D. May, *Phys. Rev. A* **65**, 012502 (2002).
- [35] P. Wcisło, F. Thibault, M. Zaborowski, S. Wójtewicz, A. Cygan, G. Kowzan, P. Masłowski, J. Komasa, M. Puchalski, K. Pachucki, R. Ciuryło, and D. Lisak, *J. Quant. Spectrosc. Radiat. Transf.* **213**, 41 (2018).
- [36] A. May, W.-K. Liu, F. McCourt, R. Ciuryło, J. S.-F. Stoker, D. Shapiro, and R. Wehr, *Can. J. Phys.* **91**, 879 (2013).
- [37] S. Hess, *Physica* **61**, 80 (1972).
- [38] J. Schaefer and W. Köhler, *Physica A* **129**, 469 (1985).
- [39] L. Demeio, S. Green, and L. Monchick, *J. Chem. Phys.* **102**, 9160 (1995).
- [40] B. W. Bakr, D. G. A. Smith, and K. Patkowski, *J. Chem. Phys.* **139**, 144305 (2013).
- [41] I. E. Gordon, L. S. Rothman, C. Hill, R. V. Kochanov, Y. Tan, P. F. Bernath, M. Birk, V. Boudon, A. Campargue, K. V. Chance, B. J. Drouin, J.-M. Flaud, R. R. Gamache, J. T. Hodges, D. Jacquemart, V. I. Perevalov, A. Perrin, K. P. Shine, M.-A. H. Smith, J. Tennyson, G. C. Toon, H. Tran, V. G. Tyuterev, A. Barbe, A. G. Császár, V. M. Devi, T. Furtenbacher, J. J. Harrison, J.-M. Hartmann, A. Jolly, T. J. Johnson, T. Karman, I. Kleiner, A. A. Kyuberis, J. Loos, O. M. Lyulin, S. T. Massie, S. N. Mikhailenko, N. Moazzen-Ahmadi, H. S. P. Müller, O. V. Naumenko, A. V. Nikitin, O. L. Polyansky, M. Rey, M. Rotger, S. W. Sharpe, K. Sung, E. Starikova, S. A. Tashkun, J. V. Auwera, G. Wagner, J. Wilzewski, P. Wcisło, S. Yu, and E. Zak, *J. Quant. Spectrosc. Radiat. Transf.* **203**, 3 (2017).
- [42] N. Jacquinet-Husson, R. Armante, N. Scott, A. Chédin, L. Crépeau, C. Boutammine, A. Bouhdaoui, C. Crevoisier, V. Capelle, C. Boone, N. Poulet-Crovisier, A. Barbe, D. C. Benner, V. Boudon, L. Brown, J. Buldyreva, A. Campargue, L. Coudert, V. Devi, M. Down, B. Drouin, A. Fayt, C. Fittschen, J.-M. Flaud, R. Gamache, J. Harrison, C. Hill, Ø. Hodnebrog, S.-M. Hu, D. Jacquemart, A. Jolly, E. Jiménez, N. Lavrentieva, A.-W. Liu, L. Lodi, O. Lyulin, S. Massie, S. Mikhailenko, H. Müller, O. Naumenko, A. Nikitin, C. Nielsen, J. Orphal, V. Perevalov, A. Perrin, E. Polovtseva, A. Predoi-Cross, M. Rotger, A. Ruth, S. Yu, K. Sung, S. Tashkun, J. Tennyson, V. Tyuterev, J. V. Auwera, B. Voronin, and A. Makie, *J. Mol. Spectrosc.* **327**, 31 (2016).
- [43] J. Tennyson, S. N. Yurchenko, A. F. Al-Refaie, E. J. Barton, K. L. Chubb, P. A. Coles, S. Diamantopoulou, M. N. Gorman, C. Hill, A. Z. Lam, L. Lodi, L. K. McKemish, Y. Na, A. Owens, O. L. Polyansky, T. Rivlin, C. Sousa-Silva, D. S. Underwood, A. Yachmenev, and E. Žak, *J. Mol. Spectrosc.* **327**, 73 (2016).
- [44] N. Stolarczyk, F. Thibault, H. Cybulski, H. Józwiak, G. Kowzan, B. Vispoel, I. Gordon, L. Rothman, R. Gamache, and P. Wcisło, *J. Quant. Spectrosc. Radiat. Transf.* **240**, 106676 (2020).
- [45] A. I. Boothroyd, P. G. Martin, and M. R. Peterson, *J. Chem. Phys.* **119**, 3187 (2003).
- [46] P. Muchnick and A. Russek, *J. Chem. Phys.* **100**, 4336 (1994).
- [47] Y. Tan, J. Wang, C.-F. Cheng, X.-Q. Zhao, A.-W. Liu, and S.-M. Hu, *J. Mol. Spectrosc.* **300**, 60 (2014).
- [48] D. Romanini, A. Kachanov, N. Sadeghi, and F. Stoeckel, *Chem. Phys. Lett.* **264**, 316 (1997).
- [49] P. Macko, D. Romanini, S. Mikhailenko, O. Naumenko, S. Kassi, A. Jenouvrier, V. Tyuterev, and A. Campargue, *J. Mol. Spectrosc.* **227**, 90 (2004).
- [50] S. Kassi and A. Campargue, *J. Chem. Phys.* **137**, 234201 (2012).
- [51] A. Campargue, S. Kassi, K. Pachucki, and J. Komasa, *Phys. Chem. Chem. Phys.* **14**, 802 (2012).
- [52] C.-F. Cheng, Y. R. Sun, H. Pan, J. Wang, A.-W. Liu, A. Campargue, and S.-M. Hu, *Phys. Rev. A* **85**, 024501 (2012).
- [53] C.-F. Cheng, Y. R. Sun, H. Pan, Y. Lu, X.-F. Li, J. Wang, A.-W. Liu, and S.-M. Hu, *Opt. Express* **20**, 9956 (2012).
- [54] D. Mondelain, S. Kassi, T. Sala, D. Romanini, D. Gatti, and A. Campargue, *J. Mol. Spectrosc.* **326**, 5 (2016).
- [55] D. Mondelain, S. Mikhailenko, E. Karlovets, S. Béguier, S. Kassi, and A. Campargue, *J. Quant. Spectrosc. Radiat. Transf.* **203**, 206 (2017).
- [56] S. Mikhailenko, D. Mondelain, E. Karlovets, S. Kassi, and A. Campargue, *J. Quant. Spectrosc. Radiat. Transf.* **206**, 163 (2018).
- [57] R. Ciuryło, A. Bielski, J. R. Drummond, D. Lisak, A. D. May, A. S. Pine, D. A. Shapiro, J. Szudy, and R. S. Trawiński, in *AIP Conf. Proc.* (American Institute of Physics, College Park, MD, 2002).
- [58] D. Lisak, J. T. Hodges, and R. Ciuryło, *Phys. Rev. A* **73**, 012507 (2006).
- [59] G. C. Corey and F. R. McCourt, *J. Chem. Phys.* **81**, 2318 (1984).

- [60] L. Monchick and L. W. Hunter, *J. Chem. Phys.* **85**, 713 (1986).
- [61] M. Nelkin and A. Ghatak, *Phys. Rev.* **135**, A4 (1964).
- [62] S. G. Rautian and I. I. Sobelman, *Sov. Phys. Usp.* **9**, 701 (1967).
- [63] P. R. Berman, *J. Quant. Spectrosc. Radiat. Transf.* **12**, 1331 (1972).
- [64] J. Schaefer and L. Monchick, *J. Chem. Phys.* **87**, 171 (1987).
- [65] R. Shafer and R. G. Gordon, *J. Chem. Phys.* **58**, 5422 (1973).
- [66] J. M. Hutson and S. Green, MOLSCAT computer code, version 14, distributed by Collaborative Computational Project No. 6 of the UK Science and Engineering Research Council (1994).
- [67] A. Ben-Reuven, *Phys. Rev.* **141**, 34 (1966).
- [68] A. Ben-Reuven, *Phys. Rev.* **145**, 7 (1966).
- [69] H. M. Pickett, *J. Chem. Phys.* **73**, 6090 (1980).
- [70] A. Pine, *J. Quant. Spectrosc. Radiat. Transf.* **62**, 397 (1999).
- [71] J. Schaefer and L. Monchick, *Astron. Astrophys.* **265**, 859 (1992).
- [72] G. Kowzan, P. Wcisło, M. Słowiński, P. Masłowski, A. Viel, and F. Thibault, *J. Quant. Spectrosc. Radiat. Transf.* **243**, 106803 (2020).
- [73] M. Ghysels, Q. Liu, A. J. Fleisher, and J. T. Hodges, *Appl. Phys. B* **123**, 124 (2017).
- [74] M. Konefał, S. Kassı, D. Mondelain, and A. Campargue, *J. Quant. Spectrosc. Radiat. Transf.* **241**, 106653 (2020).
- [75] J. Domysławska, S. Wójtewicz, P. Masłowski, K. Bielska, A. Cygan, M. Słowiński, R. S. Trawiński, R. Ciuryło, and D. Lisak, *J. Quant. Spectrosc. Radiat. Transf.* **242**, 106789 (2020).
- [76] J. Komasa, K. Piszczatowski, G. Łach, M. Przybytek, B. Jeziorski, and K. Pachucki, *J. Chem. Theory Comput.* **7**, 3105 (2011).
- [77] P. Czachorowski, M. Puchalski, J. Komasa, and K. Pachucki, *Phys. Rev. A* **98**, 052506 (2018).
- [78] A. D. May, *Phys. Rev. A* **59**, 3495 (1999).
- [79] D. A. Shapiro, R. Ciuryło, J. R. Drummond, and A. D. May, *Phys. Rev. A* **65**, 012501 (2002).
- [80] M. J. Lindenfeld, *J. Chem. Phys.* **73**, 5817 (1980).
- [81] P. F. Liao, J. E. Bjorkholm, and P. R. Berman, *Phys. Rev. A* **21**, 1927 (1980).
- [82] P. Wcisło, I. E. Gordon, H. Tran, Y. Tan, S.-M. Hu, A. Campargue, S. Kassı, D. Romanini, C. Hill, R. V. Kochanov, and L. S. Rothman, *J. Quant. Spectrosc. Radiat. Transf.* **177**, 75 (2016).



## Collisional line-shape effects in accurate He-perturbed H<sub>2</sub> spectra

Michał Słowiński<sup>a,\*</sup>, Hubert Józwiak<sup>a</sup>, Maciej Gancewski<sup>a</sup>, Kamil Stankiewicz<sup>a</sup>,  
Nikodem Stolarczyk<sup>a</sup>, Yan Tan<sup>b</sup>, Jin Wang<sup>b</sup>, An-Wen Liu<sup>b</sup>, Shui-Ming Hu<sup>b</sup>, Samir Kassi<sup>c</sup>,  
Alain Campargue<sup>c</sup>, Konrad Patkowski<sup>d</sup>, Piotr S. Żuchowski<sup>a</sup>, Roman Ciuryło<sup>a</sup>,  
Franck Thibault<sup>e</sup>, Piotr Wcisło<sup>a</sup>

<sup>a</sup> Institute of Physics, Faculty of Physics, Astronomy and Informatics, Nicolaus Copernicus University in Toruń, Grudziadzka 5, Toruń 87-100, Poland

<sup>b</sup> Hefei National Laboratory for Physical Sciences at Microscale, iChEM, University of Science and Technology of China, Hefei, 230026 China

<sup>c</sup> University of Grenoble Alpes, CNRS, LIPhy, Grenoble F-38000, France

<sup>d</sup> Department of Chemistry and Biochemistry, Auburn University, Auburn, AL 36849 USA

<sup>e</sup> Univ Rennes, CNRS, IPR (Institut de Physique de Rennes) - UMR 6251, Rennes F-35000, France



### ARTICLE INFO

#### Article history:

Received 26 March 2021

Revised 21 September 2021

Accepted 21 September 2021

Available online 23 September 2021

#### Keywords:

*ab initio* quantum-scattering Calculations

Molecular hydrogen

Spectral line shape

Collisional line-shape effects

### ABSTRACT

We investigate collisional line-shape effects that are present in highly accurate experimental spectra of the 3-0 S(1) and 2-0 Q(1) molecular hydrogen absorption lines perturbed by helium. We clearly distinguish the influence of six different collisional effects (i.e.: collisional broadening and shift, their speed dependencies and the complex Dicke effect) on the shapes of H<sub>2</sub> lines. We demonstrate that only a very specific combination of these six contributions, determined from our *ab initio* calculations, gives unprecedentedly good agreement with experimental spectra. If any of the six contributions is neglected, then the experiment-theory comparison deteriorates at least several times. We also analyze the influence of the centrifugal distortion on our *ab initio* calculations and we demonstrate that the inclusion of this effect slightly improves the agreement with the experimental spectra.

© 2021 The Author(s). Published by Elsevier Ltd.

This is an open access article under the CC BY-NC-ND license

(<http://creativecommons.org/licenses/by-nc-nd/4.0/>)

### 1. Introduction

Hydrogen molecule, which is the simplest neutral chemically bound system, colliding with a helium atom constitutes a benchmark system well suited for testing and validating [1] the *ab initio* quantum chemical calculations of potential energy surfaces (PESs) [2,3]. The way the collisional effects are manifested in rovibrational spectra is particularly interesting in the case of the H<sub>2</sub> molecule. Due to a large rotational constant [4] and the lack of low-temperature inelastic channels in H<sub>2</sub> scattering [5], the nontrivial beyond-Voigt collisional line-shape effects are atypically strong [6], which makes it a perfect system for testing the collision-induced line-shape effects together with the quantum-scattering calculations associated with them.

Recently, low-temperature experiments with coexpanded supersonic beams allowed to measure rotationally inelastic scattering of the HD molecule colliding with D<sub>2</sub> [7,8] and with He [9]. The in-

fluence of collisions of H<sub>2</sub> isotopologues or noble gas atoms with a hydrogen molecule on the shapes of the H<sub>2</sub> lines was studied in a wide temperature range, spanning from 20 to 1200 K [10–17]. In particular, the widths and shifts of the H<sub>2</sub> rovibrational lines affected by the H<sub>2</sub>-He collisions were subjected to intense theoretical and experimental studies [3,5,15,18–26]. Recently, the *ab initio* calculations carried out for two rovibrational lines of molecular hydrogen achieved a subpercent agreement with experimental spectra [1].

In this work, we investigate the shapes of two molecular hydrogen absorption lines perturbed by helium. We clearly distinguish the influence of six different collisional effects (i.e.: collisional broadening and shift, speed dependence of the broadening and the shift, and real and imaginary Dicke effect) on the shapes of H<sub>2</sub> lines. We demonstrate that only a specific combination of these six contributions, as resulting from our *ab initio* calculations, gives unprecedentedly good agreement with experimental spectra (0.87% for the 3-0 S(1) line and 0.33% for the 2-0 Q(1) line). Additionally, we extend the previous analysis [1] by introducing into our quantum-scattering calculations the impact of the centrifugal distortion (CD) on the H<sub>2</sub>-He interaction. We note that the CD is

\* Corresponding author.

E-mail addresses: [mslowinski@umk.pl](mailto:mslowinski@umk.pl) (M. Słowiński), [piotr.wcislo@umk.pl](mailto:piotr.wcislo@umk.pl) (P. Wcisło).

introduced into our quantum-scattering calculations in a twofold manner. First, CD influences the calculations of the structure of the H<sub>2</sub> molecule, i.e. the energies of the rovibrational levels. This effect was already taken into account in all our previous analyses of the He-perturbed hydrogen lines [1,3,5,21–23,26]. In fact, we used the energy levels of H<sub>2</sub> reported in Ref. [27]. Second, CD influences the H<sub>2</sub>-He interaction calculated from the PES for a given rovibrational state of H<sub>2</sub>. This is because as the H<sub>2</sub> molecule rotates, its rovibrational wave function,  $\chi_{vj}(r_{HH})$ , is slightly stretched. Thus, the full H<sub>2</sub>-He PES should be averaged over wave functions which include this stretching (see Section 4 for details). In this paper, while referring to CD, we refer to the second meaning of those stated above. In the previous works it was pointed out that CD can be crucial for purely rotational lines [5]. Here, we demonstrate that while for the 2-0 Q(1) line, CD does not impact the line-shape parameters significantly, it influences the line-shape parameters of the 3-0 S(1) line at the 6% level and, hence, cannot be neglected in the interpretation of highly accurate experimental spectra.

Besides its importance for studying molecular interactions and collisions, accurate determination of the collisional line-shape parameters is important for astrophysical research. Spectroscopic studies of the atmospheres of giant planets need an accurate determination of pressure broadening and shift for electric-quadrupole H<sub>2</sub> lines [28–31]. Higher H<sub>2</sub> overtones are also used to study the atmospheres of giant planets [32,33], where beyond-Voigt line-shape parameters were proven to be necessary to interpret the measured spectra.

## 2. Line shape description

Our line-shape calculations [1,34–37] are based on the generalized Hess method (GHM) [38–40]. Instead of fitting, we calculate the line-shape parameters, namely the speed-dependent pressure broadening,  $\Gamma(v)$ , and shift,  $\Delta(v)$  [41–43], along with the complex Dicke parameter,  $\nu_{\text{opt}}$  [3,44–48], directly from the generalized spectroscopic cross sections

$$\Gamma(v) + i\Delta(v) = \left( \frac{n_p}{2\pi c} \right) \frac{2\tilde{v}_p^2}{v\sqrt{\pi}} \exp(-v^2/\tilde{v}_p^2) \times \int_0^\infty x^2 e^{-x^2} \sinh(2vx/\tilde{v}_p) \sigma_0^q(x\tilde{v}_p) dx, \quad (1a)$$

$$\nu_{\text{opt}} = \left( \frac{n_p}{2\pi c} \right) \frac{m_p}{m + m_p} \int_0^\infty v_r f_m(v_r) \times \left[ \frac{2}{3} \frac{v_r^2}{\tilde{v}_r^2} \sigma_1^q(v_r) - \sigma_0^q(v_r) \right] dv_r, \quad (1b)$$

where  $n_p$  is the number density of the perturber,  $c$  is the speed of light,  $v_p$ ,  $v$  and  $v_r$  are the speed of the perturber with the most probable value  $\tilde{v}_p$ , the speed of the active molecule and their relative speed with mean value  $\tilde{v}_r$ , respectively, with  $x = v_r/\tilde{v}_p$ .  $m_p$  and  $m$  are the masses of the perturber and the active molecule, respectively, and  $f_m(v)$  is the Maxwell-Boltzmann speed distribution. The cross sections,  $\sigma_\epsilon^q(v)$ , are determined from the S-matrices that are obtained, from the binary impact approximation, from the quantum-scattering calculations [22], which are performed on the state-of-the-art H<sub>2</sub>-He PES, i.e. extended Bakr, Smith and Patkowski potential (BSP3) [2,3]. The  $q$  superscript denotes the tensorial rank of radiation-matter interaction, which describes the type of a spectroscopic transition. In absorption spectroscopy,  $q = 1$  corresponds to electric dipole transitions and  $q = 2$  corresponds to the electric quadrupole transitions considered here. In the case of Raman spectroscopy,  $q = 0$  describes isotropic Q lines, while  $q = 2$  corresponds

to anisotropic transitions.  $\epsilon$  denotes the rank of the velocity tensor. For  $\epsilon = 0$ , the real and imaginary part of  $\sigma_\epsilon^q(v)$  are referred to as the pressure broadening and pressure shift cross sections, respectively [49–51], which describe the damping and dephasing of the optical coherence. For  $\epsilon = 1$  the  $\sigma_\epsilon^q(v)$  provides the complex Dicke cross section [39,40,52], the real part of which describes the flow of the optical coherence between different velocity classes. The imaginary part of  $\sigma_{\epsilon=1}^q(v)$  describes the phase changing of the optical coherence during velocity-changing collisions. We note that the cross sections,  $\sigma_\epsilon^q(v)$ , include the contribution from the inelastic scattering of the diatomic molecule and the dephasing part, which involves both the reorienting collisions (induced by the anisotropic part of the PES) and purely phase-changing collisions [5].

The isolated absorption line can be described in terms of the transport-relaxation equation [53]

$$1 = -i(\omega - \omega_0 - \mathbf{k} \cdot \mathbf{v})h(\omega, \mathbf{v}) - \hat{S}^f h(\omega, \mathbf{v}), \quad (2)$$

where  $\omega$  and  $\omega_0$  are the laser frequency and the unperturbed line position, respectively,  $\mathbf{k}$  is the wave vector,  $\hat{S}^f$  is the collision operator,  $f_m(\mathbf{v})$  is the Maxwell velocity distribution of the active molecule velocity,  $\mathbf{v}$ , and  $f_m(\mathbf{v})h(\omega, \mathbf{v})$  is a scalar function proportional to the velocity distribution of the optical coherence. The shape of molecular line is calculated as [53]

$$I(\omega) = \frac{1}{\pi} \Re \int d^3\mathbf{v} f_m(\mathbf{v})h(\omega, \mathbf{v}). \quad (3)$$

The velocity distribution of the optical coherence arises as an interplay between two competing processes. On one hand, the laser light induces the optical excitation within some velocity classes. On the other, collisions change both the internal state of the molecule and its velocity [54–56]. These effects can be incorporated into the collision operator as a sum of the broadening and shift and a velocity-changing operator

$$\hat{S}^f = -(\Gamma_0 + i\Delta_0) - (\Gamma_{\text{SD}}b_\gamma(v) + i\Delta_{\text{SD}}b_\delta(v)) + (v_{\text{opt}}^r + iv_{\text{opt}}^i)\hat{M}_\xi^f, \quad (4)$$

where  $\Gamma_0$  and  $\Delta_0$  are the speed-averaged broadening and shift,  $\Gamma_{\text{SD}}$  and  $\Delta_{\text{SD}}$  are the parameters describing the magnitude of the speed-dependence of broadening and shift of the line with  $b_\gamma$  and  $b_\delta$  describing their shape [35],  $v_{\text{opt}}^r$  and  $v_{\text{opt}}^i$  are the real and imaginary part of  $\nu_{\text{opt}}$ , respectively. Finally,  $\nu_{\text{opt}}\hat{M}_\xi^f$  is the velocity-changing operator [53,57,58] within a given  $\xi$  model of collisions

$$\nu_{\text{opt}}\hat{M}_\xi^f h(\omega, \mathbf{v}) = \int [f_\xi(\mathbf{v} \leftarrow \mathbf{v}') - f_\xi(\mathbf{v}' \leftarrow \mathbf{v})]h(\omega, \mathbf{v}')d\mathbf{v}', \quad (5)$$

where  $f_\xi$  is the collision kernel. We note here that the complex Dicke parameter,  $\nu_{\text{opt}}$ , involves correlation between the internal and translational degrees of freedom [3,39,40,45]. In the original formulation of the GHM, this operator is a simple hard-collision (HC) operator [44,59] whose collision kernel depends only on the Maxwell velocity distribution [60]

$$f_{\text{HC}}(\mathbf{v} \leftarrow \mathbf{v}') = \nu_{\text{opt}}f_m(\mathbf{v}). \quad (6)$$

In this work, we replace the HC collision kernel with the more physically-justified billiard-ball (BB) model [54,57,58], in which the collision kernel takes into account not only the speed after the collision,  $v$ , but also the speed before the collision,  $v'$ , the angle  $\phi$  between aforementioned velocities and the perturber-absorber mass ratio,  $\alpha$ . The BB collision kernel can be expressed as

$$f_{\text{BB}}(\mathbf{v} \leftarrow \mathbf{v}') = \nu_{\text{opt}} \frac{1}{v_m^2} \frac{3}{32\pi} \frac{(1+\alpha)^{5/2}}{\alpha^2} \frac{1}{\sqrt{v^2 - 2vv' \cos(\phi) + v'^2}} \times \exp\left(-\frac{(1-\alpha)^2 v^2}{4\alpha v_m^2} - \frac{(1+\alpha)(1-\alpha)vv'}{2\alpha v_m^2} \cos(\phi)\right) +$$

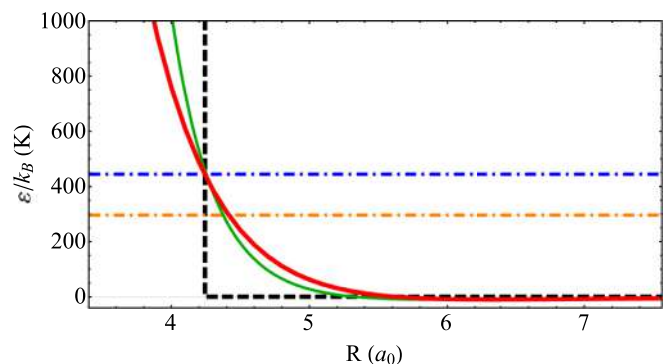


**Fig. 1.** Isotropic part of the BSP3 PES for colliding H<sub>2</sub>-He (red thick solid line) as a function of relative distance,  $R$ . The hard-sphere potential (black dashed line) was constructed so it intersects the *ab initio* potential curve at the mean collisional energy ( $\varepsilon/k_B=444$  K). Green solid line is the Lennard-Jones potential fitted to the isotropic part of the BSP3 PES. Mean collision energy and energy corresponding to the temperature  $T$  are indicated as the blue (upper) and orange (lower) dot-dashed lines respectively. The mean hard-sphere diameter  $d_{\text{H}_2\text{-He}} = 4.24$  a<sub>0</sub> at 296 K.

$$+ \frac{\alpha v^2 v'^2 \sin^2(\phi)}{v_m^2 (v^2 - 2vv' \cos(\phi) + v'^2)} - \frac{(1 + \alpha)^2 v^2}{4\alpha v_m^2}, \quad (7)$$

where  $v_m = \sqrt{2k_B T/m}$  is the most probable speed of an active molecule of mass  $m$ ,  $k_B$  is the Boltzmann constant, and  $T$  is the temperature. With the BB model of collisions included, we refer to the line shape as the speed-dependent billiard-ball profile (SDBBP).

In this work, we calculate the complex Dicke parameter from the *ab initio* calculations based on the GHM. It is interesting to compare it with the frequency of the velocity-changing collisions (real number),  $\nu_{\text{diff}}$ , calculated from the diffusion [57,61]

$$\nu_{\text{diff}} = \frac{v_m^2}{2D}, \quad (8)$$

where  $D$  is the binary diffusion coefficient. The latter can be simply calculated using a crude hard-sphere model [34,57] or an effective Lennard-Jones (LJ) potential parameters [62]. It can be also determined experimentally [63]. We estimate the mean hard-sphere diameter ( $\sigma$  in Ref. [34]) as the intersection of the true isotropic part of the PES with the mean collisional energy, see black line in Fig. 1. The effective LJ potential was obtained by fitting its parameters to the true isotropic part on the interacting pair in the ground state, see green line in Fig. 1.

Note that while this work focuses on describing the line shape in a physically justified model, we also provide a comprehensive dataset of the line-shape parameters for this system for the quadratic speed-dependent hard-collision profile in a wide temperature range in Ref. [17].

### 3. Signatures of different collisional line-shape effects in experimental spectra

In this section, we use the experimental spectra reported in Ref. [1]. The He-perturbed 2-0 Q(1) H<sub>2</sub> line was measured in the Grenoble laboratory at temperature 294.2 K and at nine pressures from 0.07 to 1.05 atm and the He-perturbed 3-0 S(1) H<sub>2</sub> line was measured in the Hefei laboratory at temperature 296.6 K and at four pressures from 0.36 to 1.35 atm. The H<sub>2</sub>-He mixing ratio is different for both experiments and for the 2-0 Q(1) line has a constant value of 4.9(1)% while for the 3-0 S(1) line spans between 10% and 33%. We perform fully quantum calculations of the line-shape parameters on the newly-developed BIGOS code [64], see Ref. [3,22] for detailed description of the methodology. Comparing to our previous work [1] we perform additional quantum-scattering calculations to check the influence of the CD (which

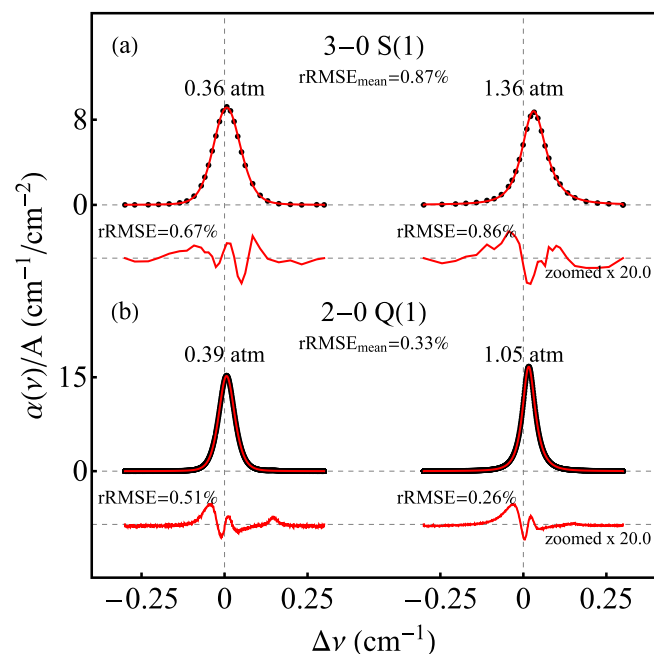


**Fig. 2.** The raw experimental spectra reported in Ref. [1] (black points) in comparison with the simulated line profiles (red lines). Linear background is subtracted from the spectra. The absorption axis is normalized to the spectral line area,  $A$ . The red lines under the line profiles show the differences between the experiment and theory enlarged twenty times. Relative root-mean-square error, rRMSE, values in the plots describe the errors relative to the profile amplitude calculated within  $\pm$ FWHM (Full-Width at Half Maximum) from the line maximum. Vertical gray lines correspond to the theoretical unperturbed line position,  $\omega_0$ . Deviation of the line maximum from  $\omega_0$  highlights that H<sub>2</sub> has atypically large pressure shift.

is usually neglected) on the shapes of molecular resonances, see Section 4 for more details. In our spectra analysis, we fit the line position,  $\omega_0$ , line intensity,  $S$ , and linear baseline. The fit of the line position was performed by means of multispectrum fitting technique [65], while the line area was fitted separately for every pressure. Line-shape parameters are not fitted, but fixed to calculated *ab initio* values. The results for two chosen pressures are presented in Fig. 2. We have already demonstrated, in Ref. [1], that the consistency between our theoretical line-shape calculations and experimental data reaches subpercent accuracy for the He-perturbed H<sub>2</sub> lines. Here we demonstrate that taking into account more sophisticated line-shape parameters is crucial to achieve this agreement. In a typical case the collisional effects in molecular absorption spectra are dominated by the speed-averaged broadening,  $\Gamma_0$ , and shift,  $\Delta_0$ , and hence the Voigt Profile (VP) suffices to describe the collision-perturbed shapes of the molecular lines [66,67]. However, the atypical properties of the hydrogen molecule give us an opportunity to experimentally study more subtle line-shape effects that our collision operator, Eq. (4), takes into account. In Sections 3.1–3.3 we demonstrate on the experimental data that none of these collisional effects can be neglected. Indeed, the excellent agreement between theory and experimental spectra, see Fig. 2, is achieved only when the contributions from all six collisional line-shape parameters are taken into account at the same time, see Fig. 3.

#### 3.1. Speed-averaged line broadening and shift

The simplest description of the line shape is based on the speed-averaged broadening and shift in conjunction with the Doppler effect. In the absence of any other collisional line-shape effects, this results in the formation of a simple VP. To quantify the impact of these collisional effects on the overall shape of the

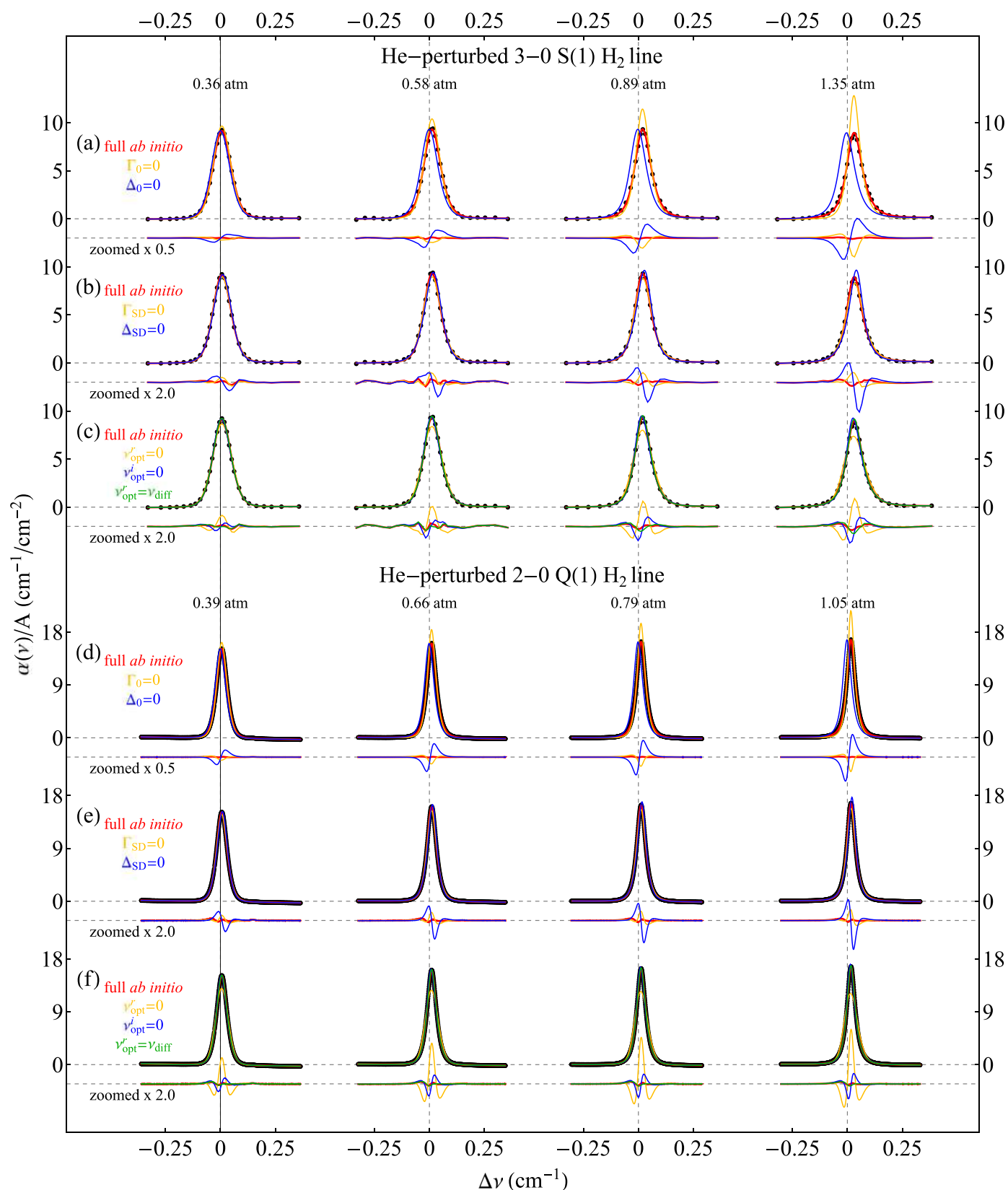


**Fig. 3.** Influence of different collisional effects on the shapes of the rovibrational transitions in  $H_2$ . Black dots are the experimental data reported in Ref. [1] and the red lines are the *ab initio* line shapes. Panels (a-c) and (d-f) correspond to the He-perturbed 3-0 S(1) and 2-0 Q(1)  $H_2$  line, respectively. Panels (a) and (d) present the line shapes in which the speed-averaged line broadening and shift is neglected, i.e.  $\Gamma_0 = 0$  (yellow line) and  $\Delta_0 = 0$  (blue line). In panels (b) and (e) the speed dependence of the line broadening,  $\Gamma_{SD} = 0$  (yellow line) and shift,  $\Delta_{SD} = 0$  (blue line) is neglected. In panels (c) and (f) we neglect the complex Dicke parameter; its real,  $v_{opt}^r = 0$  (yellow line), and imaginary,  $v_{opt}^i = 0$  (blue line), parts. These panels also present the effect of replacing  $v_{opt}^i$  with  $v_{diff}$  originating from the diffusion model calculated with the hard-sphere approach (green line).

measured H<sub>2</sub> absorption lines, we set the  $\Gamma_0$  (see yellow lines in Fig. 3a and d) and  $\Delta_0$  (see blue lines in Fig. 3a and d) parameters to zero in our *ab initio* profiles and directly superimpose them on the raw experimental data. The resulting large differences show, as expected, that both of these parameters are crucial for a proper description of the spectral profile.

### 3.2. Speed dependence of the line broadening and shift

For the present molecular system the simple VP is fairly insufficient [43,68,69]. The beyond-Voigt line-shape effects are particularly pronounced for the case of the rovibrational transitions in molecular hydrogen, see Fig. 2e–f in Ref. [1]. The dependence of the collisional width and shift on the speed of the molecules [41] has to be included to increase the agreement with experimental data. To examine its influence, we set the  $\Gamma_{SD}$  (see yellow lines in Fig. 3b and e) and  $\Delta_{SD}$  (see blue lines in Fig. 3b and e) parameters to zero in our *ab initio* profiles and directly superimpose them on the raw experimental data. The speed dependence of the line width reduces the effective width of the line via the speed class exchanges, while the speed dependence of the shift manifests as inhomogeneous broadening and asymmetry of the line [70,71]. This is clearly confirmed by our experimental data, for  $\Gamma_{SD} = 0$  (see aforementioned yellow line) the line-shape profile is broader, i.e., the peak of the line is lower, while for  $\Delta_{SD} = 0$  (blue line) the line is narrower, i.e. the line peak is higher, and the residuals are clearly asymmetric.

### 3.3. Velocity-changing collisions

The influence of the velocity-changing collisions is incredibly pronounced for the H<sub>2</sub> molecule. It is clearly visible while comparing the velocity-changing collisions frequency derived directly from the diffusion coefficient,  $\nu_{diff}$ , to the speed-averaged width,  $\Gamma_0$  (for the values refer to the Table 1). Therefore, even if the state/phase- and velocity-changing collisions are correlated, i.e. some fraction of the excited molecules undergoing the change of the velocity are damped, the effective rate of velocity-changing collisions,  $\nu_{opt}$ , is

**Table 1**

Line-shape parameters for the 3-0 S(1) and 2-0 Q(1) H<sub>2</sub> lines, determined with our *ab initio* quantum-scattering calculations that include centrifugal distortion. The calculations are done for  $T = 296.6$  K for the 3-0 S(1) line and for  $T = 294.2$  K for the 2-0 Q(1) line. As a reference, we calculated also  $\nu_{diff}$  from Eq. (8) for the hard-sphere and LJ potentials (see Fig. 1). For the hard-sphere potential,  $\nu_{diff} = 43.38$  and  $43.19$  for  $T = 296.6$  K and  $294.2$  K, respectively. For the LJ potential,  $\nu_{diff} = 38.67$  and  $38.43$  for these two temperatures, respectively. For the experimentally determined diffusion coefficient [63],  $\nu_{diff} = 40.9$  and  $41.15$  for  $T = 296.6$  K and  $294.2$  K, respectively. All the parameters are given in  $10^{-3}$  cm<sup>-1</sup> and are calculated for  $n_p = 1$  amg. Abbreviations of the PESs are given in the text.

PES	$\Gamma_0$	$\Delta_0$	$\Gamma_{SD}$	$\Delta_{SD}$	$\nu_{opt}^r$	$\nu_{opt}^i$
3-0 S(1) Line						
mMR	6.51	23.38	2.87	8.92	40.99	-13.03
SK	14.59	33.03	7.01	14.25	36.53	-19.28
BSP	12.79	31.52	5.91	12.99	37.32	-18.29
BSP2	12.36	31.15	5.70	12.67	37.57	-17.94
BSP3	12.38	31.14	5.71	12.69	37.56	-17.96
2-0 Q(1) Line						
mMR	3.45	14.28	1.59	5.53	42.63	-7.98
SK	7.04	21.89	3.35	9.25	41.25	-12.62
BSP	5.85	19.58	2.73	8.15	41.59	-11.51
BSP2	5.74	19.36	2.68	7.99	41.66	-11.33
BSP3	5.75	19.36	2.68	8.00	41.65	-11.35

still much larger than all the other collisional line-shape parameters, see Table 1. We bring this to the fore this in Fig. 3 c and f; the yellow lines show the case when the real part of the complex Dicke parameter,  $\nu_{opt}^r$ , is neglected.

For the considered lines, the real part of the complex Dicke parameter,  $\nu_{opt}^r$ , is close to the one calculated from diffusion coefficient either using a hard-sphere model or LJ potential parameters (see the Appendix B of Ref. [3]), see Eq. (8), Fig. 1 and Table 1. The green lines in Fig. 3 c and f correspond to the case when the *ab initio* calculated  $\nu_{opt}^r$  was replaced with  $\nu_{diff}$ . Using  $\nu_{opt}^r$  we achieved lower residuals than with this approach, but the differences on the figure scale is almost negligible.

In this analysis we clearly observe in experimental spectra the contribution of the imaginary part of the complex Dicke parameter,  $\nu_{opt}^i$ . It has to be emphasized that here we do not phenomenologically fit the  $\nu_{opt}^i$  parameter to the experimental data (which was done before many times [43,69,72–75]), but we set it to the value determined from our fully *ab initio* calculations and make a direct comparison with the raw experimental spectra, see the red lines in Fig. 3. To see the contribution from the  $\nu_{opt}^i$  parameter we set it to zero and compare with experimental spectra, see the blue lines in Fig. 3 c and f. It can be clearly seen that when the contribution of  $\nu_{opt}^i$  is neglected, then the discrepancy between theory and experiment is a few times larger.

### 3.4. Other collisional line-shape effects

In this section, we discuss several other collisional line-shape effects which we do not observe in our spectra. We argue that these effects have negligible influence in the cases considered here.

#### 3.4.1. Non-impact (collision duration) effects

To estimate the influence of the collision-duration effect, we use the results obtained for the Ar-perturbed HF lines [76]. The asymmetry parameter,  $b$ , for this system is at the level of  $3 \times 10^{-3}$  amg<sup>-1</sup>. At our highest pressure this would correspond to 0.15% rRMSE, which is smaller than the rRMSE of the comparison between experiment and theory reported in this work. This estimation is conservative since the range of the H<sub>2</sub>-He interaction is smaller than for HF-Ar and the corresponding collision-duration effects for H<sub>2</sub>-He are expected to be smaller as well.

#### 3.4.2. Line mixing

To estimate the influence of the line-mixing effect, we use the results obtained for the self-perturbed HD lines [77]. The line-mixing coefficient,  $y$ , for HD-HD is at the level of  $2 \times 10^{-3}$  amg<sup>-1</sup> [77]. At our highest pressure this would correspond to 0.1% rRMSE. Also this estimation is conservative since the separation between the Q lines is much larger for H<sub>2</sub> compared to the HD lines from Ref. [77].

## 4. Improved accuracy of the *ab initio* calculations

The analysis presented in the previous sections is based on the most recent *ab initio* PES (BSP3) [3]. In Section 3, we demonstrated that the *ab initio* line-shape calculations based on the BSP3 PES agree well with the experimental data. In this section, we use our quantum-scattering and line-shape calculations to validate the PESs available in the literature [2,3,78–80] as well as to quantify the influence of the CD, which is usually neglected in the scattering calculations for rovibrational transitions. The calculations that include CD are performed on the most accurate BSP3 PES using the newly developed BIGOS code [64].

For the purpose of scattering calculations, the PES for the H<sub>2</sub>-He system,  $V(R, r_{HH}, \theta)$  is expanded over Legendre polynomi-

als [3,5,22]

$$V(R, r_{\text{HH}}, \theta) = \sum_{\lambda=0,2,4,6} V_{\lambda}(R, r_{\text{HH}}) P_{\lambda}(\cos \theta), \quad (9)$$

where  $R$  is the separation between the helium atom and the center of mass of  $\text{H}_2$ ,  $r_{\text{HH}}$  is the distance between hydrogen atoms, and  $\theta$  denotes the angle between  $R$  and  $r_{\text{HH}}$ . Radial coupling terms, which enter the coupled equations, are obtained from the rovibrational average of the  $V_{\lambda}(R, r_{\text{HH}})$  terms over the wave functions of the unperturbed  $\text{H}_2$  molecule,  $\chi_{vj}(r_{\text{HH}})$ ,

$$V_{\lambda, v'j, v''j'}(R) = \int dr_{\text{HH}} \chi_{vj}(r_{\text{HH}}) V_{\lambda}(R, r_{\text{HH}}) \chi_{v''j'}(r_{\text{HH}}), \quad (10)$$

where  $v$  and  $j$  denote vibrational and rotational quantum numbers, respectively. In this work we neglect the vibrational coupling between molecular states, which means that we use only radial coupling terms with  $v' = v$  in the scattering calculations. The non-diagonal vibrational couplings would be too expensive to include. Disregarding the CD, in turn, means that in each vibrational state the coupling terms can be approximated as  $V_{\lambda, v'j, v''j'}(R) \approx V_{\lambda, v0, v0}(R)$ .

#### 4.1. $\text{H}_2$ -He potential energy surfaces

We consider five different PESs: the PES of Schaefer and Köhler (SK PES) [78], the modified Muchnick-Russek PES (mMR) [79,80], the PES reported by Bakr, Smith and Patkowski (BSP) [2] and its two extensions: BSP2 and BSP3 [3].

The original PES of Schaefer and Köhler was based on the *ab initio* points reported in Ref. [81] with the configuration interaction techniques. The SK PES covered a relatively large range of absorber-perturber distance  $R$ , (1.6 – 11  $a_0$ ) and was calculated for five intramolecular distances  $r_{\text{HH}}$  between 0.9 and 2  $a_0$ , with three of them (1.28, 1.449, 1.618  $a_0$ ) determined at a higher level of accuracy [78]. The SK PES was originally presented in the form of  $V_{\lambda}(R, r_{\text{HH}})$  values. We made use of the form published in Ref. [80].

The mMR PES was published as a modification of the *ab initio* potential of Muchnick and Russek [79]. The original MR PES covered a narrow range of  $r_{\text{HH}}$  near 1.4  $a_0$ , but the analytic fit was expected to behave reasonably even up to 4  $a_0$ . The modification of this PES (mMR) [80] was performed to fit to the more accurate *ab initio* values reported in Ref. [82], which were calculated with the complete fourth-order Møller-Plesset approximation.

The BSP PES (and its further extensions) was obtained using the coupled-cluster method with single, double and perturbative triple (CCSD(T)) excitations, taking also into account the contributions from the higher coupled-cluster excitations [2]. This PES was determined for ten values of  $r_{\text{HH}}$  in the range of  $r_{\text{HH}} \in [1.1, 1.75] a_0$ , which turned out to be insufficient for the accurate studies of processes involving vibrationally excited  $\text{H}_2$  (see Section 2 of Ref. [5] for details). This problem was solved in the second version of this PES, BSP2, which extended the *ab initio* data points range to  $r_{\text{HH}} \in [0.65, 3.75] a_0$ . In the final extension of this potential, BSP3, an improved asymptotic behavior for the large values of  $R$  was introduced (for details see Section 2 of Ref. [3]). This PES (denoted as BSP3) was used in Ref. [1].

In Table 1, we report the *ab initio* values of the line-shape parameters for all the considered PESs. There are no fitted line-shape parameters because for the molecular hydrogen they can considerably deviate from the real ones due to a strong numerical correlation. For this reason, we adopt a methodology that is more adequate to study the collisional effects in  $\text{H}_2$ , i.e., instead of comparing the fitted values of the collisional line-shape parameters with theory, we directly compare the *ab initio* line shapes with experimental spectra and the RMSE of their difference gives us information about the agreement between the theory and experiment.

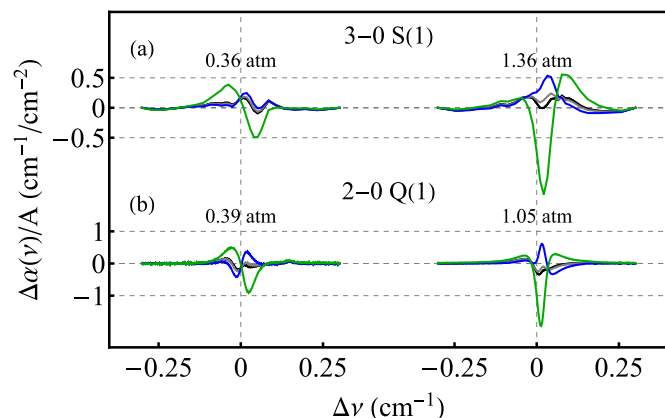


**Fig. 4.** Differences between experimental data and modelled spectra with central frequency fitted by means of the multispectrum fitting technique and line intensity fixed to the theoretical value [83]. Green, blue, gray and black lines are the residuals for the mMR, SK, BSP and BSP3 potentials, respectively. Vertical gray lines correspond to the unperturbed line position [83].

This way we can also check separately an individual influence of any of the six collisional line-shape parameters, see Fig. 3.

In Fig. 4 we show a comparison between the experiment and theory for different PESs. Contrary to the analysis from Figs. 2 and 3, here the line intensity is not adjusted but settled to the fixed theoretical value [83] (this is why the black residuals from Fig. 4 are slightly larger than the red ones from Figs. 2 and 3) to get a clear comparison and to not artificially compensate inaccurate values of some of the line-shape parameters by the line-fitting procedure.

The smallest residuals are for the most recent BSP3 PES, see the black lines in Fig. 4. The residuals for the BSP2 PES are hardly distinguishable from the ones for BSP3 (hence, we do not show them in Fig. 4). Physically, this means that any inaccuracies of the BSP2 potential at large separations between  $\text{H}_2$  and He are minor relative to the sensitivity of the line-shape parameters to the asymptotic behavior of the PES, at this level of accuracy. This is consistent with the expectation that at room-temperature energies the generalized spectroscopic cross sections are hardly sensitive to the long-range part of the PESs (see Appendix C of Ref. [3]). The asymptotic behavior influences the values of the line-shape parameters at the subpercent level, see the BSP2 and BSP3 rows in Table 1.

The residuals for the BSP PES are shown in Fig. 4 as gray lines. The main difference between BSP and BSP3 is that BSP does not cover as large a range of intramolecular separations in  $\text{H}_2$ , see Fig. 1 in Ref. [5]. For the second overtone, at higher pressures, the residuals for BSP (blue line in the top panel in Fig. 4) are larger than for BSP3 (red line). It is consistent with our expectations but at the present level of accuracy the difference is not yet large enough to unambiguously conclude that we experimentally validate the highly-stretched regions of the PESs.

The residuals for the SK and mMR PESs are shown in Fig. 4 as blue and green lines, respectively. For these two cases, the residuals are much larger (especially for the mMR PES) than for the three versions of the BSP PES. This confirms the preliminary analysis of Ref. [5].

#### 4.2. Centrifugal distortion (CD)

We performed additional scattering calculations on the BSP3 PES to determine the influence of the CD on the accuracy of theoretically modelled spectral line shapes. Figure 5 presents CD of the wave functions of  $\text{H}_2$  in the three vibrational states considered in the experiment. The difference between the

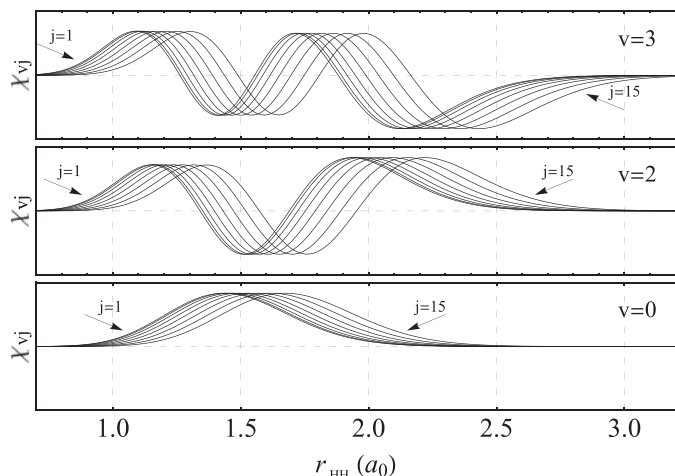


**Fig. 5.** Rovibrational wave functions of ortho- $\text{H}_2$ ,  $\chi_{vj}(r_{\text{HH}})$  ( $j = 1$  to  $j = 15$ ) considered in our scattering calculations. For small  $j$  numbers the wave functions are overlapped.

purely vibrational state,  $\chi_{v0}(r_{\text{HH}})$ , and the true wave function,  $\chi_{vj}(r_{\text{HH}})$ , increases with both  $j$  and  $v$ . Due to the fact that  $\text{H}_2$  has a remarkably large rotational constant ( $B = 60.853 \text{ cm}^{-1}$  [4]), this effect should be pronounced in the rovibrational spectra of this molecule. The influence of the CD on the pressure broadening and shift coefficients was studied by Green [84] in the He-perturbed Q lines of  $\text{D}_2$  from the fundamental band and by Shafer and Gordon [49] and Dubernet and Tuckey [85] in the He-perturbed isotropic Raman Q lines of the fundamental band and S purely rotational lines of  $\text{H}_2$ . These studies concluded that CD has a relatively small effect on both the pressure broadening and shift in the fundamental band (about 1–3%), but can significantly modify the pressure shift of the purely rotational lines, which is very sensitive to the difference in the elastic scattering in two rotational states. The majority of recent theoretical investigations [3,5,21–23] took this effect into account for purely rotational lines, but neglected it for rovibrational transitions. It was suggested [5] that in the latter case, CD might be masked due to the large contribution from the vibrational dephasing.

Here, we report values of the six line-shape parameters calculated with and without CD, see Table 2. In Fig. 6 we show the com-

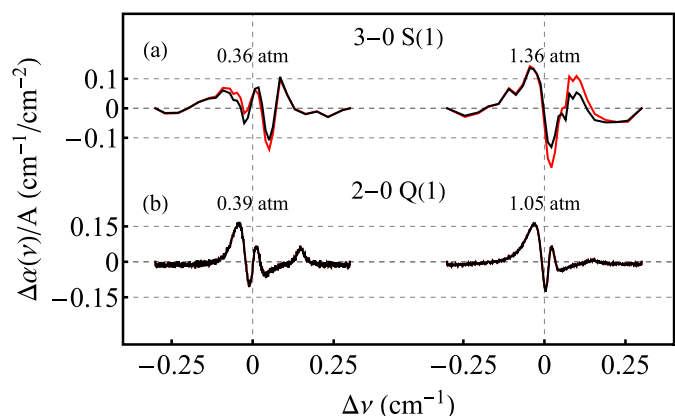


**Fig. 6.** The influence of centrifugal distortion (CD) on the theory-to-experiment consistency. We present differences between experimental data and modeled spectra with central frequency fitted by means of multispectrum fitting technique and line intensity fitted individually for each pressure. Black and red lines correspond to the cases when the CD was and was not taken into account, respectively. CD has a negligible effect on the Q line, therefore the lines are overlapping. Vertical gray lines correspond to the theoretical unperturbed line position.

parison between the experimental spectra and the theoretical line shape calculated with and without including the CD.

For the 3-0 S(1) line, CD modifies the  $\Gamma_0$  and  $\Gamma_{\text{SD}}$  by over 5%. The rest of the parameters, in particular, the pressure shift  $\Delta_0$ , are modified by over 2.5%. CD leads to lower differences between theoretical and experimental spectra, and reduces the mean rRMSE calculated for  $\pm\text{FWHM}$  from 0.99% to 0.89%. In the case of the 2-0 Q(1) line, CD has almost no effect on the calculated line-shape parameters and the spectra calculated with and without it overlap. This result agrees with the observation of Dubernet and Tuckey [85], who reported that the influence of CD on the Q( $j$ ) lines is significantly smaller than on the S( $j$ ) lines.

The fact that the collisional broadening for the two rovibrational lines which differ only in the final spectroscopic state differs by a factor of two might be surprising. As it turns out, collisional widths of rovibrational lines in  $\text{H}_2$  (both He- and self-perturbed) exhibit an unusually strong dependence on the vibrational quantum number (see, for example Fig. 6 in Ref. [17] or Fig. 4 in Ref. [6]). This is caused by a large contribution to the line broadening from the vibrational dephasing, which mainly originates from the difference between the isotropic parts of the PES in initial and final vibrational states. As discussed in Refs. [3,5,22], this difference increases for 0- $\nu$  transitions with  $\nu$ . Apart from the dephasing part, there is also a significant difference in the inelastic contribution to the collisional broadening between the  $Q_{\nu}(1)$  and  $S_{\nu}(1)$  lines. The former have significantly smaller inelastic contribution to  $\Gamma_0$ , due to the fact that the first inelastic transition from either initial or final spectroscopic state is possible once the first inelastic channel becomes accessible (here, for  $E_{\text{kin}} \approx 500 \text{ cm}^{-1}$ ). On the other hand, for the  $S_{\nu}(1)$  line the inelastic contribution from the scattering in the final spectroscopic state ( $\nu, J = 3$ ) is non-zero even at very low kinetic energies. Moreover, the inelastic contribution increases with  $\nu$  because the spacing between the rotational energy levels in a given vibrational state decreases with  $\nu$ .

#### 4.3. Propagation of the uncertainties of the line-shape parameters on the residuals

In the previous section, we demonstrate that an almost-6% change on the line-shape parameters can be introduced with the addition of the CD for the case of the 3-0 S(1) line, see Table 2. At the same time, in Fig. 2 we show that adding the CD improves the mean rRMSE for the 3-0 S(1) line by approximately 0.38% for the highest pressure (from 1.24% in Ref. [1] down to 0.86% in Fig. 2). In this section we explain this apparent inconsistency by analysing how the changes of the line-shape parameters propagate to the magnitude of the residuals. To do it, we directly simulate the line-shape profile for the original and corrected values of the line-shape parameters (the first and middle columns in Table 2, respectively) and we calculate rRMSE of the difference. All of the following discussion is made for the case of the 3-0 S(1) hydrogen line since CD, at this level of accuracy, has insignificant impact on the Q-branch lines [85].

The perturbations of  $\Gamma_0$  and  $\Delta_0$  (by 5.65% and 2.06%, respectively) have the largest impact and change the profile by almost 2% for each of the two parameters in the high-pressure limit, see the top panel in Fig. 7. Curves overlapping with each other are a coincidence. For the case of our experiment, perturbations introduce an approximately 0.2% profile change (rRMSE) for the lowest and approximately 0.8% for the highest pressure. This is over 7 times less than the magnitude of the  $\Gamma_0$  correction. As a reference for the numerical tests, we derive a simple analytical formula that describes propagation of the  $\Gamma_0$  and  $\Delta_0$  uncertainties on the residuals for the case of the Lorentz Profile (LP), see Appendix A. The analytical values, which are valid in the high-pressure limit in which the profile is close to the LP, are shown in the top panel in

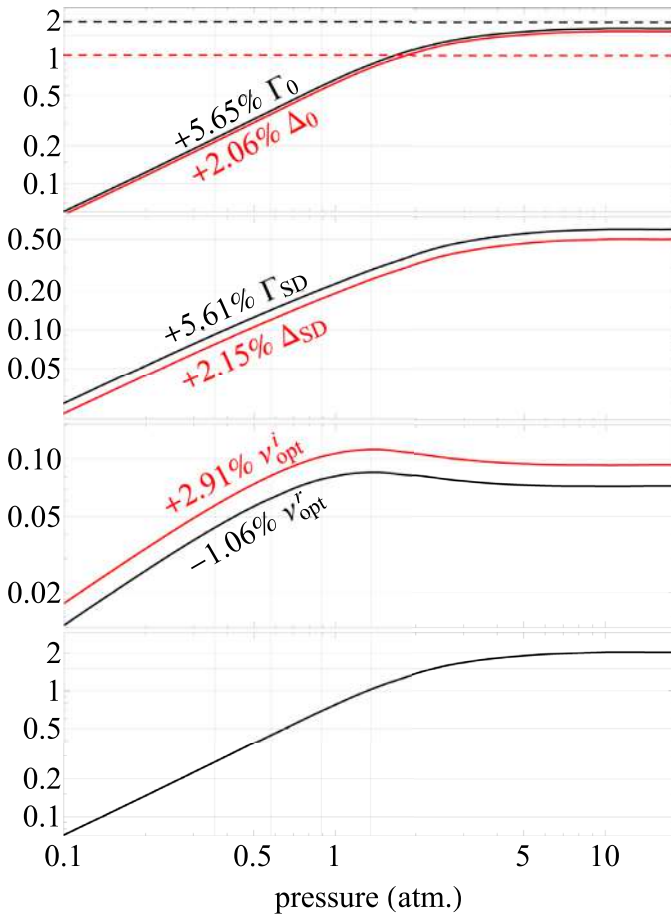


**Fig. 7.** Propagation of the uncertainties of the line-shape parameters on the residuals for the case of the He-perturbed 3-0 S(1) H<sub>2</sub> line. The vertical axis is rRMSE of the difference between the SDBBP generated for the uncorrected and centrifugal-distortion corrected values of the line-shape parameters (see Table 2). The first three panels show the results for the case when only one line-shape parameter is changed (see the labels in the plots). It is a coincidence that the two lines in the top panel overlap. The bottom panel shows the overall difference when all six line-shape parameters are changed. The dashed lines in the top panel are the analytical reference values (the same color notation as for solid lines), see Appendix A. The gray vertical lines correspond to the experimental pressures covered in this paper.

**Table 2**

Line-shape parameters for the 3-0 S(1) and 2-0 Q(1) H<sub>2</sub> lines, determined with our *ab initio* quantum-scattering calculations, using the BSP3 PES. Columns show the impact of the centrifugal distortion (CD) included in the calculations, showing both the line-shape parameter values and differences relative to the ones reported in Ref. [1]. The calculations are done for  $T = 296.6$  K for the 3-0 S(1) line and for  $T = 294.2$  K for the 2-0 Q(1) line with the corresponding Doppler frequency equal to  $\omega_D = 64.01 \times 10^{-3} \text{ cm}^{-1}$  and  $41.96 \times 10^{-3} \text{ cm}^{-1}$ , respectively. All the parameters are given in  $10^{-3} \text{ cm}^{-1}$  and are calculated for  $n_p = 1 \text{ amg}$ .

		Ref. [1]	Ref. [1]+CD	$\Delta$ [%]
3-0 S(1) Line	$\Gamma_0$	11.72	12.38	5.65
	$\Delta_0$	30.51	31.14	2.06
	$\Gamma_{SD}$	5.40	5.71	5.61
	$\Delta_{SD}$	12.42	12.69	2.15
	$v_{opt}^r$	37.96	37.56	-1.06
	$v_{opt}^i$	-17.45	-17.96	2.91
2-0 Q(1) Line	$\Gamma_0$	5.74	5.75	0.17
	$\Delta_0$	19.51	19.36	-0.77
	$\Gamma_{SD}$	2.68	2.68	0.00
	$\Delta_{SD}$	8.06	8.00	-0.74
	$v_{opt}^r$	41.64	41.65	0.02
	$v_{opt}^i$	-11.31	-11.35	0.35

Fig. 7 as the dashed horizontal lines (black for  $\Gamma_0$  and red for  $\Delta_0$ ). The full numerical values (solid lines in the top panel in Fig. 7) in the high-pressure limit are close to the analytical values. The slight difference is caused by the influence of the speed-dependent effects, the velocity-changing collisions, and the competition between them [70] that are present in our full line-shape model.

The perturbations of  $\Gamma_{SD}$  and  $\Delta_{SD}$  have an approximately four-times smaller impact on the profile than the speed-averaged ones, with a maximum change of approximately 0.5% in the high-pressure limit and changes approximately 0.07% and 0.3% for lowest and highest experimental pressure, respectively, see the second panel in Fig. 7. The corrections of both  $v_{opt}^r$  and  $v_{opt}^i$  change the rRMSE by approximately 0.1% in the high-pressure limit and by approximately 0.05% and 0.1% for the low and high experimental pressures, respectively, see the third panel in Fig. 7. It is worth mentioning that for the differences introduced by the complex Dicke narrowing changes, the rRMSE curve has a different shape and has a maximum around 1.5 atm instead of an infinite pressure.

Introducing all corrections at once leads to an approximately 2% rRMSE change in the high-pressure limit, see the bottom panel in Fig. 7. For the case of our experiment, the changes are approximately 0.3% and 1% for the lowest and highest experimental pressure, which are impressively low taking into account the almost-6% magnitude of perturbations. The actual difference between residuals (from the theory-experiment comparison) for the cases with and without CD is even smaller than 0.3% and 1% for the lowest and highest experimental pressures. This is caused by the fact that the line intensity and linear baseline were fitted to the experimental data.

#### 4.4. Relation of the present results with the previous works

It is true that the standard phenomenological models, taking into account the speed-dependent broadening and shift and complex Dicke-narrowing, with fitted parameters can provide a better representation of the data. Let us recall some recent works for the H<sub>2</sub> isotopologues. In Ref. [35] for a self-broadened D<sub>2</sub> line, it was shown that the SDBBP is able to fit experimental data within the experimental noise when all the parameters are adjusted. Fitting all the parameters leads to a significant improvement of the quality of the fit, however, some discrepancy between the parameters obtained from the fit and those from *ab initio* calculations was observed. In the case of the pressure broadening parameter it leads to a 14% deviation, while in the case of the parameter characterizing the speed dependence of the collisional width and shift, the deviation can even exceed an order of magnitude. Several D<sub>2</sub> lines from the same band were analyzed in Ref. [86] using the speed-dependent Nelkin-Ghatak profile (SDNGP) with a quadratic speed dependence of collisional broadening and shift. This profile was also able to fit the experimental data within the experimental noise when all the line-shape parameters were fitted. It should be pointed out, however, that the narrowing parameter obtained from the SDNGP fit differs by a factor of about 3 from the SDBBP fit. Also, SDNGP with a quadratic speed dependence of collisional broadening and shifting was applied to the H<sub>2</sub> lines in Ref. [35] and was able to fit experimental data within the experimental noise. The narrowing parameter obtained from this fit differs by a factor of 2 from the expected value and the speed dependence was overestimated ( $\Gamma_{SD}$  was larger than  $2/3 \Gamma_0$ , which is unphysical). These examples as well as older works in literature considering H<sub>2</sub> lines clearly show that the phenomenological models can fit experimental data well, however, the physical meaning of the parameters is problematic. Therefore, in this work we are focused on a direct comparison of *ab initio* calculations and exper-

imental data rather than on fitting some phenomenological line-shape profiles.

We would like to emphasize that in the present work we performed an advanced analysis of the H<sub>2</sub> spectra that has not been done before. Our analysis provides a deep physical understanding of the collisional effects imprinted in the shapes of the H<sub>2</sub> lines. The key result of the present work is shown in Fig. 3. In contrast to the previous works, here we analyze step-by-step the contribution of each of the six collisional line-shape effects. For instance, the blue line in Fig. 3b shows that the very strong speed dependence of the collisional shift is essential for an accurate description of the spectra. Furthermore, in Fig. 3 we demonstrate the importance of the contribution of the imaginary part of the Dicke parameter. We show that if we set the imaginary part of the Dicke parameter to zero, then the agreement between theory and experiment is a few times worse. In Fig. 3, we also demonstrate that all of these six collisional contributions have to be taken into account to reach this high agreement with experiment. This is a very interesting case in molecular spectroscopy. For most molecular species, the line shape is greatly dominated by one, two, or sometimes three contributions, and others are either completely negligible or have a small impact. Here, we were able to properly interpret all the collisional contributions in the case when all six effects play an important role.

## 5. Conclusion

In this work, we used the highly accurate experimental spectra of the 3-0 S(1) and 2-0 Q(1) molecular hydrogen absorption lines perturbed by helium to study collisional line-shape effects. We clearly distinguished the influence of six different collisional effects (i.e.: collisional broadening and shift, their speed dependencies, and the complex Dicke effect) on the shapes of the H<sub>2</sub> lines. We showed that only the specific combination of these six contributions, obtained from our *ab initio* calculations, gives unprecedentedly good agreement with experimental spectra. If any one of the six contributions is neglected, then the agreement between the experiment and theory worsens at least several times. We also included the centrifugal distortion in our *ab initio* calculations, which further improved the agreement with the experimental spectra.

## Declaration of Competing Interest

The authors declare that they have no known competing financial interests or personal relationships that could have appeared to influence the work reported in this paper.

## CRediT authorship contribution statement

**Michał Słowiński:** Methodology, Software, Validation, Formal analysis, Investigation, Writing – original draft, Writing – review & editing, Visualization. **Hubert Józwiak:** Methodology, Software, Validation, Formal analysis, Investigation, Writing – original draft, Writing – review & editing, Visualization. **Maciej Gancewski:** Software, Validation, Investigation. **Kamil Stankiewicz:** Software, Validation, Investigation. **Nikodem Stolarczyk:** Methodology, Validation, Investigation, Writing – original draft, Writing – review & editing, Visualization. **Yan Tan:** Investigation. **Jin Wang:** Investigation. **An-Wen Liu:** Investigation. **Shui-Ming Hu:** Investigation. **Samir Kassi:** Investigation. **Alain Campargue:** Investigation. **Konrad Patkowski:** Software, Investigation, Writing – review & editing. **Piotr S. Żuchowski:** Software, Investigation. **Roman Ciuryło:** Conceptualization, Methodology. **Franck Thibault:** Conceptualization, Methodology, Software, Validation. **Piotr Wcisło:** Conceptualization, Methodology, Validation, Writing – original draft, Writing – review & editing, Project administration.

## Acknowledgments

M.S., M.G. and K.S. contributions are supported by the *A next-generation worldwide quantum sensor network with optical atomic clocks* project carried out within the TEAM IV Programme of the Foundation for Polish Science cofinanced by the European Union under the European Regional Development Fund. P.W. and H.J. contributions are supported by the National Science Centre, Poland, Project No. 2018/31/B/ST2/00720. N.S. contribution is supported by the National Science Centre, Poland, Project No. 2019/35/B/ST2/01118. S.-M.H. acknowledges the support from National Natural Science Foundation of China (21688102). S.K. and A.C. acknowledge funding support from the Agence Nationale de la Recherche (Equipex REFIMEVE+ANR-11-EQPX-0039). K.P. is supported by the U.S. National Science Foundation award CHE-1955328. The project is cofinanced by the Polish National Agency for Academic Exchange under the PHC Polonium program (dec. PPN/X/PS/318/2018). The research is part of the program of the National Laboratory FAMO in Toruń, Poland. It is also supported by the COST Action CM1405 MOLIM.

## Appendix A

In this Appendix we derive analytical formulas representing the relative root-mean-square error (rRMSE) for the small perturbation of the broadening and shift parameters. By this analysis one can quantify how an error on the line-shape parameters propagates on the final spectral line-shape-profile accuracy. We utilize a simple example of the normalized Lorentz profile

$$L(\omega; \Gamma, \Delta) = \frac{1}{\pi} \frac{\Gamma}{\Gamma^2 + (\omega - \Delta)^2}. \quad (\text{A.1})$$

### Perturbation of the broadening parameter

We analyze a small change of the broadening parameter  $\Gamma \rightarrow \Gamma + \epsilon\Gamma$ . The relative difference caused by the perturbation of the profile is

$$D_{\Gamma}(\omega; \epsilon\Gamma) = \frac{L(\omega; \Gamma + \epsilon\Gamma, \Delta) - L(\omega; \Gamma, \Delta)}{L(0; \Gamma, \Delta)}. \quad (\text{A.2})$$

To quantify the error on the final line-shape profile, we utilize rRMSE at  $\pm$  FWHM of the line center, which can be expressed as

$$rRMSE(\epsilon\Gamma) = \sqrt{\frac{1}{4\Gamma} \int_{-2\Gamma}^{2\Gamma} [D_{\Gamma}(\omega; \epsilon\Gamma)]^2 d\omega}. \quad (\text{A.3})$$

Because  $L(0; \Gamma, \Delta)$  is independent on  $\omega$ , one can calculate typical RMSE and divide it by  $L(0; \Gamma, \Delta)$  to determine rRMSE as well.

Since our goal is only to quantify the errors, the actual position of the line is irrelevant and the vertical axis can be adjusted so that  $\Delta = 0$ , which simplifies the further formulas. The integration in Eq. (A.3) can be analytically performed and, since we consider small perturbations of the line-shape parameters, expanded into a series, the linear term of which is

$$rRMSE(\epsilon\Gamma) \approx \frac{\sqrt{\frac{73}{15} + \frac{25\text{atan}^2}{2}}}{10} \frac{\epsilon\Gamma}{\Gamma} \approx 0.433 \frac{\epsilon\Gamma}{\Gamma}. \quad (\text{A.4})$$

The above formula allows to estimate the rRMSE caused by the change  $\epsilon\Gamma$  of broadening line-shape parameter,  $\Gamma$ .

### Perturbation of the shift parameter

We repeat above discussion for the case of a small change of the shift parameter  $\Delta \rightarrow \Delta + \epsilon\Delta$ . The relative difference caused by the perturbation of the profile is

$$D_{\Delta}(\omega; \epsilon\Delta) = \frac{L(\omega; \Gamma, \Delta + \epsilon\Delta) - L(\omega; \Gamma, \Delta)}{L(0; \Gamma, \Delta)}. \quad (\text{A.5})$$

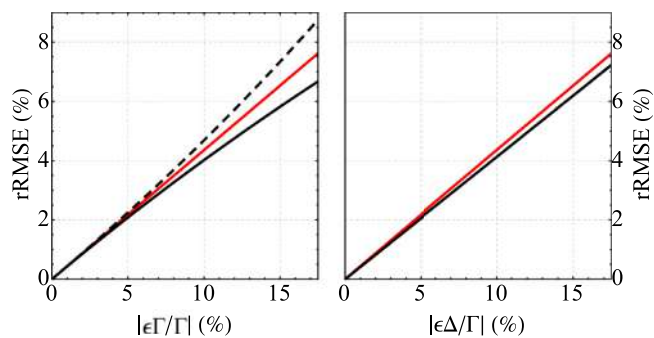


**Fig. A1.** The numerical validation of the analytical formulas for the relative root mean square errors (see text for more details). The black curves represent the numerical values and the red ones stand for analytical ones. Dashed and plain black curves of left panel corresponds to the negative and positive values of  $\epsilon\Gamma/\Gamma$ , respectively.

The same reason as mentioned before allows us to exclude  $\Delta$  parameter and focus only on its distortion, i.e.,  $\epsilon\Delta$ . Again, we quantify the error by calculating rRMSE at  $\pm$ FWHM, which is

$$rRMSE(\epsilon\Delta) = \sqrt{\frac{1}{4\Gamma} \int_{-2\Gamma}^{2\Gamma} [D_{\Delta}(\omega; \epsilon\Delta)]^2 d\omega}. \quad (A.6)$$

Similarly, rRMSE can be determined by dividing typically calculated RMSE by  $L(0; \Gamma, \Delta)$ . The integral can be analytically performed, expanded into series and since we consider small perturbations again, approximated by linear term which is

$$rRMSE(\epsilon\Delta) \approx \frac{\sqrt{\frac{77}{15} + \frac{25\text{atan}^2}{2}}}{10} \frac{\epsilon\Delta}{\Gamma} \approx 0.436 \frac{\epsilon\Delta}{\Gamma}. \quad (A.7)$$

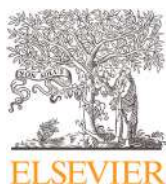
The above formula allows to estimate the rRMSE caused by the change  $\epsilon\Delta$  of shift line-shape parameter,  $\Delta$ .

The direct comparison of the numerical results with Eqs. (A.4) and (A.7) is presented in Fig. A.1.

## References

- [1] Słowiński M, Thibault F, Tan Y, Wang J, Liu A-W, Hu S-M, Kassı S, Campargue A, Konefał M, Józwiak H, Patkowski K, Zuchowski P, Ciuryło R, Lisak D, Wcisło P. H<sub>2</sub>-He collisions: *ab initio* theory meets cavity-enhanced spectra. *Phys Rev A* 2020;101(5):052705. doi:10.1103/physreva.101.052705.
- [2] Bakr BW, Smith DGA, Patkowski K. Highly accurate potential energy surface for the He-H<sub>2</sub> dimer. *J Chem Phys* 2013;139(14):144305. doi:10.1063/1.4824299.
- [3] Thibault F, Patkowski K, Zuchowski PS, Józwiak H, Ciuryło R, Wcisło P. Rovibrational line-shape parameters for H<sub>2</sub> in He and new H<sub>2</sub>-He potential energy surface. *J Quant Spectrosc Radiat Transf* 2017;202:308–20. doi:10.1016/j.jqsrt.2017.08.014.
- [4] Herzberg G, Howe LL. The Lyman bands of molecular hydrogen. *Can J Phys* 1959;37(5):636–59. doi:10.1139/p59-070.
- [5] Thibault F, Wcisło P, Ciuryło R. A test of H<sub>2</sub>-He potential energy surfaces. *Eur Phys J D* 2016;70(11):236. doi:10.1140/epjd/e2016-70114-9.
- [6] Wcisło P, Gordon IE, Tran H, Tan Y, Hu S-M, Campargue A, Kassı S, Romanini D, Hill C, Kochanov RV, Rothman LS. The implementation of non-Voigt line profiles in the HITRAN database: H<sub>2</sub> case study. *J Quant Spectrosc Radiat Transf* 2016;177:75–91. doi:10.1016/j.jqsrt.2016.01.024.
- [7] Perreault WE, Mukherjee N, Zare RN. Quantum control of molecular collisions at 1 kelvin. *Science* 2017;358(6361):356–9. doi:10.1126/science.aao3116.
- [8] Perreault WE, Mukherjee N, Zare RN. Cold quantum-controlled rotationally inelastic scattering of HD with H<sub>2</sub> and D<sub>2</sub> reveals collisional partner reorientation. *Nat Chem* 2018;10(5):561–7. doi:10.1038/s41557-018-0028-5.
- [9] Perreault WE, Mukherjee N, Zare RN. HD ( $v = 1, j = 2, m$ ) orientation controls HD-He rotationally inelastic scattering near 1 K. *J Chem Phys* 2019;150(17):174301. doi:10.1063/1.5096531.
- [10] Hout KVD, Hermans P, Mazur E, Knaap H. The broadening and shift of the rotational Raman lines for hydrogen isotopes at low temperatures. *Physica A* 1980;104(3):509–47. doi:10.1016/0378-4371(80)90012-6.
- [11] Bragg SL, Smith WH, Brault JW. Line positions and strengths in the H<sub>2</sub> quadrupole spectrum. *Astrophys J* 1982;263:999. doi:10.1086/160568.
- [12] Bischel WK, Dyer MJ. Temperature dependence of the Raman linewidth and line shift for the Q(1) and Q(0) transitions in normal and para-H<sub>2</sub>. *Phys Rev A* 1986;33(5):3113–23. doi:10.1103/physreva.33.3113.
- [13] Rahn LA, Rosasco GJ. Measurement of the density shift of the H<sub>2</sub> Q(0–5) transitions from 295 to 1000 K. *Phys Rev A* 1990;41(7):3698–706. doi:10.1103/physreva.41.3698.
- [14] Rahn LA, Farrow RL, Rosasco GJ. Measurement of the self-broadening of the H<sub>2</sub> Q(0–5) Raman transitions from 295 to 1000 K. *Phys Rev A* 1991;43(11):6075–88. doi:10.1103/physreva.43.6075.
- [15] Forsman JW, Bonamy J, Robert D, Berger JP, Saint-Loup R, Berger H. H<sub>2</sub>-He vibrational line-shape parameters: measurement and semiclassical calculation. *Phys Rev A* 1995;52(4):2652–63. doi:10.1103/physreva.52.2652.
- [16] Sinclair PM, Berger JP, Michaut X, Saint-Loup R, Chauv R, Berger H, Bonamy J, Robert D. Collisional broadening and shifting parameters of the Raman Q branch of H<sub>2</sub> perturbed by N<sub>2</sub> determined from speed-dependent line profiles at high temperatures. *Phys Rev A* 1996;54(1):402–9. doi:10.1103/physreva.54.402.
- [17] Wcisło P, Thibault F, Stolarczyk N, Józwiak H, Słowiński M, Gancewski M, Stankiewicz K, Konefał M, Kassı S, Campargue A, Tan Y, Wang J, Patkowski K, Ciuryło R, Lisak D, Kochanov R, Rothman L, Gordon I. The first comprehensive dataset of beyond-Voigt line-shape parameters from *ab initio* quantum scattering calculations for the HITRAN database: He-perturbed H<sub>2</sub> case study. *J Quant Spectrosc Radiat Transf* 2021;260:107477. doi:10.1016/j.jqsrt.2020.107477.
- [18] Hermans P, Die AV, Knaap H, Beenakker J. Measurements on the influence of binary collisions on the depolarized Rayleigh and rotational Raman lines for H<sub>2</sub>-noble gas systems at low temperatures. *Physica A* 1985;132(2–3):233–52. doi:10.1016/0378-4371(85)90010-x.
- [19] Blackmore R, Green S, Monchick L. Dicke narrowing of the polarized Stokes-Raman Q branch of the  $v=0 \rightarrow 1$  transition of D<sub>2</sub> in He. *J Chem Phys* 1989;91(7):3846–53. doi:10.1063/1.457640.
- [20] Michaut X, Saint-Loup R, Berger H, Dubernet ML, Joubert P, Bonamy J. Investigations of pure rotational transitions of H<sub>2</sub> self-perturbed and perturbed by He. I. Measurement, modeling, and quantum calculations. *J Chem Phys* 1998;109(3):951–61. doi:10.1063/1.476638.
- [21] Martínez RZ, Bermejo D, Thibault F, Wcisło P. Testing the *ab initio* quantum-scattering calculations for the D<sub>2</sub>-He benchmark system with stimulated Raman spectroscopy. *J Raman Spectrosc* 2018;49(8):1339–49. doi:10.1002/jrs.5391.
- [22] Józwiak H, Thibault F, Stolarczyk N, Wcisło P. *Ab initio* line-shape calculations for the S and O branches of H<sub>2</sub> perturbed by He. *J Quant Spectrosc Radiat Transf* 2018;219:313–22. doi:10.1016/j.jqsrt.2018.08.023.
- [23] Thibault F, Martínez RZ, Bermejo D, Wcisło P. Line-shape parameters for the first rotational lines of HD in He. *Mol Astrophys* 2020;19:100063. doi:10.1016/j.molap.2020.100063.
- [24] Morita M, Balakrishnan N. Stereodynamics of rotationally inelastic scattering in cold He+HD collisions. *J Chem Phys* 2020a;153(9):091101. doi:10.1063/1.5002190.
- [25] Morita M, Balakrishnan N. Stereodynamics of ultracold rotationally inelastic collisions. *J Chem Phys* 2020b;153(18):184307. doi:10.1063/1.5003080.
- [26] Stankiewicz K, Józwiak H, Gancewski M, Stolarczyk N, Thibault F, Wcisło P. *Ab initio* calculations of collisional line-shape parameters and generalized spectroscopic cross-sections for rovibrational dipole lines in HD perturbed by He. *J Quant Spectrosc Radiat Transf* 2020;254:107194. doi:10.1016/j.jqsrt.2020.107194.
- [27] Komasa J, Piszczatowski K, Lach G, Przybytek M, Jeziorski B, Pachucki K. Quantum electrodynamic effects in rovibrational spectra of molecular hydrogen. *J Chem Theory Comput* 2011;7(10):3105–15. doi:10.1021/ct200438t.
- [28] Feuchtgruber H, Lellouch E, Bézard B, Encrenaz T, de Graauw T, Davis GR. Detection of HD in the atmospheres of Uranus and Neptune: a new determination of the D/H ratio. *Astron Astrophys* 1999;341:L17–21. <https://ui.adsabs.harvard.edu/abs/1999A&A...341L..17F>
- [29] Lellouch E, Bézard B, Fouchet T, Feuchtgruber H, Encrenaz T, de Graauw T. The deuterium abundance in Jupiter and Saturn from ISO-SWS observations. *Astron Astrophys* 2001;370(2):610–22. doi:10.1051/0004-6361/20010259.
- [30] Lellouch E, Hartogh P, Feuchtgruber H, Vandenbussche B, de Graauw T, Moreno R, Jarchow C, Cavalié T, Orton G, Banaszekiewicz M, Blecka MI, Bockelée-Morvan D, Crovisier J, Encrenaz T, Fulton T, Küppers M, Lara LM, Lis DC, Medvedev AS, Rengel M, Sagawa H, Swinyard B, Szutowicz S, Bensch F, Bergin E, Billebaud F, Biver N, Blake GA, Blommaert JADL, Cernicharo J, Courtin R, Davis GR, Decin L, Encrenaz P, Gonzalez A, Jehin E, Kidger M, Naylor D, Portyankina G, Schieder R, Sidher S, Thomas N, de Val-Borro M, Verdugo E, Waelkens C, Walker H, Aarts H, Comito C, Kawamura JH, Maestrini A, Peacocke T, Teipen R, Tils T, Wildeman K. First results of Herschel-PACS observations of Neptune. *Astron Astrophys* 2010;518:L152. doi:10.1051/0004-6361/201014600.
- [31] Feuchtgruber H, Lellouch E, Orton G, de Graauw T, Vandenbussche B, Swinyard B, Moreno R, Jarchow C, Billebaud F, Cavalié T, Sidher S, Hartogh P. The D/H ratio in the atmospheres of Uranus and Neptune from Herschel-PACS observations. *Astron Astrophys* 2013;551:A126. doi:10.1051/0004-6361/201220857.
- [32] Smith WH. The H<sub>2</sub> 4–0 S(0, 1 and 2) quadrupole features in Jupiter. *Icarus* 1989;81(2):429–40. doi:10.1016/0019-1035(89)90062-6.
- [33] Baines KH, Mickelson ME, Larson LE, Ferguson DW. The abundances of methane and ortho/para hydrogen on Uranus and Neptune: implications of new laboratory 4–0 h<sub>2</sub> quadrupole line parameters. *Icarus* 1995;114(2):328–40. doi:10.1006/icar.1995.1065.
- [34] Ciuryło R, Shapiro DA, Drummond JR, May AD. Solving the line-shape problem with speed-dependent broadening and shifting and with Dicke narrowing. II. Application. *Phys Rev A* 2002a;65(1):012502. doi:10.1103/physreva.65.012502.
- [35] Wcisło P, Thibault F, Zaborowski M, Wójtewicz S, Cygan A, Kowzan G, Maślowski P, Komasa J, Puchalski M, Pachucki K, Ciuryło R, Lisak D. Accu-

- rate deuterium spectroscopy for fundamental studies. *J Quant Spectrosc Radiat Transf* 2018;213:41–51. doi:10.1016/j.jqsrt.2018.04.011.
- [36] Ciuryło R, Bielski A, Drummond JR, Lisak D, May AD, Pine AS, Shapiro DA, Szudy J, Trawiński RS. High-resolution studies on the influence of velocity-changing collisions on atomic and molecular line shapes. *AIP Conf Proc*, AIP 2002b. doi:10.1063/1.1525447.
- [37] Lisak D, Hodges J, Ciuryło R. Comparison of semiclassical line-shape models to rovibrational H<sub>2</sub>O spectra measured by frequency-stabilized cavity ring-down spectroscopy. *Phys Rev A* 2006;73(1):012507. doi:10.1103/physreva.73.012507.
- [38] Hess S. Kinetic theory of spectral line shapes. The transition between doppler broadening and collisional broadening. *Physica* 1972;61(1):80–94. doi:10.1016/0031-8914(72)90035-3.
- [39] Corey GC, McCourt FR. Dicke narrowing and collisional broadening of spectral lines in dilute molecular gases. *J Chem Phys* 1984;81(5):2318–29. doi:10.1063/1.447930.
- [40] Monchick L, Hunter LW. Diatomic–diatomic molecular collision integrals for pressure broadening and Dicke narrowing: a generalization of Hess's theory. *J Chem Phys* 1986;85(2):713–18. doi:10.1063/1.451277.
- [41] Berman PR. Speed-dependent collisional width and shift parameters in spectral profiles. *J Quant Spectrosc Radiat Transf* 1972;12(9):1331–42. doi:10.1016/0022-4073(72)90189-6.
- [42] Pickett HM. Effects of velocity averaging on the shapes of absorption lines. *J Chem Phys* 1980;73(12):6090–4. doi:10.1063/1.440145.
- [43] Pine A. Asymmetries and correlations in speed-dependent Dicke-narrowed line shapes of argon-broadened HF. *J Quant Spectrosc Radiat Transf* 1999;62(4):397–423. doi:10.1016/s0022-4073(98)00112-5.
- [44] Rautian SG, Sobelman IL. The effect of collisions on the Doppler broadening of spectral lines. *Sov Phys Usp* 1967;9(5):701–16. doi:10.1070/pu1967v009n05abeh003212.
- [45] Demeio L, Green S, Monchick L. Effects of velocity changing collisions on line shapes of HF in Ar. *J Chem Phys* 1995;102(23):9160–6. doi:10.1063/1.468864.
- [46] Schaefer J, Monchick L. Line broadening of HD immersed in He and H<sub>2</sub> gas. *Astron Astrophys* 1992;265(2):859–68. doi:10.1063/1.453612.
- [47] Stolarczyk N, Thibault F, Cybulski H, Jóźwiak H, Kowzan G, Vispoel B, Gordon I, Rothman L, Gamache R, Wcisło P. Evaluation of different parameterizations of temperature dependences of the line-shape parameters based on ab initio calculations: case study for the HITRAN database. *J Quant Spectrosc Radiat Transf* 2020;240:106676. doi:10.1016/j.jqsrt.2019.106676.
- [48] Kowzan G, Wcisło P, Słowiński M, Maślowski P, Viel A, Thibault F. Fully quantum calculations of the line-shape parameters for the Hartmann-Trans profile: A CO-Ar case study. *J Quant Spectrosc Radiat Transf* 2020;243:106803. doi:10.1016/j.jqsrt.2019.106803.
- [49] Shafer R, Gordon RG. Quantum scattering theory of rotational relaxation and spectral line shapes in H<sub>2</sub>-He gas mixtures. *J Chem Phys* 1973;58(12):5422–43. doi:10.1063/1.1679162.
- [50] Ben-Reuven A. Symmetry considerations in pressure-broadening theory. *Phys Rev* 1966a;141(1):34–40. doi:10.1103/PhysRev.141.34.
- [51] Ben-Reuven A. Impact broadening of microwave spectra. *Phys Rev* 1966b;145(1):7–22. doi:10.1103/PhysRev.145.7.
- [52] Schaefer J, Monchick L. Line shape cross sections of HD immersed in HE and H<sub>2</sub> gas. I. Pressure broadening cross sections. *J Chem Phys* 1987;87(1):171–81. doi:10.1063/1.453612.
- [53] Shapiro DA, Ciuryło R, Drummond JR, May AD. Solving the line-shape problem with speed-dependent broadening and shifting and with Dicke narrowing. I. Formalism. *Phys Rev A* 2002;65(1):012501. doi:10.1103/physreva.65.012501.
- [54] Blackmore R. A modified Boltzmann kinetic equation for line shape functions. *J Chem Phys* 1987;87(2):791–800. doi:10.1063/1.453286.
- [55] Smith EW, Cooper J, Chappell W, Dillon T. An impact theory for Doppler and pressure broadening II. Atomic and molecular systems. *J Quant Spectrosc Radiat Transf* 1971;11(10):1567–76. doi:10.1016/0022-4073(71)90114-2.
- [56] Nienhuis G. Effects of the radiator motion in the classical and quantum-mechanical theories of collisional spectral-line broadening. *J Quant Spectrosc Radiat Transf* 1978;20(3):275–90. doi:10.1016/0022-4073(78)90133-4.
- [57] Lindenfeld MJ. Self-structure factor of hard-sphere gases for arbitrary ratio of bath to test particle masses. *J Chem Phys* 1980;73(11):5817–29. doi:10.1063/1.440066.
- [58] Liao PF, Bjorkholm JE, Berman PR. Effects of velocity-changing collisions on two-photon and stepwise-absorption spectroscopic line shapes. *Phys Rev A* 1980;21(6):1927–38. doi:10.1103/physreva.21.1927.
- [59] Nelkin M, Ghatak A. Simple binary collision model for Van Hove's  $G_2(r, t)$ . *Phys Rev* 1964;135(1A):A4–9. doi:10.1103/PhysRev.135.A4.
- [60] Wcisło P, Tran H, Kassi S, Campargue A, Thibault F, Ciuryło R. Velocity-changing collisions in pure H<sub>2</sub> and H<sub>2</sub>-Ar mixture. *J Chem Phys* 2014;141(7):074301. doi:10.1063/1.4892414.
- [61] Chapman S, Cowling TG. *The mathematical theory of non-Uniform gases*. Cambridge University Press; 1970.
- [62] Hirshfelder JO, Curtiss CF, Bird RB. *Nonequilibrium phenomena in polyatomic gases*. Wiley; 1954.
- [63] Taylor WL, Hurlly JJ, Meyer BA, Dunlop PJ. Binary diffusion coefficients of helium/hydrogen isotope mixtures. *J Chem Phys* 1995;103(16):6959–65. doi:10.1063/1.470373.
- [64] Jóźwiak H., Gancewski M., Grabowski A., Stankiewicz K., Wcisło P. BIGOS computer code, to be published.
- [65] Benner DC, Rinsland CP, Devi VM, Smith MAH, Atkins D. A multispectrum nonlinear least squares fitting technique. *J Quant Spectrosc Radiat Transf* 1995;53(6):705–21. doi:10.1016/0022-4073(95)00015-d.
- [66] Humlíček J. An efficient method for evaluation of the complex probability function: The Voigt function and its derivatives. *J Quant Spectrosc Radiat Transf* 1979;21(4):309–13. doi:10.1016/0022-4073(79)90062-1.
- [67] Schreier F. Optimized implementations of rational approximations for the Voigt and complex error function. *J Quant Spectrosc Radiat Transf* 2011;112(6):1010–25. doi:10.1016/j.jqsrt.2010.12.010.
- [68] Duggan P, Sinclair P, Berman R, May A, Drummond JR. Testing lineshape models: measurements for  $v = 1-0$  CO broadened by He and Ar. *J Mol Spectrosc* 1997;186(1):90–8. doi:10.1006/jmsp.1997.7420.
- [69] Ngo N, Lisak D, Tran H, Hartmann JM. An isolated line-shape model to go beyond the Voigt profile in spectroscopic databases and radiative transfer codes. *J Quant Spectrosc Radiat Transf* 2013;129:89–100. doi:10.1016/j.jqsrt.2013.05.034.
- [70] Wcisło P, Thibault F, Cybulski H, Ciuryło R. Strong competition between velocity-changing and phase- or state-changing collisions in H<sub>2</sub> spectra perturbed by Ar. *Phys Rev A* 2015;91(5):052505. doi:10.1103/physreva.91.052505.
- [71] Farrow RL, Rahn LA, Sitz GO, Rosasco GJ. Observation of a speed-dependent collisional inhomogeneity in H<sub>2</sub> vibrational line profiles. *Phys Rev Lett* 1989;63(7):746–9. doi:10.1103/physrevlett.63.746.
- [72] Joubert P, Bonamy J, Robert D, Domenech J-L, Bermejo D. A partially correlated strong collision model for velocity- and state-changing collisions. Application to Ar-broadened HF rovibrational line shape. *J Quant Spectrosc Radiat Transf* 1999;61(4):519–31. doi:10.1016/s0022-4073(98)00038-7.
- [73] Ciuryło R, Pine A, Szudy J. A generalized speed-dependent line profile combining soft and hard partially correlated Dicke-narrowing collisions. *J Quant Spectrosc Radiat Transf* 2001;68(3):257–71. doi:10.1016/s0022-4073(00)00024-8.
- [74] Lisak D, Rusciano G, Sasso A. Speed-dependent and correlation effects on the line shape of acetylene. *Phys Rev A* 2005;72(1):012503. doi:10.1103/physreva.72.012503.
- [75] Lisak D, Cygan A, Bermejo D, Domenech J, Hodges J, Tran H. Application of the Hartmann-Trans profile to analysis of H<sub>2</sub>O spectra. *J Quant Spectrosc Radiat Transf* 2015;164:221–30. doi:10.1016/j.jqsrt.2015.06.012.
- [76] Marteau P, Boulet C, Robert D. Finite duration of collisions and vibrational dephasing effects on the Ar broadened HF infrared line shapes: asymmetric profiles. *J Chem Phys* 1984;80(8):3632–9. doi:10.1063/1.447184.
- [77] Sheldon G, Sinclair P, Flohic ML, Drummond J, May A. Line mixing and broadening in the Raman Q branch of HD at 304.6 K. *J Mol Spectrosc* 1989;192(2):406–16. doi:10.1006/jmsp.1998.7696.
- [78] Schaefer J, Köhler W. Quantum calculations of rotational and NMR relaxation, depolarized Rayleigh and rotational Raman line shapes for H<sub>2</sub>(HD)-He mixtures. *Physica A* 1985;129(3):469–502. doi:10.1016/0378-4371(85)90181-5.
- [79] Muchnick P, Russek A. The HeH<sub>2</sub> energy surface. *J Chem Phys* 1994;100(6):4336–46. doi:10.1063/1.466316.
- [80] Boothroyd AI, Martin PG, Peterson MR. Accurate analytic He-H<sub>2</sub> potential energy surface from a greatly expanded set of ab initio energies. *J Chem Phys* 2003;119(6):3187–207. doi:10.1063/1.1589734.
- [81] Meyer W, Hariharan PC, Kutzelnigg W. Refined ab initio calculation of the potential energy surface of the He-H<sub>2</sub> interaction with special emphasis to the region of the van der Waals minimum. *J Chem Phys* 1980;73(4):1880–97. doi:10.1063/1.440324.
- [82] Tao FM. An accurate ab initio potential energy surface of the He-H<sub>2</sub> interaction. *J Chem Phys* 1994;100(7):4947–54. doi:10.1063/1.467214.
- [83] Campargue A, Kassi S, Pachucki K, Komasa J. The absorption spectrum of H<sub>2</sub>: CRDS measurements of the (2-0) band, review of the literature data and accurate ab initio line list up to 35000 cm<sup>-1</sup>. *Phys Chem Chem Phys* 2012;14(2):802–15. doi:10.1039/c1cp22912e.
- [84] Green S, Blackmore R, Monchick L. Comment on linewidths and shifts in the Stokes-Raman Q branch of D<sub>2</sub> in He. *J Chem Phys* 1989;91(1):52–5. doi:10.1063/1.457489.
- [85] Dubernet M-L, Tuckey P. Raman Q and S line broadening and shifting coefficients: some commonly used assumptions revisited. *Chem Phys Lett* 1999;300(3-4):275–80. doi:10.1016/s0009-2614(98)01334-7.
- [86] Mondelain D, Kassi S, Campargue A. Transition frequencies in the (2-0) band of D<sub>2</sub> with MHz accuracy. *J Quant Spectrosc Radiat Transf* 2020;253:107020. doi:10.1016/j.jqsrt.2020.107020.



Contents lists available at ScienceDirect

Journal of Quantitative Spectroscopy &amp; Radiative Transfer

journal homepage: [www.elsevier.com/locate/jqsrt](http://www.elsevier.com/locate/jqsrt)

# Fully quantum calculations of the line-shape parameters for the Hartmann-Tran profile: A CO-Ar case study



Grzegorz Kowzan<sup>a,\*</sup>, Piotr Wcisło<sup>a</sup>, Michał Słowiński<sup>a</sup>, Piotr Masłowski<sup>a</sup>, Alexandra Viel<sup>b</sup>, Franck Thibault<sup>b</sup>

<sup>a</sup> Institute of Physics, Faculty of Physics, Astronomy and Informatics, Nicolaus Copernicus University in Toruń, ul. Grudziądzka 5, 87-100 Toruń, Poland

<sup>b</sup> Univ Rennes, CNRS, IPR (Institut de Physique de Rennes)-UMR 6251, Rennes F-35000, France

## ARTICLE INFO

### Article history:

Received 9 October 2019

Revised 15 December 2019

Accepted 16 December 2019

Available online 18 December 2019

### Keywords:

Hartmann-Tran profile

Databases

Molecular collisions

Spectral line shapes

## ABSTRACT

We present a procedure for generating the parameters of the Hartmann-Tran profile (HTP) from purely first principles calculations. Starting from an absorber-perturber interaction potential, we calculate  $S$ -matrices describing the effect of collisions on the absorbing molecule. We then use the generalized Hess method to calculate speed-dependent pressure shift and broadening parameters, and the complex Dicke parameter,  $\nu_{\text{opt}}$ , which accounts for such effects as the Dicke effect and correlations between dephasing and velocity-changing collisions. Based on these *ab initio* results, we derive the Hartmann-Tran profile parameters and evaluate the validity of the quadratic approximation of speed dependence and the hard-collision model of velocity-changing collisions adopted in the Hartmann-Tran profile. We also discuss the interpretation and speed dependence of  $\nu_{\text{opt}}$ . Finally, we evaluate the approximation scheme for temperature dependence of HTP line-shape parameters adopted in the 2016 edition of the HITRAN database.

© 2019 The Authors. Published by Elsevier Ltd.

This is an open access article under the CC BY license. (<http://creativecommons.org/licenses/by/4.0/>)

## 1. Introduction

The availability of accurate line-shape parameters, including the ones accounting for speed-dependent effects [1–3] and velocity-changing collisions [4], combined with an appropriate line-shape model permitting efficient evaluation of molecular line shapes are crucial for faithful reconstruction and interpretation of accurate molecular spectra [5–9] and for reduction of model-induced errors in atmospheric measurements of the Earth and other planets [10]. Various beyond-Voigt profiles [2,11–17] have been successfully used in analysis of molecular spectra exhibiting influence of speed dependence of broadening and shift as well as the influence of the Dicke effect, but their complexity and high computational cost made them unsuitable for use beyond interpretation of laboratory spectra. Since then, it was shown that the computational cost of a class of such profiles can be significantly lowered by employing the quadratic approximation of speed dependence [18–20], reducing it to at most five times that of the Voigt profile. The Hartmann-Tran profile utilizes this development and encompasses several beyond-Voigt profiles, allowing for fast and accurate line-shape modeling. This led to its recommendation by

the IUPAC [21] and its adoption in the 2016 edition of the HITRAN database [22].

The HTP is described by the Doppler width of the transition and six collisional parameters. The 2016 edition of the HITRAN database allows for inclusion of the values of four of them at four reference temperatures corresponding to different temperature ranges. Of the remaining two, the correlation parameter is assumed to be temperature independent and the frequency of velocity-changing collisions is provided at a single temperature and described by a single power law for all temperature ranges. For two parameters, pressure broadening half-width and pressure shift, and for each temperature range, the temperature dependence coefficients also have to be provided. The parameters introduced into the database should primarily allow for accurate modeling of measured spectra in a wide temperature range. The task of filling the database with experimentally determined values of these parameters is made difficult by high demands on signal-to-noise ratio of the spectra, imperfections of the line-shape model and strong numerical correlation between fitted parameters [20,21,23]. An alternate approach to the technically difficult and time-consuming measurements was recently proposed by Ngo and Hartmann [24]. It combines requantized classical molecular dynamics simulations (rCMDS) and currently available measurements of pressure broadening halfwidths to generate a subset of HTP parameters. Here, we

\* Corresponding author.

E-mail address: [gkowzan@fizyka.umk.pl](mailto:gkowzan@fizyka.umk.pl) (G. Kowzan).

validate a method of obtaining *all* the HTP parameters from purely *ab initio* quantum-mechanical calculations.

Pressure broadening and shift parameters based on *ab initio* quantum-mechanical calculations have already been obtained for a number of systems [25,26], including CO-Ar [27–30]. In contrast, the complex Dicke parameter [31]  $\nu_{\text{opt}}$ , has so far been only obtained in this manner for the hydrogen molecule isotopologues in helium baths [32–34] and D<sub>2</sub>-D<sub>2</sub> [35], which are not representative of most systems relevant to atmospheric studies. Here, we derive a complete set of HTP parameters from *ab initio* calculations for the first time for an atmospherically relevant system, namely CO-Ar.

More specifically, we apply this approach to the two P(2) and P(8) CO-Ar fundamental band lines. We calculate pressure broadening and shift coefficients, and the complex Dicke parameter for a broad temperature range and provide thermally-averaged and quadratic-speed-dependent values of these parameters directly applicable to evaluation of the HTP. We establish the accuracy of the obtained pressure broadening and shift values by comparing them with the most accurate experimental values available, measured by Luo et al. [27] and Wehr et al. [30]. Further, we investigate the validity of the HTP approximations in several ways. First, we evaluate the model of velocity-changing collisions assumed in the HTP by comparing the HTP line shapes with the speed-dependent billiard ball profile (SDBBP) [36]. Second, we evaluate the quadratic approximation of the speed dependence of broadening and shift by directly comparing the *ab initio* and quadratic speed dependence of the parameters and by comparing the HTP line shapes calculated with *ab initio* and approximate speed dependence. Third, we examine the speed dependence of  $\nu_{\text{opt}}$  and the consequences of including it in the HTP. We also validate a procedure for obtaining quadratic-speed-dependent parameters from otherwise known temperature dependence of thermally-averaged parameters [37,38].

The theoretical framework is described in Section 2. The CO-Ar results are gathered in Section 3. Tests of validity of various approximations are presented in Section 4 before Section 5 that concludes.

## 2. Theoretical framework

The HTP is described by a set of seven parameters:

$$\text{HTP}(\Gamma_D, \Gamma_0, \Delta_0, \Gamma_2, \Delta_2, \nu_{\text{VC}}, \eta; \Delta\nu), \quad (1)$$

where  $\Gamma_D$  is the Doppler half-width,  $\Gamma_0$  is the pressure-broadened half-width at half-maximum (HWHM),  $\Delta_0$  is the pressure shift,  $\Gamma_2$  and  $\Delta_2$  are the quadratic-speed-dependent pressure broadening and shift,  $\nu_{\text{VC}}$  is the frequency of velocity-changing collisions and  $\eta$  is the correlation parameter. The argument,  $\Delta\nu$ , of the function is the detuning from the transition frequency. The pressure-independent equivalents of the five pressure-dependent parameters are defined as:  $\gamma_0 = \Gamma_0/p$ ,  $\delta_0 = \Delta_0/p$ ,  $\gamma_2 = \Gamma_2/p$ ,  $\delta_2 = \Delta_2/p$  and  $\tilde{\nu}_{\text{VC}} = \nu_{\text{VC}}/p$ .

The HTP is otherwise known as partially-correlated quadratic-speed-dependent hard-collision profile. The hard-collision profiles are usually derived by solving the classical Boltzmann transport-relaxation equation for the distribution function  $f(\mathbf{r}, \mathbf{v}_1, t)$  of the active molecule [13,39]. The arguments of the function are: the position  $\mathbf{r}$  and velocity  $\mathbf{v}_1$  of the active molecule, and time  $t$ . The spectral line shape profile is obtained from the distribution function through the Fourier-Laplace transform. The solution of the Boltzmann equation is determined by the collision operator, which is separated into two terms: a first one, corresponding to dephasing collisions [40], responsible for pressure broadening and shift, and a second one, corresponding to combined velocity-changing and dephasing collisions. This description results in the general shape of the resonances which is specialized to a particular absorber-perturber pair by the speed-dependent pressure

broadening and shift functions,  $\Gamma(\nu_1)$  and  $\Delta(\nu_1)$ , the frequency of velocity-changing collisions,  $\nu_{\text{VC}}$ , and the degree of correlation between those, through  $\eta$ . These four parameters are determined by the nature of absorber-perturber collisions, and provide a way to introduce precise *ab initio* quantum scattering calculations into the determination of line shapes.

### 2.1. Broadening, shift and their dependence on speed

Since the seminal works of Baranger [41–43], Fano [44] and Ben-Reuven [45,46] the formulas for spectroscopic cross sections are well known. They rely on expressing spectral lines as Liouville space elements and pressure broadening and shift coefficients as diagonal matrix elements of the relaxation operator in the line basis. For a diatomic molecule of mass  $m_1$  perturbed by an atom of mass  $m_2$  such elements are proportional to generalized cross sections given by:

$$\begin{aligned} \sigma_{\lambda=0}^q(\nu_a, j_a, \nu_b, j_b; E_{\text{kin}}) &= \frac{\pi}{k^2} \sum_{J_a, J_b, l, l'} [J_a][J_b] (-1)^{l-l'} \\ &\times \begin{Bmatrix} j_a & q & j_b \\ J_b & l & J_a \end{Bmatrix} \begin{Bmatrix} j_a & q & j_b \\ J_b & l' & J_a \end{Bmatrix} \\ &\times \left( \delta_{ll'} - S^{*j_b}(\nu_b, j_b, l'; \nu_b, j_b, l) S^j(\nu_a, j_a, l'; \nu_a, j_a, l) \right), \end{aligned} \quad (2)$$

where  $J_a, J_b$  are total angular momenta,  $l, l'$  are orbital angular momenta and  $\nu_a, j_a, \nu_b, j_b$  are initial and final rovibrational quantum numbers of the diatomic before and after the optical transition.  $\{ : : \}$  is the 6-j symbol,  $[x]$  stands for  $(2x+1)$ ,  $q$  denotes the tensor order of the optical transition and  $\lambda$  denotes the rank of the molecular velocity tensor associated with the cross section. For electric dipole transitions considered in this article  $q=1$  and for the dephasing cross section  $\lambda=0$ . S-matrix elements are expressed in the total angular momentum coupling scheme for fixed kinetic energy  $E_{\text{kin}}$ . The magnitude of the wavevector  $k$  is determined by the relative center-of-mass kinetic energy  $k^2 = 2\mu E_{\text{kin}}/\hbar^2$ , where  $\mu = m_1 m_2 / (m_1 + m_2)$  is the reduced mass of the system. Subsequently, the  $j$  and  $\nu$  indices will be omitted for brevity. Similarly, all the HTP line-shape parameters, Eq. (1), are implicit functions of temperature  $T$ , through energy dependence of  $\sigma_{\lambda=0}^q(E_{\text{kin}})$  averaged over Maxwell-Boltzmann distribution, but in the following the argument  $T$  will be omitted, e.g.  $\Gamma_0 \equiv \Gamma_0(T)$ . The formulas are given for line-shape parameters expressed in units of angular frequency. The thermally-averaged parameters at a given concentration of the perturbing atom,  $n$ , are obtained from the following expression [47,48]:

$$\Gamma_0 - i\Delta_0 = n \langle \nu_r \rangle \langle \sigma_{\lambda=0}^q(E_{\text{kin}} = \mu \nu_r^2 / 2) \rangle, \quad (3)$$

where  $\langle \nu_r \rangle = \sqrt{8k_B T / \pi \mu}$  is the mean relative speed and  $\langle \dots \rangle$  denotes integration over the Maxwell-Boltzmann energy distribution,

$$\langle \sigma_{\lambda=0}^q(E_{\text{kin}}) \rangle = \left( \frac{1}{k_B T} \right)^2 \int_0^\infty E_{\text{kin}} \sigma_{\lambda=0}^q(E_{\text{kin}}) e^{-\frac{E_{\text{kin}}}{k_B T}} dE_{\text{kin}}. \quad (4)$$

The speed-dependent parameters are obtained by averaging the cross sections over the distribution function  $f(\nu_r | \nu_1)$  of relative velocity  $\nu_r$  with respect to the absorber velocity  $\nu_1$  at a given  $T$  [49]:

$$\Gamma(\nu_1) - i\Delta(\nu_1) = n \int_0^\infty \nu_r \sigma_{\lambda=0}^q(E_{\text{kin}} = \mu \nu_r^2 / 2) f(\nu_r | \nu_1) d\nu_r. \quad (5)$$

The obtained *ab initio* parameters are used to determine the quadratic-speed-dependent parameters (see Eq. (A.7)),  $\Gamma_2, \Delta_2$ , by requiring the derivatives of both *ab initio* and quadratic speed dependence to be equal at the most probable speed of the active

molecule  $v_p = \sqrt{2k_B T/m_1}$ , hence:

$$\Gamma_2 = \frac{v_p}{2} \frac{d}{dv} \Gamma(v_1) \Big|_{v_1=v_p} \quad (6)$$

### 2.2. The complex Dicke parameter

In the framework of the classical Boltzmann equation the physics of velocity-changing collisions and their effect on the line shape is encapsulated in the probability rate  $A(v_1', v_1)$ , describing the probability per unit time for velocity change  $v_1' \rightarrow v_1$  of the absorber to occur. In order to obtain a closed-form solution, permitting fast evaluation of the line shape, a simplifying assumption is made. It assumes that the effect of a collision is independent of the initial collision velocity and that the final velocity is determined only by the frequency of velocity-changing collisions  $\nu_{VC}$  and the equilibrium velocity distribution  $f_{MB}(v_1)$ , i.e.,  $A(v_1', v_1) = \nu_{VC} f_{MB}(v_1)$ ; this assumption leads to the familiar hard-collision model.

The separate treatment of confinement narrowing, collisional broadening and shift depends on the assumption that the associated velocity-changing and dephasing collisions occur independently. If velocity-changing collisions are correlated with dephasing collisions, then the  $\nu_{VC}$  frequency is replaced by the  $\nu_{opt}$  frequency which is in general smaller than  $\nu_{VC}$ . The reason for this substitution is that the  $\nu_{VC}$  frequency includes velocity changes of the part of optical coherence which was damped (or phase-shifted) by dephasing collisions. The HTP's hard collision model takes into account this effect by defining  $\nu_{opt}$  as

$$\nu_{opt}^{HTP}(v_1) = \nu_{VC} - \eta[\Gamma(v_1) + i\Delta(v_1)]. \quad (7)$$

In Eq. (7),  $\eta$  is a phenomenological correlation parameter and  $\nu_{VC}$  is the constant frequency of velocity-changing collisions from the uncorrelated model. The imaginary part of  $\nu_{opt}$  leads to an asymmetry of the profile distinct from the asymmetry caused by the speed dependence of pressure shift.

Similarly to pressure broadening and shift coefficients, the complex Dicke parameter,  $\nu_{opt}$ , can be calculated from first principles, provided an accurate interaction potential is available. The theory of Hess [50,51] connects the developments of Baranger [41-43], Fano [44] and Ben-Reuven [45,46] with the quantum treatment of transport-relaxation phenomena [52,53]. In the resultant quantum Boltzmann-like kinetic equation the effect of correlated velocity-changing and dephasing collisions on the line shape is explicitly included and described in terms of the flow of the spectral transition operator through the gas. Within the generalized Hess method (GHM) [54], this leads to a definition of the cross section for velocity change of an optical coherence. A formula for this cross section in terms of S-matrix elements and in the case of an isolated line of a diatomic molecule perturbed by an atom is provided below [54-57]:

$$\begin{aligned} \sigma_{\lambda=1}^q(v_a, j_a, v_b, j_b; E) &= \frac{\pi}{k^2} \sum_{J_a J_b} [U_a][U_b] \sqrt{[l_a][l'_a][l_b][l'_b]} \\ &\times \begin{pmatrix} l_a & l_b & \lambda \\ 0 & 0 & 0 \end{pmatrix} \begin{pmatrix} l'_a & l'_b & \lambda \\ 0 & 0 & 0 \end{pmatrix} \begin{bmatrix} j_a & j_a & l_b & l'_b \\ j_b & l_a & j_b & l'_a \\ q & J_b & J_a & \lambda \end{bmatrix} \\ &\times i^{l'_a-l_a+l'_b-l_b} \left( \delta_{l_a l'_a} \delta_{l_b l'_b} - S^{j_b}(v_b, j_b, l'_b; v_b, j_b, l_b) \right) \\ &\times S^{j_a}(v_a; j_a, l'_a; v_a, j_a, l_a), \end{aligned} \quad (8)$$

the same notation as in Eq. (2) is used. In addition,  $(: : :)$  refers to the 3-j symbol and  $[: : : :]$  to the 12-j symbol of the second

kind [58]. Introducing the collision integrals,  $\omega_{\lambda}^{s,s'}(q)$ , as being the thermally averaged cross sections [56,57]:

$$\omega_{\lambda}^{s,s'}(q) = \langle v_r \rangle \int_0^{\infty} x^{(s+s'+2)/2} e^{-x} \sigma_{\lambda}^q(E_{kin} = xk_B T) dx, \quad (9)$$

the thermally-averaged frequency  $\nu_{opt}$  is defined by

$$\nu_{opt}^{GHM} = nM_2 \left[ \frac{2}{3} \omega_1^{11}(q)^* - \omega_0^{00}(q)^* \right], \quad (10)$$

with  $M_i = m_i/(m_1 + m_2)$ . Clearly, for  $s = s' = 0$  and  $\lambda = 0$  we retrieve the results from the earlier theories and  $n\omega_0^{00}(q) = \Gamma_0 - i\Delta_0$ , see Eq. (3).

The form of  $\nu_{opt}$  assumed by the HTP, Eq. (7), is different from the one in the GHM, Eq. (10). Eq. (7) defines  $\nu_{opt}$  as a function of absorber's speed and restricts  $\nu_{VC}$  to real values. We obtain the values of  $\nu_{VC}$  and  $\eta$  by requiring the thermally-averaged value of  $\nu_{opt}^{HTP}(v_1)$  to be equal to  $\nu_{opt}^{GHM}$ , which implies the following relations:

$$\nu_{VC} = \text{Re } \nu_{opt}^{GHM} + \eta \Gamma_0, \quad (11)$$

$$\eta = - \frac{\text{Im } \nu_{opt}^{GHM}}{\Delta_0}. \quad (12)$$

Together with the speed-dependent broadening  $\Gamma(v_1)$  and shift  $\Delta(v_1)$ , obtained according to Eq. (5), this indirect identification of the HTP parameters,  $\nu_{VC}$  and  $\eta$ , enables evaluation of the HTP based on quantum mechanical calculations.

### 3. Results for Ar-perturbed CO lines

*Ab initio* calculations of spectroscopic cross sections require a potential describing the interaction between the active molecule and the perturber molecule. In the case of CO and Ar, i.e. a diatomic molecule and a structureless atom, the interaction potential is expressed as a function of the distance  $R$  between the CO center of mass and the Ar atom, the distance  $r$  between C and O atoms, and the angle  $\theta$  between the corresponding vectors  $\mathbf{R}$  and  $\mathbf{r}$ . In the current calculations, we used the potential of Sumiyoshi and Endo [59], which was expanded in the basis of Legendre polynomials [60] up to 10th order. The extent of values for the CO bond length determined in [59], namely 1.0 to 1.35 Å, covered 99.98% of the squared wave function amplitude of the upper vibrational state (for a non-rotating,  $j = 0$ , CO), which from our experience can be considered as sufficient for accurate calculations of  $\nu = 0 \rightarrow 1$  transitions.

The S-matrix calculations were performed with the MOLSCAT code [61] and its implementation of the modified log-derivative propagator [62,63]. The grid of collision energies at which S-matrices were calculated was limited to  $1700 \text{ cm}^{-1}$  [64] and its density was adjusted to obtain smooth  $\sigma_{\lambda}^q$  curves, with denser sampling at low collision energies and sparser sampling at high collision energies. Fig. 1 shows the spectroscopic cross sections for the P(2) and P(8) lines with insets for collision energies below the potential well depth i.e. below  $107.1 \text{ cm}^{-1}$ . A power-law dependence was used to fit cross sections, see Eq. (A.4), ignoring low-energy points. For  $\text{Re}(\sigma_0^1)$ ,  $\text{Re}(\sigma_1^1)$  the cut off was set at  $50 \text{ cm}^{-1}$ , for  $\text{Im}(\sigma_0^1)$  it was set at  $100 \text{ cm}^{-1}$ , and for  $\text{Im}(\sigma_1^1)$  at  $200 \text{ cm}^{-1}$ . The cut offs for the fits of the real parts of cross sections were set to ignore low-energy points because they do not contribute significantly to Boltzmann integrals, Eqs. (4), (9), at most temperatures accessible to experiment and cause the fits to have different asymptotic limits than the *ab initio* data. For the imaginary parts of the cross sections, it was clear from visual inspection that the low-energy part could not be fitted well with a single power-law, therefore the limit was set even higher. The fitted values are provided in Table A.1 and were used for evaluation of hypergeometric

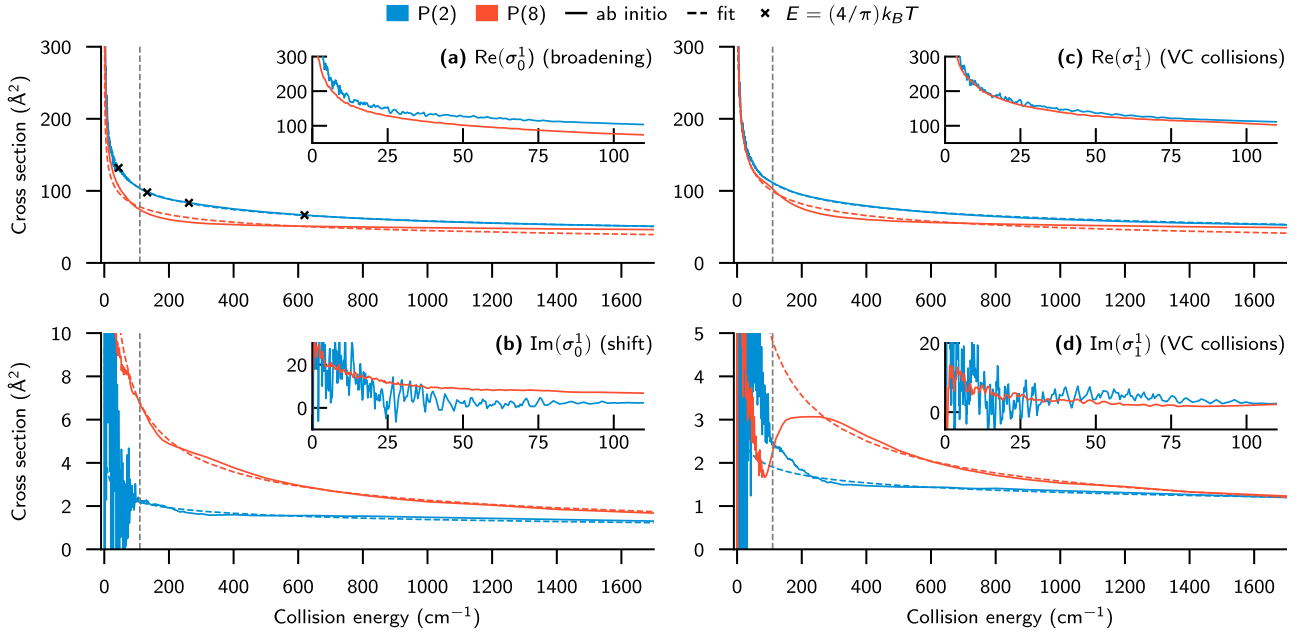


**Fig. 1.** Spectroscopic cross sections describing the effects of dephasing (a, b) and velocity-changing (c, d) collisions. Insets show the cross sections for collision energies below the potential well depth ( $107.1 \text{ cm}^{-1}$ ) and vertical dashed lines mark the well depth energy. The dashed lines show the fits of cross sections to power-law dependence from Eq. (A.4). The crosses in (a) mark the mean relative speed energies ( $= \frac{4}{\pi} \frac{k_B T}{\hbar c}$ ) corresponding to HITRAN reference temperatures: 50 K, 150 K, 296 K and 400 K.

speed dependence according to Eq. (A.6); all the other results presented in this paper are based on interpolated and extrapolated raw data, *i.e.* the solid lines in Fig. 1. The P(2) line cross sections at low collision energies exhibit strong signatures of Ar-CO resonances [65], which are much diminished for the P(8) line due to higher degree of centrifugal screening.

The cross sections were extrapolated to higher energies if necessary and interpolated with cubic B-splines, before performing the numerical integration of Eqs. (4), (5), (9). The upper limit of integration for thermal averaging at a given temperature, Eqs. (4), (9), was set by the 0.9999 quantile of  $\langle x^2 \exp(-x) \rangle$  distribution and the maximum absorber speed for which  $\gamma(v_1; T)$  (and  $\delta(v_1; T)$ ) was calculated was the 0.999 quantile of the Maxwell-Boltzmann speed distribution.

The calculations were carried out using the computer cluster of Institute of Physics of Rennes. The calculation time increases with increasing  $j_a$  value for a P( $j_a$ ) line due to increasing number of basis states. It amounts to a few hours for the P(2) line and up to a few days for, *e.g.* the P(14) line. The full determination of the line-shape parameters for all lines between rotational states populated at the considered temperatures would thus be in principle doable with only some more human time investment. However, since the purpose of the study is to demonstrate the general procedure and to investigate its broader implications, we restrict ourselves to the two P(2) and P(8) lines.

Table 1 presents the line-shape parameters obtained from *ab initio* calculations cast into parametrization of the HTP adopted in the 2016 edition of the HITRAN database. Pressure-independent HTP parameters,  $\gamma_0$ ,  $\delta_0$ ,  $\gamma_2$ ,  $\delta_2$ ,  $\tilde{\nu}_{VC}$ , were obtained in units of  $\text{cm}^{-1}/\text{atm}$  by evaluating Eqs. (3), (10) for  $n = n_0(T_0/T)$  and multiplying the result by  $(2\pi c)^{-1}$ , where  $n_0$  is the Loschmidt constant,  $T_0 = 273.15 \text{ K}$  and  $c$  is the speed of light in vacuum. The parameters are provided at four temperatures, together with coefficients allowing to approximate them at other temperatures with a linear function:  $\delta'_0$  (Eq. (A.2)), and with a power-law function:  $n_{\gamma_0}$  (Eq. (A.1)) and  $\kappa$  (Eq. (A.3)). The details of the approximation scheme are provided in Appendix A, following Ref. [38].

**Table 1**

HTP parameters of the P(2) and P(8) line within the parametrization adopted in the 2016 edition of HITRAN:  $\gamma_0$ , pressure half-width;  $n_{\gamma_0}$ , temperature dependence coefficient of  $\gamma_0$ ;  $\delta_0$ , pressure shift;  $\delta'$ , temperature dependence coefficient of  $\delta_0$ ;  $\gamma_2$ , speed-dependence of pressure half-width;  $\delta_2$ , speed-dependence of pressure shift;  $\tilde{\nu}_{VC}$ , frequency of velocity-changing collisions;  $\kappa$ , temperature dependence coefficient of  $\tilde{\nu}_{VC}$ ;  $\eta$ , correlation parameter. The parameters  $n_{\gamma_0}$ ,  $\kappa$  and  $\eta$  are dimensionless. All the other parameters are expressed in  $10^{-3} \text{ cm}^{-1}/\text{atm}$ . The approximation scheme for temperature dependence of the parameters is described in Appendix A.

Line	Param.	$T_{\text{ref}}$			
		50 K	150 K	296 K	400 K
P(2)	$\gamma_0$	252.2	109.8	65.68	34.16
	$n_{\gamma_0}$	0.760	0.754	0.759	0.758
	$\gamma_2$	31.02	14.16	8.494	4.268
	$\delta_0$	-8.61	-2.6	-1.48	-0.812
	$\delta'$	0.105	0.0156	0.0035	0.00103
	$\delta_2$	2.15	0.014	-0.14	-0.132
	$\tilde{\nu}_{VC}$	—	10.50	—	—
	$\kappa$	—	1.16	—	—
	$\eta$	—	-0.045	—	—
P(8)	$\gamma_0$	202.0	79.99	47.90	27.08
	$n_{\gamma_0}$	0.856	0.799	0.71	0.641
	$\gamma_2$	16.62	6.759	5.988	4.739
	$\delta_0$	-18.4	-6.76	-3.55	-1.51
	$\delta'$	0.19	0.043	0.0111	0.00297
	$\delta_2$	-1.15	-0.318	-0.113	0.00305
	$\tilde{\nu}_{VC}$	—	36.46	—	—
	$\kappa$	—	0.861	—	—
	$\eta$	—	0.231	—	—

Fig. 2 shows the *ab initio* (solid line) and approximate values (dashed line) of the HTP parameters. For the P(8) line  $\gamma_0$  values, the differences between *ab initio* and approximate values stay below 1% in the whole temperature range considered here. For the P(2) line the agreement is even better and discrepancies are not larger than 0.1%, except in the lowest temperature range, *i.e.* below 150 K. This can be seen to be consistent and indicative of how well the appropriate cross sections, see Fig. 1, themselves agree with the power-law dependence. The temperature dependence of  $\gamma_2$  is

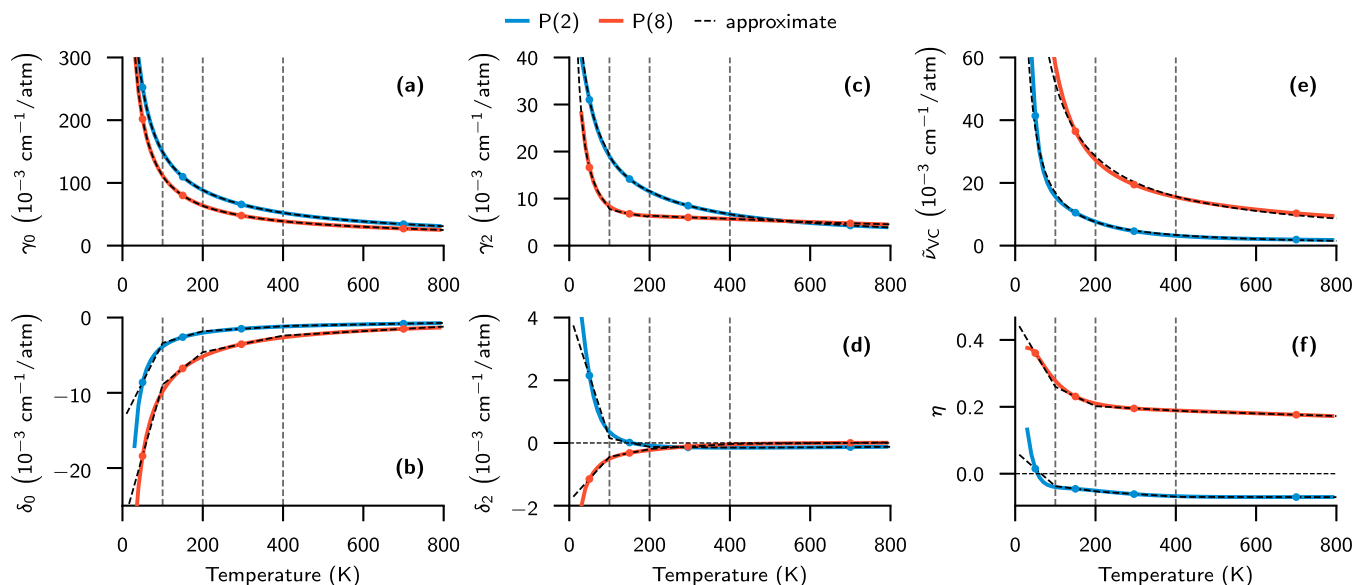


**Fig. 2.** Temperature dependence of pressure-independent line-shape parameters of P(2) and P(8) lines: (a) pressure half-width  $\gamma_0$ , (b) pressure shift  $\delta_0$ , (c) speed-dependence of pressure half-width  $\gamma_2$ , (d) speed-dependence of pressure shift  $\delta_2$ , (e) frequency of velocity-changing collisions  $\bar{\nu}_{VC}$ , (f) correlation parameter  $\eta$ . The vertical dashed lines delimit the temperature ranges and the circles mark the line-shape parameters at the reference temperatures defined in the 2016 edition of the HITRAN database. The black dashed curves show the results of applying linear approximation, Eq. (A.2), in panels (b, d, f) and power-law approximation, Eqs. (A.1), (A.3), in panels (a, c, e). The horizontal dashed lines in (d) and (f) mark the zero level.

not explicitly included in the 2016 edition of the HITRAN database, with only the values at reference temperatures being given, but it can also be seen in Fig. 2c that it is well described by power-law dependence. The approximate  $\gamma_2$  values match the *ab initio* values within 1% above 100 K for the P(2) line and above 200 K for the P(8) line, while at lower temperatures the discrepancies reach several percent for both lines. It should be noted at this point that the effect on the line shapes of these several-percent approximation errors of  $\gamma_2$  is negligible compared to the effect of the quadratic approximation itself. We fitted  $\bar{\nu}_{VC}$  values to a power law with exponent  $\kappa$  in the whole temperature range based on the reference value of  $\bar{\nu}_{VC}$  evaluated at 150 K. The error of approximation is within 4% in the whole range for the P(2) line. For the P(8) line, the perfect agreement at the reference temperature worsens to 10% and 20% at higher and lower edges of temperature range, respectively. For both lines approximation errors of  $\delta_0$  stay below 10% and only increase beyond that value at temperatures below 100 K. For  $\delta_2$ , the relative error between the full quantum and the approximation is not a relevant quantity to discuss as  $\delta_2$  is close (or even equal) to zero. The approximated and reference  $\delta_2$  values differences are however found to be small and the error made when using the approximation would have a negligible influence on the actual line shape.

The spectroscopic cross sections used in Fig. 1 and in all subsequent calculations are available in the supplementary material [dataset] [66]. Also included are the HTP parameters for temperatures from 30 K to 800 K in step of 10 K, i.e. the data for solid lines in Fig. 2, and the contents of Table 1.

We estimate the accuracy of the calculations by comparing our  $\gamma_0$  and  $\delta_0$  values with the ones reported in [27,30]. Luo et al. [27] provided broadening and shift parameters for P and R branch transitions up to rotational level  $j = 24$ , whereas the overall more accurate results of Wehr et al. [30] are available only for P( $j_a$ ) lines with  $j_a = 1, 2, 5, 7, 10, 13, 16$ . Table 2 presents the comparison for the P(2) line at the experimental temperatures. The pressure broadening parameters  $\gamma_0$  were found to all agree at sub-percent level, but for pressure shifts  $\delta_0$  the observed discrepancies were larger, reaching to about 3% for two of the considered tempera-

**Table 2**

Comparison of pressure broadening  $\gamma_0$  and shift  $\delta_0$  coefficients calculated in this work and measured by Wehr et al. [30] for the P(2) line. The values in the table are in  $10^{-3} \text{ cm}^{-1}/\text{atm}$  unless specified differently in the parentheses.

Param.	T (K)	Wehr	Calc.	Diff.	Diff. (%)
$\gamma_0$	323.9	60.99(5)	61.34	-0.35	-0.57
	294.5	65.33(3)	65.94	-0.61	-0.93
	258.7	72.53(5)	72.75	-0.22	-0.30
	236.4	77.81(4)	77.89	-0.08	-0.10
	214.1	83.89(5)	83.95	-0.06	-0.07
$\delta_0$	323.8	-1.37(4)	-1.39	0.02	-1.38
	295.0	-1.46(2)	-1.49	0.03	-1.94
	258.7	-1.70(4)	-1.64	-0.06	3.24
	236.4	-1.82(3)	-1.77	-0.05	3.00
	214.0	-1.90(3)	-1.91	0.01	-0.68

tures. The shifts are in general considered more difficult to calculate accurately because of their higher sensitivity to the shape of the potential, slower convergence with total angular momentum  $J_{tot}$  and their lower absolute values. The last factor is especially important for the fundamental band transitions considered here, which are characterized by very weak pressure shifts. As an example of relatively slow convergence of  $\text{Im}(\sigma_0^1)$  with  $J_{tot}$ , at  $E_{kin} = 300 \text{ cm}^{-1}$  the required  $J_{tot}$  value for 1% accuracy was 328, but for  $\text{Re}(\sigma_0^1)$  it was only 109. Comparing the calculated pressure broadening of the P(8) line at 296 K equal to  $47.90 \times 10^{-3} \text{ cm}^{-1}/\text{atm}$  with the value of  $46.96 \times 10^{-3} \text{ cm}^{-1}/\text{atm}$  measured by Luo et al. [27], we see a discrepancy of 2%, which is to be expected considering that broadening of other transitions measured both by Luo et al. [27] and Wehr et al. [30] was found to be underestimated by the former by a similar amount. Because the variations in pressure shift of P-branch lines for  $j_a$  values between 7 to 13 are smaller than 1% [30], which is less than the disagreement between  $\delta_0$  values of Luo et al. [27] and Wehr et al. [30], we compare our value of P(8) line pressure shift of  $-3.56 \times 10^{-3} \text{ cm}^{-1}/\text{atm}$  with the pressure shift of the P(7) line from Ref. [30] equal to  $-3.51 \times 10^{-3} \text{ cm}^{-1}/\text{atm}$ . The difference between these values is

–1.4%, which confirms the accuracy of our calculated pressure shift coefficient for the P(8) line.

#### 4. Validity of the HTP approximations

##### 4.1. Validity of the quadratic approximation

Fig. 3 shows the *ab initio* speed dependence of the line-shape parameters and their approximation (see Appendix A) with quadratic and hypergeometric functions at 296 K. The quadratic speed dependence was derived from *ab initio* dependence based on Eq. (6) and the hypergeometric speed dependence was obtained with Eq. (A.6) from power-law fits of spectroscopic cross sections shown in Fig. 1. As described in Appendix A, Eq. (A.4), different power-law dependencies of spectroscopic cross sections on collision energy give rise to different speed dependence of pressure broadening and shift. Quadratic speed dependence of  $\Gamma(v_1)$ ,  $\Delta(v_1)$  is associated with square-root energy dependence of cross sections, whereas hypergeometric speed dependence allows for an arbitrary exponent in power-law dependence. As evidenced by the fitted exponents provided in Table A.1, square-root law ( $\alpha = 1/2$  in Eq. (A.4)) would fail at modeling the cross sections in Fig. 1. Hypergeometric model can be therefore expected to better account for speed dependence of broadening and shift. For the P(2) line broadening this improvement is confirmed, but for the P(8) line broadening the quadratic model better matches the *ab initio* data. For line shifts the situation is reverse. This shows that better physical justification of the power law [67] and more accurate modeling of  $\sigma_{\lambda}^q(E)$  cross sections it offers, does not simply translate to improved performance of the hypergeometric model over the quadratic model. The work of Lance et al. [68] on  $C_2H_2$ -Xe line shapes and the recent developments by Gamache and Vispoel [69] suggest that a sum of hypergeometric functions or a higher order polynomial model would be required to unequivocally im-

**Table 3**

Integrated absolute-value percent differences between *ab initio*, quadratic (quad) and hypergeometric (hg) speed dependence. The residuals were weighted by Maxwell-Boltzmann speed distribution and divided by thermally-averaged values of the parameters at 296 K. All the values are given in percents.

Param.	P(2)		P(8)	
	quad	hg	quad	hg
$\gamma$	2.8	0.2	0.8	1.5
$\delta$	0.8	3.0	1.7	1.6

prove on the quadratic approximation. The level of disagreement between different models is quantified and summarized in Table 3.

In order to study the influence of the quadratic approximation on the line shapes, we have simulated several profiles, see Fig. 4. The three selected pressures – 10, 40 and 300 Torr – correspond to  $\Gamma_0/\Gamma_D$  ratios of about 0.13, 1.0, 3.9. The top panel shows the SDBBP with *ab initio* speed dependence (aiSDBBP), which we treat here as the reference line-shape model following its success in describing the line shapes of a variety of molecular systems, see references in [26], and CO-Ar in particular [29]. The remaining profiles are: HTP (qHTP), HTP with *ab initio* speed dependence (aiHTP) and SDBBP with quadratic speed dependence (qSDBBP). The top panel profiles and profile differences in lower panels are normalized to the peak value of aiSDBBP at each pressure. The lack of appreciable differences between aiHTP – aiSDBBP and qHTP – qSDBBP curves shows that the differences between quadratic and *ab initio* speed dependence are not large enough to affect the comparison between hard-collision and billiard ball model. That is to say, the effects of quadratic and hard-collision approximations are additive and considering them separately here is justified. The differences (qHTP–aiHTP) between the quadratic HTP and *ab initio* HTP obtained using the HTP in conjunction with Eqs. (5) and (6) exhibit the expected increase with increasing pressure and qualitatively

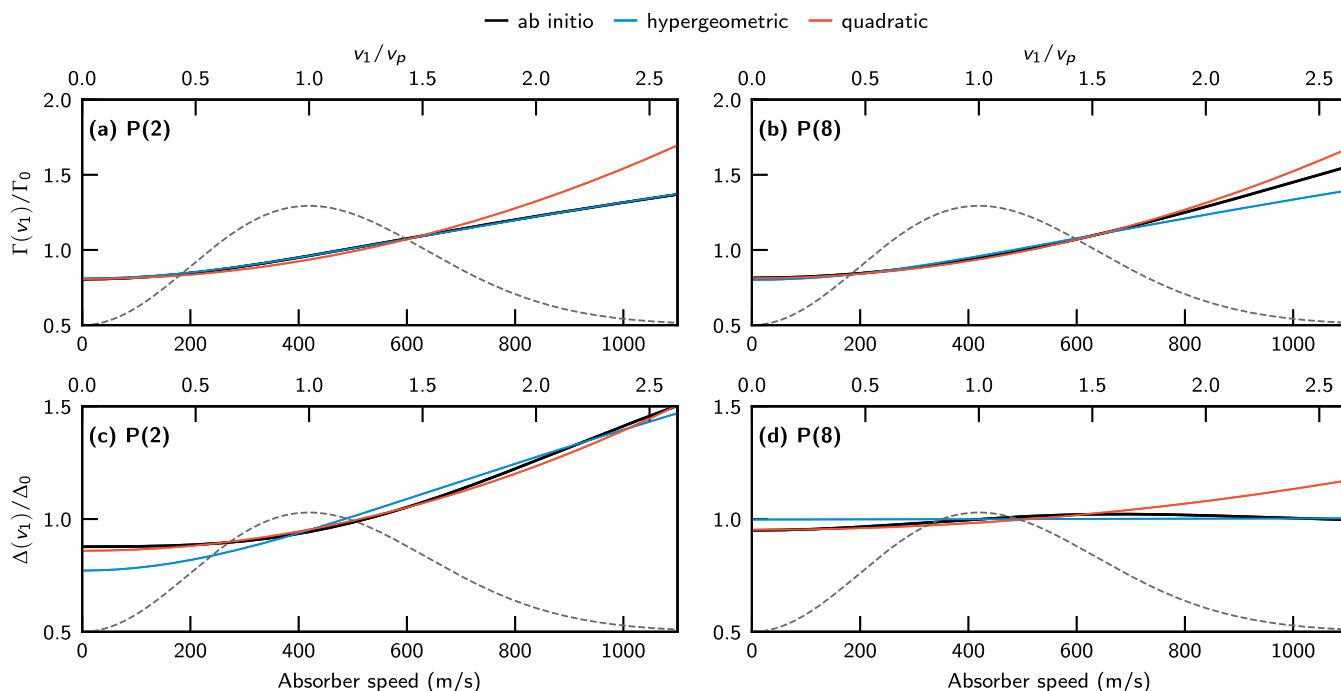


**Fig. 3.** Speed-dependent broadening and shift of P(2), (a, c), and P(8), (b, d), lines at 296 K. Black lines show the speed dependence obtained by evaluating Eq. (5) directly on the cross sections; blue lines show the hypergeometric speed dependence described by Eq. (A.6) evaluated with power-law fit coefficients from Table A.1; red lines show quadratic speed dependence described by Eq. (A.7) evaluated with coefficients obtained from Eq. (6). On panel (a) the black and blue curves overlap and are indistinguishable. Maxwell-Boltzmann speed distribution of CO at 296 K is shown as a dashed curve. (For interpretation of the references to colour in this figure legend, the reader is referred to the web version of this article.)

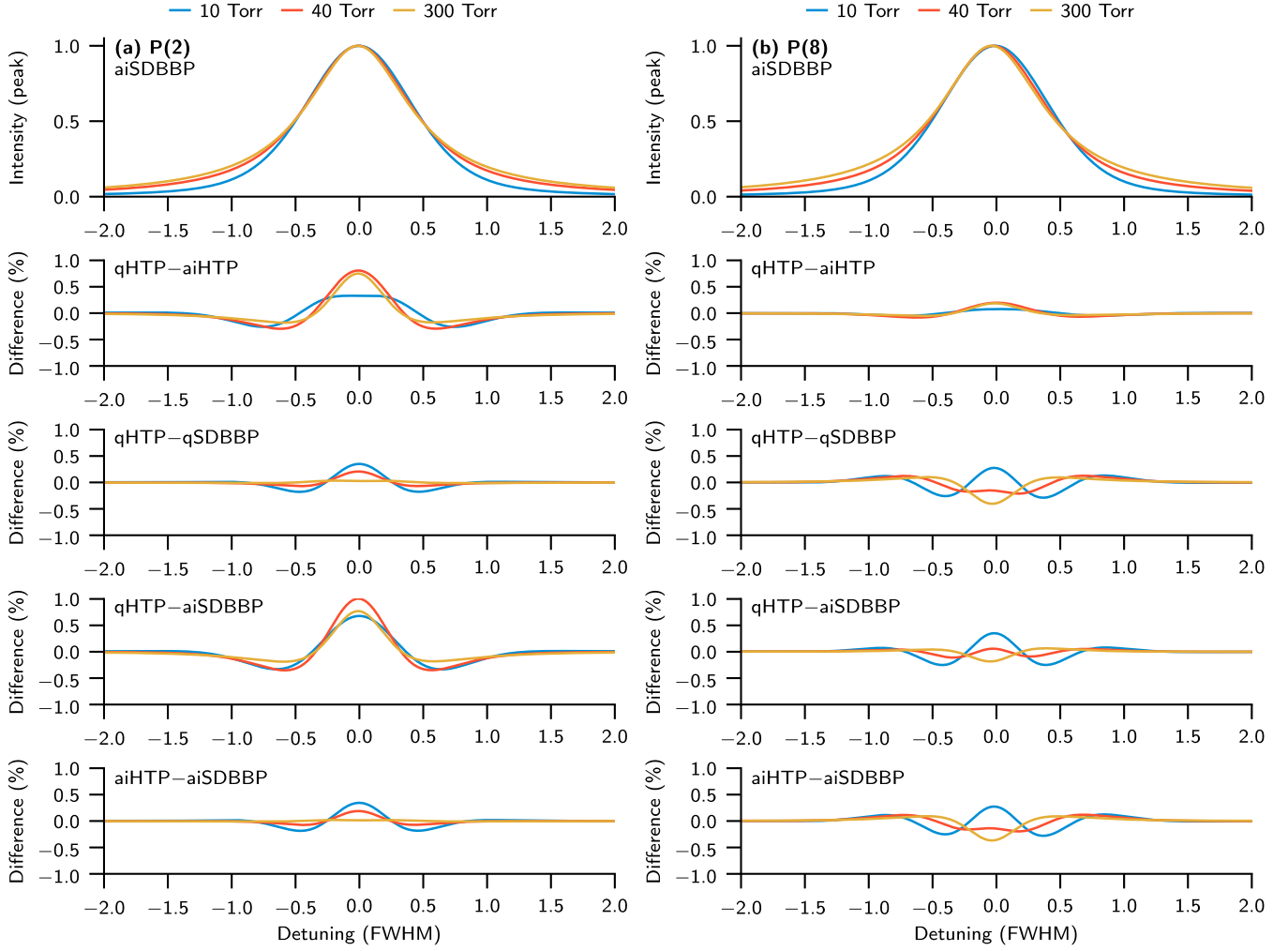


**Fig. 4.** P(2) line (left column) and P(8) line (right column) simulated line-shape profiles at 296 K. Top row shows the SDBBP with *ab initio* speed dependence (aiSDBBP) normalized to the peak value of the profile at each pressure. Lower rows show the differences between HTP (qHTP), HTP with substituted *ab initio* speed dependence (aiHTP), SDBBP with quadratic speed dependence (qSDBBP) and aiSDBBP. The differences between profiles were normalized by dividing them by the peak value of aiSDBBP profile at the same pressure. The frequency axis in each plot is in units of full-width at half-maximum (FWHM) of the aiSDBBP.

follow the results from Table 3; the P(8) line speed dependence is more faithfully modeled by quadratic speed dependence than the P(2) line. Notably, for the P(8) line the combined effect of quadratic and hard-collision approximations reduces the residuals relative to only hard-collision approximation, see the qHTP–aiSDBBP curve, showing strong correlation between  $\Gamma_2$  and  $\nu_{VC}$ . The accuracy of the quadratic approximation is on the order of a single percent, which is similar to the level of disagreement between hard-collision and billiard ball models (qHTP–qSDBBP). This shows that for these CO-Ar lines a more accurate description of both effects would be required for an overall better agreement with *ab initio* line shapes.

#### 4.2. Validity of the approximation of the velocity-changing model

The HTP, GHM profile and SDBBP can all be derived by using the generalized Waldmann-Snyder equation [50] to express the molecular line shape in terms of  $\phi(\omega, \mathbf{v}_1)$ , the velocity distribution of the optical coherence associated with the transition:

$$f_{MB}(\mathbf{v}_1) = [-i(\omega - \omega_0 - \mathbf{k} \cdot \mathbf{v}_1) - \hat{S}] \phi(\omega, \mathbf{v}_1), \quad (13)$$

where  $f_{MB}(\mathbf{v}_1)$  is the equilibrium (Maxwell) velocity distribution,  $\mathbf{k} \cdot \mathbf{v}_1$  describes the Doppler shift and  $\omega$ ,  $\omega_0$  are, respectively, the angular frequency of the incident radiation and of the transition.

In both the uncorrelated hard-collision model and the SDBBP the collision operator is of the form:

$$\hat{S} = -\Gamma(v_1) - i\Delta(v_1) + \nu_{VC}\hat{M}, \quad (14)$$

where  $\hat{M} \equiv \hat{M}_{BB}$  is the hard-sphere kernel (billiard-ball kernel) for the SDBBP and  $\hat{M} \equiv \hat{M}_{HC}$  is the hard-collision kernel. Analogously to the correlated hard-collision model, see Section 2.2, the influence of velocity-changing and dephasing collisions can be taken into account in the billiard ball model by substituting  $\nu_{VC}$  with  $\nu_{opt}$ . In this case, both the SDBBP and HTP collision operator can be expressed as:

$$\hat{S} = -\Gamma(v_1) - i\Delta(v_1) + \nu_{opt}\hat{M}. \quad (15)$$

In the GHM, the collision operator is given by:

$$\hat{S}\phi(\omega, \mathbf{v}_1) = -\omega_A \langle \phi(\omega, \mathbf{v}_1) \rangle - \omega_R [\phi(\omega, \mathbf{v}_1) - \langle \phi(\omega, \mathbf{v}_1) \rangle], \quad (16)$$

where  $\langle \dots \rangle$  denotes integration over  $f_{MB}(\mathbf{v}_1)$ ,  $\omega_A = \Gamma_0 + i\Delta_0$  and  $\omega_R$  is a complex coefficient chosen to minimize the error of approximating the collision operator by only two complex numbers. In order to obtain a closed-form formula for  $\omega_R$ , the coefficient is expanded in powers of  $\mathbf{k} \cdot \mathbf{v}_1$  and the expansion is truncated to retain only the first-order term in  $\mathbf{k}$ . This leads to identification of  $\omega_R$  with the collision integral for the flow of optical coherence, which

in terms of  $\omega_0^{00}(q)$  and  $\omega_1^{11}(q)$ , Eq. (9), is given by:

$$\omega_R = n \left[ \frac{2}{3} M_2 \omega_1^{11}(q)^* + M_1 \omega_0^{00}(q)^* \right]. \quad (17)$$

Reducing  $\omega_R$  to a term linear in concentration also results in a closed-form solution of Eq. (13) with the GHM collision operator, Eq. (16). The GHM line-shape profile is formally equivalent [32] to speed-independent HTP, i.e. correlated Rautian-Sobel'man profile. With  $\nu_{\text{opt}}^{\text{GHM}}$  defined as  $\nu_{\text{opt}}^{\text{GHM}} = \omega_R - \omega_A$ , leading to Eq. (10), this equivalence allowed us to identify the GHM line-shape parameters with  $\Gamma_0$ ,  $\Delta_0$  and  $\nu_{\text{opt}}$  parameters and express in their terms the  $\nu_{\text{VC}}$  and  $\eta$  parameters used in the HTP, Eqs. (11), (12). Using the same  $\nu_{\text{opt}}^{\text{GHM}}$  in both SDBBP and HTP lets us directly compare the effects of different treatments of velocity-changing collisions on the line shapes via different kernels  $\hat{M}$ . Contrary to the hard-collision model of the HTP, the billiard ball kernel is based on the actual interaction potential, depends on the perturber-to-absorber mass ratio, pre-collision velocity and the scattering angle, and has been shown previously to describe well the velocity-changing collisions of CO and Ar [29]. Eq. (13) is solved numerically in SDBBP, either with a simple diagonalization method [70] or with an iterative method [71].

Velocity-changing collisions interrupt the free molecular flow of the absorber and cause a reduction of the Doppler width. Additionally, they homogenize the speed distribution of the absorber, leading to a reduced influence of speed-dependent broadening and shift on the line-shapes [72]. In the two lowest pressures shown in Fig. 4, 10 Torr and 40 Torr, the dominant effect is the reduction of the Doppler width. The panels in Fig. 4 labeled qHTP–qSDBBP quantify the difference in modeling the Dicke effect by the two profiles. Despite a large difference between  $\tilde{\nu}_{\text{VC}}$  values for the two lines,  $19.5 \times 10^{-3} \text{ cm}^{-1}/\text{atm}$  for the P(8) line and  $4.61 \times 10^{-3} \text{ cm}^{-1}/\text{atm}$  for the P(2) line, the amplitudes of line-shape profile differences are close to each for both lines. The large difference between these  $\tilde{\nu}_{\text{VC}}$  values does not indicate the relative strength of the Dicke effect but it is an artifact of the adopted procedure for obtaining  $\nu_{\text{opt}}^{\text{HTP}}(\nu_1)$  from  $\nu_{\text{opt}}^{\text{GHM}}$ , Eqs. (11), (12). Indeed, the parameter actually determining the degree of collisional narrowing in the HTP is  $\text{Re } \nu_{\text{opt}}^{\text{GHM}}(\nu_1) = \nu_{\text{VC}} - \eta \Gamma(\nu_1)$ , whose speed-averaged value is equal to  $8.49 \times 10^{-3} \text{ cm}^{-1}/\text{atm}$  for the P(2) line and  $9.99 \times 10^{-3} \text{ cm}^{-1}/\text{atm}$  for the P(8) line.

At the highest plotted pressure, 300 Torr, the Doppler width is completely reduced and the differences between qHTP and qSDBBP profiles are indicative of the strength of the competition between dephasing and velocity-changing collisions [72]. HTP is known to overestimate the effect of velocity-changing collisions and with the speed-dependent broadening in CO-Ar narrowing the lines, this should lead to the qHTP lines being broader than the qSDBBP lines. This effect is found to be negligible for the P(2) line and clearly visible for the P(8) line. The contrast between the lines is surprising, considering that the  $\gamma_2$  values, see Table 1, and the  $\langle \text{Re } \nu_{\text{opt}}^{\text{HTP}}(\nu_1) \rangle$  values are similar for both lines. We have found the reason for the excessive broadening to be the speed dependence of  $\nu_{\text{opt}}$  introduced into the HTP by the  $\eta$  parameter. Evaluating the HTP with speed-independent  $\nu_{\text{opt}}$  reduced the peak-to-peak differences for the P(8) line at 300 Torr to 0.13%.

Close analysis of the definition of  $\omega_R$  reveals the interpretation of the  $\eta$  parameter within the GHM. The decomposition of  $\omega_R$  given by Eq. (17) into two terms, one of them proportional to  $\omega_0^{00}(q)$  and the other one to  $\omega_1^{11}(q)$ , comes from the fact that the  $\omega_R$  collision integral is associated with the molecular velocity vector, which can be expressed as a combination of center-of-mass velocity and relative velocity vectors. The part associated with relative motion, viz.  $(2/3)M_2\omega_1^{11}(q)$ , is responsible for the velocity-changing contribution to the  $\omega_R$  integral, whereas the part associated with center-of-mass motion,  $M_1\omega_0^{00}(q)$ , cannot contribute to

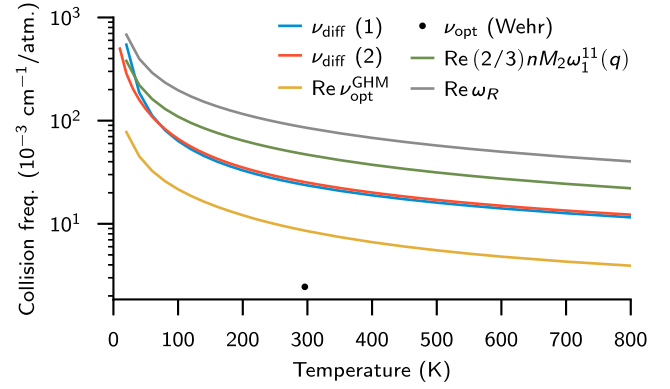


Fig. 5. Comparison between collision frequencies for the P(2) line:  $\nu_{\text{diff}}(1)$  (blue), calculated from the classical model of Boushehri et al. [73] for the mass diffusion constant  $D$ ;  $\nu_{\text{diff}}(2)$  (red), based on quantum dynamics on isotropic part of the interaction potential [59];  $\text{Re } \nu_{\text{opt}}^{\text{GHM}}$  from Eq. (10) (yellow);  $\nu_{\text{opt}}$  from Wehr's [29] SDBBP fits (black circle); the contribution to  $\text{Re } \nu_{\text{opt}}^{\text{GHM}}$  from the  $\omega_1^{11}(q)$  integral (green); the  $\text{Re } \omega_R$  frequency from Eq. (17) (gray). (For interpretation of the references to colour in this figure legend, the reader is referred to the web version of this article.)

velocity changes and it is responsible for the dephasing contribution [74,75]. Expressing  $\nu_{\text{opt}}^{\text{GHM}}$ , Eq. (10), in terms of  $\Gamma_0 + i\Delta_0$ ,

$$\nu_{\text{opt}}^{\text{GHM}} = (2/3)nM_2(\omega_1^{11}(q))^* - M_2(\Gamma_0 + i\Delta_0), \quad (18)$$

and comparing it to Eq. (7) for  $\nu_{\text{opt}}^{\text{HTP}}$ , we can associate the HTP parameters  $\nu_{\text{VC}}$  and  $\eta$  with the quantities defined within the quantum-mechanical GHM method. The frequency of velocity-changing collisions  $\nu_{\text{VC}}$  corresponds to the complex conjugate of  $(2/3)nM_2\omega_1^{11}(q)$  and the correlation parameter  $\eta$  to  $M_2$ . The GHM identification shows the  $\eta = M_2$  parameter to be a purely kinetic factor, which is the same for all the lines for a given absorber-perturber pair and which does not account for all the correlation between velocity-changing and dephasing collisions. The GHM distinguishes a dephasing-only contribution in the form of  $\omega_A = \Gamma_0 + i\Delta_0$  but no analogous velocity-changing-only contribution is defined, since both  $\omega_1^{11}(q)$  and  $\nu_{\text{opt}}^{\text{GHM}}$  also contain a dephasing contribution. It is worth noting that in the case of CO-Ar adopting the value of  $M_2 = 0.59$  as that of  $\eta$  would lead to larger speed dependence of  $\nu_{\text{opt}}^{\text{HTP}}(\nu_1)$ , Eq. (7), and larger deviations of HTP high-pressure line shapes from SDBBP line shapes.

Similarly as in [32] for the H<sub>2</sub>-He system, Fig. 5 presents the temperature dependence of the collision frequencies involved in describing the effects of velocity-changing collisions on spectral line shapes.  $\nu_{\text{diff}}(1)$  is the velocity-changing collision frequency deduced from the mass diffusion coefficient  $D$ :

$$\nu_{\text{diff}} = \frac{\nu_p^2}{2D}, \quad (19)$$

for which the value of  $D$  was calculated based on the classical model and reference data of Boushehri et al. [73].  $\nu_{\text{diff}}(2)$  was obtained from quantum scattering calculation of momentum-transfer cross section on the isotropic part of the CO-Ar interaction potential [59] in the vibrational ground state, i.e. by evaluating Eq. (8) for CO treated as a structureless particle scattered by an isotropic potential. The  $\nu_{\text{opt}}$  value (black circle) is the one obtained by Wehr et al. [29] from SDBBP fits to experimental data, labeled as  $\nu$  in [29]. The GHM collision frequencies,  $\text{Re } \nu_{\text{opt}}^{\text{GHM}}$ ,  $\text{Re } \omega_R$  and  $\text{Re } (2/3)nM_2\omega_1^{11}(q)$ , were calculated as described in the current article. Contrary to the results for H<sub>2</sub>-He [32–34], we see a clear difference between the plotted collision frequencies, illustrating that these are distinct quantities. Both  $\text{Re } \omega_R$  and  $\text{Re } (2/3)nM_2\omega_1^{11}(q)$  frequencies are significantly larger than  $\nu_{\text{diff}}(1)$  and  $\nu_{\text{diff}}(2)$ , owing to both the small rotational constant of CO and anisotropy of

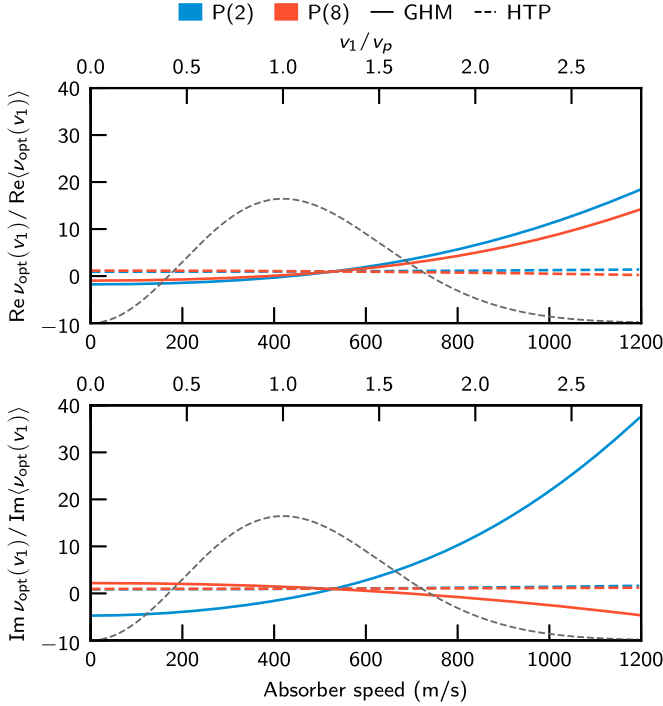


**Fig. 6.** Relative speed-dependence of GHM and HTP complex Dicke parameters at 296 K. Blue and red lines correspond to, respectively, P(2) and P(8) transitions. Solid lines show the values for  $v_{\text{opt}}(v_1) \equiv v_{\text{opt}}^{\text{GHM}}(v_1)$ , Eq. (21), and dashed lines for  $v_{\text{opt}}(v_1) \equiv v_{\text{opt}}^{\text{HTP}}(v_1)$ , Eq. (7).  $\langle v_{\text{opt}}(v_1) \rangle$  is the Maxwell–Boltzmann speed average of the complex Dicke parameter with  $\langle v_{\text{opt}}^{\text{GHM}}(v_1) \rangle = \langle v_{\text{opt}}^{\text{HTP}}(v_1) \rangle$ . The Maxwell–Boltzmann speed distribution of CO at 296 K is shown as a gray dashed curve. (For interpretation of the references to colour in this figure legend, the reader is referred to the web version of this article.)

CO–Ar potential increasing the rate of collisional dephasing as compared to H<sub>2</sub>–He. Compared to H<sub>2</sub>–He, the CO–Ar colliding system is closer to various atmospheric molecular systems when considering rotational constant values and anisotropy of the interaction potential. As a consequence the presented conclusions are expected to hold for these systems also. The  $\text{Re } v_{\text{opt}}^{\text{GHM}}$  frequency and  $v_{\text{opt}}$  frequency obtained from SDBBP fits were found to be much smaller than  $v_{\text{diff}}$ 's (see Fig. 5).

By analogy with the expression for speed-dependent broadening and shift, Eq. (5), we can formally define a speed-dependent collision integral  $\omega_1^{11}(q; v_1)$  as [34]:

$$\omega_1^{11}(q; v_1) = \frac{\mu}{k_B T} \int_0^\infty v_r^3 \sigma_{\lambda=1}^q(E_{\text{kin}} = \mu v_r^2/2) f(v_r|v_1) dv_r, \quad (20)$$

which can be used to define the speed-dependent  $v_{\text{opt}}^{\text{GHM}}(v_1)$  as:

$$v_{\text{opt}}^{\text{GHM}}(v_1) = \frac{2}{3} n M_2 \omega_1^{11}(q; v_1)^* - M_2 [\Gamma(v_1) + i\Delta(v_1)], \quad (21)$$

which properly reduces to thermally-averaged  $v_{\text{opt}}^{\text{GHM}}$  after integrating over absorber's speed distribution. Fig. 6 compares  $v_{\text{opt}}^{\text{GHM}}(v_1)$  defined in Eq. (21) and  $v_{\text{opt}}^{\text{HTP}}(v_1)$  defined in Eq. (7). The reason for the strong speed dependence of  $v_{\text{opt}}^{\text{GHM}}(v_1)$  as compared to  $\Gamma(v_1)$  or  $\Delta(v_1)$ , see Fig. 3, lies in the definition of the speed-dependent collision integral  $\omega_1^{11}(q; v_1)$ , which is independent of the specific molecular system under consideration. This is most apparent when comparing  $\text{Re } v_{\text{opt}}^{\text{GHM}}(v_1)$  and  $\Gamma(v_1)$  for the P(2) line. The cross section  $\text{Re } \sigma_1^1$  involved in determining  $\text{Re } \omega_1^{11}(q; v_1)$  and the cross section  $\text{Re } \sigma_0^1$  involved in determining  $\Gamma(v_1)$  are of similar magnitude for the P(2) line, see Fig. 1, but  $\text{Re } \sigma_0^1$  cross section is weighted by  $v_r$  in Eq. (5) whereas  $\text{Re } \sigma_1^1$  cross section is weighted by  $v_r^3$  in Eq. (20). This is also the main factor causing the large difference

between  $v_{\text{opt}}^{\text{HTP}}(v_1)$ , in which the speed-dependence is solely determined by the quantity  $\eta(\Gamma(v_1) + i\Delta(v_1))$ , and  $v_{\text{opt}}^{\text{GHM}}(v_1)$ . The speed dependence of  $v_{\text{opt}}^{\text{HTP}}(v_1)$  is additionally reduced relative to  $v_{\text{opt}}^{\text{GHM}}(v_1)$  because the value of  $\eta$  determined from Eq. (12) is smaller than that of  $M_2$ . A notable feature of  $\text{Re } v_{\text{opt}}^{\text{GHM}}(v_1)$  at low absorber speeds seen in Fig. 6 is its negativity, which makes it difficult to assign an intuitive physical interpretation to the quantity.

It has been noted previously by Pine [2] within the framework of classical Boltzmann equation that evaluating profiles based on the hard-collision model with speed-dependent  $v_{\text{opt}}$  invalidates the assumptions of the model, specifically the detailed balance for separate collision channels is not satisfied. Similarly, the  $\omega_R$  parameter in the GHM is in general dependent on velocity, but the closed-form formula is obtained only when it is taken to be a speed-independent collision integral, see Eq. (17). Considering additionally the obvious failure of  $v_{\text{opt}}^{\text{HTP}}(v_1)$  to reproduce the *ab initio* speed dependence, see Fig. 6, the incomplete accounting for correlations by the  $\eta$  parameter and the inconsistency between high-pressure HTP and SDBBP line shapes exacerbated by  $v_{\text{opt}}$ 's speed dependence, it seems more reasonable to evaluate the HTP with  $v_{\text{VC}}$  set to thermal average of the complex Dicke parameter  $v_{\text{opt}}^{\text{GHM}}$  and  $\eta$  set to zero.

#### 4.3. Quadratic speed dependence from temperature dependence

For a simple power-law dependence of pressure broadening and shift cross sections on relative speed (or collision energy), the thermally-averaged values of line-shape parameters and their speed dependence can be expressed analytically (see Appendix A) [67,68]. The resulting expressions can be manipulated to obtain approximate quadratic or hypergeometric speed-dependent parameters from the temperature dependence of averaged parameters, Eqs. (A.8), (A.9). These relations form the basis of the method proposed by Lisak et al. [37] to alleviate the problem of numerical correlation between  $\Gamma_2$ ,  $\Delta_2$  and  $v_{\text{VC}}$ ,  $\eta$  in multispectrum fits [76]. In this method,  $\Gamma_2$  and  $\Delta_2$  parameters are fixed in the fit to the approximate values to facilitate retrieval of accurate  $v_{\text{VC}}$ ,  $\eta$  values. We examine the agreement of such approximate parameters with the values obtained directly from the *ab initio* data. Fig. 7 shows the results of the comparison. Black lines show the reference  $\gamma_2$  and  $\delta_2$  values obtained from applying Eq. (6) to the *ab initio* speed dependence. Blue lines show the results of applying Eq. (A.8) directly to the *ab initio* widths and shifts, representing the best-case scenario. Yellow lines show the more likely case, in which the temperature dependence is known from a fit of an analytical dependence to a set of points. For both  $\gamma_0$  and  $\delta_0$ , we used the approximate form adopted in the 2016 edition of the HITRAN database, i.e. linear for  $\delta_0$ , Eq. (A.11), and power-law for  $\gamma_0$ , Eq. (A.10). Additionally, seeing that power-law dependence approximately matches the cross sections in Fig. 1 and the line-shape parameters in Fig. 2, which implies hypergeometric speed dependence, we have attempted a different method of arriving at quadratic-speed-dependent parameters. We have used Eq. (A.9) on *ab initio* temperature dependence to determine the parameter  $\alpha$  describing hypergeometric speed dependence and evaluated the implied hypergeometric speed-dependence at  $v_1 = v_p$  to obtain  $\gamma_2$  and  $\delta_2$  from Eq. (6). The results are shown in red in Fig. 7.

The agreement between *ab initio*-derived speed-dependent parameters (black) and either one of two methods (blue and red curves) applied directly to *ab initio* temperature dependence does not consistently favor any one of them. The indirect hypergeometric method (red) shows excellent agreement in the case of P(2) line broadening, which matches the agreement of power-law fit to the broadening cross sections in Fig. 1, and converges to the *ab initio*-derived parameters at high temperatures. The same method

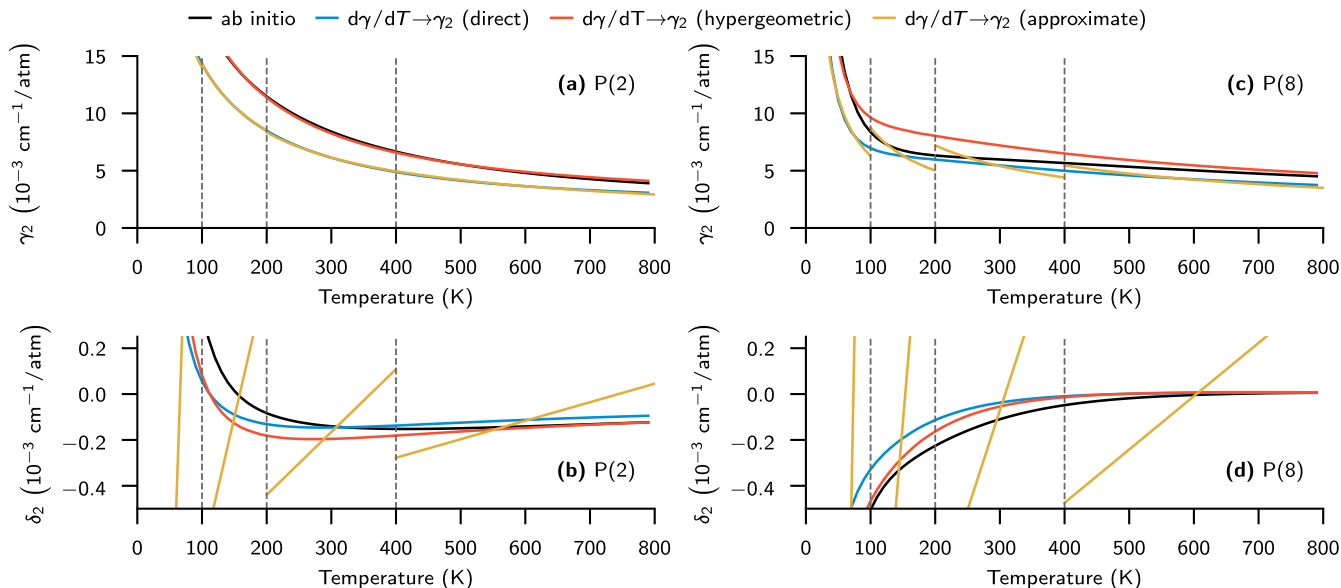


**Fig. 7.** Quadratic-speed-dependent coefficients obtained by: directly using Eq. (6) on *ab initio* speed-dependent widths and shifts (black); directly using Eq. (A.8) on *ab initio* temperature-dependent widths and shifts (blue); using Eq. (A.9) to obtain hypergeometric speed dependence from temperature dependence of *ab initio* widths and shifts and then using Eq. (6) on such speed dependence (red); using analytical formulas, Eqs. (A.10), (A.11), for temperature derivatives of approximate (exponential or linear) temperature dependence of widths and shifts (yellow). (For interpretation of the references to colour in this figure legend, the reader is referred to the web version of this article.)

applied to the P(8) line results in  $\Gamma_2$  values differing by as much as 28% from *ab initio*-derived ones. On the other hand, direct differentiation (blue) offers better agreement with P(2) line shift and P(8) line broadening in the temperature range most easily accessible for laboratory measurements, but the P(2) line broadening is shifted by about 25% from the *ab initio*-derived values in the same temperature range. Speed-dependent shifts obtained from linear temperature dependence of pressure shifts (yellow) perform worse than a simple approximation by a constant value would, which provides an additional point in favor of the double-exponential model of Gamache and Vispoel [69,77].

The direct (blue and yellow) and indirect methods (red) assume that  $\sigma_\lambda^q(E)$  cross sections are described by a square-root function, for the former, or a single power law, for the latter. These assumptions are fulfilled only to a limited degree for the CO-Ar lines shown here, as seen in Fig. 1. Examining  $\sigma_\lambda^q(E)$  reported for other molecular systems, see Table 1 in [26] for references, we can expect these simple approximations to be inaccurate in other cases as well. Another indirect evidence for the cross sections not following a single power-law dependence is also given by a large improvement in accuracy when using the double-exponential model in modeling temperature dependence of  $\gamma$  and  $\delta$  [69,77]. Nevertheless, despite their serious limitations, either of these simple methods we have evaluated can be useful in roughly estimating the importance of speed-dependent effects and providing initial guesses for a multispectrum fitting routine.

## 5. Conclusions

We have described and demonstrated a procedure for obtaining a full set of HTP line-shape parameters in a broad temperature range based on purely *ab initio* calculations utilizing an accurate interaction potential. A comparison with experimental data [27,30] has shown the accuracy of pressure broadening coefficients to be at sub-percent level and of pressure shift coefficients to be at 1%–3% level for the chosen two benchmark lines of CO perturbed by Ar. For the Dicke effect, this is the first *ab initio* cal-

ulation of  $\nu_{\text{opt}}$  for a system exhibiting collision dynamics typical of Earth atmospheric species.

Based on the *ab initio* parameters, we examine the approximations of the HTP. In particular, we compare the quadratic and hypergeometric approximations of speed-dependence, finding no consistent improvement of one over another. We examine how discrepancies between *ab initio* and approximate  $\Gamma(v_1)$  translate into actual line-shape residuals, finding small but significant deviations even when the approximated value of  $\Gamma(v_1)$  deviates only by a few percent from the actual value. We examine the hard-collision model of velocity-changing collisions as adopted in the HTP. In particular, by comparing the HTP line shapes with SDBBP line shapes in different collisional regimes, we show that at high pressure the HTP overestimates the effect of velocity-changing collisions on the P(8) line shape. We provide the interpretation of  $\nu_{\text{VC}}$  and  $\eta$  parameters in terms of GHM quantities and explain the large difference between speed dependence of  $\nu_{\text{opt}}$  in HTP and GHM. We show that in contrast to H<sub>2</sub>-He lines [32–34], for CO-Ar there is a substantial disagreement between mass transport and optical coherence transport coefficients. This behavior is also expected to occur for other atmospheric species with closely-lying rotational states. Finally, we examine the accuracy of the approximation schemes for temperature dependence of line-shape parameters adopted in the 2016 edition of the HITRAN database and the accuracy of a previously proposed scheme for deriving speed-dependent parameters from temperature dependence of averaged parameters. We find the approximate speed-dependent widths to be accurate within around 30% when obtained from power-law temperature dependence of pressure widths. In contrast, describing temperature dependence of pressure shifts by a linear function causes the approximate speed-dependent shifts to be up to a few tens of times larger in absolute value than the actual speed-dependent shifts.

The described procedure of obtaining the HTP line-shape parameters is directly applicable to other linear molecule-atom systems such as CO<sub>2</sub>-Ar [78]. It can be extended in a straightforward manner to linear-linear systems [54], such as C<sub>2</sub>H<sub>2</sub>-N<sub>2</sub> [79], although the higher density of rotational states would make it necessary to use an approximate method [80] for the determination

of the S-matrix, such as the coupled states method [81], due to higher computational cost. The procedure will be further validated by performing calculations on other systems and comparing them with accurate experimental measurements. In particular, there are ongoing works on applying the GHM method to previously measured [82] second-overtone transitions of CO-Ar and to the more common diatom-diatom collisions represented by CO-N<sub>2</sub>.

### Declaration of Competing Interest

The authors declare that they have no known competing financial interests or personal relationships that could have appeared to influence the work reported in this paper.

### CRediT authorship contribution statement

**Grzegorz Kowzan:** Conceptualization, Methodology, Software, Investigation, Funding acquisition, Writing - original draft, Writing - review & editing, Visualization. **Piotr Wcisło:** Conceptualization, Methodology, Software, Writing - original draft, Writing - review & editing. **Michał Słowiński:** Software, Investigation. **Piotr Masłowski:** Supervision, Funding acquisition. **Alexandra Viel:** Software, Investigation, Resources, Writing - original draft, Writing - review & editing. **Franck Thibault:** Conceptualization, Methodology, Software, Investigation, Resources, Writing - original draft, Writing - review & editing.

### Acknowledgments

We thank prof. R. Ciuryło for fruitful discussions. This research was supported by National Science Centre, Poland project no. 2016/21/N/ST2/00334 and 2016/23/B/ST2/00730. G. K. was supported by National Science Centre, Poland scholarship 2017/24/T/ST2/00242. P. W. contribution is supported by National Science Centre, Poland through projects no. 2015/19/D/ST2/02195 and 2018/31/B/ST2/00720. M. S. contribution is supported by the National Science Centre, Poland through Project 2014/15/D/ST2/05281 and by the "A next-generation worldwide quantum sensor network with optical atomic clocks" project carried out within the TEAM IV Programme of the Foundation for Polish Science cofinanced by the European Union under the European Regional Development Fund. The project is supported by the French-Polish PHC Polonium program (project 42769ZK for the French part). The project is co-financed by the Polish National Agency for Academic Exchange under the PHC Polonium program (dec. PPN/X/PS/318/2018). The research is a part of the program of the National Laboratory FAMO (KL FAMO) in Toruń, Poland, and is supported by a subsidy from the Polish Ministry of Science and Higher Education.

### Appendix A. Approximate temperature and speed dependence of line-shape parameters

In order to provide temperature dependence of line-shape parameters, the 2016 edition of the HITRAN database divides the whole temperature range into four subranges: 0 K–100 K, 100 K–200 K, 200 K–400 K, 400 K–∞ and assigns to each subrange a reference temperature:  $T_{\text{ref}}^{(1)} = 50$  K,  $T_{\text{ref}}^{(2)} = 150$  K,  $T_{\text{ref}}^{(3)} = 296$  K,  $T_{\text{ref}}^{(4)} = 400$  K. Values of  $\gamma_0$  and  $\delta_0$  are provided at each reference temperature, which combined with  $n_{\gamma_0}^{(i)}$  and  $\delta_0^{(i)}$  coefficients can be used to approximate collisional broadening and shift at different temperatures with, respectively, power-law and linear functions:

$$\gamma_0^{(i)}(T) = \gamma_0(T_{\text{ref}}^{(i)}) \left( \frac{T}{T_{\text{ref}}^{(i)}} \right)^{n_{\gamma_0}^{(i)}}, \quad (\text{A.1})$$

$$\delta_0^{(i)}(T) = \delta_0(T_{\text{ref}}^{(i)}) + \delta_0^{(i)}(T - T_{\text{ref}}^{(i)}), \quad (\text{A.2})$$

**Table A1**  
Power-law fit coefficients, Eq. (A.4), of spectroscopic cross sections from Fig. 1.

Line	Cross section	$\sigma_{\lambda,0}$ ( $\text{\AA}^2/\text{cm}^{-\alpha}$ )	$\alpha$
P(2)	$\text{Re}(\sigma_{0,0}^1)$	356.4	-0.262
	$\text{Re}(\sigma_{1,0}^1)$	389.5	-0.267
	$\text{Im}(\sigma_{0,0}^1)$	5.77	-0.207
	$\text{Im}(\sigma_{1,0}^1)$	4.16	-0.167
P(8)	$\text{Re}(\sigma_{0,0}^1)$	251.0	-0.246
	$\text{Re}(\sigma_{1,0}^1)$	447.2	-0.320
	$\text{Im}(\sigma_{0,0}^1)$	70.6	-0.498
	$\text{Im}(\sigma_{1,0}^1)$	51.9	-0.506

where the index  $i$  denotes the temperature range. The  $\tilde{\nu}_{\text{VC}}$  parameter is also approximated with a power law but based only on a single exponent  $\kappa$ , for the whole range and a reference value of  $\tilde{\nu}_{\text{VC}}$  at  $T_{\text{ref}}^{(2)}$ :

$$\tilde{\nu}_{\text{VC}}(T) = \tilde{\nu}_{\text{VC}}(T_{\text{ref}}^{(2)}) \left( \frac{T}{T_{\text{ref}}^{(2)}} \right)^{\kappa}. \quad (\text{A.3})$$

The temperature dependence of  $\gamma_2$  and  $\delta_2$  is not explicitly modeled by HITRAN 2016, but the values of the parameters are provided at the four reference temperatures. The correlation parameter  $\eta$  is assumed to be temperature-independent and provided at  $T_{\text{ref}}^{(2)}$ . The values of  $\gamma_0$ ,  $n_{\gamma_0}$ ,  $\delta_0$ ,  $\delta_0'$ ,  $\tilde{\nu}_{\text{VC}}$  and  $\kappa$  for the P(2) line and P(8) line of CO-Ar are given in Table 1. In addition the supplementary material [dataset] [66] contains power-law coefficients for  $\gamma_2$  ( $n_{\gamma_2}$ ) and linear coefficients for  $\delta_2$  ( $\delta_2'$ ) and  $\eta$  ( $\eta'$ ).

Power-law temperature dependence of line-shape parameters can be obtained by assuming power-law form of spectroscopic cross sections,

$$\sigma_{\lambda}^q(E_{\text{kin}}) = \sigma_{\lambda,0}^q E_{\text{kin}}^{\alpha}. \quad (\text{A.4})$$

For the P(2) line of CO-Ar fundamental band, Wehr et al. [28] has previously obtained fit parameters  $\text{Re}(\sigma_{0,0}^1) = 361 \text{ \AA}^2/\text{cm}^{-\alpha}$  and  $\alpha = 0.250$ . The difference between these values and ours, shown in Table A.1, mostly comes from the different values of collision energy at which the fit was cut off, which was  $E_{\text{kin}} = 10 \text{ cm}^{-1}$  for [28] and  $E_{\text{kin}} = 50 \text{ cm}^{-1}$  for our fit.

Evaluating analytically the Boltzmann integrals from Eqs. (4), (9) with spectroscopic cross sections obeying the power law, Eq. (A.4), we obtain [67,68]:

$$\Gamma_0(T) = n \sigma_{\lambda,0}^q k_B^{\alpha+1/2} \sqrt{\frac{8}{\pi \mu}} \tilde{\Gamma}(\alpha+2) T^{\alpha+1/2}, \quad (\text{A.5})$$

where  $\tilde{\Gamma}$  is the gamma function. The exponent  $\alpha$  is related to the temperature-dependence exponent  $n_{\gamma_0}$  from Eq. (A.1) by  $\alpha = 1/2 - n_{\gamma_0}$  and to the exponent  $n$  from Ref. [37] by  $\alpha = (n-1)/2$ . Similarly, for speed-dependent parameters evaluating Eq. (5) for power-law cross section results in [14,49,67]:

$$\Gamma(v_1; T) = \frac{\Gamma_0(T)}{(\beta+1)^{\alpha+1/2}} \text{M} \left( -\alpha - 1/2, \frac{3}{2}, -\beta \frac{v_1^2}{v_p^2} \right), \quad (\text{A.6})$$

where M is the confluent hypergeometric function [83, Sec. 13.2] and  $\beta = m_2/m_1$ . The commonly used quadratic speed dependence [84] can be obtained for  $\alpha = 1/2$  [83, Eq. 13.2.2]:

$$\Gamma(v_1; T) = \Gamma_0(T) + \Gamma_2(T) \left( \frac{v_1^2}{v_p^2} - \frac{3}{2} \right), \quad (\text{A.7})$$

implying unphysical kinetic energy square-root law for cross sections.

The preceding relations, Eqs. (A.5) and (A.7), can be used to derive quadratic and hypergeometric speed-dependent parameters from temperature dependence of  $\Gamma_0$  and  $\Delta_0$  [37]. The  $\Gamma_2$  (or  $\Delta_2$ )

parameter is given by:

$$\Gamma_2(T) = \zeta T \frac{d\Gamma_0(T)}{dT}, \quad (\text{A.8})$$

where  $\zeta = (2/3)\beta/(1 + \beta)$ , and  $\alpha$  exponent is given by:

$$\alpha(T) = \frac{T}{\Gamma_0} \frac{d\Gamma_0(T)}{dT} - \frac{1}{2}. \quad (\text{A.9})$$

As applied to the form of temperature dependence adopted in the 2016 edition of the HITRAN database, Eqs. (A.1), (A.2), this results in analytical formulas for quadratic speed-dependent width and shift:

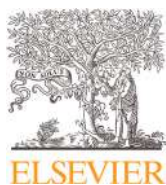
$$\gamma_2^{(i)}(T) = \zeta(-n + 1)\gamma_0(T_{\text{ref}}^{(i)}) \left(\frac{T}{T_{\text{ref}}^{(i)}}\right)^{n_{\gamma_0}^{(i)}}, \quad (\text{A.10})$$

$$\delta_2^{(i)}(T) = \zeta \left[ \delta_0(T_{\text{ref}}^{(i)}) + \delta_0'(i)(2T - T_{\text{ref}}^{(i)}) \right]. \quad (\text{A.11})$$

## References

- [1] Duggan P, Sinclair PM, Berman R, May AD, Drummond JR. Testing lineshape models: measurements for  $\nu=1-0$  CO broadened by He and Ar. *J Mol Spectrosc* 1997;186(1):90–8. doi:10.1006/jmsp.1997.7420.
- [2] Pine AS. Asymmetries and correlations in speed-dependent Dicke-narrowed line shapes of argon-broadened HF. *J Quant Spectrosc Radiat Transfer* 1999;62(4):397–423. doi:10.1016/S0022-4073(98)00112-5.
- [3] Chaussard F, Michaut X, Saint-Loup R, Berger H, Joubert P, Lance B, et al. Collisional effects on spectral line shape from the doppler to the collisional regime: a rigorous test of a unified model. *J Chem Phys* 1999;112(1):158–66. doi:10.1063/1.480570.
- [4] Dicke RH. The effect of collisions upon the doppler width of spectral lines. *Phys Rev* 1953;89(2):472–3. doi:10.1103/PhysRev.89.472.
- [5] De Vizia MD, Castrillo A, Fasci E, Amodio P, Moretti L, Gianfrani L. Experimental test of the quadratic approximation in the partially correlated speed-dependent hard-collision profile. *Phys Rev A* 2014;90(2):022503. doi:10.1103/PhysRevA.90.022503.
- [6] Campargue A, Karlovets EV, Kassi S. The 4-0 band of carbon monoxide by high sensitivity Cavity Ring Down spectroscopy near 8200  $\text{cm}^{-1}$ . *J Quant Spectrosc Radiat Transfer* 2015;154:113–19. doi:10.1016/j.jqsrt.2014.12.011.
- [7] Wójtewicz S, Masłowski P, Cygan A, Wcisło P, Zaborowski M, Piwiński M, et al. Speed-dependent effects and Dicke narrowing in nitrogen-broadened oxygen. *J Quant Spectrosc Radiat Transfer* 2015;165:68–75. doi:10.1016/j.jqsrt.2015.06.022.
- [8] Sironneau VT, Hodges JT. Line shapes, positions and intensities of water transitions near 1.28  $\mu\text{m}$ . *J Quant Spectrosc Radiat Transfer* 2015;152:1–15. doi:10.1016/j.jqsrt.2014.10.020.
- [9] Hashemi R, Predoi-Cross A, Nikitin AV, Tyuterev VG, Sung K, Smith MAH, et al. Spectroscopic line parameters of  $^{12}\text{CH}_4$  for atmospheric composition retrievals in the 4300–4500  $\text{cm}^{-1}$  region. *J Quant Spectrosc Radiat Transfer* 2017;186:106–17. doi:10.1016/j.jqsrt.2016.03.024.
- [10] Hayden Smith WM, Conner CP, Simon J, Schempp WV, Macy W. The  $\text{H}_2$  4-0 S(0, 1, and 2) quadrupole features in Jupiter. *Icarus* 1989;81(2):429–40. doi:10.1016/0019-1035(89)90062-6.
- [11] Galatry L. Simultaneous effect of doppler and foreign gas broadening on spectral lines. *Phys Rev* 1961;122(4):1218–23. doi:10.1103/PhysRev.122.1218.
- [12] Nelkin M, Ghatak A. Simple binary collision model for Van Hove's  $G_s(r, t)$ . *Phys Rev* 1964;135(1A):A4–9. doi:10.1103/PhysRev.135.A4.
- [13] Rautian SG, Sobel'man II. The effect of collisions on the doppler broadening of spectral lines. *Soviet Physics Uspekhi* 1967;9(5):701–16. doi:10.1070/PU1967v009n05ABEH003212.
- [14] Berman PR. Speed-dependent collisional width and shift parameters in spectral profiles. *J Quant Spectrosc Radiat Transfer* 1972;12(9):1331–42. doi:10.1016/0022-4073(72)90189-6.
- [15] Lance B, Blanquet G, Walrand J, Bouanich J-P. On the speed-dependent hard collision lineshape models: application to  $\text{C}_2\text{H}_2$  perturbed by Xe. *J Mol Spectrosc* 1997;185(2):262–71. doi:10.1006/jmsp.1997.7385.
- [16] Ciuryło R, Szudy J. Speed-dependent pressure broadening and shift in the soft collision approximation. *J Quant Spectrosc Radiat Transfer* 1997;57(3):411–23. doi:10.1016/S0022-4073(96)00078-7.
- [17] Wcisło P, Ciuryło R. Influence of the interaction potential shape on the Dicke narrowed spectral line profiles affected by speed-dependent collisional broadening and shifting. *J Quant Spectrosc Radiat Transfer* 2013;120:36–43. doi:10.1016/j.jqsrt.2013.02.023.
- [18] Boone CD, Walker KA, Bernath PF. Speed-dependent Voigt profile for water vapor in infrared remote sensing applications. *J Quant Spectrosc Radiat Transfer* 2007;105(3):525–32. doi:10.1016/j.jqsrt.2006.11.015.
- [19] Tran H, Ngo NH, Hartmann JM. Efficient computation of some speed-dependent isolated line profiles. *J Quant Spectrosc Radiat Transfer* 2013;129:199–203. doi:10.1016/j.jqsrt.2013.06.015.
- [20] Ngo NH, Lisak D, Tran H, Hartmann J-M. An isolated line-shape model to go beyond the Voigt profile in spectroscopic databases and radiative transfer codes. *J Quant Spectrosc Radiat Transfer* 2013;129:89–100. doi:10.1016/j.jqsrt.2013.05.034.
- [21] Tennyson J, Bernath PF, Campargue A, Császár AG, Daumont L, Gamache RR, et al. Recommended isolated-line profile for representing high-resolution spectroscopic transitions (IUPAC Technical Report). *Pure Appl Chem* 2014;86(12):1931–43. doi:10.1515/pac-2014-0208.
- [22] Gordon L, Rothman L, Hill C, Kochanov R, Tan Y, Bernath P, et al. The HITRAN2016 molecular spectroscopic database. *J Quant Spectrosc Radiat Transfer* 2017;203:3–69. doi:10.1016/j.jqsrt.2017.06.038.
- [23] Lisak D, Cygan A, Bermejo D, Domenech JL, Hodges JT, Tran H. Application of the Hartmann-Tran profile to analysis of  $\text{H}_2\text{O}$  spectra. *J Quant Spectrosc Radiat Transfer* 2015;164:221–30. doi:10.1016/j.jqsrt.2015.06.012.
- [24] Ngo NH, Hartmann J-M. A strategy to complete databases with parameters of refined line shapes and its test for CO in He, Ar and Kr. *J Quant Spectrosc Radiat Transfer* 2017. doi:10.1016/j.jqsrt.2017.01.031.
- [25] Hartmann J-M, Boulet C, Robert D. Collisional effects on molecular spectra. laboratory experiments and models, consequences for applications. Amsterdam: Elsevier; 2008. ISBN 9780444520173.
- [26] Hartmann J-M, Tran H, Armante R, Boulet C, Campargue A, Forget F, et al. Recent advances in collisional effects on spectra of molecular gases and their practical consequences. *J Quant Spectrosc Radiat Transfer* 2018;213(nil):178–227. doi:10.1016/j.jqsrt.2018.03.016.
- [27] Luo C, Wehr R, Drummond JR, May AD, Thibault F, Boissoles J, et al. Shifting and broadening in the fundamental band of CO highly diluted in He and Ar: A comparison with theory. *J Chem Phys* 2001;115(5):2198–206. doi:10.1063/1.1383049.
- [28] Wehr R, Vitcu A, Ciuryło R, Thibault F, Drummond JR, May AD. Spectral line shape of the  $P(2)$  transition in CO-Ar: Uncorrelated *ab initio* calculation. *Phys Rev A* 2002;66(6):062502. doi:10.1103/PhysRevA.66.062502.
- [29] Wehr R, Ciuryło R, Vitcu A, Thibault F, Drummond JR, May AD. Dicke-narrowed spectral line shapes of CO in Ar: Experimental results and a revised interpretation. *J Mol Spectrosc* 2006;235(1):54–68. doi:10.1016/j.jms.2005.10.009.
- [30] Wehr R, Vitcu A, Thibault F, Drummond JR, May AD. Collisional line shifting and broadening in the fundamental P-branch of CO in Ar between 214 and 324 K. *J Mol Spectrosc* 2006;235(1):69–76. doi:10.1016/j.jms.2005.10.004.
- [31] The parameter  $\nu_{\text{opt}}$  has also been called previously the frequency of optical velocity-changing collisions or the optical frequency of velocity-changing collisions.
- [32] Thibault F, Patkowski K, Żuchowski PS, Józwiak H, Ciuryło R, Wcisło P. Rovibrational line-shape parameters for  $\text{H}_2$  in He and new  $\text{H}_2$ -He potential energy surface. *J Quant Spectrosc Radiat Transfer* 2017;202:308–20. doi:10.1016/j.jqsrt.2017.08.014.
- [33] Józwiak H, Thibault F, Stolarczyk N, Wcisło P. *Ab initio* line-shape calculations for the S and O branches of  $\text{H}_2$  perturbed by He. *J Quant Spectrosc Radiat-Transf* 2018;219(nil):313–22. doi:10.1016/j.jqsrt.2018.08.023.
- [34] Martínez RZ, Bermejo D, Thibault F, Wcisło P. Testing the *ab initio* quantum-scattering calculations for the  $\text{D}_2$ -He benchmark system with stimulated raman spectroscopy. *J Raman Spectrosc* 2018;49(8):1339–49. doi:10.1002/jrs.5391.
- [35] Wcisło P, Thibault F, Zaborowski M, Wójtewicz S, Cygan A, Kowzan G, et al. Accurate deuterium spectroscopy for fundamental studies. *J Quant Spectrosc Radiat Transfer* 2018;213:41–51. doi:10.1016/j.jqsrt.2018.04.011.
- [36] Shapiro DA, Ciuryło R, Drummond JR, May AD. Solving the line-shape problem with speed-dependent broadening and shifting and with Dicke narrowing. I. Formalism. *Phys Rev A* 2001;65(1):012501. doi:10.1103/PhysRevA.65.012501.
- [37] Lisak D, Cygan A, Wcisło P, Ciuryło R. Quadratic speed dependence of collisional broadening and shifting for atmospheric applications. *J Quant Spectrosc Radiat Transfer* 2015;151:43–8. doi:10.1016/j.jqsrt.2014.08.016.
- [38] Wcisło P, Gordon IE, Tran H, Tan Y, Hu S-M, Campargue A, et al. The implementation of non-Voigt line profiles in the HITRAN database:  $\text{H}_2$  case study. *J Quant Spectrosc Radiat Transfer* 2016;177:75–91. doi:10.1016/j.jqsrt.2016.01.024.
- [39] Ciuryło R, Pine AS, Szudy J. A generalized speed-dependent line profile combining soft and hard partially correlated Dicke-narrowing collisions. *J Quant Spectrosc Radiat Transfer* 2001;68(3):257–71. doi:10.1016/S0022-4073(00)00024-8.
- [40] For short we call dephasing collisions those phase- and state-changing collisions which affect the internal motion of the molecule and lead to broadening as well as to shifting of transitions. Such collisions can be both elastic and inelastic. In addition, we remind the reader that the classical Dicke effect is tied to the translational motion, which is related only to elastic collisions.
- [41] Baranger M. Simplified quantum-mechanical theory of pressure broadening. *Phys Rev* 1958;111(2):481–93. doi:10.1103/PhysRev.111.481.
- [42] Baranger M. Problem of overlapping lines in the theory of pressure broadening. *Phys Rev* 1958;111(2):494–504. doi:10.1103/PhysRev.111.494.
- [43] Baranger M. General impact theory of pressure broadening. *Phys Rev* 1958;112(3):855–65. doi:10.1103/PhysRev.112.855.
- [44] Fano U. Pressure broadening as a prototype of relaxation. *Phys Rev* 1963;131(1):259–68. doi:10.1103/PhysRev.131.259.
- [45] Ben-Reuven A. Symmetry considerations in pressure-broadening theory. *Phys Rev* 1966;141(1):34–40. doi:10.1103/PhysRev.141.34.
- [46] Ben-Reuven A. Impact broadening of microwave spectra. *Phys Rev* 1966;145(1):7–22. doi:10.1103/PhysRev.145.7.
- [47] For absorption processes the sign convention is to take the negative of the imaginary part of a spectroscopic cross section, or equivalently to consider the cross section  $\sigma_{\lambda}^q(j_b, j_a; e) = \sigma_{\lambda}^q(j_a, j_b; e)^*$ . The same remark applies to the velocity-changing cross sections further in the text.

- [48] Fitz DE, Marcus RA. Semiclassical theory of molecular spectral line shapes in gases. *J Chem Phys* 1973;59(8):4380–92. doi:10.1063/1.1680636.
- [49] Pickett HM. Effects of velocity averaging on the shapes of absorption lines. *J Chem Phys* 1980;73(12):6090–4. doi:10.1063/1.440145.
- [50] Tip A. Transport equations for dilute gases with internal degrees of freedom. *Physica* 1971;52(4):493–522. doi:10.1016/0031-8914(71)90161-3.
- [51] Hess S. Kinetic theory of spectral line shapes. The transition between doppler broadening and collisional broadening. *Physica* 1972;61(1):80–94. doi:10.1016/0031-8914(72)90035-3.
- [52] Tip A. A kinetic equation for dilute polyatomic gases. *Phys Lett A* 1969;30(3):147–8. doi:10.1016/0375-9601(69)90901-3.
- [53] Snider RF, Sanctuary BC. Generalized Boltzmann equation for molecules with internal states. *J Chem Phys* 1971;55(4):1555–66. doi:10.1063/1.1676279.
- [54] Monchick L, Hunter LW. Diatomic-diatom molecular collision integrals for pressure broadening and Dicke narrowing: A generalization of Hess's theory. *J Chem Phys* 1986;85(2):713–18. doi:10.1063/1.451277.
- [55] Corey GC, McCourt FR. Dicke narrowing and collisional broadening of spectral lines in dilute molecular gases. *J Chem Phys* 1984;81(5):2318–29. doi:10.1063/1.447930.
- [56] Schaefer J, Monchick L. Line broadening of HD immersed in He and H<sub>2</sub> gas. *Astron Astrophys* 1992;265:859–68.
- [57] Demeio L, Green S, Monchick L. Effects of velocity changing collisions on line shapes of HF in Ar. *J Chem Phys* 1995;102(23):9160–6. doi:10.1063/1.468864.
- [58] Yutsis AP, Levinson IB, Vanagas VV. *Mathematical apparatus of the theory of angular momentum*. Jerusalem: Israel Program for Scientific Translations; 1962.
- [59] Sumiyoshi Y, Endo Y. Three-dimensional potential energy surface of Ar–CO. *J Chem Phys* 2015;142(2):024314. doi:10.1063/1.4905268.
- [60] Child MS. *Molecular Collision Theory*. Academic Press; 1974.
- [61] Hutson JM, Sueur CRL. Molscat: a program for non-reactive quantum scattering calculations on atomic and molecular collisions. CoRR 2018.
- [62] Manolopoulos DE. An improved log derivative method for inelastic scattering. *J Chem Phys* 1986;85(11):6425–9. doi:10.1063/1.451472.
- [63] Alexander MH, Manolopoulos DE. A stable linear reference potential algorithm for solution of the quantum close-coupled equations in molecular scattering theory. *J Chem Phys* 1987;86(4):2044–50. doi:10.1063/1.452154.
- [64] For convenient comparison with rovibrational energy level structure commonly given in cm<sup>-1</sup>, we provide collision energies also in cm<sup>-1</sup> through  $E/hc$  with  $c$  in cm/s.
- [65] Havenith M, Schwaab GW. Attacking a small beast: Ar–CO, a prototype for intermolecular forces. *Zeitschrift für Physikalische Chemie* 2009;219(8):1053–88. doi:10.1524/zpch.2005.219.8.1053.
- [66] Kowzan G, Wcisło P, Słowiński M., Masłowski P., Viel A., Thibault F. Spectroscopic cross sections and HTP line-shape parameters for CO–Ar 0–1 P(2), P(8) lines. Mendeley Data; 2019.
- [67] Ward J, Cooper J, Smith EW. Correlation effects in the theory of combined doppler and pressure broadening—I. Classical theory. *J Quant Spectrosc Radiat Transfer* 1974;14(7):555–90. doi:10.1016/0022-4073(74)90036-3.
- [68] Lance B, Blanquet G, Walrand J, Populaire J-C, Bouanich J-P, Robert D. Inhomogeneous lineshape profiles of C<sub>2</sub>H<sub>2</sub> perturbed by Xe. *J Mol Spectrosc* 1999;197(1):32–45. doi:10.1006/jmsp.1999.7892.
- [69] Gamache RR, Vispoel B. On the temperature dependence of half-widths and line shifts for molecular transitions in the microwave and infrared regions. *J Quant Spectrosc Radiat Transf* 2018;217(nil):440–52. doi:10.1016/j.jqsrt.2018.05.019.
- [70] Ciuryło R, Bielski A, Drummond JR, Lisak D, May AD, Pine AS, et al. High resolution studies on the influence of velocity hanging collisions on atomic and molecular line shapes. *AIP Conf Proc* 2002;645(1):151–60. doi:10.1063/1.1525447.
- [71] Wcisło P, Cygan A, Lisak D, Ciuryło R. Iterative approach to line-shape calculations based on the transport-relaxation equation. *Phys Rev A* 2013;88(1):012517. doi:10.1103/PhysRevA.88.012517.
- [72] Wcisło P, Thibault F, Cybulski H, Ciuryło R. Strong competition between velocity-changing and phase- or state-changing collisions in H<sub>2</sub> spectra perturbed by Ar. *Phys Rev A* 2015;91(5):052505. doi:10.1103/PhysRevA.91.052505.
- [73] Boushehri A, Bzowski J, Kestin J, Mason EA. Equilibrium and transport properties of eleven polyatomic gases at low density. *J Phys Chem Ref Data* 1987;16(3):445–66. doi:10.1063/1.555800.
- [74] Coombe DA, Snider RF, Sanctuary BC. Definitions and properties of generalized collision cross sections. *J Chem Phys* 1975;63:3015–30. doi:10.1063/1.431727.
- [75] McCourt FRW, Liu W-K. Anisotropic intermolecular potentials and transport properties in polyatomic gases. *Faraday Discussion Chem Soc* 1982;73(nil):241. doi:10.1039/dc9827300241.
- [76] Benner DC, Rinsland CP, Devi VM, Smith MAH, Atkins D. A multispectrum nonlinear least squares fitting technique. *J Quant Spectrosc Radiat Transfer* 1995;53(6):705–21. doi:10.1016/0022-4073(95)00015-D.
- [77] Stolarczyk N, Thibault F, Cybulski H, Jóźwiak H, Kowzan G, Vispoel B, et al. Evaluation of different parameterizations of temperature dependences of the line-shape parameters based on ab initio calculations: case study for the HITRAN database. *J Quant Spectrosc Radiat Transfer* 2019;nil(nil):106676. doi:10.1016/j.jqsrt.2019.106676.
- [78] Thibault F, Calil B, Buldyreva J, Chrysos M, Hartmann J-M, Bouanich J-P. Experimental and theoretical CO<sub>2</sub>–Ar pressure-broadening cross sections and their temperature dependence. *Phys Chem Chem Phys* 2001;3(18):3924–33. doi:10.1039/B103625B.
- [79] Thibault F, Corretja B, Viel A, Bermejo D, Martinez RZ, Bussery-Honvault B. Linewidths of C(2)H(2) perturbed by H(2): experiments and calculations from an ab initio potential. *Phys Chem Chem Phys* 2008;10(35):5419–28. doi:10.1039/b804306j. WOS:000258949000013
- [80] *Atom-molecule collision theory*. Bernstein RB, editor. New York: Plenum Press; 1979.
- [81] McGuire P, Kouri DJ. Quantum mechanical close coupling approach to molecular collisions. *j<sub>2</sub>-conserving coupled states approximation*. *J Chem Phys* 1974;60(6):2488–99. doi:10.1063/1.1681388.
- [82] Kowzan G, Stec K, Zaborowski M, Wójtewicz S, Cygan A, Lisak D, et al. Line positions, pressure broadening and shift coefficients for the second overtone transitions of carbon monoxide in argon. *J Quant Spectrosc Radiat Transfer* 2017;191:46–54. doi:10.1016/j.jqsrt.2016.12.035.
- [83] NIST Digital Library of Mathematical Functions. <http://dlmf.nist.gov/>, Release 1.0.18 of 2018-03-27. F. W. J. Olver, A. B. Olde Daalhuis, D. W. Lozier, B. I. Schneider, R. F. Boisvert, C. W. Clark, B. R. Miller, and B. V. Saunders, eds. <http://dlmf.nist.gov/>;
- [84] Priem D, Rohart F, Colmont J-M, Włodarczyk G, Bouanich J-P. Lineshape study of the  $j=3 \leftarrow 2$  rotational transition of CO perturbed by N<sub>2</sub> and O<sub>2</sub>. *J Mol Struct* 2000;517–518:435–54. doi:10.1016/S0022-2860(99)00268-9.



Contents lists available at ScienceDirect

## Journal of Quantitative Spectroscopy &amp; Radiative Transfer

journal homepage: [www.elsevier.com/locate/jqsrt](http://www.elsevier.com/locate/jqsrt)

# Analytical-function correction to the Hartmann–Tran profile for more reliable representation of the Dicke-narrowed molecular spectra

M. Konefał<sup>a,b,\*</sup>, M. Słowiński<sup>a</sup>, M. Zaborowski<sup>a</sup>, R. Ciuryło<sup>a</sup>, D. Lisak<sup>a</sup>, P. Wcisło<sup>a</sup><sup>a</sup> Institute of Physics, Faculty of Physics, Astronomy and Informatics, Nicolaus Copernicus University in Toruń, ul. Grudziadzka 5, Toruń 87-100, Poland<sup>b</sup> University Grenoble Alpes, CNRS, LIPhy, Grenoble 38000, France

## ARTICLE INFO

## Article history:

Received 15 August 2019

Revised 28 October 2019

Accepted 2 December 2019

Available online 03 December 2019

## Keywords:

Velocity-changing collisions

Hartmann–Tran profile

HTP

Speed-dependent billiard-ball profile

 $\beta$  correction

Atmospheric molecular systems

## ABSTRACT

The  $\beta$ -corrected Hartmann–Tran profile (HTP) constitutes an approximation of the partially correlated quadratic speed-dependent billiard-ball profile (SDBBP) easily applicable in calculations. We extend the approach originally developed for self-perturbed molecules [Wcisło et al. J. Quant. Spectrosc. Radiat. Transf. 177, 75–91 (2016)] to systems with a wide range of perturber-to-absorber mass ratios, including those relevant for atmospheric studies. This approach combines the computational simplicity of the HTP with the more physically justified rigid-sphere model for velocity-changing collisions. It is important for the analysis of high-resolution spectra influenced by the Dicke-narrowing effect. The  $\beta$ -corrected HTP enables high quality analytical representation of experimental spectra without incurring the high computational cost of more advanced line-shape models. This correction is directly applicable to any other line-shape model based on the hard-collision model for velocity-changing collisions.

© 2019 The Authors. Published by Elsevier Ltd.

This is an open access article under the CC BY-NC-ND license.

<http://creativecommons.org/licenses/by-nc-nd/4.0/>

## 1. Introduction

For an accurate description of spectral line shapes of isolated molecular transitions in the gas phase, it is typically required to go beyond [1,2] the Voigt profile, which ignores the influence of the speed-dependence of collisional broadening and shift [3,4] as well as velocity-changing (VC) collisions [5–8] on the line shapes. It has been shown in several publications that the choice of the VC collision model and the resulting spectral line-shape profile is of fundamental importance in the analysis of high-resolution spectra [9,10]. Following Lance et al. [2] and Pine [11], in the Hartmann–Tran profile (HTP) [12], which was recommended for high-accuracy spectroscopic applications [13] and implemented in the 2016 edition of the HITRAN database [14,15], the hard-collision (HC) model [7,8] for VC collisions is used. It assumes that the active molecule after the collision has a velocity randomly selected from the Maxwellian distribution. However, it was shown that the HC model does not satisfactorily reproduce line shapes with a prominent Dicke narrowing [5] caused by VC collisions, e.g. molecular hydrogen transitions [10]. The simplest physically justified model for the VC collisions is the rigid-sphere model (also called

the billiard ball (BB) model) [16–18], which takes into account the mass ratio of colliding molecules and models the relative importance of speed- and direction-changing collisions [10,18–20]. The rigid-sphere model is used in the billiard-ball profile [16] and the speed-dependent billiard-ball profile (SDBBP) [18]. The perturber-to-absorber mass ratio  $\alpha$  is a crucial parameter in determining the respective influence of velocity- and speed-changing collisions on the line shapes. Moreover, it is important to emphasize that calculations of a ratio of speed- and velocity-changing collision rates as well as a collision kernel based on the rigid-sphere model are in good agreement with classical molecular dynamics simulations (CMDS) [10,19,21].

In this work, we propose a correction to the frequency of VC collisions,  $\nu_{VC}$ , of the HC model adopted in the HTP, in order to achieve percent-level agreement between the corrected HTP and the SDBBP. This approach was first proposed in Ref. [15] for  $H_2$  spectra and was called the  $\beta$  correction. Typically when the original HC model is used to interpret experimental data, the obtained  $\nu_{VC}$  scales non-linearly with pressure, which is not physical. The reason for it is that the HC model oversimplifies the actual description of the velocity changes. The correction reduces the non-linearity of the HC-based  $\nu_{VC}$  with pressure. It allows finding a single  $\nu_{VC}$ /pressure coefficient in multispectrum fit analysis of experimental data [22,23], which results in fidelity of spectra representation comparable to the one of the rigid-sphere model but at

\* Corresponding author.

E-mail addresses: [konefal@fizyka.umk.pl](mailto:konefal@fizyka.umk.pl) (M. Konefał), [piotr.wcislo@fizyka.umk.pl](mailto:piotr.wcislo@fizyka.umk.pl) (P. Wcisło).

the same time keeps the low computational cost of the Hartmann–Tran algorithm. Here, we extend this approach to other molecular systems characterized by  $\alpha$  from 0 to 5. It should be noted that the  $\beta$  correction does not add any extra fitted parameter to the HTP.

The proposed correction is important considering the recent rapid developments of ultra-accurate spectroscopic measurements, where accuracy is no longer limited only by experimental imperfections but also by the use of oversimplified line-shape models. The latter contribution is currently the dominant factor limiting the improvement of the accuracy of spectroscopic data. The correction will allow increasing the accuracy of line shape modeling in various fields of optical metrology, such as Doppler-broadening thermometry [24,25].

## 2. Velocity-changing collisions

The velocity-changing collisions reduce the mean free path of an active molecule and lead to the Dicke narrowing [5] of Doppler broadened spectral lines. One of the simplest models describing the VC collisions is the HC model, which is the one adopted in the HTP. In the HC model the velocity after the collision is randomly chosen from the Maxwell distribution  $f_m(\vec{v})$  of the active molecule velocity  $\vec{v}$ . The corresponding HC kernel

$$f_{\text{HC}}(\vec{v} \leftarrow \vec{v}') = \nu_{\text{VC}} f_m(\vec{v}) \quad (1)$$

describes the rate of velocity changes from the velocity before the collision  $\vec{v}'$  to the velocity after the collision  $\vec{v}$ . A more physically justified description of the VC collisions is given by the BB model [16–18]. The BB collision model is based on the assumption that the molecular interaction potential can be approximated by a hard-sphere wall, see e.g. Refs. [10,26]. The BB kernel is given by the following analytical formula [27]:

$$f_{\text{BB}}(\vec{v} \leftarrow \vec{v}') = \nu_{\text{VC}} f_D \frac{3}{32\pi v_m^2} \frac{(1+\alpha)^{5/2}}{\alpha^2} \frac{1}{\sqrt{v^2 - 2vv'\cos\theta + v'^2}} \times \exp\left(-\frac{(1-\alpha)^2 v'^2}{4\alpha v_m^2} - \frac{(1+\alpha)^2 v^2}{4\alpha v_m^2} - \frac{(1+\alpha)(1-\alpha)vv'}{2\alpha v_m^2}\right) \times \cos\theta + \frac{\alpha \sin^2\theta}{v^2 - 2vv'\cos\theta + v'^2} \frac{v^2 v'^2}{v_m^2}, \quad (2)$$

where  $\nu_{\text{VC}} = v_m^2 / (2D^{(0)} f_D)$  [17,18] is the effective frequency of the VC collisions,  $v_m$  is the most probable speed of the active molecule and

$$D^{(0)} = \frac{3}{8} \sqrt{\frac{k_B T}{2\pi \mu}} \frac{1}{N\sigma^2} \quad (3)$$

is the first-order mass diffusion coefficient for rigid spheres,  $f_D = D/D^{(0)}$  and  $D$  is the exact mass diffusion coefficient for the rigid spheres [17]. The notation in Eqs. (2) and (3) is as follows:  $\alpha = m_p/m_a$  is the perturber-to-absorber mass ratio,  $\mu = m_a m_p / (m_a + m_p)$  is the reduced mass of the collision pair,  $\theta$  is the scattering angle between the velocity vectors  $\vec{v}$  and  $\vec{v}'$ ,  $\sigma$  is the average of the rigid-sphere diameter of the absorber and the perturber,  $N$  is the number density of the perturber,  $k_B$  is the Boltzmann constant and  $T$  is temperature. As shown in Ref. [10,26], the BB collision kernel is in a good agreement with the CMDS collision kernel, provided that  $\sigma$  in Eq. (3) is chosen so that the hard-sphere wall intersects the short-range repulsive part of the actual potential at the mean collision energy.

## 3. Correction of $\nu_{\text{VC}}$ in the HTP

In Ref. [12], an algorithm for evaluating the partially-correlated quadratic speed-dependent hard-collision profile (pCqS-DHCP) [11] with the computational time comparable to that of

the standard Voigt profile was introduced. The IUPAC Task Group [13,14] recommended to call this fast algorithm the Hartmann–Tran profile and demonstrated its utility by applying it to the analysis of water spectra. In Refs. [12,28] the HTP was applied to spectral analysis of other molecules. The way of storing the HTP parameters in the HITRAN2016 database was presented in Ref. [15] and recently extended to the double-power-law representation of the temperature dependencies of the line-shape parameters [29]. The HTP is described by the following set of parameters:

$$\text{HTP}(\Gamma_D, \Gamma_0, \Delta_0, \Gamma_2, \Delta_2, \nu_{\text{VC}}, \eta, \Delta\nu), \quad (4)$$

where  $\Gamma_D$  is the Doppler half-width,  $\Gamma_0$  and  $\Delta_0$  are, respectively, the pressure-induced broadening and shift,  $\Gamma_2$  and  $\Delta_2$  are the parameters that quantify the speed dependence of the broadening and shift,  $\nu_{\text{VC}}$  is the frequency of VC collisions,  $\eta$  is the correlation parameter and  $\Delta\nu$  is the detuning from the line center,  $\nu_0$ , at zero pressure.

The limited reliability of the description of VC collisions given by Eq. (1) and adopted in the HTP can be improved by correcting  $\nu_{\text{VC}}$  in the way proposed in Ref. [15]. Here, we follow this approach by replacing  $\nu_{\text{VC}}$  in Eq. (4) with  $\nu_{\text{VC}}$  multiplied by a simple analytical function of the  $\nu_{\text{VC}}/\Gamma_D$  ratio. This function, called the  $\beta$  correction, is chosen to make the HTP as close as possible to a profile in which the VC collisions are described by a much more realistic BB model (Eq. (2)). We determine the  $\beta$ -correction function for a wide range of perturber-to-absorber mass ratios  $\alpha$ .

The  $\beta$  correction is determined as follows. The SDBBP [18] and the HTP are simulated in a wide range of pressures corresponding to  $\chi = \nu_{\text{VC}}/\Gamma_D$  from 0.01 to 100 and to  $\alpha$  from 0 to 5. We limit our study to  $\alpha = 5$  as it covers most of the mass ratios of typical atmospheric systems. For the calculations of the reference SDBBP we use the diagonalization [18,30–33] and iterative [34] approaches. Following Ref. [15] we simulate the SDBBP and HTP with the same set of the line-shape parameters, setting  $\Gamma_0$ ,  $\Delta_0$ ,  $\Gamma_2$ ,  $\Delta_2$  to zero, keeping  $\Gamma_D$  constant and varying  $\nu_{\text{VC}} = \chi \cdot \Gamma_D$ . Afterwards, the SDBBP and HTP simulated in this way are compared. In order to best reproduce the SDBBP by the HTP we fit the value of  $\nu_{\text{VC}}$  in the HTP. In these fits, we minimize the maximum absolute value of the difference between the two profiles:  $|\text{SDBBP} - \text{HTP}|$ . This procedure is repeated to cover the considered here ranges of  $\chi$  and  $\alpha$ . Subsequently, we find values of  $\beta_\alpha(\chi)$  defined as the ratio of  $\nu_{\text{VC}}$  fitted in the HTP to the original  $\nu_{\text{VC}}$  used in the simulations with the SDBBP.

Determination of the  $\beta$  correction is performed including only the Doppler broadening and velocity-changing collisions, in order to get a universal  $\beta$ -correction function, which is independent of the differences in collisional dephasing affecting various molecules and lines. It was shown in Ref. [15], that when  $\Gamma_0$ ,  $\Delta_0$ ,  $\Gamma_2$ ,  $\Delta_2$  are different from zero, the  $\beta$ -corrected HTP gives a significantly better approximation of the SDBBP than the ordinary HTP. We call the  $\beta$ -corrected HTP simply the  $\beta$ HTP. We propose to use the  $\beta$ HTP in which  $\nu_{\text{VC}}$  in the HTP is replaced by  $\beta_\alpha(\chi)\nu_{\text{VC}}$  as an approximation of the SDBBP:

$$\text{SDBBP}(\dots, \nu_{\text{VC}}, \dots) \approx \beta \text{HTP}(\dots, \nu_{\text{VC}}, \dots) = \text{HTP}(\dots, \beta_\alpha(\chi)\nu_{\text{VC}}, \dots). \quad (5)$$

As the BB collision operator depends on the mass ratio of colliding molecules, we model the  $\beta$  correction as a mass ratio function. In Fig. 1, a comparison between the simulated SDBBP and HTP with and without the  $\beta$  correction is shown. A full dot, for a given  $\chi$  and  $\alpha$ , is obtained by taking the maximum of the absolute value of the difference between the simulated profiles ( $|\text{SDBBP} - \text{HTP}|$ ) and divided by the HTP value at its maximum. Open dots show the same difference but in the case when the value of  $\nu_{\text{VC}}$  in the HTP is adjusted in a way to make the  $\beta$ HTP as close as possible to

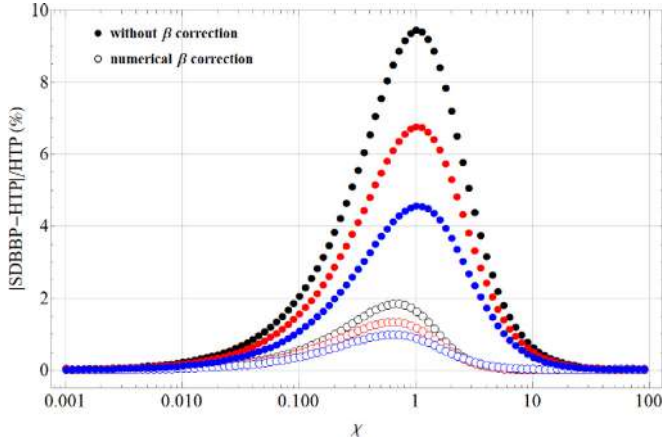


**Fig. 1.** Dependence of the maximum of the absolute value of the difference between simulated profiles  $|SDBBP-HTP|$  divided by the HTP value at its maximum on  $\chi = \nu_{VC}/\Gamma_D$ . Full dots show the results for the HTP without the  $\beta$  correction and open dots show the results for the HTP with the  $\beta$  correction. Black, red and blue colors correspond to calculations for  $\alpha = 0.1, 1.0$  and  $2.5$ , respectively (note logarithmic scale of horizontal axis). (For interpretation of the references to colour in this figure legend, the reader is referred to the web version of this article.)

the simulated SDBBP. Black, red and blue colors correspond to  $\alpha$  equal to 0.1, 1.0 and 2.5, respectively.

The shape of  $|SDBBP - HTP|/HTP$  strongly depends on  $\chi$ : (i) at low  $\chi$ —the low-pressure limit—the impact of  $\nu_{VC}$  on the line-shape profile is negligible and the line-shape profile is dominated by the Doppler broadening, (ii) at medium  $\chi$ —the Dicke narrowing and the Doppler broadening are comparable and the model for the VC collisions plays the most pronounced role, (iii) at high  $\chi$ —the high-pressure limit—the Dicke narrowing dominates the Doppler width and the line-shape converges to the Lorentz profile [5,8,18], independent of the model for the VC collision operator. In the proposed approach, the application of the  $\beta$  correction in HTP allows a fivefold reduction of the difference between the two profiles in the medium pressure range.

#### 4. Analytical representation of the $\beta$ correction and its applicability

We introduce the  $\beta$ -correction as a function of two arguments:  $\chi$  and  $\alpha$ , determined in a two-dimensional fitting approach. In the first step, in order to find the best mathematical representation of  $\beta$  with respect to  $\chi$  for every considered  $\alpha$ , we look for a function which best reproduces numerical values of  $\beta$  calculated in the way described in Section 3.

The observed dependence of the  $\beta$ -correction function on  $\chi$  can be approximated by the following expression:

$$\beta_\alpha(\chi) = A_\alpha \tanh(B_\alpha \log_{10} \chi + C_\alpha) + D_\alpha. \quad (6)$$

In the second step, this function is independently fitted to numerical values of  $\beta_\alpha(\chi)$  for various  $\alpha$  in order to find values of parameters. We do it in a way to obtain the smallest difference between the SDBBP and  $\beta$ HTP when applying numerical and analytical values of  $\beta_\alpha(\chi)$ , see Fig. 4. Next, we determine analytical expressions for each of these parameters, which are provided below:

$$A_\alpha = 0.0534 + 0.1585e^{-0.4510\alpha}, \quad (7a)$$

$$B_\alpha = 1.9595 - 0.1258\alpha + 0.0056\alpha^2 + 0.0050\alpha^3, \quad (7b)$$

$$C_\alpha = -0.0546 + 0.0672\alpha - 0.0125\alpha^2 + 0.0003\alpha^3, \quad (7c)$$

$$D_\alpha = 0.9466 - 0.1585e^{-0.4510\alpha}. \quad (7d)$$

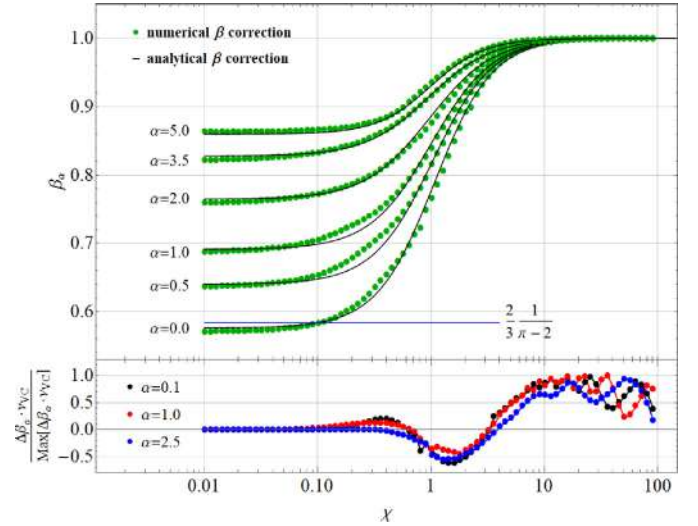


**Fig. 2.** Upper panel: The analytical  $\beta$ -correction function given by Eq. (6) is plotted as black lines (note logarithmic scale of the horizontal axis). Green dots are the numerical calculations of  $\beta$ . Both quantities,  $\chi$  and  $\alpha$ , are dimensionless. The horizontal blue line indicates the correction value taken from Eq. (8), see text for details. Lower panel: Relative differences between numerical and analytical values of the  $\beta_\alpha(\chi)\nu_{VC}$  product according to Eq. (5). (For interpretation of the references to colour in this figure legend, the reader is referred to the web version of this article.)

Fig. 2 shows numerical  $\beta$  values (green dots) for  $\chi$  ranging from 0.01 to 100 and for  $\alpha$  from 0 to 5. The black lines correspond to the phenomenological  $\beta$ -correction function. At high  $\chi$  the  $\beta$ -correction function goes to 1 as at high pressure the VC collisions lead to the same Lorentzian shape of the Doppler component for any reasonable VC collision operator [5,8,18]. On the other hand, at low  $\chi$  the  $\beta$  correction converges to the low pressure limit which is different for collisional operators with different  $\alpha$  [35]. The lower panel of Fig. 2 shows the relative differences between numerical and analytical values of the  $\beta_\alpha(\chi)\nu_{VC}$  product, which is the quantity entering into the  $\beta$ HTP according to Eq. (5). It is especially important to minimize this differences at higher  $\chi$  values, in order to minimize the discrepancies between numerical and analytical values of  $\beta_\alpha(\chi)$ , as shown in Fig. 4. We want to emphasize that the  $\beta$ -correction function is a phenomenological function and it does not have a strict physical meaning. However, it can be seen as a quantity which tells how many hard VC collisions are needed to give a similar effect to BB collisions at given  $\alpha$ . Finally, in Fig. 3 we present the functions given by Eqs. (7a)–(7d) for  $A_\alpha$ ,  $B_\alpha$ ,  $C_\alpha$  and  $D_\alpha$  (linear plots) together with numerical values (discrete data points).

In Fig. 4, we demonstrate how well the determined here  $\beta$ -correction function, Eq. (6), is able to improve the HTP. The relative differences between the SDBBP and the  $\beta$ HTP are plotted as open dots when the numerical values of  $\beta$  are taken, and as lines when applying analytical values of  $\beta$  according to Eq. (6). The analytical  $\beta$ -correction function captures well the behavior of numerical calculations. Although the analytical formula performs worse for  $\chi > 4$ , it still provides a significant improvement over the uncorrected HTP. The presented analytical function is a compromise between the simplicity of mathematical expressions and the agreement with numerical calculations. The  $\beta$ -correction function has been successfully applied in spectral analysis of lines of helium perturbed  $H_2$  [36] and of pure  $D_2$  lines [37].

In Ref. [38], the relation between the effective frequency of the VC collisions in the soft collision model  $\nu_{opt}^{SC}$  and in the HC model

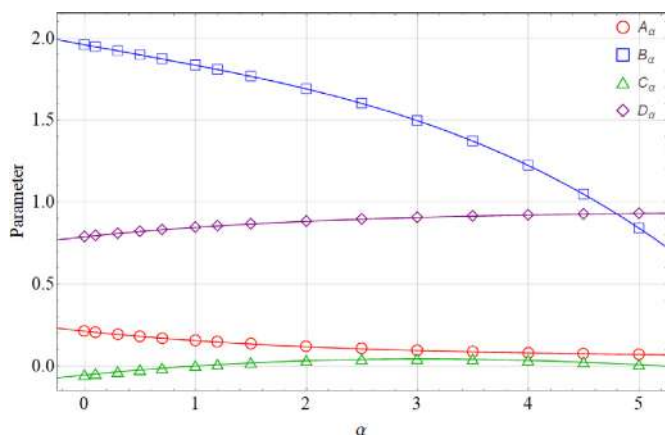


**Fig. 3.** Overview of the parameters of the  $\beta$ -correction function as a function of  $\alpha$ . Numerical values of  $A_\alpha$  are plotted as red circles,  $B_\alpha$  as blue squares,  $C_\alpha$  as green triangles and  $D_\alpha$  as purple diamonds. Analytical functions of these parameters, given by Eq. (7a)–(7d), are plotted as lines in corresponding colors. (For interpretation of the references to colour in this figure legend, the reader is referred to the web version of this article.)

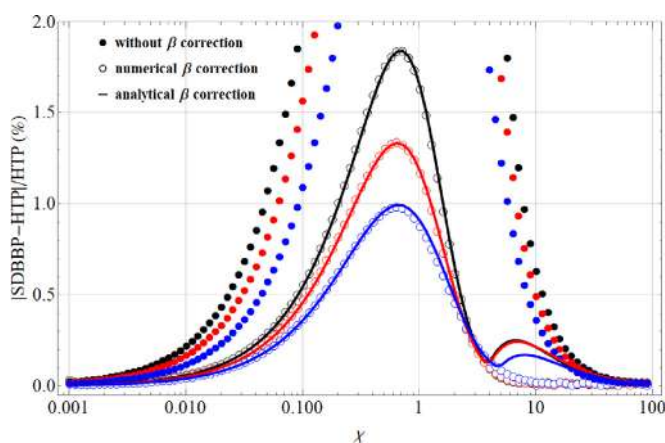


**Fig. 4.** The relative differences between the SDBBP and the HTP simulated with the same set of parameters (note logarithmic scale of the horizontal axis). This figure partially reproduces Fig. 1. Black, red and blue colors correspond to  $\alpha = 0.1$ , 1.0 and 2.5, respectively. Open dots represent the difference between the two profiles when numerical values of  $\beta$  are used and lines represent the same difference when analytical  $\beta$  values based on Eq. (6) are applied. (For interpretation of the references to colour in this figure legend, the reader is referred to the web version of this article.)

$\nu_{\text{opt}}^{\text{HC}}$  in the Doppler limit was shown to be

$$\frac{\nu_{\text{opt}}^{\text{HC}}}{\nu_{\text{opt}}^{\text{SC}}} = \frac{2}{3} \frac{1}{\pi - 2} \approx 0.584. \quad (8)$$

This relation was derived at low pressure regime from the expression given by Rautian and Sobel'man [8] describing simultaneous influence of the soft and hard collisions on the Doppler broadening. As the soft collisions are equivalent to the BB collisions with  $\alpha = 0$ , Eq. (8) corresponds to the  $\beta$  correction value at its zero limit, which found numerically equals:  $\beta_0(0) \approx 0.576$ . This value is about 1.4% lower than the result in Eq. (8), see Fig. 2. This difference is likely a consequence of different approaches to residual minimization used in this work and in Ref. [38]. Here, the residuals were minimized over the entire line, whereas in Ref. [38] only at the maximum residual value.

Calculated values of the  $\beta$ -correction function parameters for selected molecular systems are listed in Table 1. The values were calculated based on Eqs. (7a)–(7d).

**Table 1**  
Values of the  $\beta$ -correction function parameters for selected molecular systems.

System	$\alpha$	$A_\alpha$	$B_\alpha$	$C_\alpha$	$D_\alpha$
CO <sub>2</sub> -N <sub>2</sub>	1.57	0.1314	1.7954	0.0213	0.8686
CO <sub>2</sub> -O <sub>2</sub>	1.38	0.1384	1.8099	0.0151	0.8616
CO-N <sub>2</sub>	1.00	0.1543	1.8444	0.0004	0.8457
CO-O <sub>2</sub>	0.88	0.1599	1.8566	-0.0050	0.8401
HF-N <sub>2</sub>	0.71	0.1684	1.8749	-0.0131	0.8316
HF-O <sub>2</sub>	0.63	0.1726	1.8838	-0.0172	0.8274
HCl-N <sub>2</sub>	1.30	0.1415	1.8166	0.0123	0.8585
HCl-O <sub>2</sub>	1.14	0.1481	1.8309	0.0062	0.8519
CH <sub>4</sub> -N <sub>2</sub>	0.57	0.1759	1.8906	-0.0203	0.8241
CH <sub>4</sub> -O <sub>2</sub>	0.50	0.1798	1.8987	-0.0241	0.8202

## 5. Conclusions

In this paper a simple analytical correction for the frequency of VC collisions,  $\nu_{\text{VC}}$ , of the HC model adopted in the HTP is presented. The HC model overestimates the frequency of VC collisions in real molecular systems, as it was shown for H<sub>2</sub> perturbed by argon in Ref. [10] or by helium in Ref. [20], as well as in the case of VC collisions described by the Fokker-Planck operator [8,38]. Presented, the  $\beta$ -correction function applied to the HTP reduces the disagreement between the HTP and the more physically justified but more computationally demanding SDBBP [16,18,32] to the percent level, enabling more accurate reproduction of molecular spectra.

In this paper, we propose the  $\beta$ -correction function, which is a function of  $\chi = \nu_{\text{VC}}/\Gamma_{\text{D}}$  and four heuristic parameters dependent on the perturber-to-absorber mass ratio  $\alpha$ . Application of the  $\beta$  correction is of particular significance for studies involving line shapes characterized by a large Dicke narrowing effect and involving multi-spectrum fitting analysis by a line-shape profile assuming the HC model. This correction allows one to maximize the agreement between the HC-based model and experimental spectra with linear dependence of  $\nu_{\text{VC}}$  on pressure. Its implementation does not add any extra fitted parameter and has a negligible influence on the computation time of the line profile.

## Declaration of Competing Interests

The authors declare that they have no known competing financial interests or personal relationships that could have appeared to influence the work reported in this paper.

## Acknowledgements

The authors would like to thank Grzegorz Kowzan for language corrections of the manuscript. MK and DL contributions are supported by the National Science Centre, Poland, Project 2015/18/E/ST2/00585. MS contribution is supported by the National Science Centre in Poland through Projects 2014/15/D/ST2/05281 and 2017/26/D/ST2/00371 and by the TEAM IV Programme of the Foundation for Polish Science co-financed by the European Union under the European Regional Development Fund. MZ contribution is supported by the National Science Centre, Poland, Project 2015/17/B/ST2/02115. PW contribution is supported by the National Science Centre in Poland through Projects nos. 2015/19/D/ST2/02195 and 2018/31/B/ST2/00720. The research is a part of the program of the National Laboratory FAMO (KL FAMO) in Torun, Poland, and is supported by a subsidy from the Polish Ministry of Science and Higher Education. The research effort is also supported by the COST Action CM1405 MOLIM.

## References

- [1] Ciuryło R, Szudy J. Speed-dependent pressure broadening and shift in the soft collision approximation. *J Quant Spectrosc Radiat Transf* 1997;57(1997):411–23. doi:10.1016/S0022-4073(96)00078-7.
- [2] Lance B, Blanquet G, Walrand J, Bouanich J-P. On the speed-dependent hard collision lineshape models: application to  $c_2h_2$  perturbed by xe. *J Mol Spectrosc* 1997;185(1997):262–71. doi:10.1006/jmsp.1997.7385.
- [3] Berman PR. Speed-dependent collisional width and shift parameters in spectral profiles. *J Quant Spectr Radiat Transf* 1972;12(9):1331–42. doi:10.1016/0022-4073(72)90189-6.
- [4] Farrow RL, Rahn IA, Sitz GO, Rosasco GJ. Observation of a speed-dependent collisional inhomogeneity in  $H_2$  vibrational line profiles. *Phys Rev Lett* 1989;63(7):746–9. doi:10.1103/PhysRevLett.63.746.
- [5] Dicke RH. The effects of collisions upon the doppler width of spectral lines. *Phys Rev* 1953;89(2):472–3. doi:10.1103/PhysRev.89.472.
- [6] Galatry L. Simultaneous effect of doppler and foreign gas broadening on spectral lines. *Phys Rev* 1961;122(4):1218–23. doi:10.1103/PhysRev.122.1218.
- [7] Nelkin M, Ghatak A. Simple binary collision model for van hove's  $G_s(r, t)$ . *Phys Rev* 1964;135(1A):A4–9. doi:10.1103/PhysRev.135.A4.
- [8] Rautian SG, Sobel'man II. The effect of collisions on the doppler broadening of spectral lines. *Sov Phys Uspekhi* 1967;9(5):701–16. doi:10.1070/PU1967v09n05ABEH003212.
- [9] Tran H, Hartmann JM, Chaussard F, Gupta M. An isolated line-shape model based on the keilson storer function for velocity changes. ii. molecular dynamics simulations and the  $q(1)$  lines for pure  $H_2$ . *J Quant Spectr Radiat Transf* 2009;131:154303. doi:10.1063/1.3247898.
- [10] Wcisło P, Tran H, Kassi S, Campargue A, Thibault F, Ciuryło R. Velocity-changing collisions in pure  $H_2$  and  $H_2$ -Ar mixture. *J Chem Phys* 2014;141(141):074301. doi:10.1063/1.4892414.
- [11] Pine AS. Asymmetries and correlations in speed-dependent dicke-narrowed line shapes of argon-broadened hf. *J Quant Spectr Radiat Transf* 1999;62(4):397–423. doi:10.1016/S0022-4073(98)00112-5.
- [12] Ngo NH, Lisak D, Tran H, Hartmann JM. An isolated line-shape model to go beyond the Voigt profile in spectroscopic databases and radiative transfer codes. *J Quant Spectr Radiat Transf* 2013;129:89–100. doi:10.1016/j.jqsrt.2013.05.034.
- [13] Tennyson J, Bernath PF, Campargue A, Császár AG, Daumont L, Gamache RR, et al. Recommended isolated-line profile for representing high-resolution spectroscopic transitions (IUPAC technical report). *Pure Appl Chem* 2014;86(12):1931–43. doi:10.1515/pac-2014-0208.
- [14] Gordon IE, Rothman LS, Hill C, Kochanov R, Tan Y, Bernath PF, et al. The HITRAN2016 molecular spectroscopic database. *J Quant Spectr Radiat Transf* 2017;203:3–69. doi:10.1016/j.jqsrt.2017.06.038.
- [15] Wcisło P, Gordon I-E, Tran H, Tan Y, Hu S-M, Campargue A, et al. The implementation of non-Voigt line profiles in the HITRAN database:  $H_2$  case study. *J Quant Spectr Radiat Transf* 2016;177(177):75–91. doi:10.1016/j.jqsrt.2016.01.024.
- [16] Blackmore R. A modified Boltzmann kinetic equation for line shape functions. *J Chem Phys* 1987;87(1987):791–800. 0021-9606/87/140791-10002.10
- [17] Lindenfeld M. Self-structure factor of hard-sphere gases for arbitrary ratio of bath to test particle masses. *J Chem Phys* 1979;73(1979):5817–29. 0021-9606/80/235817-13001.00
- [18] Ciuryło R, Shapiro D, Drummond JR, May A. Solving the line-shape problem with speed-dependent broadening and shifting and with Dicke narrowing. II. application. *Phys Rev A* 2002;65(2002):12502. doi:10.1103/PhysRevA.65.012502.
- [19] Ciuryło R, Lisak D, Szudy J. Role of velocity- and speed-changing collisions an speed-dependent line shapes of  $H_2$ . *Phys Rev A* 2002;66(66):472–3. doi:10.1103/PhysRevA.66.032701.
- [20] Wcisło P, Thibault F, Cybulski H, Ciuryło R. Strong competition between velocity-changing and phase- or state-changing collisions in  $H_2$  spectra perturbed by ar. *Phys Rev A* 2015;91(91):052505. doi:10.1103/PhysRevA.91.052505.
- [21] Hoang PNM, Joubert P, Robert D. Speed-dependent line-shape models analysis from molecular dynamics simulations: the collision regime. *Phys Rev A* 2001;65(65):12507. doi:10.1103/PhysRevA.65.012507.
- [22] Benner D, Rinsland C, Devi V, Smith M, Atkins D. A multispectrum nonlinear least squares fitting technique. *J Quant Spectr Radiat Transf* 1995;53:705–21. doi:10.1016/0022-4073(95)00015-D.
- [23] Pine A, Ciuryło R. Multispectrum fits of ar-broadened HF with a generalized asymmetric lineshape: effects of correlation, hardness, speed dependence, and collision duration. *J Mol Spectrosc* 2001;208(2001):180–7. doi:10.1006/jmsp.2001.8375.
- [24] Bielska K, Havey, G E Scace DK, Lisak D, Hodges JT. Spectroscopic measurement of the vapour pressure of ice. *Phil Trans R Soc A* 2012;370:2509–19. doi:10.1098/rsta.2011.0188.
- [25] Gotti R, Moretti L, Gatti D, Castrillo A, Galzerano G, Laporta P, et al. Cavity-ring-down doppler-broadening primary thermometry. *Phys Rev A* 2018;97:012512. doi:10.1103/PhysRevA.97.012512.
- [26] Wcisło P, Thibault F, Zaborowski M, Wójtewicz S, Cygan A, Kowzan G, et al. Accurate deuterium spectroscopy for fundamental studies. *J Quant Spectr Radiat Transf* 2018;213(213):41–51. doi:10.1016/j.jqsrt.2018.04.011.
- [27] Liao PF, Bjorkholm JE, Berman PR. Effects of velocity-changing collisions on two-photon and stepwise-absorption spectroscopic line shapes. *Physical Review A* 1980;21(6):1927–38. doi:10.1103/PhysRevA.21.1927.
- [28] Lisak D, Cygan A, Bermejo D, Domenech J, Hodges J, Tran H. Application of the Hartmann Tran profile to analysis of  $H_2O$  spectra. *J Quant Spectr Radiat Transf* 2015;164:221–30. doi:10.1016/j.jqsrt.2015.06.012.
- [29] Stolarczyk N, Thibault F, Cybulski H, Wójtewicz S, Cygan A, Kowzan G, et al. Evaluation of different parameterizations of temperature dependences of the line-shape parameters based on ab initio calculations: case study for the HITRAN database. *J Quant Spectrosc Radiat Transf* 2019;106676. doi:10.1016/j.jqsrt.2019.106676.
- [30] Dolbeau S, Berman R, Drummond JR, May AD. Dicke narrowing as an example of line mixing. *Phys Rev A* 1998;59(5):3506–12.
- [31] Robert D, Bonamy L. Memory effects in speed-changing collisions and their consequences for spectral lineshape: i. collision regime. *Eur Phys J D* 1998;2(3):245. doi:10.1007/s100530050137.
- [32] Shapiro D, Ciuryło R, Drummond JR, May A. Solving the line-shape problem with speed-dependent broadening and shifting and with Dicke narrowing. I. formalism. *Phys Rev A* 2002;65(2002):12501.
- [33] Lisak D, Bielski A, Ciuryło R, Domysławska J, Trawiński RS, Szudy J. On the role of dicke narrowing in the formation of atomic line shapes in the optical domain. *J Phys B: At Mol Opt Phys* 2003;36:3985–98.
- [34] Wcisło P, Cygan A, Lisak D, Ciuryło R. Iterative approach to line-shape calculations based on the transport-relaxation equation. *Phys Rev A* 2013;88(88):012517. doi:10.1103/PhysRevA.88.012517.
- [35] Chandrasekhar S. Stochastic problems in physics and astronomy. *Rev Mod Phys* 1943;15(1):1–89. doi:10.1103/RevModPhys.15.1.
- [36] Stowiński M, Konefał M, Zaborowski M, Józwiak H, Nishiyama A, Stolarczyk N, et al. in preparation.
- [37] Zaborowski M, Thibault F, Cygan A, Józwiak H, Kowzan G, Masłowski P, et al. in preparation.
- [38] Wójtewicz S, Cygan A, Masłowski P, Domysławska J, Trawiński R, Lisak D, et al. Spectral line shapes of self-broadened P-branch transitions of oxygen B band. *J Quant Spectr Radiat Transf* 2014;144(144):36–48. doi:10.1016/j.jqsrt.2014.03.029.



## Ultrahigh finesse cavity-enhanced spectroscopy for accurate tests of quantum electrodynamics for molecules

MIKOŁAJ ZABOROWSKI,<sup>1,\*</sup> MICHAŁ SŁOWIŃSKI,<sup>1</sup> KAMIL STANKIEWICZ,<sup>1</sup>  
FRANCK THIBAUT,<sup>2</sup> AGATA CYGAN,<sup>1</sup> HUBERT JÓZWIAK,<sup>1</sup> GRZEGORZ KOWZAN,<sup>1</sup>  
PIOTR MASŁOWSKI,<sup>1</sup> AKIKO NISHIYAMA,<sup>1</sup> NIKODEM STOLARCZYK,<sup>1</sup> SZYMON WÓJTEWICZ,<sup>1</sup>  
ROMAN CIURYŁO,<sup>1</sup> DANIEL LISAK,<sup>1</sup> AND PIOTR WCISŁO<sup>1,3</sup>

<sup>1</sup>Institute of Physics, Faculty of Physics, Astronomy and Informatics, Nicolaus Copernicus University in Toruń, Grudziądzka 5, 87-100 Toruń, Poland

<sup>2</sup>Université de Rennes, CNRS, IPR (Institut de Physique de Rennes)—UMR 6251, F-35000 Rennes, France

<sup>3</sup>e-mail: piotr.wcislo@umk.pl

\*Corresponding author: mzab@doktorant.umk.pl

Received 27 January 2020; revised 19 February 2020; accepted 20 February 2020; posted 20 February 2020 (Doc. ID 389268); published 17 March 2020

**We report the most accurate, to the best of our knowledge, measurement of the position of the weak quadrupole S(2) 2–0 line in D<sub>2</sub>. The spectra were collected with a frequency-stabilized cavity ringdown spectrometer (FS-CRDS) with an ultrahigh finesse optical cavity ( $\mathcal{F} = 637000$ ) and operating in the frequency-agile, rapid scanning spectroscopy (FARS) mode. Despite working in the Doppler-limited regime, we reached 40 kHz of statistical uncertainty and 161 kHz of absolute accuracy, achieving the highest accuracy for homonuclear isotopologues of molecular hydrogen. The accuracy of our measurement corresponds to the fifth significant digit of the leading term in quantum electrodynamics (QED) correction. We observe  $2.3\sigma$  discrepancy with the recent theoretical value.** © 2020 Optical Society of America

<https://doi.org/10.1364/OL.389268>

Molecular hydrogen, in the view of its simplicity, is well suited for testing quantum electrodynamics (QED) for molecules [1,2] as well as for searching for new physics beyond the standard model such as new forces [3] or extra dimensions [4]. Furthermore, molecular hydrogen possesses a wide structure of ultranarrow rovibrational transitions [5] with different sensitivities to the proton charge radius and proton-to-electron mass ratio. Therefore, the recent large progress in both theoretical [1,2,6] and experimental [7–11] determinations of the rovibrational splitting in different isotopologues of molecular hydrogen makes it a promising system for adjusting several physical constants [12,13]. The most accurate measurements were performed for the HD isotopologue with absolute accuracy claimed to be 20 kHz [14] and 80 kHz [8] for the R(1) 2–0 line. Such accuracy was obtained by saturating the transition and measuring the sub-Doppler structure. These two results [8,14]

differ, however, by almost 1 MHz. Recently, it was reported [7] that the uncertainty from Ref. [14] was underestimated due to a complex hyperfine structure and should be 50 kHz. Although HD possesses electric dipole transitions, they are extremely weak, and a high-finesse optical cavity (with finesse of the order of  $10^5$ ) is necessary to build a sufficiently large intracavity power and saturate the transitions. Homonuclear isotopologues (due to the symmetry of molecules) do not possess even weak electric dipole lines in the ground electronic state, and direct studies of the rovibrational structure were performed on the quadrupole transitions, which are almost 3 orders of magnitude weaker than the dipole lines used in HD. For this reason, their transitions were not saturated and measurements were performed with the cavity-enhanced Doppler-limited techniques. The most accurate measurements for the D<sub>2</sub> isotopologue were performed for the first overtone [the S(2) line] and reached an absolute accuracy of 500 kHz [10] and 400 kHz [11]. For the case of the H<sub>2</sub> isotopologue, the most accurate measurements that directly probe the rovibrational lines reached an accuracy of 6.6 MHz [15] (performed for second overtone), and the measurement based on the subtraction of the energies of two electronic transitions provided the energy of the fundamental band lines with an accuracy of 4.5 MHz [16,17].

In this Letter, we report the most accurate measurement of the position of the weak quadrupole S(2) 2–0 line in D<sub>2</sub>. The spectra were collected with a frequency-stabilized cavity ringdown spectrometer (FS-CRDS) linked to an optical frequency comb (OFC) referenced to a primary frequency standard [18,19]. We developed an ultrahigh finesse optical cavity ( $\mathcal{F} = 637000$ ), and we implemented frequency-agile, rapid scanning spectroscopy (FARS) [20], which allowed us to reduce the absorption noise from  $3 \times 10^{-10} \text{ cm}^{-1}$  in our previous study [11] to  $8 \times 10^{-12} \text{ cm}^{-1}$  in the present work. In spectra analysis, we used the speed-dependent billiard-ball

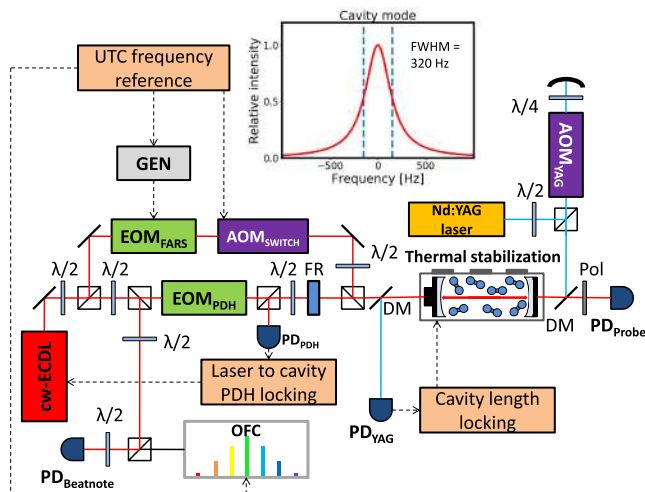


**Fig. 1.** Frequency-stabilized cavity ringdown spectrometer FS-CRDS referenced to the primary frequency standard UTC (AOS). Light from a continuous-wave external cavity diode laser (cw-ECDL) is polarization split into two beams. One of them is used for PDH locking of the ECDL frequency to the cavity mode and to determine its absolute frequency by measuring the heterodyne beat with the OFC.  $EOM_{PDH}$  modulates the phase of light to create the PDH error signal. Second beam probes the gas sample inside the cavity by ringdown decay signals initiated by an acousto-optic modulator ( $AOM_{SWITCH}$ ). The cavity length is actively stabilized to the iodine stabilized Nd:YAG laser. The  $EOM_{FARS}$ , also referenced to the UTC (AOS), is used for fast full-spectrum scanning by stepping a laser sideband to successive optical cavity modes. FR, Faraday rotator; GEN, generator; DM, dichroic mirror; Pol, polarizer; PD, photodiodes.

profile (SDBBP) [21], whose parameters were determined in Ref. [11] based on the analysis that merged both *ab initio* calculations and high-pressure measurement. This allowed us to reduce the systematic effects related to collisional perturbation to the shapes of molecular lines [15]. Despite operating in the Doppler-limited regime, we reached 40 kHz of statistical uncertainty and 161 kHz of absolute accuracy of the  $S(2) 2-0$  transition energy determination, achieving the highest accuracy for homonuclear isotopologues of molecular hydrogen and

only 3.2 times lower accuracy compared to the most accurate sub-Doppler measurements in HD [7] whose line intensities are almost 3 orders of magnitude stronger [7,22]. The accuracy of our measurement corresponds to the fifth significant digit of the leading term in QED correction. We observe  $2.3\sigma$  discrepancy between our experimental and most recent theoretical value [2].

The experimental setup is shown in Fig. 1. The enhancement cavity of the FS-CRDS spectrometer is length-stabilized with respect to the  $I_2$ -stabilized Nd:YAG laser operating at 1064 nm to prevent the thermal drift of the cavity modes. The fractional frequency stabilities measured at 1 s are below  $7 \times 10^{-13}$  for Nd:YAG laser and OFC, and below  $4 \times 10^{-12}$  for a continuous-wave external cavity diode laser (cw-ECDL) and cavity modes (see Fig. 3 in Ref. [18] for details). The deuterium sample has a purity of 99.96%. The length of the cavity is 73.5 cm, which corresponds to a free spectral range (FSR) of 204 MHz. We use an acousto-optic modulator ( $AOM_{YAG}$ ) arranged in a double-pass configuration to control the cavity length and, hence, tune the laser frequency on a denser grid than the FSR spacing. We measure the absolute frequency of the laser with an OFC, which is referenced to the Coordinated Universal Time (UTC), the primary time standard provided by the Astro-Geodynamic Observatory in Borowiec (Poland) [18].

In this work, we improved the previous experimental setup [11] by developing a cavity with much higher finesse and implementing the FARS technique [20]. We improved the finesse of the previous cavity [11] from  $\mathcal{F} = 4 \times 10^4$  to  $6.4 \times 10^5$ ; hence, the light-molecule interaction path increased by more than 1 order of magnitude. It corresponds to an ultranarrow mode width of 320 Hz (0.5 ms ringdown decay time), and, to our knowledge, it is the highest finesse used in molecular spectroscopy measurements. The intracavity optical power was 5.8 W, which is several orders of magnitude apart from the line saturation regime. We implemented the FARS technique by using an electro-optic modulator ( $EOM_{FARS}$ , see Fig. 1), which rapidly tunes the frequency of the modulator sideband over successive modes of the optical cavity (15 GHz tuning range). On average, we acquired approximately 230 spectral points per full scan and 7000 scans per every pressure (this corresponds to approximately 50 MHz frequency step and 11 GHz scan range).

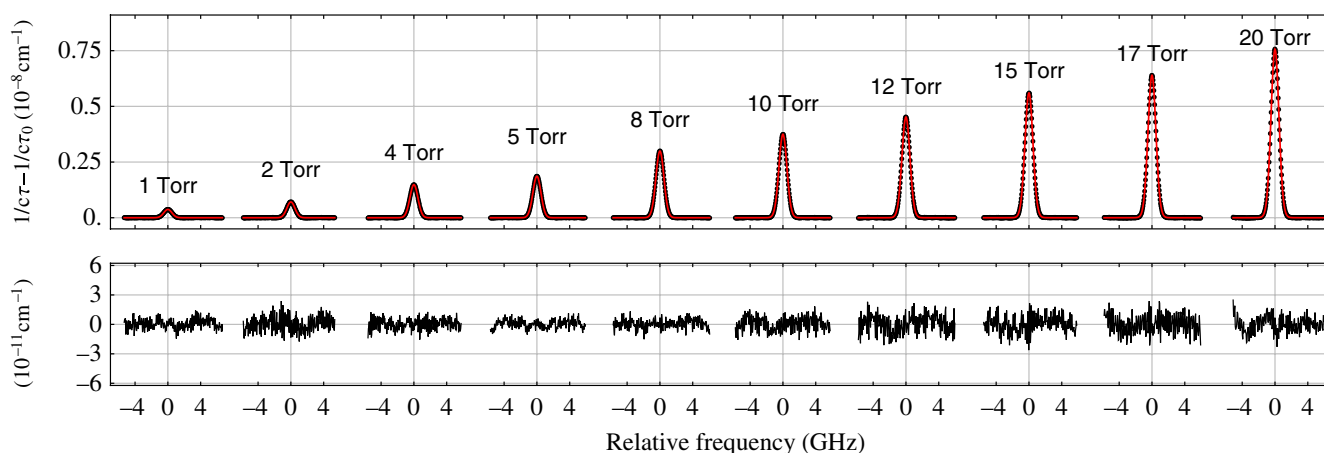


**Fig. 2.** Upper panel,  $2-0 S(2)$  line of  $D_2$  at 10 pressures from 1 to 20 Torr (black points are the experimental spectra, and red lines are the fitted profiles). Lower panel, the residuals obtained with SDBBP fit (standard deviation of residuals varies from  $4.5 \times 10^{-12} \text{ cm}^{-1}$  to  $9.6 \times 10^{-12} \text{ cm}^{-1}$ , and is  $8 \times 10^{-12} \text{ cm}^{-1}$  on average).

**Table 1. Standard Uncertainty Budget to Experimental Determination of the Frequency of the S(2) 2–0 Transition in D<sub>2</sub><sup>a</sup>**

Uncertainty Contribution	$u(v_0)$ (kHz)	$u(v_0)$ (kHz)
	1 to 20 Torr	1 to 40 Torr
1. Line shape profile	111	222
2. Statistics, $1\sigma$	96	40
3. Instrumental systematic shift [18]	47	47
4. Etalons	46	21
5. Temperature instability	5	5
6. Relativistic asymmetry [27]	3	3
7. Laser source stability	< 1	< 1
8. Pressure gauge nonlinearity	1	1
<b>Standard combined uncertainty</b>	<b>161</b>	<b>231</b>

<sup>a</sup>Middle and right column show uncertainties estimated for the fitted datasets of 1–20 Torr and 1–40 Torr, respectively.

Excluding experimental setup and gas sample preparations, the measurement time per each pressure took on average 24 h. With a standard FS-CRDS method, the frequency tuning takes much longer time than an individual ringdown decay (the decay time is approximately 0.5 ms, and we recorded seven decay times per every ringdown event, while the laser tuning, cavity mode searching and Pound-Drever-Hall (PDH) relocking takes from few seconds up to a minute) [11]. Therefore, the implementation of the FARS technique allowed us to considerably reduce the experimental dead time related to laser tuning and relocking. Furthermore, the ability to quickly jump over the cavity modes allowed us to completely reverse the sequence of a measurement cycle, and, instead of averaging the signal at every frequency point until reaching the Allan variance minimum, we scan the whole line spectrum in a subsecond time and average consecutive spectra, which considerably reduces the common experimental noise of the spectrum background. We developed an active feedback loop for cavity temperature stabilization that ensures 10 mK stability including temperature gradients [23], which reduces the slow drifts of a spectrum baseline and collisional line shape parameters.

The experimental setup developments allowed us to reach 37-fold lower noise-equivalent absorption level comparing to our previous experiment [11] [see the fit residuals in Fig. 2 and the comparison with the previous experiment in Fig. 3(a)] and, hence, move the experiment into the regime of much lower pressures where the systematic uncertainties related to collisional effects are much smaller. We collected the spectra of the S(2) 2–0 line in D<sub>2</sub> at 18 pressures from 1 to 40 Torr (see Fig. 2). In this figure, we show the spectra only for 10 pressures ranging from 1 to 20 Torr, which were used for our final determination of the line position. It was shown in Ref. [15] that simple fits of the spectra with symmetric line profile and linear extrapolation of the line position to the zero-pressure limit results in a systematic error that comes from the fact that the effective line position does not scale linearly with pressure. The reason is that the actual shapes of D<sub>2</sub> lines are asymmetric, mainly due to strong speed dependence of the collisional shift. To reduce the influence of this asymmetry, in our analysis, we used one of the most physically justified line shape models describing the collisional effects, SDBBP, whose parameters are derived from *ab initio* quantum-scattering calculations, and some of them were adjusted to the high-pressure spectra (see Ref. [11] for details). The spectra for

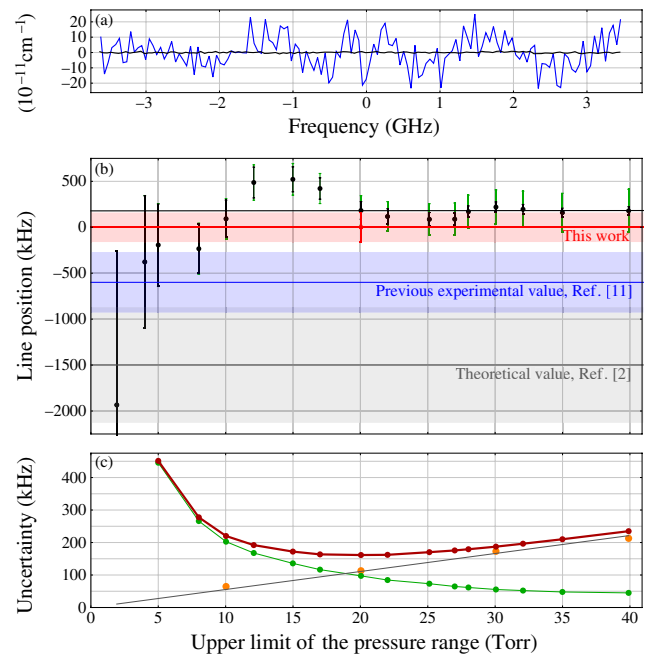


**Fig. 3.** (a) Residuals from the best fits of line shape models to experimental spectra of the S(2) 2–0 line of D<sub>2</sub> for the case of the present work for 4.9 Torr (black line) and the previous work [11] for 984.4 Torr (blue line). The goal of this figure is not to compare the systematic structure of the residuals but the level of the noise before and after experimental improvements reported here. The acquisition time is similar in both cases. (b) Comparison of our determination of the energy of the S(2) 2–0 transition obtained with SDBBP fit [red point, 0 kHz value corresponds to 187,104,300.40(17) MHz] with the best previous experimental result (blue line [11]) and theoretical prediction (gray line [2]); the blue and gray shadows are the corresponding uncertainties. To show how the determined line position and its uncertainty depend on the choice of experimental conditions, we repeated the fitting analysis for different upper limits of the used pressure range (see black points). Due to numerical expense of the SDBBP evaluation, we did this test with its approximated version, i.e., the beta-corrected speed-dependent hard-collision profile ( $\beta$ SDHCP) [24,25]. Although the line position determination with  $\beta$ SDHCP is systematically shifted from our ultimate value (by 179 kHz at 20 Torr upper limit), it properly shows the dependence of line position determination and its statistical uncertainty (black error bars) on the upper limit of the pressure range. The green error bars are total uncertainties. (c) Dependence of the total combined standard uncertainty of line position determination (red points) on the used pressure range of experimental data. The gray line is the systematic part determined from four fits with perturbed values of the fixed line shape parameters (orange points) and approximated with linear function. The statistical part was determined as a standard uncertainty of the fitted line position (green points).

all the pressures were fitted simultaneously, enforcing the same value of unperturbed line position and linear scaling of the line shape parameters, including the pressure shift. In contrast to the ordinary multispectrum fit approach [26], all six collisional line shape coefficients [11] (i.e., the pressure broadening and shift, speed-dependence of the broadening and shift, and the real and imaginary parts of the complex Dicke parameter) and the Doppler broadening were fixed in experimental spectra fitting (this enforced also a proper linear scaling of the line

shape parameters with pressure). Besides what is common to all pressures line position, for each pressure, we also fitted separate values of the line area, linear baseline, and the amplitude and phase of a baseline etalon [11]. To estimate the influence of the fixed collisional line shape parameters, we repeated the fits with varied values of the collisional line shape parameters by a conservative amount of 10% [11]. In Figs. 3(b) and 3(c), we show how the line position determination and different sources of uncertainties depend on the pressure range taken in the analysis. For every point in these plots, we fitted all the spectra from the lowest pressure to the upper limit of the pressure range specified on the horizontal axis. When only the low-pressure range is taken into account, the uncertainty is dominated by the statistical contribution, and the uncertainty due to collisional effects is negligible. In the opposite regime, in which all the pressures are included, the uncertainty is dominated by the contribution of the collisional perturbation of the line. The smallest combined uncertainty is reached when the two dominating uncertainty sources (i.e., statistics and line shape profile) are equal, which approximately corresponds to the upper limit of the pressure range equal to 20 Torr [see Fig. 3(c)]. In Table 1, we show the uncertainty budget. Our ultimate determination of the D<sub>2</sub> 2–0 S(2) line frequency is 187,104,300.40(17) MHz (wavenumber 6241.1276670(54) cm<sup>-1</sup>). In Fig. 3(b), we show a comparison of our result with the recent theoretical value [2], 6241.127617(21) cm<sup>-1</sup>, and the two previous experimental results combined [10,11], 6241.127647(11) cm<sup>-1</sup>. The difference between theory and our results is 2.3σ. The leading term in QED correction to the D<sub>2</sub> 2–0 S(2) line frequency is -0.033167(18) cm<sup>-1</sup> [2]; hence, our experimental determination allows this correction to be tested at the fifth meaningful digit. Furthermore, our uncertainty is sufficiently small to test two other higher-order QED corrections and the finite nuclear size correction (see Table V in Ref. [2]).

We demonstrated an accurate measurement of the frequency of the weak S(2) 2–0 line in deuterium. We reached the accuracy of 161 kHz by merging the FARS technique with a ultrahigh finesse cavity. The reported here value of the line position differs from previous experimental determination [11] by 600 kHz (1.6σ) and from theoretical value [2] by 1500 kHz (2.3σ).

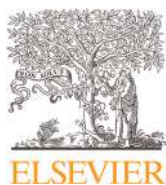
**Funding.** National Science Centre in Poland [2018/31/B/ST2/00720 (NS, HJ and PW), 2017/26/D/ST2/00371 (MZ and SW), 2015/18/E/ST2/00585 (AC, PM and DL), 2016/21/N/ST2/00334 (GK), 2017/24/T/ST2/00242 (GK)]; French-Polish PHC Polonium program (42769ZK); Polish National Agency for Academic Exchange (PPN/X/PS/318/2018); Japan Society for the Promotion of Science; European Regional Development Fund; Ministerstwo Nauki i Szkolnictwa Wyzszego.

**Acknowledgment.** AN contribution is supported by Japan Society for the Promotion of Science Overseas Research grant. MS and KS are supported by the *A next-generation worldwide quantum sensor network with optical atomic clocks* project carried out within the TEAM IV Programme of the Foundation for Polish Science cofinanced by the European Union under the European Regional Development Fund.

**Disclosures.** The authors declare no conflicts of interest.

## REFERENCES

1. J. Komasa, M. Puchalski, P. Czachorowski, G. Łach, and K. Pachucki, *Phys. Rev. A* **100**, 032519 (2019).
2. P. Czachorowski, M. Puchalski, J. Komasa, and K. Pachucki, *Phys. Rev. A* **98**, 052506 (2018).
3. E. J. Salumbides, J. C. J. Koelemeij, J. Komasa, K. Pachucki, K. S. E. Eikema, and W. Ubachs, *Phys. Rev. D* **87**, 112008 (2013).
4. E. J. Salumbides, A. N. Schellekens, B. Gato-Rivera, and W. Ubachs, *New J. Phys.* **17**, 033015 (2015).
5. L. Wolniewicz, I. Simbotin, and A. Dalgarno, *Astrophys. J.* **115**, 293 (1998).
6. K. Pachucki and J. Komasa, *Phys. Chem. Chem. Phys.* **20**, 26297 (2018).
7. M. L. Diouf, F. M. J. Cozijn, B. Darquié, E. J. Salumbides, and W. Ubachs, *Opt. Lett.* **44**, 4733 (2019).
8. L.-G. Tao, A.-W. Liu, K. Pachucki, J. Komasa, Y. R. Sun, J. Wang, and S.-M. Hu, *Phys. Rev. Lett.* **120**, 153001 (2018).
9. E. Fasci, A. Castrillo, H. Dinesan, S. Gravina, L. Moretti, and L. Gianfrani, *Phys. Rev. A* **98**, 022516 (2018).
10. D. Mondelain, S. Kassi, T. Sala, D. Romanini, D. Gatti, and A. Campargue, *J. Mol. Spectrosc.* **326**, 5 (2016).
11. P. Wcisło, F. Thibault, M. Zaborowski, S. Wójtewicz, A. Cygan, G. Kowzan, P. Masłowski, J. Komasa, M. Puchalski, K. Pachucki, R. Ciuryło, and D. Lisak, *J. Quant. Spectrosc. Radiat. Transfer* **213**, 41 (2018).
12. P. J. Mohr, D. B. Newell, and B. N. Taylor, *Rev. Mod. Phys.* **88**, 035009 (2016).
13. A. Beyer, L. Maisenbacher, A. Matveev, R. Pohl, K. Khabarova, A. Grinin, T. Lamour, D. C. Yost, T. W. Hänsch, N. Kolachevsky, and T. Udem, *Science* **358**, 79 (2017).
14. F. M. J. Cozijn, P. Dupré, E. J. Salumbides, K. S. E. Eikema, and W. Ubachs, *Phys. Rev. Lett.* **120**, 153002 (2018).
15. P. Wcisło, I. E. Gordon, C.-F. Cheng, S.-M. Hu, and R. Ciuryło, *Phys. Rev. A* **93**, 022501 (2016).
16. G. D. Dickenson, M. L. Niu, E. J. Salumbides, J. Komasa, K. S. E. Eikema, K. Pachucki, and W. Ubachs, *Phys. Rev. Lett.* **110**, 193601 (2013).
17. M. L. Niu, E. J. Salumbides, G. D. Dickenson, K. S. E. Eikema, and W. Ubachs, *J. Mol. Spectrosc.* **300**, 44 (2014).
18. A. Cygan, S. Wójtewicz, G. Kowzan, M. Zaborowski, P. Wcisło, J. Nawrocki, P. Krehlik, L. Śliwczyński, M. Lipiński, P. Masłowski, R. Ciuryło, and D. Lisak, *J. Chem. Phys.* **144**, 214202 (2016).
19. A. Cygan, P. Wcisło, S. Wójtewicz, G. Kowzan, M. Zaborowski, D. Charczun, K. Bielska, R. S. Trawiński, R. Ciuryło, P. Masłowski, and D. Lisak, *Opt. Express* **27**, 21810 (2019).
20. G. W. Truong, K. O. Douglass, S. E. Maxwell, R. D. van Zee, D. F. Plusquellic, J. T. Hodges, and D. A. Long, *Nat. Photonics* **7**, 532 (2013).
21. R. Ciuryło, D. A. Shapiro, J. R. Drummond, and A. D. May, *Phys. Rev. A* **65**, 012502 (2002).
22. K. Pachucki and J. Komasa, *Phys. Chem. Chem. Phys.* **12**, 9188 (2010).
23. M. Zaborowski, P. Wcisło, F. Thibault, S. Wójtewicz, A. Cygan, G. Kowzan, P. Masłowski, D. Lisak, and R. Ciuryło, *J. Phys. Conf. Ser.* **810**, 012042 (2017).
24. P. Wcisło, I. E. Gordon, H. Tran, Y. Tan, S.-M. Hu, A. Campargue, S. Kassi, D. Romanini, C. Hill, R. V. Kochanov, and L. S. Rothman, *J. Quant. Spectrosc. Radiat. Transfer* **177**, 75 (2016).
25. M. Konefał, M. Słowiński, M. Zaborowski, R. Ciuryło, D. Lisak, and P. Wcisło, *J. Quant. Spectrosc. Radiat. Transfer* **242**, 106784 (2020).
26. A. S. Pine and R. Ciuryło, *J. Mol. Spectrosc.* **208**, 180 (2001).
27. P. Wcisło, P. Amodio, R. Ciuryło, and L. Gianfrani, *Phys. Rev. A* **91**, 022508 (2015).



Contents lists available at ScienceDirect

Journal of Quantitative Spectroscopy &amp; Radiative Transfer

journal homepage: [www.elsevier.com/locate/jqsrt](http://www.elsevier.com/locate/jqsrt)

# The first comprehensive dataset of beyond-Voigt line-shape parameters from *ab initio* quantum scattering calculations for the HITRAN database: He-perturbed H<sub>2</sub> case study

P. Wcisło<sup>a,\*</sup>, F. Thibault<sup>b</sup>, N. Stolarczyk<sup>a</sup>, H. Jóźwiak<sup>a</sup>, M. Słowiński<sup>a</sup>, M. Gancewski<sup>a</sup>, K. Stankiewicz<sup>a</sup>, M. Konefał<sup>a,c</sup>, S. Kassi<sup>c</sup>, A. Campargue<sup>c</sup>, Y. Tan<sup>d</sup>, J. Wang<sup>d</sup>, K. Patkowski<sup>e</sup>, R. Ciuryło<sup>a</sup>, D. Lisak<sup>a</sup>, R. Kochanov<sup>f,g</sup>, L.S. Rothman<sup>f</sup>, I.E. Gordon<sup>f</sup>

<sup>a</sup> Institute of Physics, Faculty of Physics, Astronomy and Informatics, Nicolaus Copernicus University in Torun, Grudziadzka 5, 87-100 Torun, Poland

<sup>b</sup> Univ Rennes, CNRS, IPR (Institut de Physique de Rennes)-UMR 6251, F-35000 Rennes, France

<sup>c</sup> University of Grenoble Alpes, CNRS, LIPhy, F-38000 Grenoble, France

<sup>d</sup> Hefei National Laboratory for Physical Sciences at Microscale, iChEM, University of Science and Technology of China, Hefei, 230026 China

<sup>e</sup> Department of Chemistry and Biochemistry, Auburn University, Auburn, AL 36849, USA

<sup>f</sup> Harvard-Smithsonian Center for Astrophysics, Atomic and Molecular Physics Division, Cambridge, MA, USA

<sup>g</sup> QUAMER laboratory, Tomsk State University, 36 Lenin Avenue, 634050 Tomsk, Russia

## ARTICLE INFO

### Article history:

Received 15 September 2020

Revised 9 December 2020

Accepted 9 December 2020

Available online 11 December 2020

### Keywords:

Beyond-Voigt line-shape parameters

HITRAN

H<sub>2</sub>-He

Ab initio quantum scattering calculations

## ABSTRACT

We demonstrate a new method for populating line-by-line spectroscopic databases with beyond-Voigt line-shape parameters, which is based on *ab initio* quantum scattering calculations. We report a comprehensive dataset for the benchmark system of He-perturbed H<sub>2</sub> (we cover all the rovibrational bands that are present in the HITRAN spectroscopic database). We generate the entire dataset of the line-shape parameters (broadening and shift, their speed dependence, and the complex Dicke parameter) from fully *ab initio* quantum-scattering calculations. We extend the previous calculations by taking into account the centrifugal distortion for all the bands and by including the hot bands. The results are projected on a simple structure of the quadratic speed-dependent hard-collision profile. We report a simple and compact formula that allows the speed-dependence parameters to be calculated directly from the generalized spectroscopic cross sections. For each line and each line-shape parameter, we provide a full temperature dependence within the double-power-law (DPL) representation, which makes the dataset compatible with the HITRAN database. The temperature dependences cover the range from 20 to 1000 K, which includes the low temperatures relevant for the studies of the atmospheres of giant planets. The final outcome from our dataset is validated on highly accurate experimental spectra collected with cavity ring-down spectrometers. The methodology can be applied to many other molecular species important for atmospheric and planetary studies.

© 2020 Elsevier Ltd. All rights reserved.

## 1. Introduction

The collisional line-shape effects, including the beyond-Voigt effects [1–8], play an important role in atomic and molecular physics [9–13]. On one hand, they give access to studying the molecular interactions [14–16] and dynamics [17], but on the other hand they can affect the accuracy of optical metrology based on molecular spectroscopy [18]. In particular, insufficient modeling of the line-

shape effects can limit the accuracy of simulations of atmospheric measurements of the Earth [19] and other planets [20] and even modify the retrieved opacity of exoplanetary atmospheres [21,22]. To address this problem, a new relational structure [23] was introduced into the most widely used line-by-line spectroscopic database, HITRAN [24], allowing the beyond-Voigt line-shape effects to be represented [25]. It is, however, remarkably challenging to populate the entire database (all the molecules and their isotopologues over a great spectral range and thermodynamic conditions) with purely experimental beyond-Voigt line-shape parameters, not only due to a large number of transitions to be measured at different conditions and different spectral ranges, but

\* Corresponding author.

E-mail addresses: [piotr.wcislo@fizyka.umk.pl](mailto:piotr.wcislo@fizyka.umk.pl), [piotr.wcislo@umk.pl](mailto:piotr.wcislo@umk.pl) (P. Wcisło).

also due to strong numerical correlations between the line-shape parameters.

In this article, we demonstrate a new method for populating line-by-line spectroscopic databases with beyond-Voigt line-shape parameters that is based on *ab initio* quantum scattering calculations. We report a comprehensive dataset for the benchmark system of He-perturbed  $H_2$  lines. We cover all the rovibrational bands (with their branches) that are present in HITRAN. We generate the values of the line-shape parameters (broadening and shift, their speed dependence, and the complex Dicke parameter) from fully *ab initio* quantum-scattering calculations. We extend the calculations of the generalized spectroscopic cross sections reported in Refs. [15,26] by taking into account the centrifugal distortion for all the bands and by including the hot bands. We extrapolate the *ab initio* results to populate very weak lines, i.e., higher overtones,  $v' \geq 6$ , higher rotational numbers,  $J' \geq 8$ , and high- $v'$  hot bands,  $v' \geq 6$ ; following the standard HITRAN notation, we denote the final and initial states of a transition with primes and double primes, respectively. The results are projected on a simple structure of the quadratic speed-dependent hard-collision (qSDHC) profile [27–29] that is consistent with the recently recommended HITRAN parametrization [30]. We also report a simple and compact formula that allows the speed-dependence parameters (within the quadratic model) to be calculated directly from the generalized spectroscopic cross sections, which considerably speeds up the calculations and makes them numerically more stable. For each line and each line-shape parameter we provide a full temperature dependence within the double-power-law (DPL) representation, which was recently recommended for the HITRAN database [30]. The results are valid for a wide temperature range from 20 to 1000 K, with the 50–200 K range prioritized (in this range the DPL fits have 10 times larger weights), which is relevant for the studies of the atmospheres of giant planets. The final outcome from our dataset is validated on highly accurate experimental spectra collected with cavity ring-down spectrometers [31] demonstrating sub-percent agreement. Incorporation of beyond-Voigt line-shape parameters reported in this paper together with their DPL temperature dependences into the HITRAN database is possible thanks to the recently developed flexible relational structure of HITRAN [23]. The complex structure of this dataset is easily accessible for non-expert HITRAN users thanks to the HITRAN Application Programming Interface (HAPI) [32] that automatically generates spectra at the desired spectral range and thermodynamic conditions chosen by the user.

The atmospheres of the giant planets in the Solar System are greatly dominated by a mixture of molecular hydrogen and atomic helium. Moreover, atmospheres of some types of super-Earth exoplanets are predicted to be dominated by the  $H_2$ -He mixture [21]. The spectroscopic studies of giant planet atmospheres are naturally based on the main isotopologue of molecular hydrogen [33]. However, although the abundance of hydrogen deuteride is 4–5 orders of magnitude smaller, HD is noticeable in the spectroscopic studies of giant planets [20,33] due to the much larger intensity of the dipole transitions compared to the weak quadrupole lines in  $H_2$ . In total, four combinations of collision partners should be considered to provide a complete reference data for the planetary studies: self-perturbed  $H_2$ , He-perturbed  $H_2$ ,  $H_2$ -perturbed HD and He-perturbed HD. In this article, we consider the simplest benchmark case of He-perturbed  $H_2$ .

In Section 2, we discuss the general methodology of generating beyond-Voigt line-shape parameters from *ab initio* calculations. Section 3 illustrates the methodology on the examples of two rovibrational lines in He-perturbed  $H_2$ . The full comprehensive dataset for He-perturbed  $H_2$  is discussed in Section 4 and the complete dataset is provided in the supplementary material [34].

## 2. Methodology of generating datasets of the beyond-Voigt line-shape parameters based on the *ab initio* calculations

A typical approach to populating the HITRAN database with the beyond-Voigt line-shape parameters [24,32] uses the data that were obtained from fitting the advanced profiles to the high-quality experimental spectra [25,35–39], see the red boxes in the flowchart in Fig. 1. It is a challenging task to populate the entire database with the purely experimental approach due to the large number of transitions required to be accurately measured at different conditions. Another difficulty is related to strong numerical correlations between the line-shape parameters, which often results in large systematic errors in the retrieved line-shape parameters. The numerical correlation can be considerably reduced by implementing the multispectrum fitting approach [40–42] which is, however, very demanding from a technical point of view and is still difficult to automatically apply to large experimental datasets.

In this article, we present a new methodology for populating the spectroscopic databases based on *ab initio* calculations. A key factor that enables development of this approach was a demonstration that the fully *ab initio* quantum-scattering calculations can reproduce the shapes of the high-quality collision-perturbed experimental spectra at the subpercent level [31], including the deep non-Voigt regime (by subpercent agreement we mean that the root-mean-square error of the *ab initio* model relative to profile peak (rRMSE) calculated within  $\pm$ FWHM is smaller than 1%). The flowchart in Fig. 1 illustrates our methodology (see the yellow boxes). The chain of the *ab initio* calculations starts with the quantum-chemical calculations of the PESs [14,15]. In the second step, the PESs are used to perform the quantum-scattering calculations by solving the close-coupling equations, which provide the scattering S-matrices as a function of relative kinetic energy of the collision,  $E_{kin}$ . The S-matrices allow us to calculate the generalized spectroscopic cross-sections,  $\sigma_{\lambda}^q(E_{kin})$ , that describe the collision perturbation of the optical coherence associated with the considered molecular transition. This approach also allows for the calculations of off-diagonal generalized spectroscopic cross-sections. Thus, for instance, the well-known case of overlapping lines could be considered. However, in this study we limit the discussion to the case of isolated lines, which is relevant for the molecular system considered here at pressures typical for the atmospheres of gas giants. We consider two types of generalized cross-sections that differ by the rank of the velocity tensor,  $\lambda$ . For the zero rank,  $\lambda = 0$ ,  $\sigma_{\lambda}^q$  describes perturbation of internal motion of the

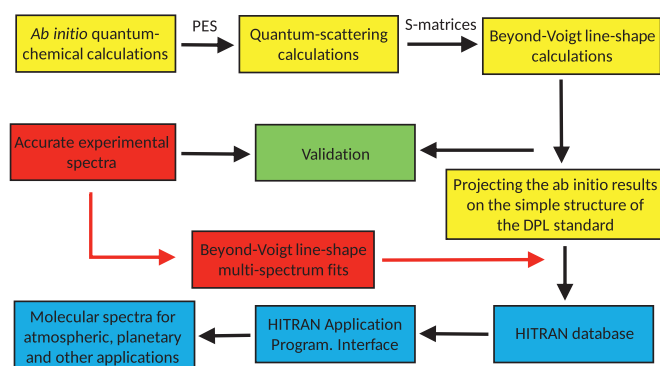


Fig. 1. Diagram illustrating our approach to generating the experimentally validated *ab initio* dataset of the beyond-Voigt line-shape parameters and its incorporation into the HITRAN database. The red arrows show the usual way of populating the database based on experimental spectra analysis only. (For interpretation of the references to color in this figure legend, the reader is referred to the web version of this article.)

molecule, and its real and imaginary parts have spectroscopic interpretation of the pressure broadening and shift cross-sections (PBXS and PSXS, respectively) [43–46]. For  $\lambda = 1$ ,  $\sigma_\lambda^q$  describes perturbation of translational motion (including the correlations with dephasing and state-changing collisions) and it has spectroscopic interpretation of the complex Dicke cross-section (its real and imaginary parts are denoted as RDXS and IDXS, respectively) [26,47–50].  $q$  is the tensor rank of the spectral transition operator (equal to 1 and 2 for dipole and quadrupole lines, respectively). In principle,  $\sigma_\lambda^q$  should also be labeled with the quantum numbers specifying the ground and excited levels of the transition (a diagonal cross-section in Liouville space); for the sake of notation clarity we skip them in this article. The two complex cross sections,  $\sigma_0^q$  and  $\sigma_1^q$ , allow us to calculate the collisional quantities that are needed for modeling the beyond-Voigt shapes of molecular lines, as depicted in the third yellow box in Fig. 1. The basic quantities are the collisional broadening,  $\gamma$ , and shift,  $\delta$ , of molecular lines expressed as a function of active molecule speed,  $v$ , which can be calculated as [3,51]

$$\gamma(v) + i\delta(v) = \frac{1}{2\pi c} \frac{1}{k_B T} \frac{2}{\sqrt{\pi} \bar{v}_p} \int_0^\infty dv_r v_r^2 e^{-\frac{v^2 + v_r^2}{\bar{v}_p^2}} \sinh\left(\frac{2vv_r}{\bar{v}_p^2}\right) \sigma_0^q(v_r), \quad (1)$$

where  $\bar{v}_p$  and  $v_r$  are the most probable speed of the perturber distribution and relative absorber-perturber speed, respectively.  $k_B$  and  $T$  are the Boltzmann constant and temperature. Two other line-shape parameters, which quantify the rate of the velocity-changing collisions, are the real,  $\tilde{v}_{\text{opt}}^r$ , and imaginary,  $\tilde{v}_{\text{opt}}^i$ , parts of the complex Dicke parameter,  $\tilde{v}_{\text{opt}}$ , which is calculated as

$$\tilde{v}_{\text{opt}} = \tilde{v}_{\text{opt}}^r + i\tilde{v}_{\text{opt}}^i = \frac{1}{2\pi c} \frac{1}{k_B T} \langle v_r \rangle M_2 \times \int_0^\infty dx x e^{-x} \left[ \frac{2}{3} x \sigma_1^q(E_{\text{kin}} = x k_B T) - \sigma_0^q(E_{\text{kin}} = x k_B T) \right], \quad (2)$$

where  $M_2 = m_2/(m_1 + m_2)$ , and  $m_1$  and  $m_2$  are the masses of the active and perturbing molecules (or atoms),  $\langle v_r \rangle = \sqrt{8k_B T/\pi\mu}$  is the average relative speed and  $\mu$  is the reduced mass of the colliding partners. The variable of integration,  $x$ , is a dimensionless kinetic energy of a collision,  $x = E_{\text{kin}}/(k_B T)$ . The quantities expressed by Eqs. (1) and (2) [i.e.,  $\gamma(v)$ ,  $\delta(v)$ ,  $\tilde{v}_{\text{opt}}^r$  and  $\tilde{v}_{\text{opt}}^i$ ] carry all the collisional information that comes from our *ab initio* calculations and enters the beyond-Voigt line-shape models. The details of the line-shape calculations based on these quantities can be found in Ref. [6,52,53].

From the perspective of spectroscopy applications and populating the HITRAN database, the full speed dependences, given by Eq. (1), and full *ab initio* line-shape models [53] are far too complex to be stored in the database and are computationally too demanding to be used to analyze large sets of molecular spectra. Therefore, following Ref. [30], we project the full *ab initio* line-shape model on a simple structure of the quadratic speed-dependent hard-collision model (qSDHC) [27–29], in which the speed dependence is approximated with a quadratic function [54]

$$\gamma(v) + i\delta(v) \approx \gamma_0 + i\delta_0 + (\gamma_2 + i\delta_2)(v^2/v_m^2 - 3/2), \quad (3)$$

where  $v_m$  is the most probable absorber speed. The speed-averaged broadening and shift,  $\gamma_0$  and  $\delta_0$ , are calculated as real and imaginary parts of a simple average of  $\sigma_0^q$  over the Maxwellian  $E_{\text{kin}}$  distribution [3,51]

$$\gamma_0 + i\delta_0 = \frac{1}{2\pi c} \frac{1}{k_B T} \langle v_r \rangle \int_0^\infty dx x e^{-x} \sigma_0^q(E_{\text{kin}} = x k_B T). \quad (4)$$

Alternatively,  $\gamma_0$  and  $\delta_0$  can be calculated by averaging  $\gamma(v)$  and  $\delta(v)$  over the Maxwell distribution of active molecule speed,  $v$ , yielding exactly the same result as Eq. (4). The two parameters

quantifying the speed dependence of the broadening and shift,  $\gamma_2$  and  $\delta_2$ , are calculated by demanding that the slope of the quadratic approximation equals the slope of the actual speed dependences at  $v = v_m$  [53],

$$\gamma_2 + i\delta_2 = \frac{v_m}{2} \frac{d}{dv} (\gamma(v) + i\delta(v))|_{v=v_m}. \quad (5)$$

Following the generalized Hess method [4,48,50], we directly take the complex Dicke parameter,  $\tilde{v}_{\text{opt}} = \tilde{v}_{\text{opt}}^r + i\tilde{v}_{\text{opt}}^i$ , as a complex rate of the velocity-changing collisions in the qSDHC model [30]. In the cases of molecules for which the Dicke narrowing is pronounced, we recommend the use of the  $\beta$  correction [25,55] that improves the hard-collision approximation without increasing the cost of the line-shape computations. Note that the  $\beta$  correction is a generic concept valid for any molecular system and does not require any additional parameter to be stored (it depends only on the perturber-to-absorber mass ratio [55]). In total, the most general form of the qSDHC profile requires six line-shape parameters to be stored:

$$\gamma_0, \delta_0, \gamma_2, \delta_2, \tilde{v}_{\text{opt}}^r, \tilde{v}_{\text{opt}}^i. \quad (6)$$

The recent approach adopted in HITRAN [30] allows the temperature dependences of all the six line-shape parameter to be represented with the double-power-law (DPL):

$$\begin{aligned} \gamma_0(T) &= g_0 (T_{\text{ref}}/T)^n + g'_0 (T_{\text{ref}}/T)^{n'}, \\ \delta_0(T) &= d_0 (T_{\text{ref}}/T)^m + d'_0 (T_{\text{ref}}/T)^{m'}, \\ \gamma_2(T) &= g_2 (T_{\text{ref}}/T)^j + g'_2 (T_{\text{ref}}/T)^{j'}, \\ \delta_2(T) &= d_2 (T_{\text{ref}}/T)^k + d'_2 (T_{\text{ref}}/T)^{k'}, \\ \tilde{v}_{\text{opt}}^r(T) &= r (T_{\text{ref}}/T)^p + r' (T_{\text{ref}}/T)^{p'}, \\ \tilde{v}_{\text{opt}}^i(T) &= i (T_{\text{ref}}/T)^q + i' (T_{\text{ref}}/T)^{q'}, \end{aligned} \quad (7)$$

where  $T_{\text{ref}} = 296$  K. The full parametrization of the collisional line-shape effects requires 24 coefficients per single line, i.e., four coefficients per each of the six line-shape parameters, see Eq. (7). It should be noted that Eq. (7) represent the most general case of the DPL representation adopted in HITRAN [30]. For many molecular systems, not all the collisional effects are important at the considered accuracy level and, for a given experimental temperature range, a simple single-power law suffices. In such cases, one of the two approaches will be adopted in HITRAN. Either a single-power law and a smaller number of line-shape parameters will be stored (e.g.,  $\gamma_0$  and  $\delta_0$  for the simple Voigt profile or  $\gamma_0$ ,  $\delta_0$ ,  $\gamma_2$  and  $\delta_2$  for the quadratic speed-dependent Voigt profile) or the full DPL parametrization will be adopted but some of the 24 coefficients will be set to zero.

In this article, we show that our approach based on *ab initio* calculations allows us to fully benefit from the DPL parametrization given by Eq. (7). We generated a comprehensive dataset of the beyond-Voigt line-shape parameters for a system for which all the six line-shape parameters are necessary to represent the shapes of molecular lines (i.e., He-perturbed  $\text{H}_2$ ) and we use the DPL parametrization to represent these parameters in a wide temperature range, see Section 3.3 for details.

The HITRAN DPL parametrization, see Eq. (7) and Ref. [30], does not use the exact form of the Hartmann-Tran profile (HT profile) [56] but its modified version, the qSDHC profile. The main difference between these profiles is that for the description of the velocity-changing collisions the HT profile uses the frequency of the velocity-changing collisions,  $\tilde{v}_{\text{vc}}$ , and the correlation parameter,  $\eta$  (first introduced by Rautian and Sobelmann [2]), while the qSDHC profile uses an explicit parametrization with the real,  $\tilde{v}_{\text{opt}}^r$ , and imaginary,  $\tilde{v}_{\text{opt}}^i$ , parts of the complex Dicke parameter. The major advantage of the parametrization used in this work [30] is that it avoids singularities in temperature dependences of the complex Dicke parameter that may appear when the HT parametrization is used [30]. Another advantage of the qSDHC profile is that it

does not require to introduce unphysical speed dependence of the complex Dicke parameter, in contrast to the original formulation of the HT profile. For details refer to the Appendices A and B in Ref. [30]; see also Ref. [57].

Hartmann proposed a different approach to populating spectroscopic databases with line-shape parameters based on *ab initio* calculations [58] (see also Section 2 in Ref. [30]). In his approach, the *ab initio* line-shape parameters are used with one of the sophisticated line-shape models to generate reference shapes in a wide range of pressures, and then the reference spectra are fitted with some simpler phenomenological model. In his scheme the fitted line-shape parameters lose their physical meaning but, in principle, the shapes of molecular lines should better agree with experiment. Similar tests were done before, for instance see Ref. [59] (in that work, due to a lack of *ab initio* parameters, a sophisticated line-shape model was used with parameters determined experimentally). Recently, this approach was tested for the requantized Classical Molecular Dynamics Simulations corrected with the use of experimental spectra [60]. However, in the case of the He-perturbed H<sub>2</sub> lines considered here, the difference between the qSDHC profile and the more sophisticated ones are much smaller than the difference with experimental data. Hence that approach [58] would not improve the accuracy of the dataset reported here.

### 3. Illustration of the methodology for the case of 2-0 Q(1) and 3-0 S(1) lines

In this section, we use an example of two rovibrational lines in He-perturbed H<sub>2</sub> to illustrate the methodology described in Section 2 and shown in Fig. 1. We consider the 2-0 Q(1) and 3-0 S(1) quadrupole lines that were recently accurately measured with the cavity enhanced techniques [31]; in this article we refer to them as reference lines. These measurements were used for accurate validation of the *ab initio* collisional line-shape calculations [31] and more recently these spectra were used for validation of improved quantum-scattering calculations that include centrifugal distortion [61].

#### 3.1. *Ab initio* quantum scattering calculations

The H<sub>2</sub>-He PES is three-dimensional, i.e., it depends on the distance between the center of mass of the hydrogen molecule and the helium atom,  $R$ , the distance between the two hydrogen atoms,  $r$ , and the angle between the intra- and intermolecular axes,  $\theta$ . The quantum-scattering calculations [15,26] that we used to generate the line-shape parameter dataset are based on the recent state-of-the-art PES that is an extension of the PES published by Bakr, Smith and Patkowski [14] (this PES will be referred to as BSP). The BSP PES was calculated using the coupled-cluster method with single, double and perturbative triple (CCSD(T)) excitations, taking into account also the contributions from the higher coupled-cluster excitations. It was determined for ten intramolecular separations, between 1.1 and 1.75  $a_0$ , which was shown to be insufficient for the detailed studies of processes involving the vibrationally excited H<sub>2</sub> molecule (see Section 2 of Ref. [46] and Appendix C of [15] for details). This issue was addressed in the second version of this PES, BSP2, which extended the range of *ab initio* data points to  $r \in [0.65, 3.75] a_0$ . The final version of this PES, BSP3 [15], which was used in this work, has improved asymptotic behavior of the H<sub>2</sub>-He interaction energy at large  $R$ . The quantum scattering calculations based on the BSP3 PES were recently tested on highly accurate cavity-enhanced measurements of the shapes of He-perturbed H<sub>2</sub> 2-0 Q(1) and 3-0 S(1) lines [31] resulting in unprecedented agreement between experimental and theoretical collision-induced line shapes. Furthermore, the BSP3 PES was em-

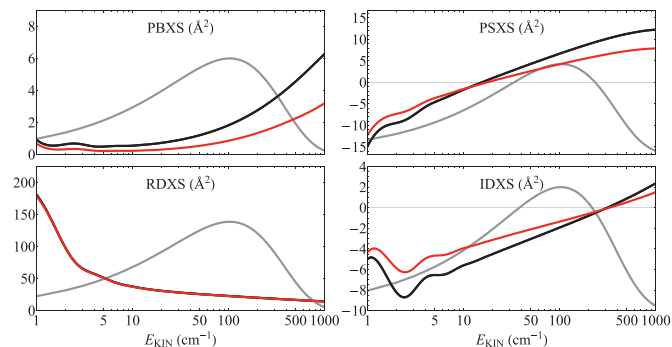


**Fig. 2.** Examples of the generalized spectroscopic cross sections for the case of 2-0 Q(1) and 3-0 S(1) lines in helium-perturbed H<sub>2</sub>, see the red and black lines, respectively. The four panels show the pressure broadening (PBXS), pressure shift (PSXS), and real (RDXS) and imaginary (IDXS) parts of the complex Dicke cross-sections as a function of collision energy. The gray line is the Maxwell-Boltzmann distribution at 296 K in arbitrary units. (For interpretation of the references to color in this figure legend, the reader is referred to the web version of this article.)

ployed in the studies of purely rotational lines of He-perturbed isotopologues of molecular hydrogen: D<sub>2</sub> [47,62] and HD [63,64].

For the purpose of dynamical calculations [15,26], the three-dimensional H<sub>2</sub>-He PES is projected over Legendre polynomials,  $P_\xi$  [15,26,46]:

$$V(R, r, \theta) = \sum_{\xi} v_{\xi}(R, r) P_{\xi}(\cos \theta). \quad (8)$$

In the case of homonuclear molecules like H<sub>2</sub>, the  $\xi$  index takes only even values. Due to the small overall anisotropy of the H<sub>2</sub>-He PES, only the first four  $\xi$  values are retained throughout the calculations. The  $v_{\xi}(R, r)$  terms are averaged over rovibrational wavefunctions of the unperturbed molecule,  $\chi_{v,J}(r)$ , leading to the radial coupling terms,  $A_{\xi,v,J,v',J'}(R)$ , which enter the close-coupled equations. At room temperature the vibrational coupling ( $v \neq v'$ ) can be neglected [15,26]. The influence of the centrifugal distortion (the  $J$  dependence of the radial coupling terms) was usually neglected in the scattering calculations for the rovibrational transitions [15,26], as it was suggested that this effect might be masked due to the large contribution from the vibrational dephasing [46]. However, it was shown recently [61,64] that if one aims for sub-percent accuracy of the line-shape parameters, the centrifugal distortion of the potential energy surface must be taken into account. Therefore, the  $J$ -dependence of the radial coupling terms  $A_{\xi,v,J,v',J'}(R)$  was included in the following analysis.

The scattering calculations were performed using the recently developed BIGOS code [65] for a wide range of relative kinetic energies. The BIGOS code solves the coupled equations in the body-fixed frame of reference using the renormalized Numerov's algorithm [66]. Calculations were carried out for intermolecular distances ranging from 1 to 200  $a_0$  and three asymptotically closed levels were kept in the basis set. Fig. 2 presents an example of the generalized spectroscopic cross sections for the 2-0 Q(1) and 3-0 S(1) lines.

#### 3.2. Speed dependence of the broadening and shift, and the quadratic approximation

The calculations of the  $\gamma_0$ ,  $\delta_0$ ,  $\tilde{\nu}_{\text{opt}}^{\text{r}}$  and  $\tilde{\nu}_{\text{opt}}^{\text{i}}$  parameters are straightforward and require only performing the averaging (with proper weights) of the generalized spectroscopic cross sections over the Maxwell distribution of the relative kinetic energy of a collision, see Eqs. (2) and (4). Calculations of the speed-dependence parameters,  $\gamma_2$  and  $\delta_2$ , are, in principle, more complex and require a few additional steps. First, the *ab initio* speed-dependent broadening and shift are calculated from Eq. (1); Fig. 3

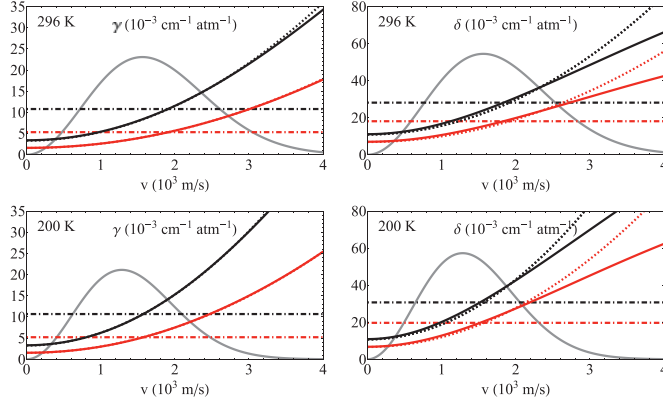


**Fig. 3.** Examples of the speed dependences of the broadening,  $\gamma$ , and shift,  $\delta$ , parameters. The red and black lines correspond to the 2-0 Q(1) and 3-0 S(1) lines in helium-perturbed  $H_2$ , respectively. The solid lines show the full *ab initio* results and the dotted lines show the quadratic approximations. The dash-dotted lines show the corresponding speed-averaged values. The calculations were done for  $T = 296$  K (upper panels) and 200 K (lower panels); the corresponding Maxwell-Boltzmann distributions (in arbitrary units) are plotted as a gray lines. (For interpretation of the references to color in this figure legend, the reader is referred to the web version of this article.)

shows the result for the case of the 2-0 Q(1) and 3-0 S(1) lines. The full speed dependences are approximated with a quadratic function, see Eq. (3). The choice of how the  $\gamma_2$  and  $\delta_2$  parameters are determined is not unique [67,68]. In our methodology we demand that the slopes of the *ab initio* and quadratic speed dependences are equal at the most probable speed, see Eq. (5). This approach is very efficient from a computational perspective. The derivative from Eq. (5) can be done analytically before the integration in Eq. (1) and, hence, the  $\gamma_2$  and  $\delta_2$  parameters can be evaluated directly by averaging the  $\sigma_0^q$  cross section with proper weights

$$\begin{aligned} \gamma_2 + i\delta_2 &= \frac{1}{2\pi c} \frac{1}{k_B T} \frac{\bar{v}_p}{\sqrt{\pi}} e^{-y^2} \\ &\times \int_0^\infty \left( 2x \cosh(2xy) - \left( \frac{1}{y} + 2y \right) \sinh(2xy) \right) \\ &\times x^2 e^{-x^2} \sigma_0^q(x\bar{v}_p) dx, \end{aligned} \quad (9)$$

where  $x = v_r/\bar{v}_p$  and  $y = v_m/\bar{v}_p$ , with  $v_r$ ,  $v_m$  and  $\bar{v}_p$  being the relative absorber to perturber speed, most probable absorber speed and most probable perturber speed, respectively. Note that  $y = \sqrt{\alpha}$ , where  $\alpha$  is the perturber-to-absorber mass ratio. The quadratic approximations for the 2-0 Q(1) and 3-0 S(1) transitions are shown in Fig. 3 as dotted lines. The results from Fig. 3 were calculated for  $T = 296$  K. The accuracy of the quadratic approximation depends on the choice of transition and line-shape parameter. In the cases considered in Fig. 3, the approximation works better for the  $\gamma$  parameter.

### 3.3. Temperature dependences of the line-shape parameters

The values of the six collisional line-shape parameters,  $\gamma_0$ ,  $\delta_0$ ,  $\gamma_2$ ,  $\delta_2$ ,  $\bar{v}_{opt}^r$  and  $\bar{v}_{opt}^i$ , were calculated in the temperature range from 20 to 1000 K using Eqs. (4), (9) and (2). The examples of these results, for the case of our reference lines, are shown in Fig. 4. To represent these temperature dependences in the HITRAN database, we use the recently recommended DPL approximation [30] for all the six line-shape parameters, see Eq. (7). The DPL fits were done for the 20 – 1000 K temperature range enforcing ten times larger fitting weights for the prioritized temperature range from 50 to 200 K (see the gray shadows in Fig. 4), which is relevant for the atmospheres of giant planets. The examples of the DPL

**Table 1**

Examples of the complete records from our DPL line-shape parameter dataset for the cases of the Q(1) 2-0 and S(1) 3-0 lines in  $H_2$  perturbed by He. Coefficients 1 and 2 are in  $cm^{-1}atm^{-1}$ . Exponents 1 and 2 are dimensionless. All the DPL coefficients are defined by Eq. (7), following the original formulation from Ref. [30].

Q(1) 2-0 line				
	Coefficient 1	Coefficient 2	Exponent 1	Exponent 2
$\gamma_0(T)$	$g_0 = 0.29611$	$g'_0 = -0.29076$	$n = -0.30724$	$n' = -0.31188$
$\delta_0(T)$	$d_0 = 1.29146$	$d'_0 = -1.27385$	$m = 0.617$	$m' = 0.622$
$\gamma_2(T)$	$g_2 = 0.114102$	$g'_2 = -0.111618$	$j = 0.2396$	$j' = 0.2453$
$\delta_2(T)$	$d_2 = 0.091305$	$d'_2 = -0.083861$	$k = -0.0013$	$k' = -0.0383$
$\bar{v}_{opt}^r(T)$	$r = 0.04277$	$r' = -0.00417$	$p = 0.6856$	$p' = -0.1236$
$\bar{v}_{opt}^i(T)$	$i = -0.27435$	$i' = 0.26376$	$q = 0.07106$	$q' = 0.05273$
S(1) 3-0 line				
	Coefficient 1	Coefficient 2	Exponent 1	Exponent 2
$\gamma_0(T)$	$g_0 = 0.012847$	$g'_0 = -0.001465$	$n = -0.11276$	$n' = -0.92775$
$\delta_0(T)$	$d_0 = 1.87405$	$d'_0 = -1.84585$	$m = 0.61066$	$m' = 0.61600$
$\gamma_2(T)$	$g_2 = 0.0493132$	$g'_2 = -0.0440504$	$j = -0.34485$	$j' = -0.38797$
$\delta_2(T)$	$d_2 = 1.5985$	$d'_2 = -1.5867$	$k = -0.01288$	$k' = -0.01602$
$\bar{v}_{opt}^r(T)$	$r = 0.05173$	$r' = -0.01689$	$p = 0.6530$	$p' = 0.2554$
$\bar{v}_{opt}^i(T)$	$i = -0.4136$	$i' = 0.39691$	$q = 0.08613$	$q' = 0.06746$

fits are shown in Fig. 4 as green lines. The DPL approximation performs best when the temperature dependence is monotonic; when an extremum is clearly seen then the accuracy is worse, see the  $\delta_0$  panels in Fig. 4. The amplitude of the residuals for most of the cases is smaller than 1%; their exact values are taken into account in the estimations of the line-shape parameter uncertainties reported in our dataset, see the supplementary materials [34].

### 3.4. Examples of a complete dataset record

In Table 1, we show examples of complete records from our line-shape parameter dataset for the cases of the two reference lines. All the coefficients are defined by Eqs. (7), following the original formulation from Ref. [30]. A set of 24 coefficients per a single molecular transition is required for a full DPL description of the six line-shape parameters. The values of the coefficients gathered in Table 1 are directly taken from the fits shown in Fig. 4. Note that at  $T = T_{ref}$ , Eqs. (7) simplify and a given line-shape parameter is simply a sum of the corresponding Coefficient 1 and Coefficient 2; for instance  $\gamma_0(T_{ref}) = g_0 + g'_0$ .

### 3.5. Experimental validation

In this section, we show experimental validation of our line-shape parameter dataset for the cases of the two reference lines. We use the experimental data reported in Ref. [31]. The 2-0 Q(1) line was measured in the Grenoble laboratory at nine pressures from 0.39 to 1.05 atm and at a temperature of 294.2 K. The 3-0 S(1) line was measured in the Hefei laboratory at four pressures from 0.36 to 1.35 atm and at temperature of 296.6 K. The experimental spectra are shown as black dots in Fig. 5. Both experiments are based on high-finesse cavity ring-down spectrometers; the experimental details are given in Ref. [31].

It was demonstrated in Ref. [31] that the synthetic profiles based on the fully *ab initio* calculations agree exceptionally well with the experimental profiles without fitting any of the line-shape parameters. The relative root mean square error (rRMSE) averaged over the pressures calculated within  $\pm$ FWHM around the line center was 0.33% and 0.99% for the 2-0 Q(1) and 3-0 S(1) lines, respectively [31]. Recently, the agreement with these experimental profiles was confirmed with an improved theoretical approach that includes the centrifugal distortion in the quantum-scattering calculation; rRMSE was 0.38% and 0.86% for the 2-0 Q(1) and 3-0 S(1) lines, respectively [61]. In this section, we show that we can reach an almost equally good agreement if we replace the

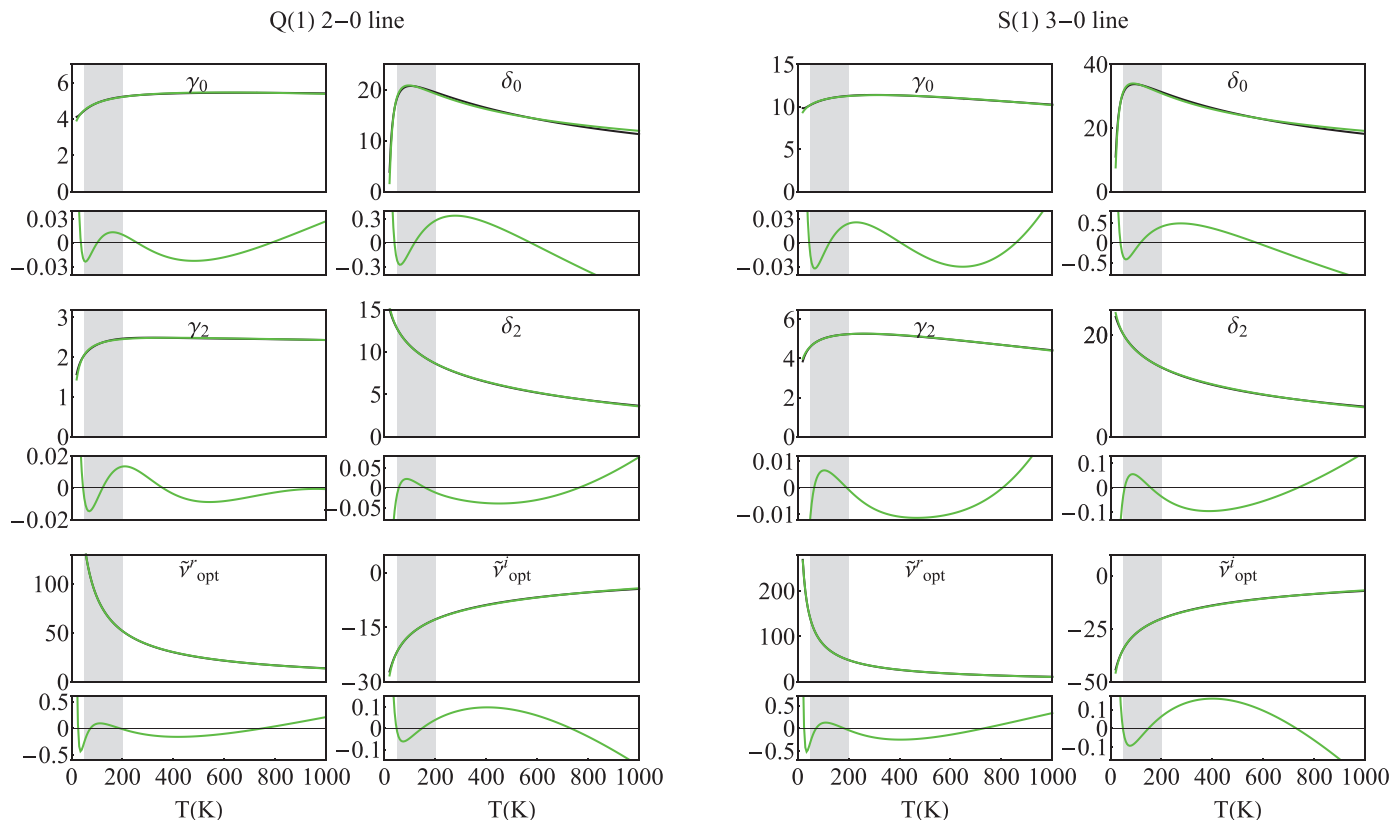


**Fig. 4.** Examples of the temperature dependences of the six collisional line-shape parameters,  $\gamma_0$ ,  $\delta_0$ ,  $\gamma_2$ ,  $\delta_2$ ,  $\tilde{\nu}_{opt}^r$  and  $\tilde{\nu}_{opt}^i$ , for the cases of the Q(1) 2-0 and S(1) 3-0 lines in  $H_2$  perturbed by He. The black and green lines are the *ab initio* results and DPL approximations, respectively. The small panels show the residuals from the DPL fits. The vertical axes for all the panels (including residuals) are in  $10^{-3} \text{cm}^{-1} \text{atm}^{-1}$ . The gray shadows indicate the temperature range prioritized in the DPL fits; this temperature range is relevant for the atmospheres of giant planets. (For interpretation of the references to color in this figure legend, the reader is referred to the web version of this article.)

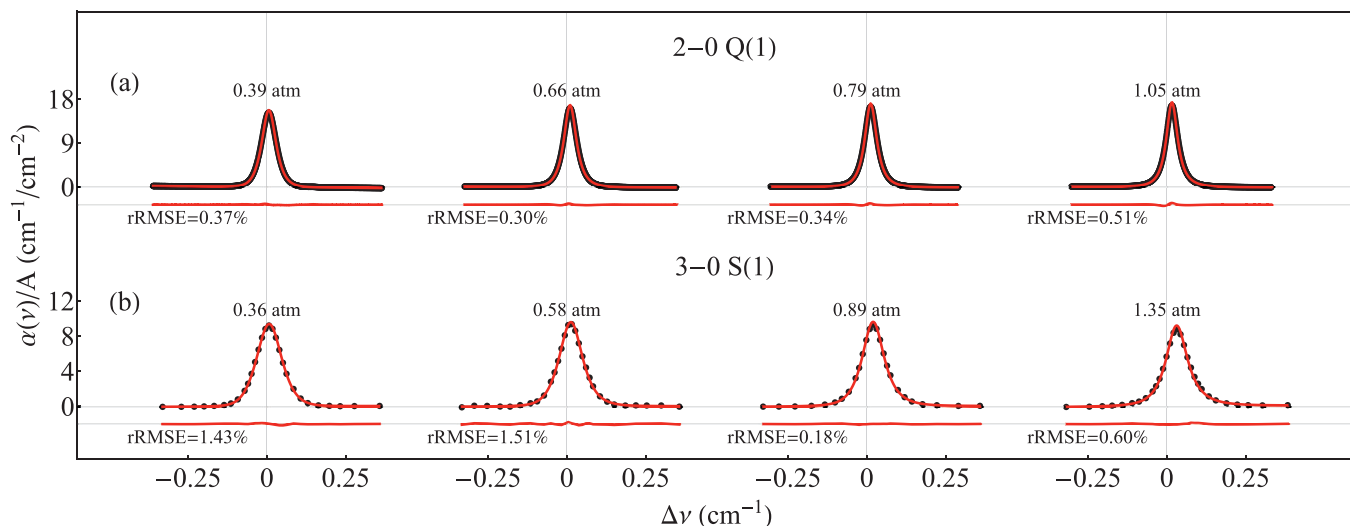


**Fig. 5.** Comparison of the synthetic spectra of the He-perturbed  $H_2$  lines generated from our DPL HITRAN-format line-shape dataset (red lines) with experimental spectra (black points) collected with cavity ring-down spectrometers. Temperatures for the experimental and synthetic spectra are 294.2 K and 296.6 K for the 2-0 Q(1) and 3-0 S(1) lines, respectively. The red lines below the profiles show the differences between the experimental and synthetic spectra; rRMSE is the corresponding relative root mean square error calculated within  $\pm \text{FWHM}$  around line center (relative means that RMSE is divided by the absorption coefficient at the line peak). (For interpretation of the references to color in this figure legend, the reader is referred to the web version of this article.)

full *ab initio* model with the approximate approach presented in this article, consistent with the HITRAN-format DPL parametrization [30]. The approximation is twofold. First, the full line-shape model [31,53,69] is replaced with a quadratic speed-dependent hard-collision (qSDHC) model. Second, the full *ab initio* tempera-

ture dependences are approximated with DPL. The comparison is shown in Fig. 5. The average rRMSE is 0.46% and 0.93% for the 2-0 Q(1) and 3-0 S(1) lines, respectively. It should be emphasized that none of the line-shapes were fitted in this comparison (all of them were taken from our dataset). For this comparison, we only fitted

the line area, baseline, background slope and line center (all the pressures were fitted simultaneously and the fitted line center was constrained to be the same for all the pressures). The profiles from Fig. 5 were calculated using the  $\beta$  correction [25,55] to the qSDHC profile, see Section 2 for details. Without the  $\beta$  correction, the average rRMSE considerably deteriorates and equals 1.43% and 1.08% for the 2-0 Q(1) and 3-0 S(1) lines, respectively.

#### 4. Comprehensive dataset of beyond Voigt line-shape parameters for the helium-perturbed H<sub>2</sub> lines

In this section, we discuss the main result of the present paper, i.e., the complete dataset of the beyond-Voigt line-shape parameters for the He-perturbed H<sub>2</sub> rovibrational lines. We provide a full set of the line-shape parameters for all the 3480 H<sub>2</sub> rovibrational electric quadrupole lines present in the HITRAN database [24]. For our basic set of 321 lines (that contains the strongest lines) we directly perform *ab initio* calculations of the generalized spectroscopic cross sections, see Section 3.1. For all the other lines (higher overtones, high- $J$  lines and high- $\nu'$  hot bands) we extrapolate the *ab initio* data. The majority of the extrapolated data concerns the hot bands. In this work, we extended the *ab initio* calculations from Refs. [15,26] by taking into account the centrifugal distortion for all the bands and by including the hot bands. We also performed *ab initio* calculations for several dozen other lines with high  $\nu$  or  $J$  numbers, which we use to adjust and validate our extrapolation scheme.

We use our *ab initio* generalized spectroscopic cross sections to calculate the line-shape parameters and their temperature dependences within the HITRAN DPL parametrization [30]. Our *ab initio* calculations of the cross sections were performed for:

- 105 lines from the Q-branches ( $J''$  ranging from 1 to 7; Q(0) is forbidden) from the  $\nu' - \nu''$  bands, with  $\nu'' = 0, \dots, 4$  and  $\Delta\nu = \nu' - \nu'' = 1, \dots, 5$ ,
- 126 lines from the S-branches ( $J''$  ranging from 0 to 5) from the  $\nu' - \nu''$  bands, with  $\nu'' = 0, \dots, 5$  and  $\Delta\nu = \nu' - \nu'' = 0, \dots, 5$ ,
- 90 lines from the O-branches ( $J''$  ranging from 2 to 7) from the  $\nu' - \nu''$  bands, with  $\nu'' = 0, \dots, 4$  and  $\Delta\nu = \nu' - \nu'' = 1, \dots, 5$ .

For each of these 321 lines, we employ the methodology introduced in Section 2 to populate a complete dataset record defined by Eqs. (7) and illustrated in Table 1.

In Fig. 6, we show an example of the vibrational,  $\nu'$ , and rotational,  $J''$ , quantum number dependences of the line-shape parameters generated from our dataset at 150 K and 296 K (the plots do not show the raw *ab initio* data, but the line-shape parameters already reconstructed from our HITRAN-format DPL dataset). We observe a strong dependence of all the six line-shape parameters on the vibrational number  $\nu'$ , and much weaker dependence on the rotational number  $J''$ , which is consistent with the phenomenological dataset for self-perturbed H<sub>2</sub> [25]. In Fig. 7, we show the results for different hot bands; the colors indicate the change of the vibrational quantum number  $\Delta\nu = \nu' - \nu''$ . In contrast to the simplest assumption that for a fixed  $\Delta\nu$  the line-shape parameters should hardly depend on  $\nu''$  (this was assumed, for instance, in the phenomenological database for the self-perturbed H<sub>2</sub> [25]), we observe a strong dependence on  $\nu''$ , especially for small  $\Delta\nu$  for the  $\gamma_0$  parameter.

The rovibrational lines in H<sub>2</sub> are exceptionally weak; the strongest line at  $T = T_{\text{ref}} = 296$  K is the 1-0 S(1) line with a line intensity of  $3.2 \times 10^{-26}$  cm/molecule. The intensity quickly decreases with  $J''$  and  $\nu'$ . For instance, the intensity of the 1-0 S(5) line is as small as  $2.2 \times 10^{-29}$  cm/molecule, and the intensity of the 5-0 S(1) line is  $0.95 \times 10^{-29}$  cm/molecule. At lower temperatures that are relevant for giant planet atmospheres, the line intensity decreases with  $J''$  and  $\nu'$  even faster. For this reason, we limit our full line-shape calculations based on the *ab initio* generalized spectroscopic cross sections to  $J' < 8$  and  $\nu' < 6$ . For the completeness of the dataset, we extrapolate our calculations for higher  $J''$  and  $\nu'$  lines that are present in HITRAN (in fact, in this procedure we combine extrapolation and interpolation). The extrapolation scheme is as follows. For every branch (O, Q and S), we calculated the values of the line-shape parameters for one high- $\nu'$  line per cold/hot band, i.e., we performed additional *ab initio* calculations for the following lines: Q(1) 9-x, S(1) 9-x, O(3) 9-x, with  $x = 0, \dots, 5$ . We assumed in our extrapolation that the proportions of the values of the line-shape parameters between the 9-0 and 5-0 bands for other  $J''$  are the same as for the three cases mentioned above (i.e.,

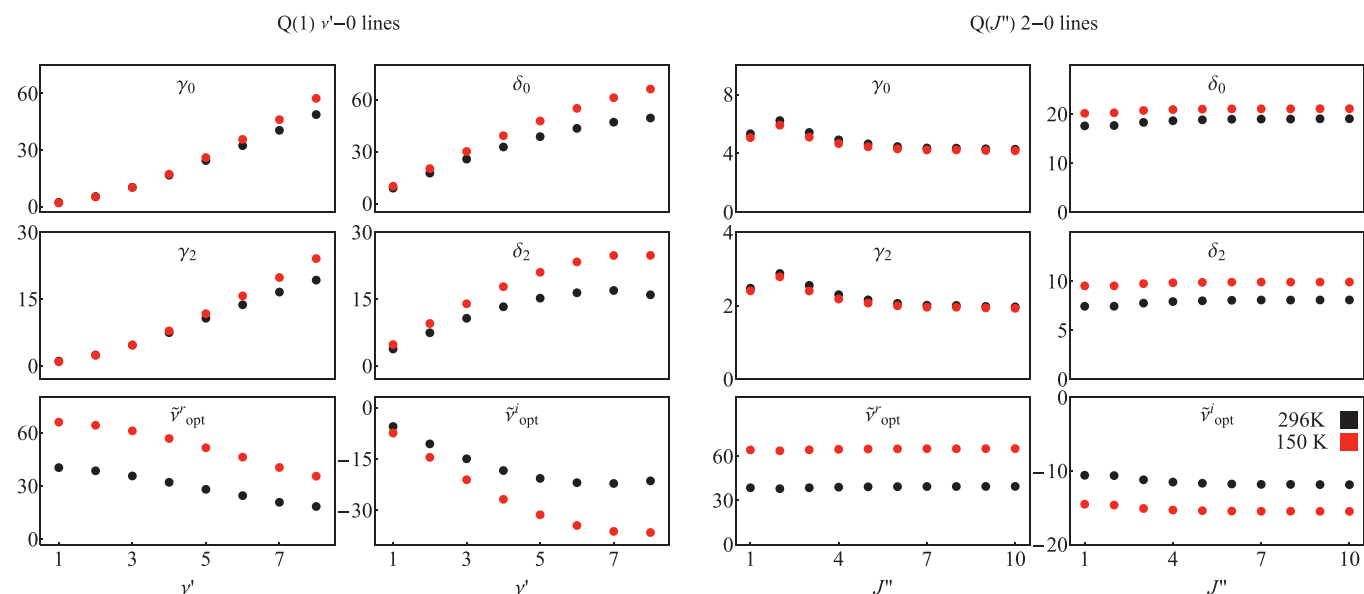


**Fig. 6.** An excerpt from our dataset illustrating the structure of the dataset and the examples of the vibrational and rotational dependences of all six line-shape parameters. The line-shape parameters are determined for the He-perturbed H<sub>2</sub> rovibrational lines at  $T = 150$  and  $296$  K; refer to red and black colors, respectively. All the parameters are expressed in units of  $10^{-3}$  cm<sup>-1</sup>atm<sup>-1</sup>. The values of the line-shape parameters shown in this plot are not directly taken from *ab initio* calculations, but reconstructed from the DPL relations, Eqs. (7), based on the coefficients from our dataset [34]. (For interpretation of the references to color in this figure legend, the reader is referred to the web version of this article.)

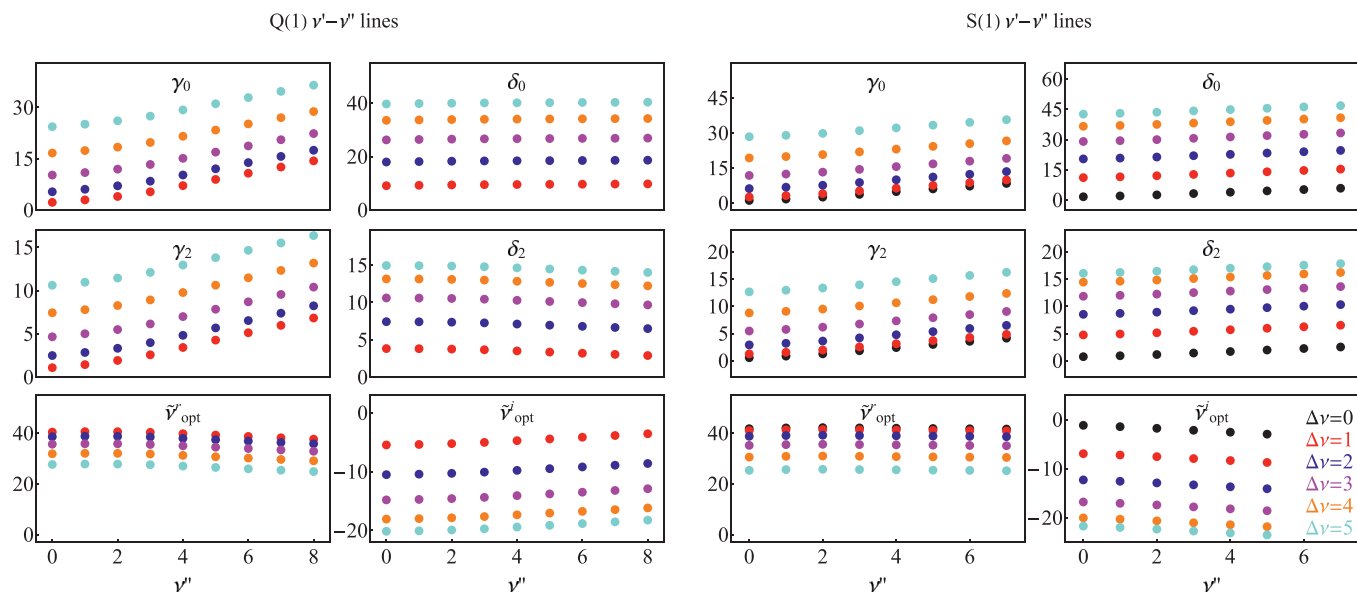


**Fig. 7.** An excerpt from our dataset illustrating the values of the beyond-Voigt line-shape parameters for different hot bands. The left and right sides of the figure show the results for the Q(1) and S(1) lines, respectively. All the parameters are expressed in units of  $10^{-3} \text{ cm}^{-1} \text{ atm}^{-1}$ . The values of the line-shape parameters shown in this plot are not directly taken from *ab initio* calculations, but reconstructed from the DPL relations, Eqs. (7), based on the coefficients from our dataset [34]. The data for  $\nu' = \nu'' + \Delta\nu \geq 6$  come from extrapolation.

the same within each branch). In the next step, we interpolated the line-shape parameters for the bands between 5-0 and 9-0 using a quadratic function fitted (separately for every  $J''$ ) to 4-0, 5-0 and 9-0 data. The same approach was applied to extrapolate the data for hot bands. To populate the dataset for higher  $J''$ , we performed fully *ab initio* calculations for the six high- $J''$  transitions belonging to the 2-0 band: O(10), O(13), Q(8), Q(11), S(8) and S(11) lines. We constrained the same proportions of the line-shape parameters between  $J'' = 5, 8$  and 11 (10 and 13 for O branches) for other bands, and we interpolated the values of the line-shape parameters between  $J'' = 5$  and 11 (13 for the O bands) with a quadratic function. For  $J'' > 11$  ( $J'' > 13$  for the O bands) we used linear extrapolation based on the last two  $J''$ . This approach (based on the data for the 2-0 band) was used to extrapolate the data for higher  $J''$  for all cold and hot bands. The scheme of data interpolation and extrapolation described above was implemented directly to the raw *ab initio* data before fitting the DPL temperature dependences. The reason for this is that the four DPL coefficients are strongly correlated with each other, and even for neighboring  $J''$  and  $\nu'$  quantum numbers their fitted values can be very different despite similar temperature dependences.

Due to a strong numerical correlation between the DPL coefficients, the uncertainties of the DPL coefficients do not suffice and a full covariance matrix would be needed. For this reason, we do not report an individual uncertainty for every DPL coefficient, but a single uncertainty for the entire DPL function for a given line-shape parameter. The uncertainty consists of two contributions, the first one comes from the DPL approximation, and the second one from *ab initio* calculations. We calculate the DPL contribution as a standard deviation of the difference between the full *ab initio* values of the line-shape parameter and their DPL approximation calculated in the range from 50 to 200 K, see the small panels in Fig. 4. We estimate the uncertainty of our *ab initio* calculations at 1%.

The complete dataset of the line-shape parameters within the DPL representation [30] for the He-perturbed  $\text{H}_2$  lines is given in the supplementary materials [34]; the definition of the reported coefficients is given by Eqs. (7). The lines are ordered with increas-

ing transition energy. The above described format of the uncertainties reported in this work does not fit the standard HITRAN uncertainty codes. For this reason, the error codes in HITRAN will be set to *unreported* (code = 0). Nevertheless, all the uncertainties are reported in the supplementary materials [34] in the columns labelled *DPL-err*. In the supplementary materials [34], we also provide the source *ab initio* data that were used to generate the DPL dataset, i.e., the generalized spectroscopic cross sections and line-shape parameters as a function of temperature.

## 5. Conclusion

We demonstrated a methodology for populating line-by-line spectroscopic databases with beyond-Voigt line-shape parameters that is based on *ab initio* quantum scattering calculations. We provided a comprehensive dataset for the benchmark system of He-perturbed  $\text{H}_2$  (we cover all the rovibrational bands that are present in HITRAN). We extended the previous quantum-scattering calculations by taking into account the centrifugal distortion for all the bands and by including the hot bands. The results were projected on a simple structure of the quadratic speed-dependent hard-collision profile. For each line and each line-shape parameter, we provided a full temperature dependence within the double-power-law (DPL) representation. The temperature dependences cover the range from 20 to 1000 K, which also includes the low temperatures relevant for the studies of the atmospheres of giant planets. We demonstrated that the synthetic spectra generated from our dataset agree with highly accurate experimental spectra collected with cavity ring-down spectrometers at a subpercent accuracy level. The methodology can be applied to many other molecular species important for atmospheric and planetary studies.

## Declaration of Competing Interest

The authors declare that they have no known competing financial interests or personal relationships that could have appeared to influence the work reported in this paper.

## CRediT authorship contribution statement

**P. Wcisło:** Conceptualization, Methodology, Validation, Writing - original draft, Writing - review & editing. **F. Thibault:** Conceptualization, Methodology, Software, Validation, Writing - original draft, Writing - review & editing. **N. Stolarczyk:** Investigation, Visualization, Methodology, Software, Validation, Data curation, Writing - original draft, Writing - review & editing. **H. Jóźwiak:** Investigation, Methodology, Software, Validation, Data curation, Writing - original draft, Writing - review & editing. **M. Słowiński:** Investigation, Visualization, Methodology, Software, Validation, Data curation, Writing - original draft, Writing - review & editing. **M. Gancewski:** Investigation, Software, Validation, Data curation, Writing - original draft, Writing - review & editing. **K. Stankiewicz:** Investigation, Software, Validation, Data curation, Writing - original draft, Writing - review & editing. **M. Konefał:** Validation. **S. Kassi:** Investigation. **A. Campargue:** Investigation. **Y. Tan:** Investigation. **J. Wang:** Investigation. **K. Patkowski:** Investigation, Software, Writing - review & editing. **R. Ciuryło:** Conceptualization, Methodology, Writing - review & editing. **D. Lisak:** Conceptualization, Methodology, Writing - review & editing. **R. Kochanov:** Conceptualization, Methodology, Data curation. **L.S. Rothman:** Conceptualization, Methodology, Data curation, Validation, Writing - review & editing. **I.E. Gordon:** Conceptualization, Methodology, Data curation, Validation, Writing - review & editing.

## Acknowledgements

P.W. was supported by Polish National Science Centre Project No. 2019/35/B/ST2/01118. N.S. and H.J. were supported by Polish National Science Centre Project No. 2018/31/B/ST2/00720. M.S., M.G. and K.S. were supported by the A next-generation worldwide quantum sensor network with optical atomic clocks project carried out within the TEAM IV Programme of the Foundation for Polish Science cofinanced by the European Union under the European Regional Development Fund. S.K. and A.C. acknowledge funding support from the Agence Nationale de la Recherche (Equipex REFIMEVE+ANR-11-EQPX-0039). M.K. and D.L. were supported by Polish National Science Centre Project No. 2015/18/E/ST2/00585. K.P. was supported by U.S. National Science Foundation CAREER award CHE-1351978. The project was cofinanced by the Polish National Agency for Academic Exchange under the PHC Polonium program (dec. PPN/X/PS/318/2018). The research was part of the program of the National Laboratory FAMO in Toruń, Poland. The HITRAN database is supported by NASA AURA NNX17AI78G and NASA PDART NNX16AG51G grants.

## Supplementary material

Supplementary material associated with this article can be found, in the online version, at doi:[10.1016/j.jqsrt.2020.107477](https://doi.org/10.1016/j.jqsrt.2020.107477).

## References

- Dicke R. The effect of collisions upon the Doppler width of spectral lines. *Phys Rev* 1953;89:472–3. doi:[10.1103/PhysRev.89.472](https://doi.org/10.1103/PhysRev.89.472).
- Rautian SG, Sobelman II. The effect of collisions on the doppler broadening of spectral lines. *Usp Fiz Nauk* 1966;90:209. [*Sov Phys Usp* 1967;9:701]
- Berman PR. Speed-dependent collisional width and shift parameters in spectral profiles. *J Quant Spectrosc Radiat Transf* 1972;12(9):1331–42. doi:[10.1016/0022-4073\(72\)90189-6](https://doi.org/10.1016/0022-4073(72)90189-6).
- Hess S. Kinetic theory of spectral line shapes. The transition between Doppler broadening and collisional broadening. *Physica* 1972;61(1):80–94. doi:[10.1016/0031-8914\(72\)90035-3](https://doi.org/10.1016/0031-8914(72)90035-3).
- Blackmore R. A modified Boltzmann kinetic equation for line shape functions. *J Chem Phys* 1987;87(2):791–800. doi:[10.1063/1.453286](https://doi.org/10.1063/1.453286).
- Ciuryło R, Bielski A, Drummond JR, Lisak D, May AD, Pine AS, et al. Spectral line shapes. In: Back CA, editor. (AIP, Melville, NY); 2002a. p. 151.
- May AD, Liu W-K, McCourt FRW, Ciuryło R, Sanchez-FortStoker J, Shapiro D, et al. The impact theory of spectral line shapes: a paradigm shift. *Can J Phys* 2013;91(11):879–95. doi:[10.1139/cjp-2012-0345](https://doi.org/10.1139/cjp-2012-0345).
- Hartmann J-M, Tran H, Ngo NH, Landsheere X, Chelin P, Lu Y, et al. *Ab initio* calculations of the spectral shapes of CO<sub>2</sub> isolated lines including non-Voigt effects and comparisons with experiments. *Phys Rev A* 2013;87:013403. doi:[10.1103/PhysRevA.87.013403](https://doi.org/10.1103/PhysRevA.87.013403).
- De Vizia MD, Castrillo A, Fasci E, Amodio P, Moretti L, Gianfrani L. Experimental test of the quadratic approximation in the partially correlated speed-dependent hard-collision profile. *Phys Rev A* 2014;90:022503. doi:[10.1103/PhysRevA.90.022503](https://doi.org/10.1103/PhysRevA.90.022503).
- Devi VM, Benner DC, Smith MAH, Mantz AW, Sung K, Crawford TJ, et al. Self- and air-broadened line shape parameters in the  $\nu_2+\nu_3$  band of <sup>12</sup>CH<sub>4</sub>: 4500–4630 cm<sup>-1</sup>. *J Quant Spectrosc Radiat Transf* 2015;152:149–65. doi:[10.1016/j.jqsrt.2014.11.011](https://doi.org/10.1016/j.jqsrt.2014.11.011).
- Campargue A, Karlovets EV, Kassi S. The 4–0 band of carbon monoxide by high sensitivity cavity ring down spectroscopy near 8200 cm<sup>-1</sup>. *J Quant Spectrosc Radiat Transf* 2015;154:113–19. doi:[10.1016/j.jqsrt.2014.12.011](https://doi.org/10.1016/j.jqsrt.2014.12.011).
- Wójtewicz S, Masłowski P, Cygan A, Wcisło P, Zaborowski M, Piwiński M, et al. Speed-dependent effects and Dicke narrowing in nitrogen-broadened oxygen. *J Quant Spectrosc Radiat Transf* 2015;165:68–75. doi:[10.1016/j.jqsrt.2015.06.022](https://doi.org/10.1016/j.jqsrt.2015.06.022).
- Sironneau VT, Hodges JT. Line shapes, positions and intensities of water transitions near 1.28 μm. *J Quant Spectrosc Radiat Transf* 2015;152:1–15. doi:[10.1016/j.jqsrt.2014.10.020](https://doi.org/10.1016/j.jqsrt.2014.10.020).
- Bakr BW, Smith DGA, Patkowski K. Highly accurate potential energy surface for the He-H<sub>2</sub> dimer. *J Chem Phys* 2013;139(14):144305. doi:[10.1063/1.4824299](https://doi.org/10.1063/1.4824299).
- Thibault F, Patkowski K, Żuchowski PS, Jóźwiak H, Ciuryło R, Wcisło P. Rovibrational line-shape parameters for H<sub>2</sub> in He and new H<sub>2</sub>-He potential energy surface. *J Quant Spectrosc Radiat Transf* 2017;202:308–20. doi:[10.1016/j.jqsrt.2017.08.014](https://doi.org/10.1016/j.jqsrt.2017.08.014).
- Wcisło P, Ciuryło R. Influence of the interaction potential shape on the Dicke narrowed spectral line profiles affected by speed-dependent collisional broadening and shifting. *J Quant Spectrosc Radiat Transf* 2013;120(0):36–43. doi:[10.1016/j.jqsrt.2013.02.023](https://doi.org/10.1016/j.jqsrt.2013.02.023).
- Wcisło P, Thibault F, Cybulski H, Ciuryło R. Strong competition between velocity-changing and phase- or state-changing collisions in H<sub>2</sub> spectra perturbed by Ar. *Phys Rev A* 2015;91:052505. doi:[10.1103/PhysRevA.91.052505](https://doi.org/10.1103/PhysRevA.91.052505).
- Wcisło P, Gordon IE, Cheng C-F, Hu S-M, Ciuryło R. Collision-induced line-shape effects limiting the accuracy in Doppler-limited spectroscopy of H<sub>2</sub>. *Phys Rev A* 2016a;93:022501. doi:[10.1103/PhysRevA.93.022501](https://doi.org/10.1103/PhysRevA.93.022501).
- Miller CE, Brown LR, Toth RA, Benner DC, Devi VM. Spectroscopic challenges for high accuracy retrievals of atmospheric CO<sub>2</sub> and the orbiting carbon observatory (OCO) experiment. *C R Phys* 2005;6(8):876–87. doi:[10.1016/j.crhy.2005.09.005](https://doi.org/10.1016/j.crhy.2005.09.005).
- Feuchtgruber H, Lellouch E, Orton G, de Graauw T, Vandenbussche B, Swinyard B, et al. The D/H ratio in the atmospheres of Uranus and Neptune from Herschel-PACS observations. *A&A* 2013;551:A126. doi:[10.1051/0004-6361/201220857](https://doi.org/10.1051/0004-6361/201220857).
- Miller-Ricci E, Seager S, Sasselov D. The atmospheric signatures of super-Earths: how to distinguish between hydrogen-rich and hydrogen-poor atmospheres. *Astrophys J* 2008;690(2):1056–67. doi:[10.1088/0004-637x/690/2/1056](https://doi.org/10.1088/0004-637x/690/2/1056).
- Fortney JJ, Robinson T.D., Domagal-Goldman S., Genio A.D.D., Gordon I.E., Gharib-Nezhad E., et al. The need for laboratory measurements and *ab initio* studies to aid understanding of exoplanetary atmospheres. [arXiv:1905.07064](https://arxiv.org/abs/1905.07064) 2019; URL <https://arxiv.org/abs/1905.07064>.
- Hill C, Gordon IE, Kochanov RV, Barrett L, Wilzewski JS, Rothman LS. HITRAN-Nonline: An online interface and the flexible representation of spectroscopic data in the HITRAN database. *J Quant Spectrosc Radiat Transf* 2016;177:4–14. doi:[10.1016/j.jqsrt.2015.12.012](https://doi.org/10.1016/j.jqsrt.2015.12.012).
- Gordon I, Rothman L, Hill C, Kochanov R, Tan Y, Bernath P, et al. The HITRAN2016 molecular spectroscopic database. *J Quant Spectrosc Radiat Transf* 2017;203:3–69. doi:[10.1016/j.jqsrt.2017.06.038](https://doi.org/10.1016/j.jqsrt.2017.06.038).
- Wcisło P, Gordon I, Tran H, Tan Y, Hu S-M, Campargue A, et al. The implementation of non-Voigt line profiles in the HITRAN database: H<sub>2</sub> case study. *J Quant Spectrosc Radiat Transf* 2016b;177:75–91. doi:[10.1016/j.jqsrt.2016.01.024](https://doi.org/10.1016/j.jqsrt.2016.01.024).
- Jóźwiak H, Thibault F, Stolarczyk N, Wcisło P. *Ab initio* line-shape calculations for the S and O branches of H<sub>2</sub> perturbed by He. *J Quant Spectrosc Radiat Transf* 2018;219:313–22. doi:[10.1016/j.jqsrt.2018.08.023](https://doi.org/10.1016/j.jqsrt.2018.08.023).
- Pine AS. Asymmetries and correlations in speed-dependent Dicke-narrowed line shapes of argon-broadened HF. *J Quant Spectrosc Radiat Transf* 1999;62(4):397–423. doi:[10.1016/S0022-4073\(98\)00112-5](https://doi.org/10.1016/S0022-4073(98)00112-5).
- Ngo N, Lisak D, Tran H, Hartmann J-M. An isolated line-shape model to go beyond the Voigt profile in spectroscopic databases and radiative transfer codes. *J Quant Spectrosc Radiat Transf* 2013;129:89–100. doi:[10.1016/j.jqsrt.2013.05.034](https://doi.org/10.1016/j.jqsrt.2013.05.034).
- Tennyson J, Bernath PF, Campargue A, Császár AG, Daumont L, Gamache RR, et al. Recommended isolated-line profile for representing high-resolution spectroscopic transitions (IUPAC technical report). *Pure Appl Chem* 2014;86(12):1931–43. doi:[10.1515/pac-2014-0208](https://doi.org/10.1515/pac-2014-0208).
- Stolarczyk N, Thibault F, Cybulski H, Jóźwiak H, Kowzan G, Vispoel B, et al. Evaluation of different parameterizations of temperature dependences of the line-shape parameters based on *ab initio* calculations: Case study for the HITRAN database. *J Quant Spectrosc Radiat Transf* 2020;240:106676. doi:[10.1016/j.jqsrt.2019.106676](https://doi.org/10.1016/j.jqsrt.2019.106676).
- Stowiński M, Thibault F, Tan Y, Wang J, Liu A-W, Hu S-M, et al. H<sub>2</sub>-He collisions: *ab initio* theory meets cavity-enhanced spectra. *Phys Rev A* 2020;101:052705. doi:[10.1103/PhysRevA.101.052705](https://doi.org/10.1103/PhysRevA.101.052705).

- [32] Kochanov R, Gordon I, Rothman L, Wcisło P, Hill C, Wilzewski J. HITRAN Application Programming Interface (HAPI): a comprehensive approach to working with spectroscopic data. *J Quant Spectrosc Radiat Transf* 2016;177:15–30. doi:10.1016/j.jqsrt.2016.03.005.
- [33] Lellouch E, Bézard B, Fouchet T, Feuchtgruber H, Encrenaz T, de Graauw T. The deuterium abundance in Jupiter and Saturn from ISO-SWS observations. *A&A* 2001;370(2):610–22. doi:10.1051/0004-6361:20010259.
- [34] Wcisło P, Thibault F, Stolarczyk N, Józwiak H, Słowiński M., Gancewski M., et al. Supplementary material 2020. doi:10.1016/j.jqsrt.2020.107477.
- [35] Long D, Havey D, Okumura M, Miller C, Hodges J. O<sub>2</sub> A-band line parameters to support atmospheric remote sensing. *J Quant Spectrosc Radiat Transf* 2010;111(14):2021–36. doi:10.1016/j.jqsrt.2010.05.011.
- [36] Devi VM, Benner DC, Smith M, Mantz A, Sung K, Brown L, et al. Spectral line parameters including temperature dependences of self- and air-broadening in the 2-0 band of CO at 2.3  $\mu\text{m}$ . *J Quant Spectrosc Radiat Transf* 2012a;113:1013–33. doi:10.1016/j.jqsrt.2012.02.010.
- [37] Devi VM, Benner DC, Smith MAH, Mantz AW, Sung K, Brown LR. Spectral line parameters including temperature dependences of air-broadening for the 2-0 bands of <sup>13</sup>C<sup>18</sup>O and <sup>12</sup>C<sup>18</sup>O at 2.3  $\mu\text{m}$ . *J Mol Spectrosc* 2012b;276-277:33–48. doi:10.1016/j.jms.2012.05.005.
- [38] Li G, Gordon IE, Hajigeorgiou PG, Coxon JA, Rothman LS. Reference spectroscopic data for hydrogen halides, Part II: The line lists. *J Quant Spectrosc Radiat Transf* 2013;130:284–95. doi:10.1016/j.jqsrt.2013.07.019.
- [39] Domysławska J, Wójtewicz S, Masłowski P, Cygan A, Bielska K, Trawiński RS, et al. A new approach to spectral line shapes of the weak oxygen transitions for atmospheric applications. *J Quant Spectrosc Radiat Transf* 2016;169:111–21. doi:10.1016/j.jqsrt.2015.10.019.
- [40] Benner DC, Rinsland CP, Devi VM, Smith MAH, Atkins D. A multispectrum nonlinear least squares fitting technique. *J Quant Spectrosc Radiat Transf* 1995;53(6):705–21. doi:10.1016/0022-4073(95)00015-D.
- [41] Pine A, Ciuryło R. Multispectrum fits of Ar-broadened HF with a generalized asymmetric lineshape: effects of correlation, hardness, speed dependence, and collision duration. *J Mol Spectrosc* 2001;208(2):180–7. doi:10.1006/jmsp.2001.8375.
- [42] Amodio P, Moretti L, Castrillo A, Gianfrani L. Line-narrowing effects in the near-infrared spectrum of water and precision determination of spectroscopic parameters. *J Chem Phys* 2014;140(4):044310. doi:10.1063/1.4862482.
- [43] Ben-Reuven A. Symmetry considerations in pressure-broadening theory. *Phys Rev* 1966a;141:34–40. doi:10.1103/PhysRev.141.34.
- [44] Ben-Reuven A. Impact broadening of microwave spectra. *Phys Rev* 1966b;145:7–22. doi:10.1103/PhysRev.145.7.
- [45] Shafer R, Gordon RG. Quantum scattering theory of rotational relaxation and spectral line shapes in H<sub>2</sub>-He gas mixtures. *J Chem Phys* 1973;58(12):5422–43. doi:10.1063/1.1679162.
- [46] Thibault F, Wcisło P, Ciuryło R. A test of H<sub>2</sub>-He potential energy surfaces. *Eur Phys J D* 2016;70:236. doi:10.1140/epjd/e2016-70114-9.
- [47] Martínez RZ, Bermejo D, Thibault F, Wcisło P. Testing the *ab initio* quantum-scattering calculations for the D<sub>2</sub>-He benchmark system with stimulated Raman spectroscopy. *J Raman Spectrosc* 2018;49(8):1339–49. doi:10.1002/jrs.5391.
- [48] Monchick L, Hunter LW. Diatomic diatomic molecular collision integrals for pressure broadening and Dicke narrowing: a generalization of Hess's theory. *J Chem Phys* 1986;85(2):713–18. doi:10.1063/1.451277.
- [49] Schaefer J, Monchick L. Line shape cross sections of HD immersed in He and H<sub>2</sub> gas. I. Pressure broadening cross sections. *J Chem Phys* 1987;87(1):171–81. doi:10.1063/1.453612.
- [50] Corey GC, McCourt FR. Dicke narrowing and collisional broadening of spectral lines in dilute molecular gases. *J Chem Phys* 1984;81(5):2318–29. doi:10.1063/1.447930.
- [51] Ward J, Cooper J, Smith EW. Correlation effects in the theory of combined Doppler and pressure broadening - I. Classical theory. *J Quant Spectrosc Radiat Transf* 1974;14(7):555–90. doi:10.1016/0022-4073(74)90036-3.
- [52] Lisak D, Hodges JT, Ciuryło R. Comparison of semiclassical line-shape models to rovibrational H<sub>2</sub>O spectra measured by frequency-stabilized cavity ring-down spectroscopy. *Phys Rev A* 2006;73:012507. doi:10.1103/PhysRevA.73.012507.
- [53] Wcisło P, Thibault F, Zaborowski M, Wójtewicz S, Cygan A, Kowzan G, et al. Accurate deuterium spectroscopy for fundamental studies. *J Quant Spectrosc Radiat Transf* 2018;213:41–51. doi:10.1016/j.jqsrt.2018.04.011.
- [54] Rohart F, Włodarczak G, Colmont J-M, Cazzoli G, Dore L, Puzzarini C. Galatry versus speed-dependent Voigt profiles for millimeter lines of O<sub>3</sub> in collision with N<sub>2</sub> and O<sub>2</sub>. *J Mol Spectrosc* 2008;251(1):282–92. doi:10.1016/j.jms.2008.03.005.
- [55] Konefał M, Słowiński M, Zaborowski M, Ciuryło R, Lisak D, Wcisło P. Analytical-function correction to the Hartmann Tran profile for more reliable representation of the Dicke-narrowed molecular spectra. *J Quant Spectrosc Radiat Transf* 2020;242:106784. doi:10.1016/j.jqsrt.2019.106784.
- [56] Tran H, Ngo N, Hartmann J-M. Efficient computation of some speed-dependent isolated line profiles. *J Quant Spectrosc Radiat Transf* 2013;129:199–203. doi:10.1016/j.jqsrt.2013.06.015.
- [57] Kowzan G, Wcisło P, Słowiński M, Masłowski P, Viel A, Thibault F. Fully quantum calculations of the line-shape parameters for the Hartmann-Tran profile: A CO-Ar case study. *J Quant Spectrosc Radiat Transf* 2020;243:106803. doi:10.1016/j.jqsrt.2019.106803.
- [58] Private communication with J.-M. Hartmann. 2018.
- [59] Wcisło P, Lisak D, Ciuryło R, Pine AS. Multispectrum-fitting of phenomenological collisional line-shape models to a speed-dependent Blackmore profile for spectroscopic analysis and databases. *J Phys* 2017;810:012061. doi:10.1088/1742-6596/810/1/012061.
- [60] Ngo N, Hartmann J-M. A strategy to complete databases with parameters of refined line shapes and its test for CO in He, Ar and Kr. *J Quant Spectrosc Radiat Transf* 2017;203:334–40. doi:10.1016/j.jqsrt.2017.01.031. HITRAN2016 Special Issue
- [61] Słowiński M., et al. In preparation.
- [62] Martínez RZ, Bermejo D, Wcisło P, Thibault F. Accurate wavenumber measurements for the S<sub>0</sub>(0), S<sub>0</sub>(1), and S<sub>0</sub>(2) pure rotational Raman lines of D<sub>2</sub>. *J Raman Spectrosc* 2019;50(1):127–9. doi:10.1002/jrs.5499.
- [63] Thibault F, Martínez RZ, Bermejo D, Wcisło P. Line-shape parameters for the first rotational lines of HD in He. *Mol Astrophys* 2020;19:100063. doi:10.1016/j.molap.2020.100063.
- [64] Stankiewicz K, Józwiak H, Gancewski M, Stolarczyk N, Thibault F, Wcisło P. *Ab initio* calculations of collisional line-shape parameters and generalized spectroscopic cross-sections for rovibrational dipole lines in HD perturbed by He. *J Quant Spectrosc Radiat Transf* 2020;254:107194. doi:10.1016/j.jqsrt.2020.107194.
- [65] Józwiak H., Gancewski M., Stankiewicz K., Wcisło P. BIGOS computer code, to be published.
- [66] Johnson BR. The renormalized Numerov method applied to calculating bound states of the coupled-channel Schrödinger equation. *J Chem Phys* 1978;69(10):4678–88. doi:10.1063/1.436421.
- [67] Rohart F, Nguyen L, Buldyreva J, Colmont J-M, Włodarczak G. Lineshapes of the 172 and 602 GHz rotational transitions of HC<sup>15</sup>N. *J Mol Spectrosc* 2007;246(2):213–27. doi:10.1016/j.jms.2007.09.009.
- [68] Lisak D, Cygan A, Wcisło P, Ciuryło R. Quadratic speed dependence of collisional broadening and shifting for atmospheric applications. *J Quant Spectrosc Radiat Transf* 2015;151:43–8. doi:10.1016/j.jqsrt.2014.08.016.
- [69] Ciuryło R, Shapiro DA, Drummond JR, May AD. Solving the line-shape problem with speed-dependent broadening and shifting and with Dicke narrowing. II. Application. *Phys Rev A* 2002b;65:012502. doi:10.1103/PhysRevA.65.012502.

Toruń, 04.02.2022

prof. dr hab. Roman Ciuryło  
Instytut Fizyki  
Uniwersytet Mikołaja Kopernika w Toruniu  
ul. Grudziądzka 5/7,  
87-100 Toruń

## STATEMENT OF CO-AUTHORSHIP

I hereby declare that my contribution to the research papers listed below involves:

1. M. Słowiński, F. Tibault, Y. Tan, J. Wang, A.-W. Liu, S.-M. Hu, S. Kassı, A. Campargue, M. Konefał, H. Jóźwiak, K. Patkowski, P. Żuchowski, R. Ciuryło, D. Lisak, P. Wcisło, *H<sub>2</sub>-He collisions: Ab initio theory meets cavity-enhanced spectra*, Phys. Rev. A **101**, 052705-7 (2020).

I brought to the project expertise about speed-dependent billiard ball profile SDBBP and initiative to use the SDBBP for interpretation of experimental spectra. I helped to put the paper in proper context in relation to earlier works and verify conclusions drawn from comparison of experimental data and *ab initio* line shape calculations.

2. M. Słowiński, H. Jóźwiak, M. Gancewski, K. Stankiewicz, N. Stolarczyk, Y. Tan, J. Wang, A.-W. Liu, S.-M. Hu, S. Kassı, A. Campargue, K. Patkowski, P. S. Żuchowski, R. Ciuryło, F. Thibault, P. Wcisło, *Collisional line-shape effects in accurate He-perturbed H<sub>2</sub> spectra*, J. Quant. Spectrosc. Radiat. Transfer **277**, 107951-11 (2022).

I brought to the project expertise about speed-dependent billiard ball profile SDBBP and initiative to use the SDBBP for interpretation of experimental spectra. I helped to put the paper in proper context in relation to earlier works and verify conclusions drawn from comparison of experimental data and *ab initio* line shape calculations. I helped choose the proper presentation of part of the results related to line shapes comparison.





3. M. Konefał, M. Słowiński, M. Zaborowski, R. Ciuryło, D. Lisak, P. Wcisło,  
*Analytical-function correction to the Hartmann–Tran profile for more reliable representation of the Dicke-narrowed molecular spectra*,  
J. Quant. Spectrosc. Radiat. Transfer **242**, 106784-5 (2020).

I brought to the project expertise about speed-dependent billiard ball profile SDBBP and mass varied comparison with hard collision model including detailed analysis of asymptotic case of soft collisions and its comparison with hard collision model. I helped to put the paper in proper context in relation to earlier works and verify conclusions drawn from comparison of hard collision profile with SDBBP. I helped choose the proper form of results presentation.

4. M. Zaborowski, M. Słowiński, K. Stankiewicz, F. Thibault, A. Cygan, H. Józwiak, G. Kowzan, P. Masłowski, A. Nishiyama, N. Stolarczyk, S. Wójtewicz, R. Ciuryło, D. Lisak, P. Wcisło,  
*Ultra-high finesse cavity-enhanced spectroscopy for accurate tests of quantum electrodynamics for molecules*,  
Opt. Lett. **45**, 1603-1606 (2020).

I brought to the project expertise about speed-dependent billiard ball profile SDBBP and initiative to use the SDBBP together with multispectrum fitting technique for analysis of experimental spectra. I helped to put the paper in proper context in relation to earlier works and verify interpretation of experimental data.



Toruń, 13.12.2021

mgr Hubert Józwiak

Szkoła Doktorska Nauk Ścisłych i Przyrodniczych

*Academia Scientiarum Thoruniensis*

Grudziądzka 5/7

87-100 Toruń

### Statement of coauthorship

I hereby declare that my contribution to the four research papers listed below involves:

1. Michał Słowiński, Franck Tibault, Yan Tan, Jin Wang, An-Wen Liu, Shui-Ming Hu, Samir Kassi, Alain Campargue, Magdalena Konefał, Hubert Józwiak, Konrad Patkowski, Piotr Żuchowski, Roman Ciuryło, Daniel Lisak, Piotr Wcisło „*H<sub>2</sub>-He collisions: Ab initio theory meets cavity-enhanced spectra*”, *Physical Review A* **101**, 052705 (2020)  
DOI: 10.1103/PhysRevA.101.052705

preparation of the five potential energy surfaces, denoted in the paper as „SK”, „mMR”, „BSP”, „BSP2” and „BSP3”, for quantum scattering calculations; performing quantum scattering calculations and determining the generalized spectroscopic cross sections for the 2-0 Q(1) and 3-0 S(1) H<sub>2</sub> lines perturbed by He

2. Michał Słowiński, Hubert Józwiak, Maciej Gancewski, Kamil Stankiewicz, Nikodem Stolarczyk, Yan Tan, Jin Wang, An-Wen Liu, Shui-Ming Hu, Samir Kassi, Alain Campargue, Konrad Patkowski, Piotr S. Żuchowski, Roman Ciuryło, Franck Thibault, Piotr Wcisło „*Collisional line-shape effects in accurate He-perturbed H<sub>2</sub> spectra*” *Journal of Quantitative Spectroscopy and Radiative Transfer* **277**, 107951 (2022)  
DOI: 10.1016/j.jqsrt.2021.107951

preparation of the quantum scattering code, performing quantum scattering calculations that involve the correction originating from the centrifugal distortion of the potential energy surface for the five considered potential energy surfaces, denoted as „SK”, „mMR”, „BSP”, „BSP2” and „BSP3” in the paper, calculations of the generalized spectroscopic cross sections

3. Mikołaj Zaborowski, Michał Słowiński, Kamil Stankiewicz, Franck Thibault, Agata Cygan, Hubert Józwiak, Grzegorz Kowzan, Piotr Masłowski, Akiko Nishiyama, Nikodem Stolarczyk, Szymon Wójtewicz, Roman Ciuryło, Daniel Lisak, Piotr Wcisło „*Ultra-high finesse cavity-enhanced spectroscopy for accurate tests of quantum electrodynamics for molecules*” *Optics Letters* **45**, 1603 (2020) DOI: 10.1364/OL.389268

preparation of the potential energy surface for the  $D_2$ - $D_2$  scattering calculations, performing quantum scattering calculations, determining the generalized optical cross sections for the self-perturbed 2-0 S(2) line in  $D_2$

4. Piotr Wcisło, Franck Thibault, Nikodem Stolarczyk, Hubert Józwiak, Michał Słowiński, Maciej Gancewski, Kamil Stankiewicz, Magdalena Konefał, Samir Kassi, Alain Campargue, Yan Tan, Jin Wang, Konrad Patkowski, Roman Ciuryło, Daniel Lisak, Roman Kochanov, Laurence S. Rothman, Iouli E. Gordon „*The first comprehensive dataset of beyond-Voigt line-shape parameters from ab initio quantum scattering calculations for the HITRAN database: He-perturbed  $H_2$  case study*” *Journal of Quantitative Spectroscopy and Radiative Transfer* **260**, 107477 (2021) DOI: 10.1016/j.jqsrt.2020.107477

preparation of the radial coupling terms of the potential that include the centrifugal distortion correction, performing quantum scattering calculations and determining the generalized spectroscopic cross sections for 321 He-perturbed lines in  $H_2$

Hubert Józwiak

dr inż. Grzegorz Kowzan  
Instytut Fizyki UMK  
Ul. Grudziądzka 5/7  
87-100 Toruń

Stony Brook, 03.01.2022

## Statement of coauthorship

I hereby declare that my contribution to the paper:

Grzegorz Kowzan, Piotr Wcisło, Michał Słowiński, Piotr Masłowski, Alexandra Viel, Franck Thibault.  
“Fully quantum calculations of the line-shape parameters for the Hartmann-Tran profile: A CO-Ar case study.” Journal of Quantitative Spectroscopy and Radiative Transfer 243, p. 106803, 2020,

included: leading the work on the paper, performing the scattering calculations, calculations of spectroscopic cross sections and of line shapes (excluding the speed-dependent billiard ball lineshape profile). I also analyzed the validity of line-shape approximations, prepared the figures and wrote the manuscript.

...Grzegorz...Kowzan  
Signature

Prof. dr hab. Daniel Lisak  
Uniwersytet Mikołaja Kopernika w Toruniu  
Instytut Fizyki, Grudziądzka 5/7, 87-100 Toruń

Toruń, 7.12.2021

### Statement about my contribution to the research papers

My contribution to the research published in paper:

Authors: Magdalena Konefał, Michał Słowiński, Mikołaj Zaborowski, Roman Ciuryło, Daniel Lisak, Piotr Wcisło

Title: Analytical-function correction to the Hartmann–Tran profile for more reliable representation of the Dicke-narrowed molecular spectra

Journal: Journal of Quantitative Spectroscopy and Radiative Transfer 242, 106784 (2020)

DOI: 10.1016/j.jqsrt.2019.106784

was related to explaining the details of the HTP line shape model to the first author, discussing the results and a way of their presentation with other authors, as well as contributing to writing and editing the manuscript.

My contribution to the research published in paper:

Authors: Piotr Wcisło, Franck Thibault, Nikodem Stolarczyk, Hubert Józwiak, Michał Słowiński, Maciej Gancewski, Kamil Stankiewicz, Magdalena Konefał, Samir Kassi, Alain Campargue, Yan Tan, Jin Wang, Konrad Patkowski, Roman Ciuryło, Daniel Lisak, Roman Kochanov, Laurence S.Rothman, Iouli E. Gordon

Title: The first comprehensive dataset of beyond-Voigt line-shape parameters from ab initio quantum scattering calculations for the HITRAN database: He-perturbed H<sub>2</sub> case study

Journal: Journal of Quantitative Spectroscopy and Radiative Transfer 260, 107477 (2021)

DOI: 10.1016/j.jqsrt.2020.107477

was related to discussing concepts and methodology with other authors as well as contributing to writing and editing the manuscript.



dr hab. Piotr Maślowski, prof. UMK

Toruń, 01.02.2022

Uniwersytet Mikołaja Kopernika w Toruniu

Instytut Fizyki, ul. Grudziądzka 5/7, 87-100 Toruń

### **Statement about my contribution to the research papers**

My contribution to the research published in the paper

Authors: Grzegorz Kowzan, Piotr Wcisło, Michał Słowiński, Piotr Maślowski, Alexandra Viel, Franck Thibault

Title: Fully quantum calculations of the line-shape parameters for the Hartmann-Tran profile: A CO-Ar case study

Journal: Journal of Quantitative Spectroscopy and Radiative Transfer 243, 106803 (2020)

DOI: 10.1016/j.jqsrt.2019.106803

was related to discussing concepts and methodology with other authors as well as contributing to the editing of the manuscript.



**Object : Contribution statement – cooperation with Michał Słowiński**

**To the Polish Ministry of Education and Science**

Dear colleagues,

By the present letter I would like to inform you about my contribution to Torun's group work, and in particular to Michał Slowinski's articles. First, I would like to mention that my group at the Institut de Physique de Rennes and the group lead by Dr Roman Ciuryło obtained two French-Polish Polonium grants during the last ten years. Michał Slowinski was involved in the second 2 years project just finished this year (due to the pandemic). He visited my laboratory during 7 days during the summer of 2018. During his stay in Rennes we have been together to MOLEC 2018 which was held in Dinard (close to Rennes, on the channel) to present our works.

We worked together on CO in argon baths, H<sub>2</sub> diluted in helium and on a quadrupolar line of D<sub>2</sub>. For all the papers listed below my contribution was essentially the same. Prepare the potential energy surfaces in a suitable form to perform the dynamics on it, and then perform quantum dynamical calculations to obtain scattering S-matrix elements that enter in spectroscopic generalized cross sections (pressure broadening and shift as well as complex Dicke cross sections. For some of the systems considered I have also determined the speed dependent line shape parameters. Such parameters are then used, by Michał and Torun's group, for an accurate line shape analysis of recorded spectra (in Torun, Grenoble or Heifei).

Our collaboration is very efficient since it allowed us to publish a number of papers during the last years.

**List of common publications:**

1. Michał Słowiński, Hubert Józwiak, Maciej Gancewski, Kamil Stankiewicz, Nikodem Stolarczyk, Yan Tan, Jin Wang, An-Wen Liu, Shui-Ming Hu, Samir Kassi, Alain Campargue, Konrad Patkowski, Piotr S. Żuchowski, Roman Ciuryło, Franck Thibault, Piotr Wcisło. "*Collisional line-shape effects in accurate He-perturbed H<sub>2</sub> spectra*". J. Quant. Spectrosc. and Radiat. Transfer 277, 107951 (2022).

<https://doi.org/10.1016/j.jqsrt.2021.107951>

2. Piotr Wcisło, Franck Thibault, Nikodem Stolarczyk, Hubert Józwiak, Michał Słowiński, Maciej Gancewski, Kamil Stankiewicz, Magdalena Konefał, Samir Kassi, Alain Campargue, Yan Tan, Jin Wang, Konrad Patkowski, Roman Ciuryło, Daniel Lisak, Roman Kochanov, Laurence S. Rothman, Iouli E. Gordon. "*The first comprehensive dataset of beyond-Voigt line-shape parameters from ab initio quantum scattering calculations for the HITRAN database: He-perturbed H<sub>2</sub> case study*". J. Quant. Spectrosc. and Radiat. Transfer 260, 107477 (2021).

<https://doi.org/10.1016/j.jqsrt.2020.107477>

3. Michał Słowiński, Franck Thibault, Yan Tan, Jin Wang, An-Wen Liu, Shui-Ming Hu, Samir Kassi, Alain Campargue, Magdalena Konefał, Hubert Józwiak, Konrad Patkowski, Piotr Żuchowski, Roman Ciuryło, Daniel Lisak, Piotr Wcisło. "*H<sub>2</sub>-He collisions: Ab initio theory meets cavity-*



*enhanced spectra*. Physical Review A 101, 052705 (2020).  
<https://doi.org/10.1103/PhysRevA.101.052705>.

4. Mikołaj Zaborowski, Michał Słowiński, Kamil Stankiewicz, Franck Thibault, Agata Cygan, Hubert Józwiak, Grzegorz Kowzan, Piotr Masłowski, Akiko Nishiyama, Nikodem Stolarczyk, Szymon Wójtewicz, Roman Ciuryło, Daniel Lisak, Piotr Wcisło. “*Ultrahigh finesse cavity-enhanced spectroscopy for accurate tests of quantum electrodynamics for molecules*”. Optics Letters 45, 1603 (2020). <https://doi.org/10.1364/OL.389268>

5. Grzegorz Kowzan, Piotr Wcisło, Michał Słowiński, Piotr Masłowski, Alexandra Viel, Franck Thibault. “*Fully quantum calculations of the line-shape parameters for the Hartmann-Tran profile: A CO-Ar case study*”. J. Quant. Spectrosc. and Radiat. Transfer 243, 106803 (2020).

<https://doi.org/10.1016/j.jqsrt.2019.106803>

Yours sincerely,

Dr Franck THIBAUT

Institut de Physique de Rennes, Université de Rennes 1, France

Email : [franck.thibault@univ-rennes1.fr](mailto:franck.thibault@univ-rennes1.fr)

Tel : +33223236182

[Franck THIBAUT \(0000-0002-1279-8588\) - ORCID | Connecting Research and Researchers](#)

January 29, 2022

### Statement of co-authorship

My contribution to the paper

*M. Słowiński, F. Thibault, Y. Tan, J. Wang, A.-W. Liu, S.-M. Hu, S. Kassı, A. Campargue, M. Konefał, H. Jóźwiak, K. Patkowski, P. Żuchowski, R. Ciuryło, D. Lisak, P. Wcisło*  
*"H<sub>2</sub>-He collisions: Ab initio theory meets cavity-enhanced spectra"*  
*Phys. Rev. A. 101 (2020), 052705*

was coordinating the project and supervising the data analysis, results interpretation and manuscript preparation. **I would like to emphasize that the contribution of Michał Słowiński to this work was dominant.** He solved the transport-relaxation equation for the velocity distribution of an optical coherence (Eq. (3)) and used it to generate the collision-perturbed shapes of the H<sub>2</sub> lines (he used the generalized spectroscopic cross sections calculated by other coauthors). He did the entire analysis of the experimental spectra and performed the comparison between theory and experiment. Michał came up with the idea of using the accurate spectra to validate potential energy surfaces and he performed such analysis (Fig. 3). Michał was very independent in his work, he developed a large part of the methodology he used for the analysis, developed the computer codes etc. He prepared all the figures, wrote almost entire article and took the responsibility of paper submission and addressing the criticism of editor and reviewers.

My contribution to the paper

*M. Słowiński, H. Jóźwiak, M. Gancewski, K. Stankiewicz, N. Stolarczyk, Y. Tan, J. Wang, A.-W. Liu, S.-M. Hu, S. Kassı, A. Campargue, K. Patkowski, P. Żuchowski, R. Ciuryło, F. Thibault, P. Wcisło*  
*"Collisional line-shape effects in accurate He-perturbed H<sub>2</sub> spectra"*  
*J. Quant. Spectrosc. Radiat. T 278 (2022), 107951*

was coordinating the project and supervising the data analysis, results interpretation and manuscript preparation. **I would like to emphasize that the contribution of Michał Słowiński to this work was dominant.** He performed all the line-shape calculations (based on the generalized spectroscopic cross sections calculated by other coauthors). Michał came up with the idea of resolving the contributions of different collisional effects by comparing the experimental spectra with theoretical *ab initio* spectra that have one of the contributions turned off, see Fig. 3. This gave us a much deeper insight into the collisional physics underlying the formation of the shapes of molecular lines. Michał was very independent in his work, he developed a large part of the methodology he used for the analysis, developed the computer codes etc. He prepared all the figure (except Fig. 5), wrote almost entire article and took the responsibility of paper submission and addressing the criticism of editor and reviewers.



My contribution to the paper

*G. Kowzan, P. Wcisło, M. Słowiński, P. Masłowski, A. Viel, F. Thibault*

*"Fully quantum calculations of the line-shape parameters for the Hartmann-Tran profile: a CO-Ar case study"*  
*J. Quant. Spectrosc. Radiat. T 243 (2020), 106803*

was supporting the project in the area of the physics of molecular collisions and line-shape modeling, and discussing the idea of validating the phenomenological profile on the *ab initio* ones.

My contribution to the paper

*M. Konefał, M. Słowiński, M. Zaborowski, R. Ciuryło, D. Lisak, P. Wcisło*

*"Analytical-function correction to the Hartmann–Tran profile for more reliable representation of the Dicke-narrowed molecular spectra"*  
*J. Quant. Spectrosc. Radiat. T 242 (2020), 106784*

was coordinating the project, and supervising the data analysis, results interpretation and manuscript preparation. **I would like to emphasize that the contributions of the first two authors (Magda Konefał and Michał Słowiński) are equal.** Michał performed almost all the calculations and prepared the computer codes necessary for them. He prepared all the figures (except Fig. 3). Michał gave also an important contribution on the conceptual level, where he participated in formulating the problem and developing the idea of the beta-correction for an arbitrary absorber-to-perturber mass ratio.

My contribution to the paper

*M. Zaborowski, M. Słowiński, K. Stankiewicz, F. Thibault, A. Cygan, H. Jóźwiak, G. Kowzan, P. Masłowski, A. Nishiyama, N. Stolarczyk, S. Wójtewicz, R. Ciuryło, D. Lisak, P. Wcisło*

*"Ultra-high finesse cavity-enhanced spectroscopy for accurate tests of quantum electrodynamics for molecules"*  
*Opt. Lett. 45 (2020), 1603-1606*

was coordinating the project, maintaining the collaboration, and supervising the measurements, data analysis, results interpretation and manuscript preparation. **I would like to emphasize that Michał Słowiński prepared the computer codes for generating the sophisticated beyond-Voigt line-shape profiles that were crucial for the experimental data analysis and reducing the systematic uncertainties.** Michał also participated in the measurement (spectra collecting) and data analysis.

My contribution to the paper

*P. Wcisło, F. Thibault, N. Stolarczyk, H. Jóźwiak, M. Słowiński, M. Gancewski, K. Stankiewicz, M. Konefał, S. Kass, A. Campargue, Y. Tan, J. Wang, K. Patkowski, R. Ciuryło, D. Lisak, R. Kochanov, L. S. Rothman, I. E. Gordon*  
*"The first comprehensive dataset of beyond-Voigt line-shape parameters from ab initio quantum scattering calculations for the HITRAN database: He-perturbed H<sub>2</sub> case study"*  
*J. Quant. Spectrosc. Radiat. T 260 (2021), 107477*

was coordinating the project, maintaining the collaboration, and supervising the data analysis, results interpretation and manuscript preparation. **I would like to emphasize that Michał Słowiński performed validation of the spectroscopic dataset on the experimental spectra**, i.e., he validated the beta-corrected quadratic speed-dependent hard-collision model (that is based on our *ab initio* line-shape parameters exported to the HITRAN format) on the accurate He-perturbed H<sub>2</sub> spectra from Grenoble and Hefei laboratories, see Fig. 5.



*Piotr Wcisło, Physicist  
dr. hab., prof. at NCU  
Institute of Physics  
Nicolaus Copernicus University  
Grudziądzka 5, 87-100 Toruń, Poland  
room: 526  
phone: + 48 56 611 32 82  
+ 48 504 130 458  
email: piotr.wcislo@umk.pl  
Google Scholar: 4umjDDsAAAAJ*

mgr inż. Mikołaj Zaborowski  
ul. Grudziądzka 5  
87-100 Toruń

Toruń, 7.12.2021

## Statement of coauthorship

I hereby declare that my contribution to the paper:

M. Zaborowski, M. Słowiński, K. Stankiewicz, F. Thibault, A. Cygan, H. Józwiak, G. Kowzan, P. Masłowski, A. Nishiyama, N. Stolarczyk, S. Wójtewicz, R. Ciuryło, D. Lisak, P. Wcisło, *Ultrahigh finesse cavity-enhanced spectroscopy for accurate tests of quantum electrodynamics for molecules*, Optics Letters **45**, 1603 (2020), DOI: 10.1364/OL.389268

included taking leading part in the measurements, data analysis and writing of the article. I created table and most of the graphs in the article. I was responsible for submitting and editing the article according to co-authors' and reviewers' remarks.

Mikołaj Zaborowski

Signature

mgr inż. Mikołaj Zaborowski  
ul. Grudziądzka 5  
87-100 Toruń

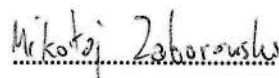
Toruń, 7.12.2021

## Statement of coauthorship

I hereby declare that my contribution to the paper:

M. Konefał, M. Słowiński, M. Zaborowski, R. Ciuryło, D. Lisak, P. Wcisło, *Analytical-function correction to the Hartmann–Tran profile for more reliable representation of the Dicke-narrowed molecular spectra*, *Journal of Quantitative Spectroscopy and Radiative Transfer* **242**, 106784 (2020), DOI: 10.1016/j.jqsrt.2019.106784

included taking part in determining and testing  $\beta$ -correction function.



Signature



# THE LIST OF ALL THE ARTICLES COAUTHORED BY ME

INCLUDING THOSE NOT SUBMITTED  
WITHIN THIS DISSERTATION

1. H<sub>2</sub>-He collisions: *Ab initio* theory meets cavity-enhanced spectra  
**Michał Słowiński**, Franck Thibault, Yan Tan, Jin Wang, An-Wen Liu, Shui-Ming Hu, Samir Kassi, Alain Campargue, Magdalena Konefał, Hubert Józwiak, Konrad Patkowski, Piotr Żuchowski, Roman Ciuryło, Daniel Lisak, Piotr Wcisło  
*Physical Review A* 101, 052705 (2020)  
DOI: 10.1103/PhysRevA.101.052705
2. Collisional line-shape effects in accurate He-perturbed H<sub>2</sub> spectra  
**Michał Słowiński**, Hubert Józwiak, Maciej Gancewski, Kamil Stankiewicz, Nikodem Stolarczyk, Yan Tan, Jin Wang, An-Wen Liu, Shui-Ming Hu, Samir Kassi, Alain Campargue, Konrad Patkowski, Piotr S. Żuchowski, Roman Ciuryło, Franck Thibault, Piotr Wcisło  
*Journal of Quantitative Spectroscopy and Radiative Transfer* 277, 107951 (2022)  
DOI: 10.1016/j.jqsrt.2021.107951
3. Fully quantum calculations of the line-shape parameters for the Hartmann-Tran profile: A CO-Ar case study  
Grzegorz Kowzan, Piotr Wcisło, **Michał Słowiński**, Piotr Masłowski, Alexandra Viel, Franck Thibault  
*Journal of Quantitative Spectroscopy and Radiative Transfer* 243, 106803 (2020)  
DOI: 10.1016/j.jqsrt.2019.106803



4. Analytical-function correction to the Hartmann–Tran profile for more reliable representation of the Dicke-narrowed molecular spectra

Magdalena Konefał, **Michał Słowiński**, Mikołaj Zaborowski, Roman Ciuryło, Daniel Lisak, Piotr Wcisło

*Journal of Quantitative Spectroscopy and Radiative Transfer* 242, 106784 (2020)

DOI: 10.1016/j.jqsrt.2019.106784

5. Ultrahigh finesse cavity-enhanced spectroscopy for accurate tests of quantum electrodynamics for molecules

Mikołaj Zaborowski, **Michał Słowiński**, Kamil Stankiewicz, Franck Thibault, Agata Cygan, Hubert Józwiak, Grzegorz Kowzan, Piotr Masłowski, Akiko Nishiyama, Nikodem Stolarczyk, Szymon Wójtewicz, Roman Ciuryło, Daniel Lisak, Piotr Wcisło

*Optics Letters* 45, 1603 (2020)

DOI: 10.1364/OL.389268

6. The first comprehensive dataset of beyond-Voigt line-shape parameters from *ab initio* quantum scattering calculations for the HITRAN database: He-perturbed H<sub>2</sub> case study

Piotr Wcisło, Franck Thibault, Nikodem Stolarczyk, Hubert Józwiak, **Michał Słowiński**, Maciej Gancewski, Kamil Stankiewicz, Magdalena Konefał, Samir Kassi, Alain Campargue, Yan Tan, Jin Wang, Konrad Patkowski, Roman Ciuryło, Daniel Lisak, Roman Kochanov, Laurence S. Rothman, Iouli E. Gordon

*Journal of Quantitative Spectroscopy and Radiative Transfer* 260, 107477 (2021)

DOI: 10.1016/j.jqsrt.2020.107477



7. Inclusion of Berry's phase into an impact treatment of self-broadening of the Lyman- $\alpha$  line in an external slowly rotating electric field  
Roman Ciuryło, **Michał Słowiński**, Józef Szudy, William E. Baylis  
*Physical Review A* 98, 023430 (2018)  
DOI: 10.1103/PhysRevA.98.023430
  
8. Line-shape analysis for high J R-branch transitions of the oxygen B band  
Jolanta Domysławska, Szymon Wójtewicz, Piotr Masłowski, Katarzyna Bielska, Agata Cygan, **Michał Słowiński**, Ryszard Trawiński, Roman Ciuryło, Daniel Lisak  
*Journal of Quantitative Spectroscopy and Radiative Transfer* 242, 106789 (2020)  
DOI: 10.1016/j.jqsrt.2019.106789
  
9. Subpercent agreement between ab initio and experimental collision-induced line shapes of carbon monoxide perturbed by argon  
Grzegorz Kowzan, Hubert Cybulski, Piotr Wcisło, **Michał Słowiński**, Alexandra Viel, Piotr Masłowski, Franck Thibault  
*Physical Review A* 102, 107477 (2021)  
DOI: 10.1103/PhysRevA.102.012821
  
10. Simultaneous observation of speed dependence and Dicke narrowing for self-perturbed P-branch lines of O<sub>2</sub> B band  
Katarzyna Bielska, Jolanta Domysławska, Szymon Wójtewicz, Alexandr Balashov, **Michał Słowiński**, Mariusz Piwiński, Agata Cygan, Roman Ciuryło, Daniel Lisak  
*Journal of Quantitative Spectroscopy and Radiative Transfer* 276, 107927 (2021)  
DOI: 10.1016/j.jqsrt.2021.107927